This thesis is the result of work done while in registered postgraduate candidature at the University of Southampton.

UNIVERSITY OF SOUTHAMPTON

TURBIDITY CURRENT PROCESSES AND DEPOSITS ON THE NORTHWEST AFRICAN MARGIN

A thesis submitted for the degree of Doctor of Philosophy

by

Russell Barry Wynn BSc (Hons)

School of Ocean and Earth Science

Faculty of Science

University of Southampton

April 2000

UNIVERSITY OF SOUTHAMPTON

ABSTRACT

FACULTY OF SCIENCE

SCHOOL OF OCEAN AND EARTH SCIENCE

Doctor of Philosophy

TURBIDITY CURRENT PROCESSES AND DEPOSITS ON THE NORTHWEST AFRICAN MARGIN

by Russell Barry Wynn

The Northwest African margin is affected by a wide variety of sedimentary processes, including pelagic/hemipelagic background sedimentation, alongslope bottom currents, and downslope gravity flows. A large section of the margin can be classified as a fine-grained clastic slope apron, although the presence of numerous volcanic islands and seamounts leads to a more complex distribution of sedimentary processes than is accounted for by existing slope apron models.

The Moroccan Turbidite System (MTS) is the largest turbidite system on the margin, with a total length of 1500 km. Individual turbidites can be correlated across three interconnected deep-water basins, giving an unprecedented insight into the turbidite depositional architecture of a system with complex seafloor topography and multiple sources. A detailed, core-based study of the turbidite fill in an intraslope basin within the MTS has revealed that sand body architecture is largely controlled by turbidity current volume. Small-volume turbidity currents deposit all of their sand around the mouth of the feeder canyon, whereas large-volume turbidity currents deposit extensive sheet sands across the basin floor. The large-volume, high efficiency flows excavate giant erosional scours at the canyon mouth, leading to development of a channel-lobe transition zone (CLTZ). Comparison with other CLTZ's has revealed that these zones form in association with flow expansion at a canyon/channel mouth, and may also be linked to major breaks in slope.

Deep-water sediment waves are widespread on the margin, and display wave heights up to 70 m, and wavelengths up to 2.4 km. The largest sediment-wave fields are found on the continental slope and rise bordering the volcanic Canary Islands. Analysis of an integrated dataset, combined with simple numerical modelling, reveals that the sediment waves are deposited as antidunes beneath unconfined, low-velocity, low concentration turbidity currents.

For my mother and grandmother

ACKNOWLEDGEMENTS

First of all I would like to thank my three supervisors, Dr Doug Masson, Prof Dorrik Stow and Dr Phil Weaver for their expertise and guidance throughout the duration of my study. In particular, I would like to thank Doug for his table tennis lessons and companionship on cruises, Dorrik for his patience in listening to my various far-flung theories and helping set up the sediment waves workshop, and Phil for teaching me how to write a paper in a week! I would also like to take this opportunity to thank the following colleagues at Southampton Oceanography Centre who have helped me in my work: Jez Evans, Neil Kenyon, Guy Rothwell, Dave Gunn, John Murray, Martin Gee, Tim le Bas, Veit Huenerbach, Rod Pearce and Barry Marsh. Of course, none of this work would have been possible without the dedication and commitment shown at sea by the masters, officers and crew of the RRS Discovery and RRS Charles Darwin, who are the unsung heroes of so much deep-water research. My time at Southampton has been punctuated by several visits to BP Amoco (Sunbury and Aberdeen) where I worked on a number of short-term technical projects. I am therefore grateful to Liz Jolley, Richard Dixon, Shelagh Baines, Andy Pulham and all my other friends at BP Amoco for making my time there so enjoyable. My colleagues at Barcelona, Gemma Ercilla, Belen Alonso and Jesus Baraza are thanked for providing data and ideas on some aspects of my work. Finally, I would like to acknowledge the University of Southampton and Challenger Division as the source of my PhD funding.

Outside of work, I would like to say a big thank you to my family, and also my girlfriend, Vikki, for their constant support and encouragement, and to the following friends and acquaintances who have made my time at Southampton so enjoyable: the 'housemates'– Mike Reeder, Katie Allen, Paul Kelly, Tim Cane, Stuart Moss, Jon Evans and Phil Scotney, the SOC football team, and also Kim and Neil Potter, Ian Harding, Frank Wigley, Thorsten Warneke, Mike Carter, Ross McGowan and anyone else who has shared a kebab with me after a Wednesday night at Ikon.

CONTENTS

Page

Abstract 3

Acknowledgements 5

Contents 6

List of figures 9

List of tables 13

List of appendices 14

Chapter 1: Introduction 15

1.1: Introduction to the study 15

1.2: Aims and objectives 16

1.3: Layout of the thesis 17

1.4: Statement on authorship 17

Chapter 2: Methodology and database 19

2.1: Cruise information 19

2.2: Multi-beam bathymetry 19

2.3: Sidescan sonar 19

2.4: Seismic profiles 20

2.5: Sediment cores 20

2.6: Other data 22

Chapter 3: Regional setting 23

3.1: Study area: the Northwest African margin 23

3.2: The volcanic Canary Islands 23

3.3: Onshore geology 23

3.4: Seafloor morphology 26

3.5: Oceanography 26

3.6: Geological history of the Northwest African margin 30

Chapter 4: Continental margin sedimentation 32

4.1: Introduction and aims 32

4.2: *Paper 1* - Continental margin sedimentation, with special reference to the Northeast Atlantic margin 34
4.3: Summary 60

Chapter 5: Sedimentary processes on the Northwest African margin 61
5.1: Introduction and aims 62
5.2: *Paper 2* - The Northwest African slope apron: a modern analogue for deep-water systems with complex seafloor topography 63
5.3: Summary 87

Chapter 6: Turbidite depositional architecture on the Northwest African margin 88
6.1: Introduction and aims 89
6.2: *Paper 3* - Turbidite depositional architecture across three interconnected deep-water basins on the Northwest African margin 90
6.3: Summary 123

Chapter 7: Channel –lobe transition zones 124
7.1: Introduction and aims 125
7.2: *Paper 4* - A new model for channel-lobe transition zones based on high-resolution seafloor mapping and modern and ancient analogues 126
7.3: Summary 161

Chapter 8: Turbidity current sediment waves (1) 162
8.1: Introduction and aims 163
8.2: *Paper 5* - Turbidity current sediment waves on the submarine slopes of the western Canary Islands 164
8.3: Summary 185

Chapter 9: Turbidity current sediment waves (2) 186
9.1: Introduction and aims 187
9.2: *Paper 6* - Sedimentary processes in the Selvage sediment-wave field, NE Atlantic: new insights into the formation of sediment waves by turbidity currents 188
9.3: Summary 216

Chapter 10: Turbidity current sediment waves (3) 217
10.1: Introduction and aims 218
10.2: *Paper 7* - Turbidity current sediment waves in subsurface sequences 219
10.3: Summary 235

Chapter 11: Discussion 236
11.1: Slope apron vs submarine fan vs turbidity current pathway 236
11.2: Sediment flux on the Northwest African margin 238
11.3: Long-distance turbidite correlation 240
11.4: Bottom current vs turbidity current sediment waves 241
11.5: Applications to hydrocarbon exploration 241

Chapter 12: Conclusions 245

Chapter 13: Future work 247

References 249
Appendices 273

LIST OF FIGURES

Chapter 3:

Figure 3.1: Location map of the study area on the Northwest African margin 24
Figure 3.2: Geological map of the Northwest African margin 25
Figure 3.3: Map showing surface current flow along the margin 28
Figure 3.4: Map showing AABW flow direction along the margin 29

Chapter 4:

Figure 4.1: Map showing the distribution of sedimentary processes on the Northeast Atlantic margin ..... Foldout 1
Figure 4.2: Schematic diagrams showing the idealised sedimentary features on a) the glaciated margin, b) the glacially-influenced margin and c) the non-glaciated margin 39
Figure 4.3: TOBI image of the edge of the Saharan debris flow 41
Figure 4.4: a) 3.5kHz and b) airgun seismic profiles across the Madeira Abyssal Plain 42
Figure 4.5: Diagram of canyon morphology on the Biscay margin 47
Figure 4.6: TOBI image of mass movements north of the Faeroe Islands 50
Figure 4.7: 3.5kHz-profile of a contourite drift with sediment waves in the north-east Rockall Trough 52
Figure 4.8: TOBI image of iceberg ploughmarks on the upper slope west of Scotland 53
Figure 4.9: Graph showing how turbidite volume (per million years) varies on four different abyssal plains 56

Chapter 5:

Figure 5.1: Sediment distribution and process map of the Northwest African margin ..... Foldout 2
Figure 5.2: Gravity-flow deposits and features on the Northwest African margin, including a) turbidity current channels, b) turbidity current sediment waves, c) the Saharan Debris Flow, and d) the Oratava-Icod-Tino debris avalanche complex 71

Figure 5.3: Turbidite sand thicknesses and sand/mud ratios in the Agadir Basin based on core data 75
Figure 5.4: Diagram showing the age of turbidite emplacement on the Madeira Abyssal Plain 77
Figure 5.5: Turbidite sand thicknesses and sand/mud ratios on the Madeira Abyssal Plain 78
Figure 5.6: Sedimentary environment models showing a) the Stow (1985) model of a fine-grained clastic slope apron and b) the Northwest African slope apron 80
Figure 5.7: Schematic profiles of the continental margin off Western Sahara showing a) a constructional margin and b) a destructive or erosional margin 82

Chapter 6:

Figure 6.1: Location map showing the main features of the Moroccan Turbidite System 93
Figure 6.2: a) Location map showing core locations, lines of cross-section/core correlation and bathymetry of the study area. b) Cross section through the Moroccan Turbidite System 96
Figure 6.3: 3.5kHz-profiles showing the acoustic character of the seafloor at various core localities 100
Figure 6.4: Core correlation for the Agadir Basin sequence showing the turbidite fill 103
Figure 6.5: Core correlation for the Madeira Abyssal Plain, Agadir Basin and the Seine Abyssal Plain 104
Figure 6.6: Graphs showing the composition of turbidites derived from a) Morocco Shelf (fine sand fraction), b) Morocco Shelf (very fine sand fraction, and c) Canary Islands/Western Sahara Shelf 105
Figure 6.7: Core photographs showing the sedimentary structures of two turbidites in the Agadir Basin 106
Figure 6.8: Coccolith ratios in turbidite *AB13/Mf/Sk* 114
Figure 6.9: Schematic diagram showing the relationship between turbidite depositional architecture and turbidite volume in the Agadir Basin 117

Chapter 7:

Figure 7.1: Location map of the CLTZ at the mouth of the Agadir Canyon 131
Figure 7.2: Interpretation of TOBI mosaic across the Agadir CLTZ 132
Figure 7.3: Sketch of TOBI 7kHz-profile across the Agadir CLTZ 133
Figure 7.4: a) TOBI image of scours within the Agadir CLTZ. b) TOBI 7kHz-profile showing scour morphology in cross-section 134
Figure 7.5: a) TOBI image of an erosional scarp within the Agadir CLTZ. b) TOBI 7kHz-profile showing scoured seafloor adjacent to the erosional scarp 135
Figure 7.6: 3.5kHz-profile across the proximal Agadir CLTZ 136
Figure 7.7: Location map of the CLTZ at the mouth of the Lisbon and Setubal Canyons 138
Figure 7.8: Interpretation of TOBI mosaic across the Lisbon and Setubal CLTZ s 139
Figure 7.9: TOBI image showing widespread seafloor erosion within the Lisbon CLTZ 140
Figure 7.10: Location map of the CLTZ on the Rhone Fan 142
Figure 7.11: Interpretation of MAK1 images across the Rhone CLTZ 143
Figure 7.12: MAK1 image showing a large erosional scour within the Rhone CLTZ 144
Figure 7.13: a) Summary diagram showing typical cross-sections through a low and high efficiency system. b) summary diagram showing the spatial distribution of erosional scours and depositional bedforms within a CLTZ in a high efficiency system 145
Figure 7.14: Chart showing the relationship between slope angle and depth of scour in CLTZ and channel floor/levee overbank environments 151
Figure 7.15: Line diagram comparing channels and scours in cross-section 154

Chapter 8:

Figure 8.1: Location map showing the regional setting and bathymetry of the sediment wave fields around the western Canary Islands 167
Figure 8.2: GEOSEA 3-D image (plan view) of the La Palma wave field 170
Figure 8.3: a) Enlarged GEOSEA 3-D image (oblique view) of the La Palma sediment waves b) Tracing of the wave crest lines shown in (a) 171

Figure 8.4: 3.5kHz-profile through the La Palma wave field 172
Figure 8.5: Airgun seismic profile through the La Palma wave field 173
Figure 8.6: Sedimentary logs of cores recovered from the La Palma wave field 174
Figure 8.7: GEOSEA 3-D image (plan view) of the El Julan sediment wave field within the El Julan debris avalanche scar 181
Figure 8.8: TOBI image of the El Julan sediment wave field 182

Chapter 9:

Figure 9.1: Location map showing sediment wave fields in the vicinity of the Canary Islands 192
Figure 9.2: Line drawing of TOPAS profile taken through the Selvage wave field 195
Figure 9.3: TOPAS profile showing poorly developed sediment waves and transparent debris flow deposit 196
Figure 9.4: TOPAS profile showing well developed sediment waves in the Selvage wave field 197
Figure 9.5: Graphs showing variations in wave height, wavelength and wave height/wavelength ratio with distance downslope for the Selvage and La Palma wave fields 198
Figure 9.6: Core description for Core D13071 recovered from the Selvage wave field 200
Figure 9.7: Drawing of a volcaniclastic turbidite in Core D13071 201

Chapter 10:

Figure 10.1: Location map of the La Palma and Selvage wave fields 222
Figure 10.2: 3.5kHz-profile through the La Palma wave field 224
Figure 10.3: Single-channel seismic profile through the La Palma wave field 225
Figure 10.4: GEOSEA 3-D image of the upper La Palma wave field 226
Figure 10.5: Sediment core descriptions from the La Palma and Selvage wave fields 228
Figure 10.6: Schematic diagram showing migrating sediment waves in the subsurface 233

LIST OF TABLES

Chapter 2:

Table 2.1: Character, location and interpretation of morphological features and sedimentary deposits on the Northwest African margin 21

Chapter 5:

Table 5.1: Character, location and interpretation of morphological features and sedimentary deposits on the Northwest African margin 67

Chapter 6:

Table 6.1: Key characteristics of cores used in this study 98

Table 6.2: Key characteristics of individual turbidites in the Agadir Basin 101

Table 6.3: Correlation of turbidites on the Madeira Abyssal Plain, Agadir Basin and Seine Abyssal Plain, with volume, thickness and age shown for each turbidite 110

Chapter 7:

Table 7.1: Dimensions of erosional scours in modern and ancient CLTZ s, and modern channel floor/levee overbank environments 149

Chapter 9:

Table 9.1: Characteristics of sediment wave fields formed beneath unconfined turbidity currents 191

Chapter 10:

Table 10.1: Dimensions and characteristics of the La Palma and Selvage wave fields, compared with published data on turbidity current sediment waves 230

LIST OF APPENDICES

Appendix 1: 274

Turbidite sand mineralogy in cores recovered from the Agadir Basin and Seine Abyssal Plain 274

CHAPTER 1

INTRODUCTION

1.1: Introduction to the thesis

The Northwest African margin is one of the most intensively studied continental margins in the world, and the wide variety of sedimentary processes and deposits recognised in this area have contributed greatly to our understanding of deep-water sedimentation. Sediment facies mapping based on 3.5kHz-profiles has revealed that the margin is affected by a complex interplay of downslope, alongslope and pelagic/hemipelagic sedimentary processes (Jacobi and Hayes, 1982; 1984; 1992). Downslope processes include debris avalanches on the submarine flanks of the Canary Islands (Watts and Masson, 1995; Masson, 1996; Urgeles et al., 1997; 1999), large-scale, long runout debris flows (Embley, 1976; 1982; Jacobi, 1976; Kidd et al., 1985; Masson et al., 1992; 1993; 1997; 1998; Gee et al., 1999), and infrequent, large-volume turbidity currents that deposit thick muds on the deep abyssal plains (Weaver and Kuijpers, 1983; Weaver and Rothwell, 1987; Searle, 1987; Pearce and Jarvis, 1992; Rothwell et al., 1992; Weaver et al., 1992; 1995; 1998; Masson, 1994; Davies et al., 1997; Lebreiro et al., 1997; Ercilla et al., 1998). Alongslope bottom currents produce bedforms and erosional features such as sediment waves and erosional furrows (Jacobi and Hayes, 1992; Masson et al., 1992).

Despite being so intensely surveyed there are still some major gaps in our knowledge of the Northwest African margin, as most previous studies have focussed on the Madeira Abyssal Plain and the seafloor adjacent to the Canary Islands. There has been no analysis of the interaction of sedimentary processes operating across the entire margin, and relatively little work has been done on the turbidite depositional architecture east of the Madeira Abyssal Plain. In addition, the nature of channel-lobe transition zones on the margin is still poorly understood, and the mode of formation of the giant deep-water sediment waves first noted by Jacobi et al. (1975) has yet to be identified.

Two cruises undertaken in 1997 provided an excellent opportunity to collect data that would contribute towards a better understanding of the topics described above. RRS

Discovery cruise 225 provided giant piston cores from the intraslope Agadir Basin and high-resolution sidescan sonar data from the Agadir channel-lobe transition zone, and Charles Darwin cruise 108 provided high-resolution bathymetry and sidescan sonar data from sediment wave fields around the Canary Islands. These new data have been investigated during the last three years and the results are presented in this thesis.

1.2: Aims and objectives of this study

The principal aims of this study are as follows:

1) Produce a detailed map showing the sedimentary processes and deposits across the Northwest African continental margin. This will allow the distribution and interaction of sedimentary processes to be analysed, and will enable comparisons to be made with the rest of the Northeast Atlantic margin. In addition, the influence of complex seafloor topography on sedimentary processes will be investigated.

2) Investigate the Moroccan Turbidite System on the Northwest African margin. This will be achieved by combining new core data obtained during RRS Discovery Cruise 225 with previously published data. Correlation of turbidites between cores will be carried out, and a provenance study of basal turbidite sands should allow source areas to be identified. Controls on sand body dimensions and distributions will be assessed.

3) Investigate channel-lobe transition zones using new geophysical data obtained from the mouth of the Agadir and Lisbon Canyons during RRS Discovery Cruise 225. The new data will then be combined with previously published data in an attempt to create a new model for channel-lobe transition zones, and establish the controls on their development.

4) Investigate deep-water sediment waves in turbidite-dominated environments using new geophysical data obtained during RRS Charles Darwin Cruise 108. The existing models for sediment wave generation beneath turbidity currents are poorly understood, and an attempt will be made to update these models. In addition, the application of sediment wave studies to hydrocarbon exploration in deep-water turbidite systems will be examined.

1.3: Thesis layout

This thesis is presented as a series of seven papers, describing turbidity current processes and deposits on the Northwest African margin. Four of the papers are already published, two are under review, and one is in press.

The thesis opens with this introduction chapter (Chapter 1) which outlines the general theme of the project, and the specific aims of the thesis. Chapter 2 contains a description of the data and how they were collected. Chapter 3 describes the geology, seafloor morphology, oceanography and geological history of the study area. Chapters 4 to 10 contain the seven papers, and make up the bulk of the thesis. The papers represent the key areas of research undertaken during this project, and all papers are linked together by a short introduction and summary. Chapter 11 contains a detailed discussion of the key findings of the research, and attempts to put these results into a global context. Finally, the conclusions are presented in Chapter 12, followed by references and appendices.

The organisation of this thesis into a series of papers means that there will inevitably be some duplication, as each paper contains a section on data collection, study area etc. However, the references for each paper have been removed and all references cited within the thesis are contained in a single reference list at the end.

1.4: Statement on authorship

Papers 2-7 in the thesis have been written by myself as the first named author, with contributions from my three supervisors, Phil Weaver, Doug Masson and Dorrik Stow. In addition, Paper 4 contains a contribution from Dr Neil Kenyon (Southampton Oceanography Centre, UK) and Paper 6 contains a contribution from Dr Gemma Ercilla (CSIC, Spain).

The text of Paper 1 was written by Phil Weaver, myself and Neil Kenyon, and Jeremy Evans was involved in figure compilation. Although, I am not the first named author of this paper it was decided to include it within the thesis as 1) I was responsible for writing a significant proportion of the text, including most of the description of the Northwest African margin and 2) this paper is an excellent introductory paper for the

thesis, as it compares the processes and deposits of the Northwest African margin, with the rest of the Northeast Atlantic margin.

CHAPTER 2

METHODOLOGY AND DATABASE

2.1: Cruise information

The data presented in this thesis have been collected on a number of research cruises on board the RRS Discovery, RRS Charles Darwin, R/V Hesperides and R/V Gelendzhik. Many of these cruises were undertaken as part of the international STEAM (Sediment Transport on Eastern Atlantic Margins) project, which ran from July 1994 to July 1997. In particular, data collected during two recent cruises (in which I participated) have provided the bulk of the results displayed in this thesis:

1) Core data displayed in Chapters 5, 6, 9 and 10 were collected during Discovery Cruise 225 in February 1997. In addition, TOBI images and profiles in Chapter 7 were also collected during this cruise.

2) Shallow seismic profiles, multibeam bathymetry and TOBI data in Chapters 8 and 10 were collected during Charles Darwin Cruise 108 in September 1997.

2.2: Multibeam bathymetry

High-resolution multibeam bathymetry was collected using the hull-mounted Simrad EM12 multibeam echo sounder. The Simrad EM12 system operates at a frequency of 13kHz, and has a swath width of >2-2.5x water depth up to a maximum water depth of 11,000 m. The bathymetric data have been processed using GEOSEA modelling software, which produces high-resolution, grey-shaded, 3-D perspective images of the seafloor.

2.3: Side-scan sonar

Three side-scan sonar systems have been used in this study:

GLORIA (Geological Long-Range Inclined Asdic) is a 6.5kHz long-range side-scan sonar with a swath width of up to 10x water depth. It is towed near the surface at speeds

of up to 10 knots, allowing large areas of the seafloor to be mapped relatively quickly. A modified version of the GLORIA interpretation scheme given by Kidd et al. (1985) and Masson et al. (1992) is shown in Table 2.1.

TOBI (Towed Ocean Bottom Instrument) is a deep-towed, 30kHz, high-resolution side-scan sonar with a swath width of about 6 km (Murton et al., 1992). The TOBI system is towed at around 400 m above the seafloor at a speed of 1-2 knots. A sub-bottom profiler operating at 7kHz is also attached to the TOBI vehicle.

MAK-1 is also a deep-towed, 30kHz, high-resolution side-scan sonar, and has a swath width of 2 km. MAK-1 has been developed by Yuzhmorgeologiya of Russia. A sub-bottom profiler operating at 5kHz is attached to the MAK-1 vehicle.

2.4: Seismic profiles

Most of the seismic profiles used in this study are 3.5kHz-profiles (see Damuth, 1980 for an overview of 3.5kHz echo characters, and how they relate to seafloor deposits and processes). Echo-character definitions for the Northwest African margin, based on summaries in Jacobi and Hayes (1992), Masson et al. (1992) and Wynn et al. (2000, a), are shown in Table 2.1. In addition, ultra high-resolution seismic profiles have been obtained using the TOPAS (TOpographic Parametric Sonar) system. TOPAS is a hull-mounted seabed and sub-bottom echo-sounder, and provides a vertical resolution of <30-40 cm within the upper 50-80 m of the sediment column at any water depth (Webb, 1993; Dybedal and Boe, 1994). Single-channel seismic profiles have also been collected using a single 300 in^3 BOLT 1500c airgun.

2.5: Sediment cores

Core data used in this study include several piston cores up to 13 m long, and three kasten cores up to 2 m long. Piston cores have been logged with the multi-sensor core logger developed at Southampton Oceanography Centre (Best and Gunn, 1999), which records P-wave velocity (ms^{-1}), wet bulk density using gamma ray attenuation (gcc^{-1}), and magnetic susceptibility (SI) of the core sediments. Cores have also been logged visually, with particular attention paid to colour and grain size changes. A number of turbidites in the piston cores have had the basal sand fraction sampled for mineralogical

No.	Echo-character	Sidescan character	Core character	Location	Interpretation
		PELAGIC AND HEMIPELAGIC SEDIMENTATION			
1	Continuous, flat, subbottom reflectors, > 50 m penetration	Low to intermediate backscatter, featureless or vaguely mottled/lineated	*On slope/rise* - interbedded marls, oozes and clays *On abyssal plains* - interbedded f-g turbidites and marls, oozes and clays	Found across large areas of the continental slope, rise and abyssal plains	Flat-lying pelagic/hemipelagic drape on slope/rise OR f-g turbidites and pelagic/ hemipelagic sediments on abyssal plain
2	Irregular, undulating > 50 m penetration	Very low backscatter patches	Marls, clays and oozes	Flanks of volcanic seamounts	Pelagic drape on seamounts
		BOTTOM CURRENT FEATURES AND DEPOSITS			
3	Very regular, overlapping hyperbolae, tangent to seafloor			Parallel to bathymetric contours, around seamounts	Erosional furrows
4	Regular, undulating, may show marked asymmetry. > 50 m penetration	Distinct, regular bands of low to intermediate backscatter	Interbedded fine-grained silts, clays, marls and oozes	Parallel to bathymetric contours, on continental rise and around seamounts	Bottom current sediment waves
		GRAVITY-FLOW FEATURES AND DEPOSITS			
5	Rough seabed with abundant large hyperbolae	Variable backscatter. Irregular, blocky texture		On, or adjacent to, slopes of volcanic islands	Debris avalanche deposits
6	Large hyperbolae with vertex elevation decreasing downslope. Rare subbottom reflectors			Continental slope/rise, slope and base of seamounts amd volcanic islands	Submarine slide deposits. Deposits grade from 'hummocky' near slide-scar to 'blocky' downslope
7	Prolonged echo with no penetration. Small-scale rough seabed with many hyperbolae	High backscatter, strongly lineated perpendicular to slope	Buried slide-scars show hiatus in sequence	Continental slope, slopes of volcanic islands and seamounts	Sediment-slide scars
8	Acoustically transparent, lens-shaped units with prolonged echo. Onlaps other facies	High backscatter lobate sheets, lineated with well-defined boundaries	Variable. Blocky unsorted material in f-g matrix OR deformed but coherent blocks of original sed sequence	Slope/rise and on slopes of volcanic islands and seamounts	Debris-flow deposits
9	Parallel-bedded with 10-30 m irregular penetration	Intermediate backscatter, lineated with variable backscatter lineations	Interbedded f-g turbidites and clays, marls, oozes. Low sand/shale ratio	Slope and rise, generally perpendicular to bathymetric contours	Turbidity current pathways and channel overbank deposits
10	Topographic lows on profiles, often with decreased penetration	Straight or curved narrow lineaments. High backscatter, or high with low central stripe	Interbedded c-g turbidites and clays, marls, oozes. High sand/shale ratio	Slope and rise, generally perpendicular to bathymetric contours	Turbidity current channels
11	Regular, undulating, often with marked asymmetry. penetration increases downslope, from < 10-> 50 m	Distinct, regular bands of low to intermediate backscatter. Spacing between bands decreases downslope.	Turbidites, interbedded with marls, clays and oozes	Slopes of volcanic islands and seamounts, levee backslopes, channel floors. Parallel to slope contours	Turbidity current sediment waves
		OTHER FEATURES AND DEPOSITS			
12	Sharp to prolonged echo with no penetration. Large-scale rough seabed with large hyperbolae	Very high backscatter, linear to irregular patches		Seamounts and volcanic island slopes. Canyon walls	Basement rock outcrop

Table 2.1: Character, location and interpretation of morphological features and sedimentary deposits on the Northwest African margin. Modified from Masson et al. (1992) and Jacobi and Hayes (1992).

analysis, and the upper mud fraction for coccolith analysis. These techniques are covered in more detail in Chapter 9. A description of the typical core sediment character for a variety of environments is shown in Table 2.1.

2.6: Other data

Bathymetric data used in the construction of location maps, and also the sedimentation maps in Chapters 4 and 5, were provided by the GEBCO Digital Atlas. (British Oceanographic Data Centre, 1995).

CHAPTER 3

REGIONAL SETTING

3.1: Study area: the Northwest African margin

The study area comprises the whole of the Northwest African margin, which runs from Cape Verde (15°N) in the south, to the Straits of Gibraltar (36°N) in the north (Figure 3.1). For the purposes of this study the margin is taken to include the shelf, slope, rise and abyssal plains. The study area is bounded to the east by the African coastlines of Senegal, Mauritania, Western Sahara and Morocco, and to the west by the lower flanks of the mid-Atlantic Ridge. Along its length, the margin is punctuated by the Canary, Madeira and Cape Verde archipelagos, as well as numerous volcanic seamounts and salt diapirs.

3.2: The volcanic Canary Islands

The volcanic Canary archipelago is the largest island group in the study area, and is made up of seven major islands. Three of the islands are over 2000 m high, with a maximum relief of nearly 3800 m on Pico de Teide, Tenerife. This giant volcano is the third largest oceanic volcano on earth, after Mauna Kea and Mauna Loa on Hawaii (Schmincke, 1982). The island chain is oriented roughly east-west, and extends for almost 500 km (Figure 3.1). The islands are located on Jurassic-age oceanic crust and are believed to have formed when the African plate moved over a mantle hotspot. Volcanism has largely occurred in the last 20 Ma, and the islands show an overall decrease in age to the west (Schmincke, 1982). The Canary Islands have had a major effect on seafloor processes within the study area, as they act as a nucleus for downslope gravity flows, and as a barrier to alongslope bottom currents.

3.3: Onshore geology

The Northwest African margin is a mature passive margin, which has evolved since the initial mid-Atlantic rifting in the late Triassic (Seibold, 1982). The onshore geology of the margin is dominated by three Mesozoic-Cenozoic sedimentary basins separated by Precambrian highs (Figure 3.2). The Atlas or Essaouira-Agadir Basin has the Moroccan

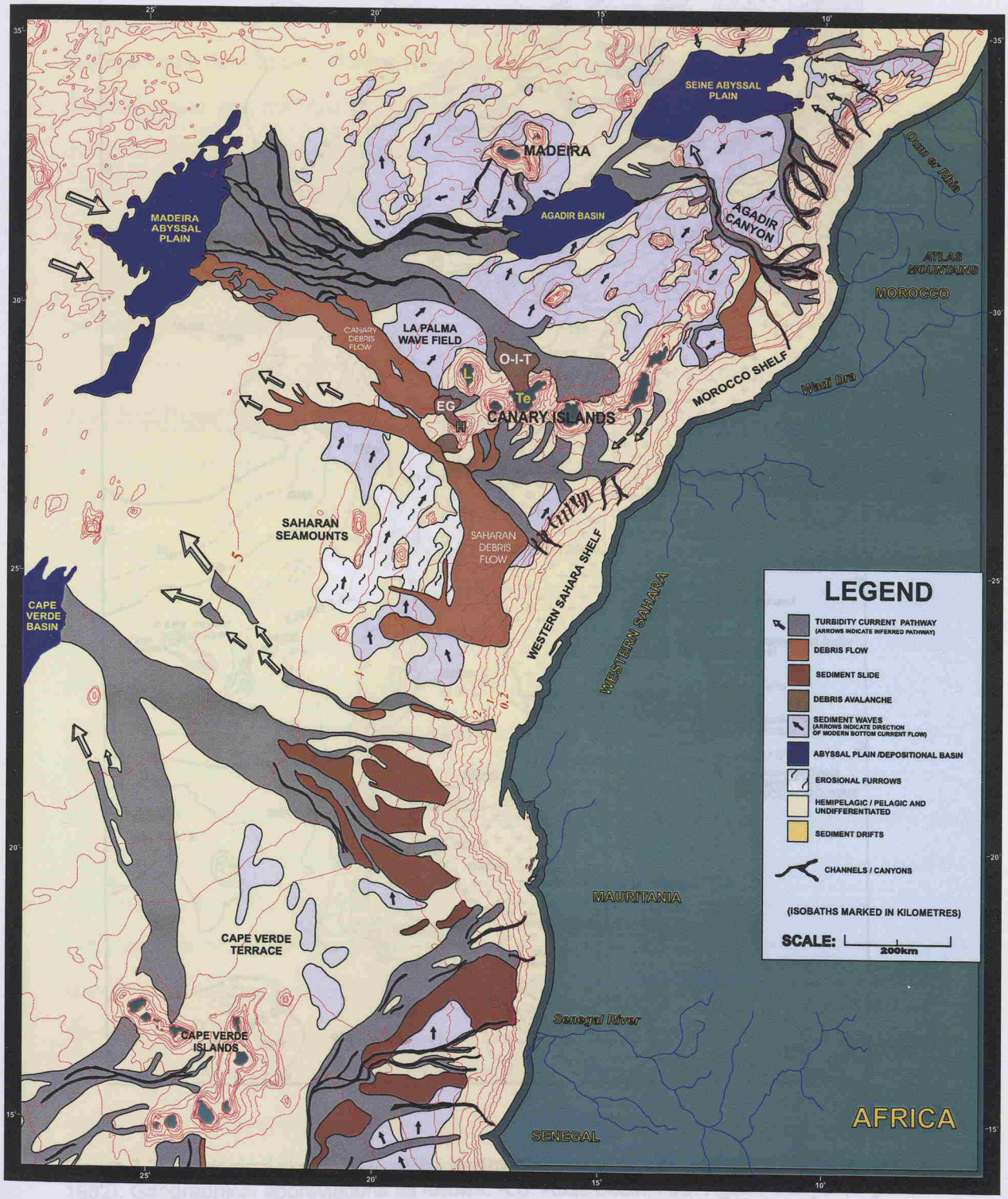

Figure 3.1: Map showing the location of the study area on the Northwest African margin, and the distribution of sedimentary features described in the thesis. A large-scale, full colour version of this map is presented in Foldout 1.

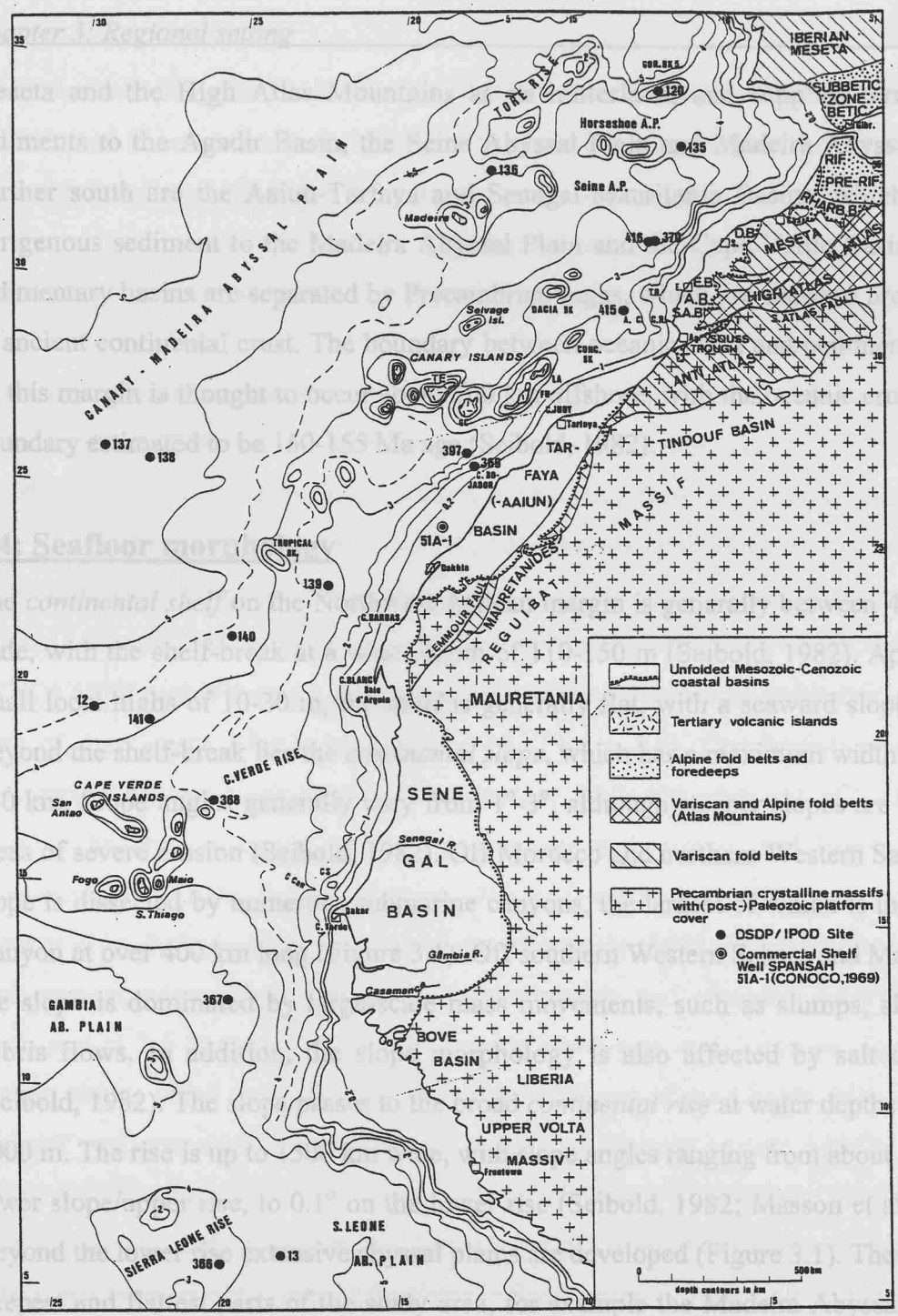

Figure 3.2: Geological sketch map of the Northwest African margin (modified from Seibold, 1982). Geographical abbreviations as follows: A.B. Atlas Basin; A.C. Agadir Canyon; Ag. Agadir; A.T.B. Aaiun-Tarfaya Basin; Cas. Casablanca; C.Can. Cayar Canyon; Conc. Bk. Conception Bank; C.R. Cap Rhir; C.S. Cayar Seamount; D.B. Doukkala Basin; E. Essaouira; E.B. Essaouira Basin; Fu. Fuerteventura; G.C. Gran Canaria; Gibr. Gibraltar; Gor. Bk. Gorringe Bank; S.A.B. South Atlas Basin; La. Lanzarote; M.P. Mazagan Plateau; S. Safi; T. Tizi n'Test Fault; Te. Tenerife; T.P. Tafelny Plateau.

Meseta and the High Atlas Mountains as its hinterland, and supplies terrigenous sediments to the Agadir Basin, the Seine Abyssal Plain and Madeira Abyssal Plain. Further south are the Aaiun-Tarfaya and Senegal-Mauritania Basins, which supply terrigenous sediment to the Madeira Abyssal Plain and the Cape Verde Basin. These sedimentary basins are separated by Precambrian highs, which are seaward protrusions of ancient continental crust. The boundary between oceanic crust and continental crust on this margin is thought to occur about 500 km offshore, with the oceanic crust at this boundary estimated to be 150-155 Ma age (Seibold, 1982).

3.4: Seafloor morphology

The *continental shelf* on the Northwest African margin is generally between 40-60 km wide, with the shelf-break at a water depth of 110-150 m (Seibold, 1982). Apart from small local highs of 10-30 m, the shelf is generally flat, with a seaward slope of $<1^{\circ}$. Beyond the shelf-break lies the *continental slope*, which has a maximum width of about 250 km. Slope angles generally vary from 1°-3°, although steeper slopes are found in areas of severe erosion (Seibold, 1982). Off Morocco and northern Western Sahara, the slope is dissected by numerous submarine canyons, the largest of which is the Agadir Canyon at over 400 km long (Figure 3.1). Off southern Western Sahara and Mauritania, the slope is dominated by large-scale mass movements, such as slumps, slides and debris flows. In addition, the slope morphology is also affected by salt diapirism (Seibold, 1982). The slope passes to the broad *continental rise* at water depths of 1500-4000 m. The rise is up to 1500 km wide, with slope angles ranging from about 1° on the lower slope/upper rise, to 0.1° on the lower rise (Seibold, 1982; Masson et al., 1992). Beyond the lower rise extensive abyssal plains are developed (Figure 3.1). These are the deepest and flattest parts of the study area, for example the Madeira Abyssal Plain is about 5400 m deep and has a slope of less than 0.01° (Searle, 1987). Surface relief is generally less than 10 m, apart from scarce abyssal hills up to 1000 m high.

3.5: Oceanography

The oceanic surface water circulation on the Northwest African margin is largely controlled by surface winds. The sluggish, wide and shallow (<100 m) Canary Current sweeps across the entire margin, and is driven by the north-easterly Trade Winds (Sarnthein et al., 1982). At 15°N the Canary Current divides, with most of the current

driven westwards by the Trade Winds to form the westward-flowing North Equatorial Current, and the remainder continuing south along the coast (Figure 3.3). This simple pattern is locally modified by upwelling around oceanic islands, variations in shelf morphology and the position of the shelf-break, and the influence of seasonal local winds (Schemainda et al., 1975).

A number of different bottom currents flow along the Northwest African margin at water depths of <2000 m, and these are summarised by Sarnthein et al. (1982). At water depths >2000 m there are two main bottom currents that flow along the lower slope and rise. North Atlantic Deep Water (NADW) has been poorly studied, but is believed to flow southwards between 2000-3800 m and is rather unstructured (Sarnthein et al, 1982). Antarctic Bottom Water (AABW) flows northwards below the NADW up to 35°N. AABW passes through, and west of, the Saharan Seamounts and is then deflected west of the Canary Islands before splitting (Figure 3.4). One branch of the flow continues north-east along the Moroccan margin, while the other curves back around Madeira before continuing northwards (Jacobi, Rabinowitz and Embley, 1975; Lonsdale, 1978; 1982; Sarnthein et al., 1982). Generally, NADW and AABW are thought to be fairly weak at the present-day. Lonsdale (1978; 1982) conducted short-term current measurements on the Moroccan margin and recorded AABW flowing north-east at 3-6 cm/sec and NADW flowing south-east at 1-2 cm/sec. In addition, bottom photos taken from the slope and rise north-east of the Canary Islands show a tranquil seafloor, with no evidence of significant bottom current activity (Jacobi, Rabinowitz and Embley, 1975; Embley, 1976). However, in places the bottom current flow can be affected by topographic forcing; for example, AABW flowing at up to 18 cm/sec has been recorded around the Saharan Seamounts (Lonsdale 1978; 1982).

Coastal upwelling occurs off Northwest Africa throughout the year between 20°N and 25°N. During the summer months the upwelling zone extends northwards to the Iberian margin, and in winter southwards to the Sierra Leone margin. In contrast to the Southwest African margin, only a small fraction of the high organic input from surface waters reaches the sediment, with slope and rise sediments containing 0.3-4% organic carbon (Seibold, 1982).

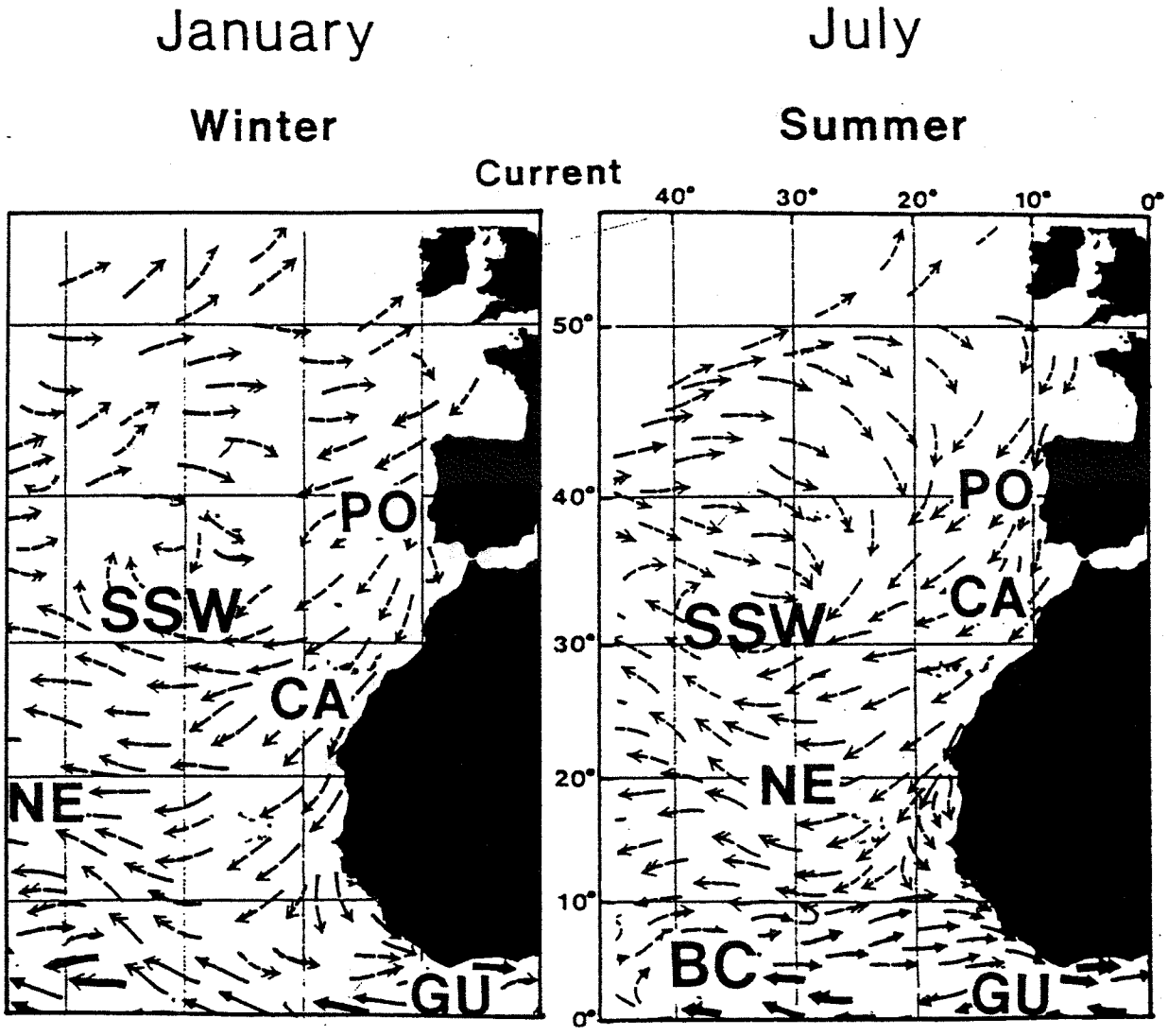

Figure 3.3: Surface water currents off Northwest Africa. Abbreviations as follows: PO = Portugal Current; CA = Canary Current; GU = Guinea Current; NE = North-Equatorial Current; SSW = Sargasso Sea Water; BC = Benguela Current.

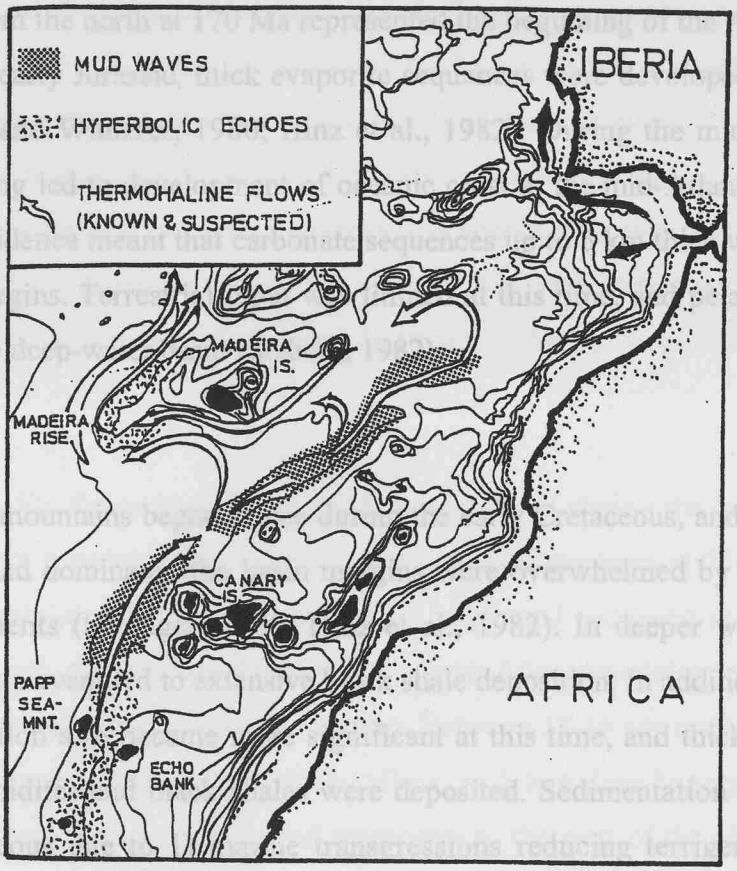

Figure 3.4: Deep-water bottom current flow off Northwest Africa, as inferred from the distribution of current induced bedforms and current meter results. Unfilled arrows = AABW (Antarctic Bottom Water). Filled arrows = MOW (Mediterranean Outflow Water) (modified from Lonsdale, 1978).

3.6: Geological history of the Northwest African margin

Triassic-Jurassic

Initial rifting between the continents of Africa and America occurred in the late Triassic, with the first marine evaporites appearing at this time (Seibold, 1982). A marine transgression from the north at 170 Ma represented the beginning of the Atlantic Ocean and, during the early Jurassic, thick evaporite sequences were developed (Bhat et al., 1975; Lancelot and Winterer, 1980; Hinz et al., 1982). During the mid-late Jurassic seafloor spreading led to development of oceanic crust at the mid-Atlantic Ridge, and rapid basin subsidence meant that carbonate sequences up to 5 km thick were deposited at the ocean margins. Terrestrial input was limited at this time, and pelagic sediments dominated in the deep-water basin (Seibold, 1982).

Cretaceous

The High Atlas mountains began to rise during the early Cretaceous, and the carbonate platforms that had dominated the basin margins were overwhelmed by fluvial deltaic and shelf sediments (Schlager, 1980; Hinz et al., 1982). In deeper water, the mid-Cretaceous anoxic event led to extensive black shale deposition. In addition, deep-water turbidite deposition also became more significant at this time, and thick sequences of interbedded turbidites and black shales were deposited. Sedimentation slowed during the late Cretaceous due to 1) marine transgressions reducing terrigenous input, 2) shallowing of the CCD leading to carbonate dissolution and 3) increased bottom current activity causing sediment erosion/non-deposition (Seibold, 1982). Off Morocco, mass movements became more frequent in response to the emergence of the western High Atlas Mountains, and salt diapirism was widespread (Lancelot and Winterer, 1980; Hinz et al., 1982).

Cenozoic

On the Northwest African margin, submarine erosion was the dominant process operating from the Palaeocene to the Oligocene. In particular, a major sea-level fall in the Oligocene (Vail et al., 1977) led to more frequent mass movements, and an increase in turbidity current and bottom current erosion of the margin. In the Miocene the volcanic Canary Islands and Cape Verde Islands began to form, and volcaniclastic sediments were deposited in adjacent deep-water basins (Schmincke, 1982). Turbidity

currents and bottom currents were diverted around these new obstacles, leading to considerable changes in the pattern of sedimentation.

Investigations undertaken by the Ocean Drilling Program on the Madeira Abyssal Plain (MAP) have revealed that turbidites deposited on the plain since the mid-Miocene are sourced from three main areas: the north-west African margin, the volcanic Canary Islands, and seamounts to the west of the plain (Weaver et al., 1998). Detailed geochemical and micropalaeontological studies of the turbidite sequence on the MAP indicates major changes in turbidite frequency and source area over time. This form of basin analysis is a particularly useful method for understanding variations in terrigenous-to-marine sediment flux on the Northwest African margin over a long time period.

Significant turbidite deposition on the MAP was initiated during the mid-Miocene at about 17 Ma. This may have been a result of the lowered sea level at this time, leading to sediment instability on the outer shelf/upper slope and increased turbidity current activity. In addition, the continued uplift of the High Atlas mountains led to high rates of terrigenous sediment output onto the margin. Between 17-16 Ma turbidite deposition on the MAP was confined to fracture zone valleys, with turbidites largely being derived from the north-west African margin and seamounts to the west of the plain. By 16 Ma these valleys were almost full, and some turbidites derived from seamounts to the west were deposited across most of the MAP. Between 16 and 13 Ma organic-rich flows from the Northwest African margin increased in volume and were also deposited across a larger area. Turbidite frequency was highest at this time, with organic turbidites deposited at a rate of up to 100 flows/m.y. After 13 Ma, most turbidites can be correlated across the whole plain, indicating that the fracture zone valleys had become infilled and/or flow volumes were increasing. Between 13-6.5 Ma turbidite frequency decreased, with organic turbidites reduced to <4 flows/m.y from 6.5-7 Ma. However, at 6.5 Ma organic turbidite frequency increased again, and remained at a high level through to the present-day. In addition, volcanic and calcareous turbidites became more frequent at this time, and were also deposited at a high frequency through to the present-day (Weaver et al., 1998).

CHAPTER 4

CONTINENTAL MARGIN SEDIMENTATION

4.1: Introduction and aims

Continental margins are host to a wide variety of sedimentary processes that are controlled by factors such as climate, bottom current regime and margin morphology. On the Northeast Atlantic margin the construction of sedimentation maps for large areas, e.g. sections of the Northwest African margin (Jacobi and Hayes, 1984; 1992; Masson et al., 1992), has given us a greater understanding of the link between sedimentary processes and their driving forces. However, no attempt has yet been made to map the whole Northeast Atlantic margin, in order to look at large-scale variations in seafloor processes at different latitudes.

This chapter therefore contains the following paper, entitled 'Continental margin sedimentation with special reference to the Northeast Atlantic margin'. The principal aim of this paper is to present a new map of seafloor sedimentary features across the whole Northeast Atlantic margin, from Northwest Africa, to northern Norway. This will allow detailed analysis of the sedimentary processes and interactions at varying latitudes, and enable large-scale, process-based subdivision of the margin.

4.2: Paper 1

Continental margin sedimentation, with special reference to the Northeast Atlantic margin

Philip P E Weaver, Russell B Wynn, Neil H Kenyon and Jeremy M Evans

SOES/Challenger Division, Southampton Oceanography Centre, European Way, Southampton, SO14 3ZH, UK

This paper was submitted to Sedimentology in October 1999. It was reviewed by David Piper, William Morris and Ian Jarvis, and was accepted for publication in November 1999. It was published in the Sedimentology 'Millenium Reviews Special Issue' in March 2000, v.47 (Supplement 1), p.239-256.

Abstract

The Northeast Atlantic continental margin displays a wide range of sediment transport systems with both alongslope and downslope processes. Off most of the Northwest African margin, south of 26°N, upwelling produces elevated accumulation rates, though there is little fluvial input. This area is subject to infrequent but large-scale mass movements, giving rise to debris flows and turbidity currents. The latter traverse the slope and deposit thick layers on the abyssal plains, whilst debris flows deposit on the continental slope and rise. From the Atlas Mountains northwards to 56°N the margin is less prone to mass movements, but is cut by a large number of canyons, which also funnel turbidity currents to the abyssal plains. The presence of a lithospheric plate boundary off Southwest Iberia is believed to have led to high rates of sediment transport to the deep sea. Even larger quantities of coarse sediments have fed the canyons and abyssal plains in the Bay of Biscay as a result of drainage from melting ice sheets. Bottom currents have built sediment waves off the Northwest African and Iberian margins, and created erosional furrows south of the Canary Islands. The Mediterranean outflow is a particularly strong bottom current near the Straits of Gibraltar, depositing sediment waves in the Gulf of Cadiz. North of 56°N the margin is heavily influenced by glacial and glaciomarine processes active during glacial times, which built glacial trough-mouth fans such as the North Sea Fan, and left iceberg scour marks on the upper slope and shelf. Over a long period, especially during interglacials, this part of the margin has been greatly influenced by alongslope currents, with less influence by turbidity currents than on the lower latitude margins. Mass movements are again a prominent feature, particularly off Norway and the Faeroe Islands. Some of these mass movements have occurred during the Holocene, although high glacial sedimentation rates may have contributed to the instability.

Introduction

In this paper we describe the sedimentary processes, and map the major sedimentary features, on the Northeast Atlantic continental margin from Northwest Africa to northern Norway (Figure 4.1, see foldout 1). This region includes areas of passive margin with low sediment input, areas with high glacial sedimentation, areas incised by canyons, areas of fan sedimentation, areas with low gradient continental slopes, and areas with steep continental slopes.

Continental margins are important areas for investigation since they form a 'new frontier' for exploitation by the hydrocarbons industry, and increasing numbers of telecommunication cables are laid across them. Nevertheless, many of the sedimentary processes displayed here remain poorly understood. Major advances in our knowledge of continental margins have followed the development and deployment of long-range side-scan sonars such as GLORIA, which can image large areas in relatively short time intervals. Further advances have been achieved following the development of much higher resolution deep-towed side-scan, and of swath bathymetry. There has been some ocean drilling of passive continental margins by DSDP and ODP, especially of modern fans (Legs 96, 116, 155), sediment drifts (e.g. Legs 94, 172, 181), and abyssal plains (Legs 149, 157). Downslope processes have not been specifically targeted except in Legs 150 and 174A, both on the New Jersey margin, where a downslope transect of cores was drilled.

In this paper we have limited our discussion to sedimentary processes operating from the shelf edge to the abyssal plain, thus including the continental slope, continental rise and abyssal plain. In all cases it is important to include the sediments of the abyssal plains as part of the continental margin, since the plains are formed by sediments derived from the margin. Within this area the dominant sedimentary processes are alongslope sediment transport, which builds sediment drifts and waves, and downslope processes involving mass wasting (sediment slides, debris flows and turbidity currents). In addition, canyons can be incised into the slope, in some cases cutting across the shelf, and large submarine fans may be built off major points of sediment supply. The scale of some of the processes can be very large, for example, the Storegga slide off Norway has an estimated volume of 5700 km^3 (Bugge et al., 1988), whilst a single turbidite in the Madeira Abyssal Plain has a volume in excess of 250 km^3 (Weaver et al., 1992, 1995).

Main sedimentary processes

Submarine slides and debris flows

Sediment instability resulting in submarine slides and debris flows is very common on some continental margins and single events are frequently very large (in the order of hundreds of km^3). Should failure occur, the ocean floor offers unimpeded slopes and flat-floored basins hundreds of kilometres in length, allowing flow over enormous distances. Slides are defined as the downward and outward movement of slope forming

materials, wherein shear failure occurs along one or several surfaces (see Hampton et al., 1996 for a thorough review). Many submarine slides disintegrate downslope into debris flows, which are described as the movement of granular solids, sometimes mixed with minor amounts of entrained water on a low slope. The typical end product is a mass of displaced blocks of sediment or rock embedded in a more highly disrupted matrix. Debris avalanches are used here to describe submarine slides where little or no water entrainment occurs, and the resulting run-out distances are less. High-latitude slopes commonly consist of stacked debris flows (Vorren et al., 1998). Such flows have been studied in the field and experimentally (e.g. Mohrig et al., 1999), and are believed to flow on a lubricating layer of water between the debris flow and the underlying material, a process referred to as hydroplaning.

Turbidity currents

Turbidity currents occur on a variety of scales, and are a common feature of many continental margins. The largest turbidity currents form deposits in the deep ocean that are termed megaturbidites, and are often linked to mass movements occurring higher up the slope. These currents transport tens to hundreds of cubic kilometres of sediment, and appear to be able to travel immense distances over extremely low gradient slopes. They dump their sediment load only when they become ponded on the flat abyssal plains at the base of the slope. Individual mud-dominated turbidites commonly form layers up to a few metres in thickness over the whole abyssal plain (Pilkey, 1987; Rothwell et al., 1992).

On the continental slope and rise, turbidity currents are usually funnelled downslope by canyons and channels. Canyons are generally V-shaped in profile and are often eroded into bedrock. In plan view they display tributary canyon systems with a number of orders of tributary, including steep, gullied slopes. They may originate offshore of a sediment point source such as a river, and generally occur on, or just seaward of the shelf-break. Canyons commonly pass downslope into channels, which are shallower than canyons, more U-shaped in profile, and may have depositional elements such as levees and aggradational floors. Deep-water channels occur in a variety of forms, from deep, narrow erosive channels to broad, shallow distributary channels. Meandering channels tend to occur on fans with gentle gradients and a dominantly fine-grained

sediment supply (e.g. Clark et al., 1992). Both canyon and channel floors can have bedforms such as sediment waves and erosional scours.

Turbidity currents generally deposit the majority of their load on turbidite fans. The rivers running into the Northeast Atlantic are relatively small and the resultant fans are usually built near the foot of the slope, beyond the canyon mouths.

Bottom currents

Bottom currents often play a major role in continental margin sedimentation. They can erode, mould, transport and redistribute sediments supplied to the slope and rise by downslope flows and vertical settling. Bottom current features include erosional furrows and moats, and depositional bedforms such as contourite drifts and sediment waves.

Contourite drifts are the primary deposits of bottom currents, and are widespread throughout the World Ocean. Contourite drifts occur on a variety of scales, from small patch drifts (<100 km^2) to giant elongate drifts (>100,000 km^2). Controls on contourite accumulation include: (1) active geostrophic circulation - this varies through time, for example, bottom currents are generally more active during interglacials and therefore contourite deposition is increased during these periods, (2) sea-floor topography - this can influence bottom current flow velocity, leading to sediment erosion or deposition in certain areas, (3) sediment supply - many contourite deposits actually derive the majority of their sediment from turbidite systems, as turbidity currents are one of the main mechanisms for sediment to be transported to the slope, rise and basins, (4) nepheloid layer turbidity - this also affects the ability of bottom currents to deposit or erode sediment (Faugeres et al., 1993).

Process interaction on the Northeast Atlantic margin

The non-glaciated margin south of 26°N (mass-wasting processes dominant)

Downslope processes

The passive continental margin off Northwest Africa, between 15° and 26°N, is dominated by mass wasting processes (submarine slides, debris flows and turbidity currents) (Figure 4.2c). This is due to a number of factors, including low terrigenous input and local upwelling. This part of the margin receives very little fluvial sediment, particularly the margin off Western Sahara. However, a number of upwelling cells

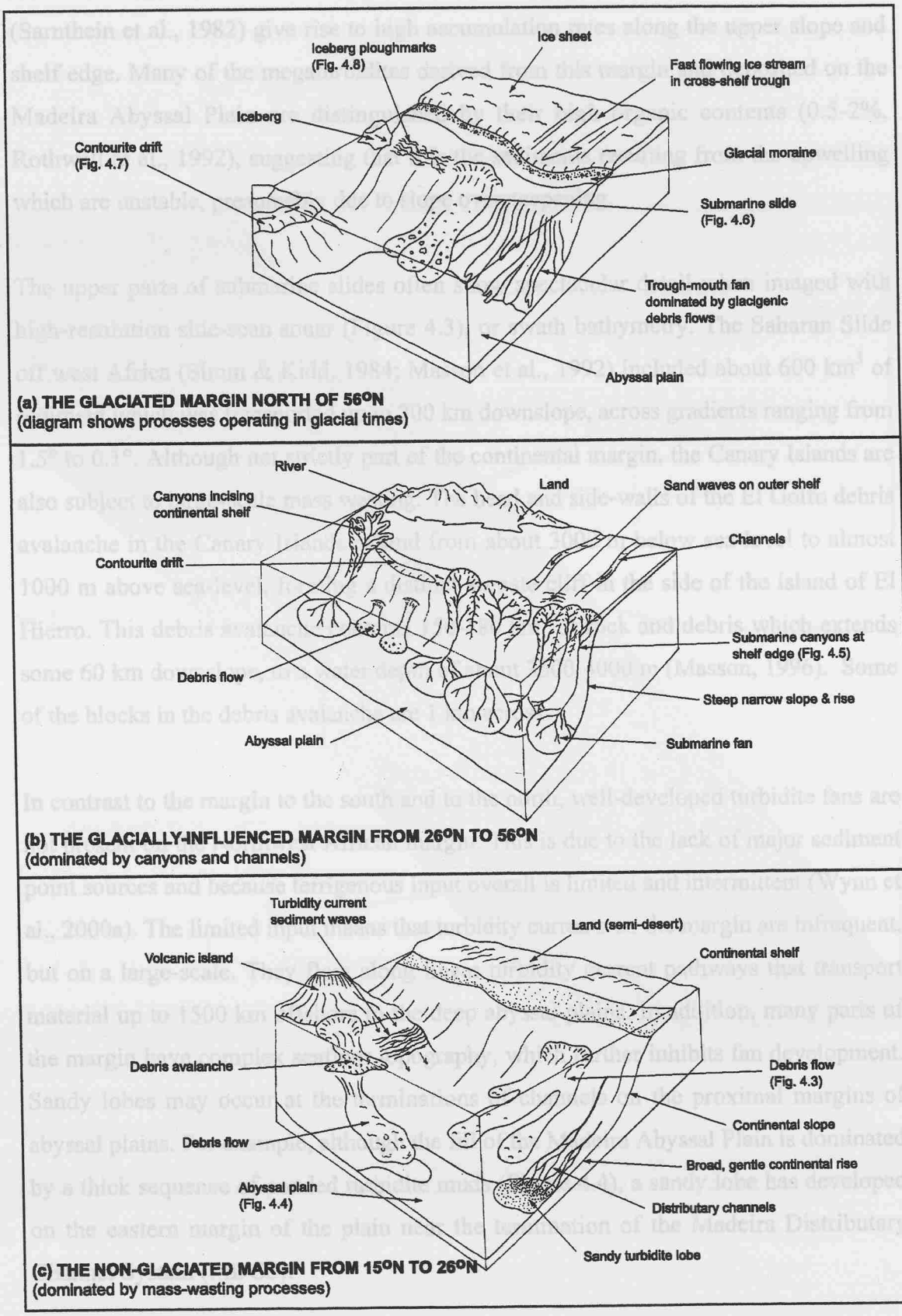

Figure 4.2: Schematic diagrams showing the idealised sedimentary features on (a) the glaciated margin north of 56°N, (b) the glacially influenced margin from 26°N to 56°N, and (c) the non-glaciated margin from 15°N to 26°N.

(Sarnthein et al., 1982) give rise to high accumulation rates along the upper slope and shelf edge. Many of the megaturbidites derived from this margin and deposited on the Madeira Abyssal Plain are distinguished by their high organic contents (0.5-2%, Rothwell at al., 1992), suggesting that it is the sediments resulting from the upwelling which are unstable, presumably due to slope oversteepening.

The upper parts of submarine slides often show spectacular detail when imaged with high-resolution side-scan sonar (Figure 4.3), or swath bathymetry. The Saharan Slide off west Africa (Simm & Kidd, 1984; Masson et al., 1992) included about 600 km^3 of sediment which was transported up to 700 km downslope, across gradients ranging from 1.5° to 0.1°. Although not strictly part of the continental margin, the Canary Islands are also subject to large-scale mass wasting. The head and side-walls of the El Golfo debris avalanche in the Canary Islands extend from about 3000 m below sea-level to almost 1000 m above sea-level, forming a distinct arcuate cliff in the side of the island of El Hierro. This debris avalanche contains 150-180 km^3 of rock and debris which extends some 60 km downslope, to a water depth of about 3500-4000 m (Masson, 1996). Some of the blocks in the debris avalanche are 1 km across.

In contrast to the margin to the south and to the north, well-developed turbidite fans are not present on the Northwest African margin. This is due to the lack of major sediment point sources and because terrigenous input overall is limited and intermittent (Wynn et al., 2000a). The limited input means that turbidity currents on the margin are infrequent, but on a large-scale. They flow along linear turbidity current pathways that transport material up to 1500 km offshore to the deep abyssal plains. In addition, many parts of the margin have complex seafloor topography, which further inhibits fan development. Sandy lobes may occur at the terminations of channels on the proximal margins of abyssal plains. For example, although the fill of the Madeira Abyssal Plain is dominated by a thick sequence of ponded turbidite muds (Figure 4.4), a sandy lobe has developed on the eastern margin of the plain near the termination of the Madeira Distributary Channel System (MDCS).

The MDCS is the best-developed distributary channel network on the Northwest African margin and is some 500 km long. It extends from the western edge of the intraslope Agadir Basin to the eastern edge of the Madeira Abyssal Plain, and occurs on

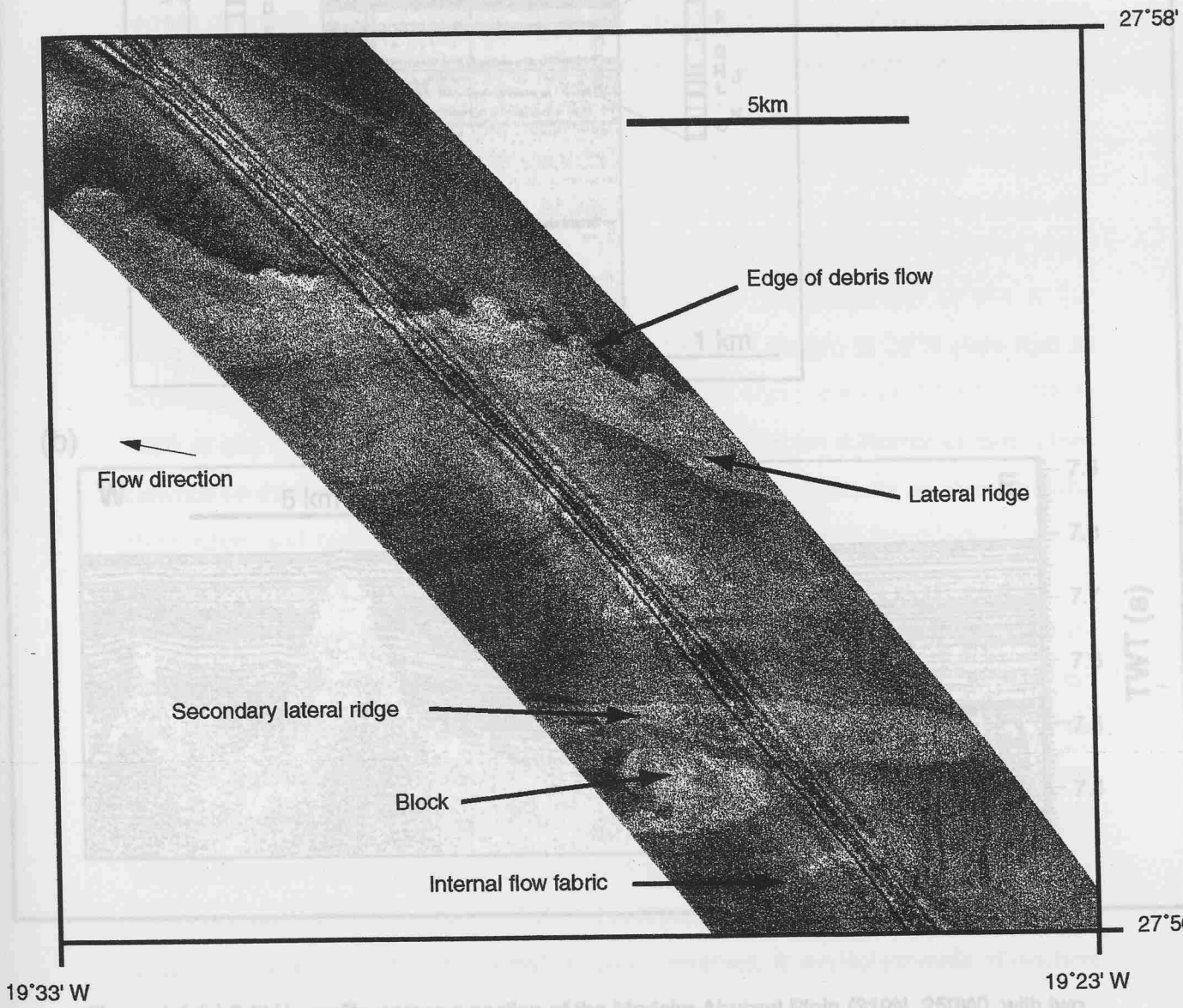

Figure 4.3: TOBI sidescan sonar image showing the edge of the Saharan debris flow, west of the relatively starved Northwest African margin. High levels of backscatter are shown as light tones. For location see Figure 4.1.

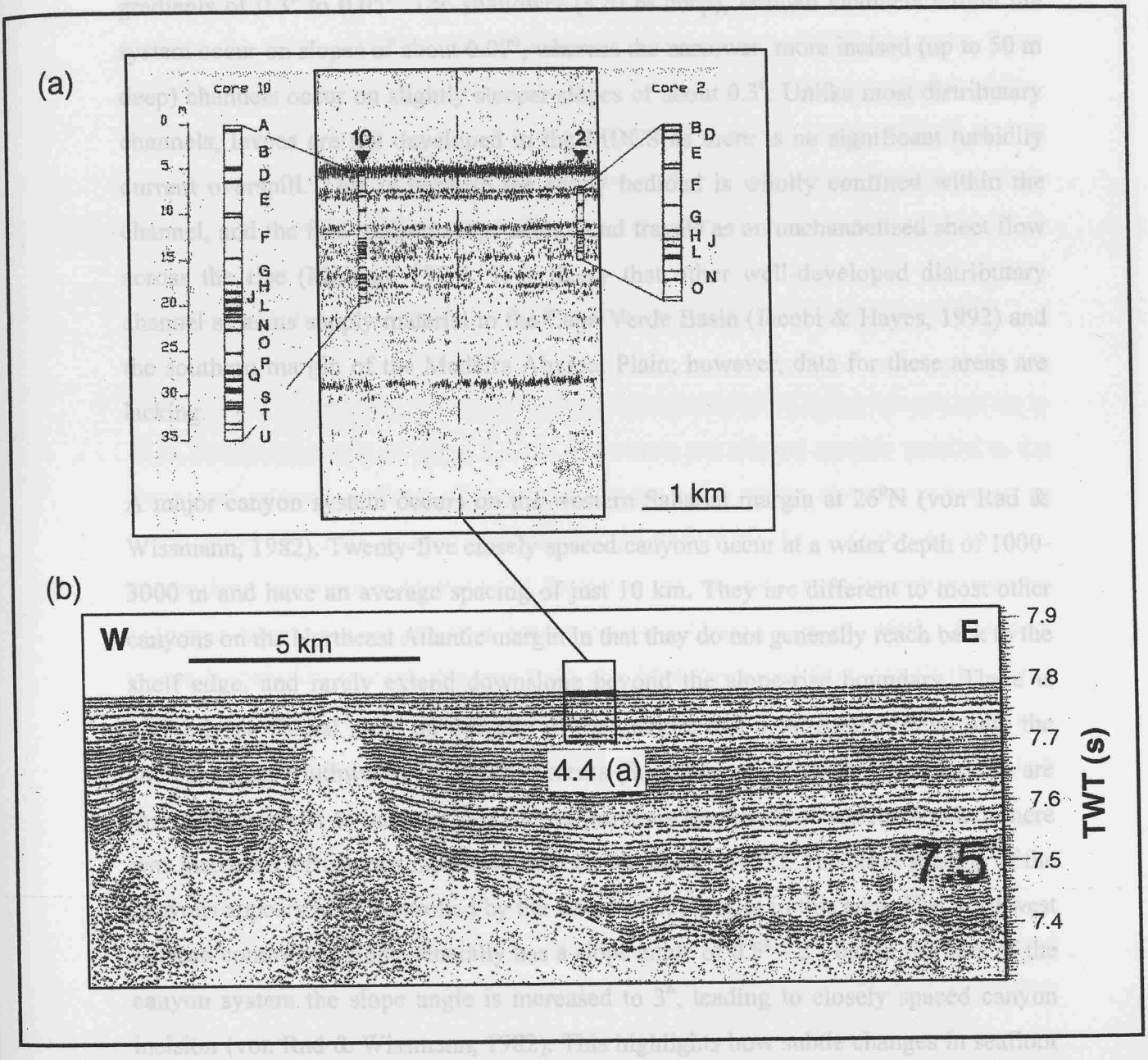

Figure 4.4 (a) 3.5kHz profile across a section of the Madeira Abyssal Plain (31ºN, 25ºW), with two cores showing how the turbidite sequence can be roughly correlated with seismic reflectors. The lettering scheme on the two cores represents individual turbidites as defined by Weaver et al. (1992). (b) Airgun seismic profile of ponded turbidites from the Madeira Abyssal Plain. Boxed area represents the high resolution profile shown in (a). For location see Figure 4.1.

gradients of 0.3° to 0.05°. The shallower (<20 m deep), braided channels within the system occur on slopes of about 0.07°, whereas the narrower, more incised (up to 50 m deep) channels occur on slightly steeper slopes of about 0.3°. Unlike most distributary channels, levees are not developed in the MDCS as there is no significant turbidity current overspill. This is because the sandy bedload is wholly confined within the channel, and the fine-grained suspension cloud travels as an unchannelised sheet flow across the rise (Masson, 1994). It is likely that other well-developed distributary channel systems supply material to the Cape Verde Basin (Jacobi & Hayes, 1992) and the southern margin of the Madeira Abyssal Plain; however, data for these areas are lacking.

A major canyon system occurs on the western Saharan margin at 26°N (von Rad & Wissmann, 1982). Twenty-five closely spaced canyons occur at a water depth of 1000-3000 m and have an average spacing of just 10 km. They are different to most other canyons on the Northeast Atlantic margin in that they do not generally reach back to the shelf edge, and rarely extend downslope beyond the slope-rise boundary. There is currently no fluvial input on this part of the margin, and most aeolian input onto the shelf is swept southwards by strong currents (Sarnthein et al., 1982). The canyons are therefore believed to have formed during previous lowstands of sea level, when there was increased terrigenous input (von Rad & Wissmann, 1982). The close spacing of the canyons appears to be controlled by the steeper slope angles in this area. The Northwest African continental slope generally has a slope angle of 0.5° - 2°, but in the area of the canyon system the slope angle is increased to 3°, leading to closely spaced canyon incision (von Rad & Wissmann, 1982). This highlights how subtle changes in seafloor gradients can have a dramatic control on slope processes. A similar example of gradient control on canyon formation is found in the Porcupine Seabight (Kenyon, 1987).

Recent investigations on the lower slope and rise north-west of the Canary Islands have revealed that fields of sediment waves on open slopes may be generated by unconfined turbidity currents (Wynn et al., 2000b). Sediment waves can also be generated by bottom currents, but a number of criteria can be used to distinguish the two types: (1) Turbidity current sediment waves typically show a regular downslope decrease in dimensions, bottom current waves are generally more irregular; (2) Turbidity current wave crestlines are aligned roughly parallel to the slope, and are often sinuous and

bifurcating; bottom current wave crestlines on slopes are generally developed at an angle to the slope, and are more uniform, (3) Core studies of different wave types typically reveal evidence of turbidity current deposition or bottom current deposition, (4) Bottom current sediment waves only form beneath bottom currents of 9-50 cm/sec (e.g. Flood, 1988); they do not occur in areas with weak or absent bottom currents (although the bottom current regime in the past must be taken into account), (5) A thorough examination of the oceanography, seafloor topography, and sedimentary regime in the area of a wave field will often give conclusive evidence of its origin.

Wave heights of turbidity current sediment waves around the Canary Islands are up to 70 m, and wavelengths are up to 2.4 km. The waves are aligned roughly parallel to the slope and migrate upslope. Cores taken through the waves show a sequence of interbedded turbidites and pelagic/hemipelagic sediments. Overall, the dimensions, morphology and mode of formation of the waves are very similar to those described for sediment waves on channel-levee backslopes (e.g. Nakajima et al., 1998). Sediment waves in turbidity current channels have also been described from the flanks of the western and northern Canary Islands (Wynn et al., 2000b). These waves are smaller and coarser-grained than those formed by unconfined flows. They have wave heights up to 6 m and wavelengths up to 1.2 km.

Alongslope processes

Antarctic Bottom Water (AABW) is responsible for forming erosional furrows and sediment waves on the continental rise off Northwest Africa (Jacobi & Hayes, 1984; 1992). In the area of the Saharan Seamounts, AABW is funnelled between the seamounts and strengthened by topographic forcing, leading to the formation of erosional furrows (Jacobi and Hayes, 1992).

The glacially-influenced margin from 26°N to 56°N (canyon and channel processes dominant)

Downslope processes

This margin has a series of large submarine canyons and little or no evidence of submarine slides (Figure 4.2b). North-east of the Canary Islands is an area of canyoned margin beginning with the Agadir Canyon. These canyons funnel sediment derived

from the Atlas Mountains across a continental slope which is considerably narrower than that to the south. The turbidity currents deliver sediments directly to the Seine Abyssal Plain (Davies et al., 1997) and the Agadir Basin. The Agadir Basin is an intraslope basin from which sediment flows now spill over and flow downslope to the Madeira Abyssal Plain (Masson, 1994; Wynn et al., 2000a).

TOBI deep-towed sidescan sonar surveys at the mouth of the Agadir and Lisbon Canyons (see Chapter 7) have revealed extensive zones of erosional scours and bedforms associated with the transition zone between canyon mouth and depositional lobe. These transition zones are commonly developed at the mouths of submarine canyons and channels (see Normark & Piper, 1991 for a review), and are created by the increased turbulence and erosive power of turbidity currents undergoing flow expansion. The flow expansion may be linked to a hydraulic jump (Komar, 1971) in areas where there is a significant break-of-slope at the canyon/channel mouth. At the mouth of the Agadir and Lisbon Canyons individual erosional scours up to 21 m deep and 500 m wide have been imaged. In addition, fields of chevron-shaped scours, erosional scarps and sediment waves have all been imaged in this zone. The Agadir Canyon system feeds infrequent (1 every 30,000 years), large-volume (up to 250 km^3) turbidity currents to the Agadir Basin (Weaver et al., 1992). These turbidity currents spread out and flow as sheet flows across the basin floor, which is topographically constrained by volcanic islands and seamounts. Many of the flows continue westwards to the Madeira Abyssal Plain, but in doing so they often deposit much of their sandy bedload in the Agadir Basin as a sheet sand (Ercilla et al., 1998; Wynn et al., 2000a).

The margin from Iberia to the southern Rockall Trough is dominated by canyons, which are often deeply incised. The canyons on the eastern side of the Rockall Trough are as yet poorly mapped but are known to exist even on the Porcupine Bank margin, which is relatively isolated from areas of fluvial input (Roberts, 1975). It has been noted before (e.g. Emery & Uchupi, 1984) that this concentration of canyons is near the southern limits of the Quaternary ice cover, and coarse sediment carried by meltwater may have cut them. Canyons were most active during lowstands of sea level, as more material was transported to canyon heads at these times. Many canyons were largely inactive during interglacials, and often become partly infilled with pelagic and hemipelagic sediments. However, infrequent events such as earthquakes may trigger large turbidity currents at

any time. For example, the 1755 Lisbon earthquake triggered a massive turbidity current that is believed to have travelled along the Setubal Canyon and out onto the Tagus Abyssal Plain (Thomson & Weaver, 1994). Location, morphology and spacing of canyons are controlled by a combination of sediment supply, slope angle, seafloor topography and structure (e.g. faults). On the west Portuguese margin, the canyons are dominantly controlled by the positions of river mouths, which would have been closer to the canyon heads during lowstands of sea level. Several canyons on this margin (e.g. Setubal Canyon) even cut back to the inner shelf, and feed directly from the lower reaches of major river valleys. The west Portuguese continental margin is steep and narrow and the turbidity currents have built large abyssal plains at the foot of the slope (Milkert & Weaver, 1996; Lebreiro et al., 1997). On the extensively canyoned north Biscay margin the canyons are fed by cross-shelf glacial drainage channels, and by tidal shelf sand transport (Kenyon et al., 1978; Reynaud et al., 1999). The canyons are restricted to areas of steeper gradients with an angle of 4^{o} - 9^{o}. Many of the canyons are aligned oblique to the slope, and their morphology is clearly related to underlying basement topography and faulting (Kenyon et al., 1978; Lallemand & Sibuet, 1986).

Most canyons in the study area have gullied walls and a number of minor tributary canyons feeding sediment from the continental shelf (Figure 4.5). They merge downslope into one major canyon before terminating directly onto a basin floor. Small distributary channels are known in a few cases to have developed beyond the canyon mouths, e.g. on the Celtic Fan (Droz, et al., 1999), and beyond the Gollum Canyon system in the Porcupine Seabight. The Gollum Canyon system has canyons up to 280 m deep and 1.5 km wide that develop downslope into a dendritic pattern of slightly sinuous channels running across the floor of the Seabight (Kenyon et al., 1978). Levees are absent from this channel system, probably for the same reasons as for the MDCS. Beyond the Seabight, distributary channels are only up to 40 m deep. The largest abyssal plains are found on this sector of the margin, as demonstrated on Figure 4.1 (which is an equal area projection). This is presumably due to higher turbidity current activity in this area, as a result of increased glaciomarine sediment supply at the edge of the Quaternary ice sheet.

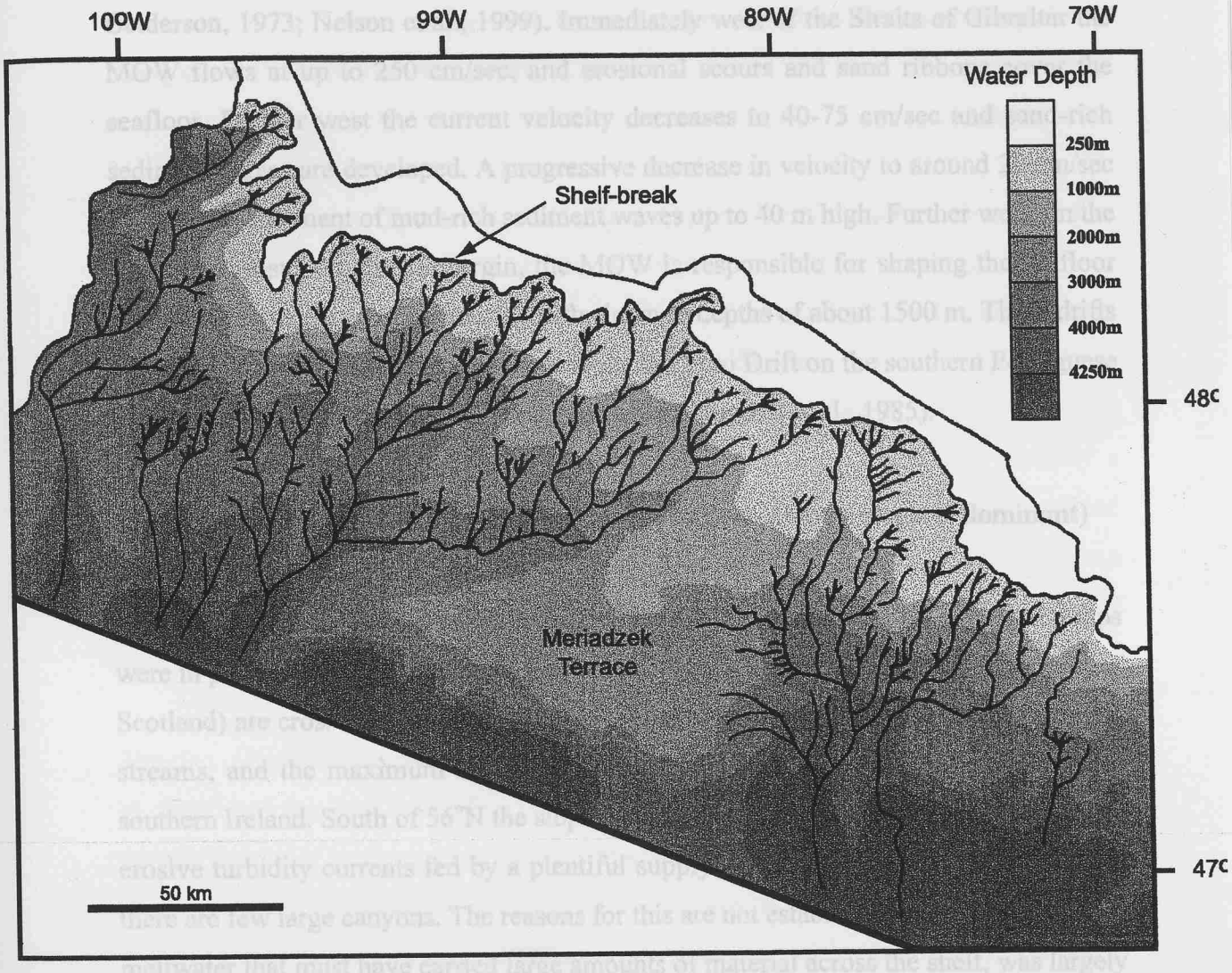

Figure 4.5: Line diagram based on swath bathymetry, showing the detailed and complex morphology of canyons on the continental slope bordering the Celtic Sea Shelf (Biscay margin). Modified from Bourillet and Loubrieu (1995). For location see Figure 4.1.

Alongslope processes

The Mediterranean Outflow Water (MOW) is responsible for the creation of a wide range of bottom current features on the south and west Iberian margin (Kenyon & Belderson, 1973; Nelson et al., 1999). Immediately west of the Straits of Gibraltar the MOW flows at up to 250 cm/sec, and erosional scours and sand ribbons cover the seafloor. Further west the current velocity decreases to 40-75 cm/sec and sand-rich sediment waves are developed. A progressive decrease in velocity to around 20 cm/sec leads to development of mud-rich sediment waves up to 40 m high. Further west, on the south and west Portuguese margin, the MOW is responsible for shaping the seafloor sediments into a series of contourite drifts down to depths of about 1500 m. These drifts are generally small and isolated, for example, the Faro Drift on the southern Portuguese margin is about 50 km long and 10 - 25 km wide (Faugeres et al., 1985).

The glaciated margin north of 56°N (glacial and alongslope processes dominant)

Downslope processes

There is a marked change in shelf and slope morphology where the Quaternary icecaps were in proximity to the margin (Figure 4.2a). The shelves as far south as 56°N (west of Scotland) are crossed by troughs that were cut near to the shelf edge by fast flowing ice streams, and the maximum southerly extent of ice sheets during glaciations was to southern Ireland. South of 56°N the slope is dominated by canyons, probably formed by erosive turbidity currents fed by a plentiful supply of coarse sediment. North of 56°N there are few large canyons. The reasons for this are not established. Possibly the glacial meltwater that must have carried large amounts of material across the shelf, was largely diverted into the cross-shelf troughs and fed to the slope at these few point sources, causing sliding rather than turbidity currents and canyon cutting. It has also been suggested that the strong currents along the upper slope have prevented canyon formation, as is the case on the Northwest Atlantic margin to the south of Cape Canaveral (Kenyon, 1987).

The geometry and processes of sedimentation along the margin in the Norwegian Sea have been reviewed by Vorren et al. (1998), and similar processes act along the margin west of Scotland. At the mouth of the cross-shelf troughs there are usually trough-mouth fans; accumulations of sediment on the slope that have a characteristic internal

geometry very different to typical low-latitude turbidite fans. Of the two main small-scale geometries, the most common are stacks of glacial debris flows: long, narrow tongues of a fairly consistent size and composition that extend downslope. Less frequent are classic debris flows which are usually much more extensive and varied in thickness (King et al., 1996; Baltzer et al., 1998).

Modelling of the flows within ice sheets by Dowdeswell & Siegert (1999) shows the predicted pattern of ice flux to the shelf edge along the Eurasian margin. Sediment flux transported by the icestreams has also been modelled and agrees well with the known distribution and size of trough mouth fans. The southernmost glacial fan is the Barra Fan. The presence of extensive turbidite deposition at the foot of the Barra Fan (Roberts 1975; Faugeres et al., 1981) and the network of tributary gullies at the top of the fan (Armishaw et al., 1998) are unusual glacial fan features, and so this is possibly a transitional example of a glacial fan. A further example of a glacial fan west of Scotland is the Sula Sgeir Fan (Baltzer et al., 1998). West of the Shetland Islands there are no well-developed cross-shelf troughs and no major depocentres. The extensive areas of both classic and glacial debris flows form what could be called a slope apron.

The two major areas of glacial drainage result in the enormous North Sea Fan (King et al. 1996) and the Bear Island Fan (Dowdeswell et al., 1997; Vorren et al., 1998). Both consist mainly of large numbers of stacked glacial debris flows. The Bear Island Fan is comparable in size to the largest low-latitude turbidite fans such as the Mississippi Fan, which consists mainly of large numbers of stacked channel-levee complexes. Both of the two largest fans are modified by major slides. The slides either bound the fans, such as the Storegga and North Faeroes Slides (Figure 4.6) on the northern and southern margins of the North Sea Fan (van Weering et al., 1998a, b), or are on top of them, such as the Bjornoyrenna Slide (Laberg & Vorren, 1993) on top of the Bear Island Fan. The best-studied slide is the Storegga Slide (Bugge et al., 1987, 1988; Evans et al., 1996). This is a site of repeated failure. Less well studied slides include those east of Rockall Bank (Roberts, 1972; Flood et al., 1979), the Traenadjupet Slide (e.g. Dowdeswell et al., 1996), and the Andoya Slide (Laberg et al., 1999). It seems likely that seismic investigations will reveal a complex history of repeated failure for most of these slides. It has been suggested that these slides could be caused by detachment of slabs of sediment charged with solid gas hydrate, released as the seawater warms up (Bugge et

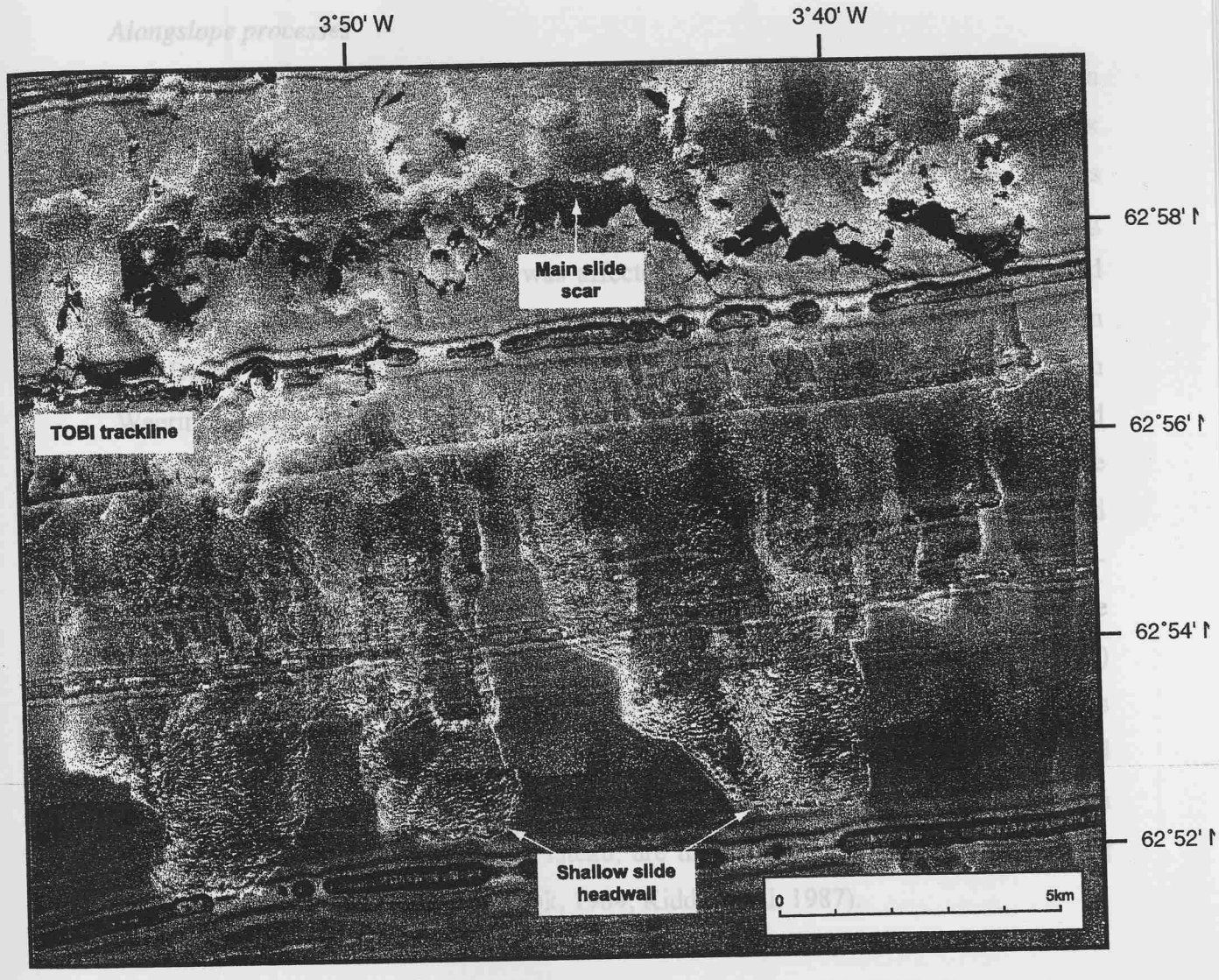

Figure 4.6: TOBI sidescan sonar mosaic showing an area of mass movements north of the Faeroe Islands. Shallow slides occur upslope of a major slide scar (seen as black shadows), representing a deeper failure. Downslope is to the north. High levels of backscatter are shown as light tones. Modified from van Weering et al. (1998). For location see Figure 4.1.

al., 1988; Mienert et al., 1998). Bottom simulating reflectors have been detected near the Storegga Slide and modelling predicts that the Norwegian Sea margin should be a likely place for gas hydrate formation (Miles, 1995).

Alongslope processes

Bottom currents have developed an extensive suite of contourite drifts and mud waves in the Northeast Rockall Trough area (Figure 4.7). In this region there is a complex circulation of bottom water, and mixing between three or four different water masses may occur. Generally, bottom currents have a greater influence on sedimentation during interglacials, as most of the slope was affected by large-scale mass movements and turbidity currents during glacial periods. North-east of the Faeroe Islands the Norwegian Sea Deep Water (NSDW) has formed contourite deposits on the upper slope (van Weering et al., 1998a). Part of the NSDW then flows south through the Faeroe-Shetland Channel as Norwegian Sea Overflow Water (NSOW), before moving west over the Wyville-Thomson Ridge. It partially mixes with Labrador Sea Water (LSW) and AABW to form North Atlantic Deep Water (NADW), which circulates as an anti-clockwise gyre in the Rockall Trough. In this region a number of contourite drifts have formed, and three distinct types can be recognised (Stoker et al., 1994). These are 1) distinctly mounded elongate drifts, 2) broad sheet drifts, and 3) isolated patch drifts (including moat-related drifts). Sediment waves occur on the flanks of the drifts, and have wave heights up to 20 m and wavelengths up to 2 km (Figure 4.7). Further south and west, adjacent to the Rockall Plateau, are the giant Feni and Hatton Drifts (e.g Roberts et al., 1984; Stow & Holbrook, 1984; Kidd & Hill, 1987).

During glacial periods the currents moved large icebergs around the Northeast Atlantic. Where they impinge on the continental slope and outer shelf they form patterns of iceberg plough marks (Figure 4.8; Belderson et al., 1973). They generally occur down to about 700 m except where buried by later sedimentation. It is usual to find a dense network of criss-crossing iceberg plough marks on the shelf and upper slope and isolated ploughmarks running alongslope in deeper water. The southernmost limit of known ploughmarks is west of Ireland.

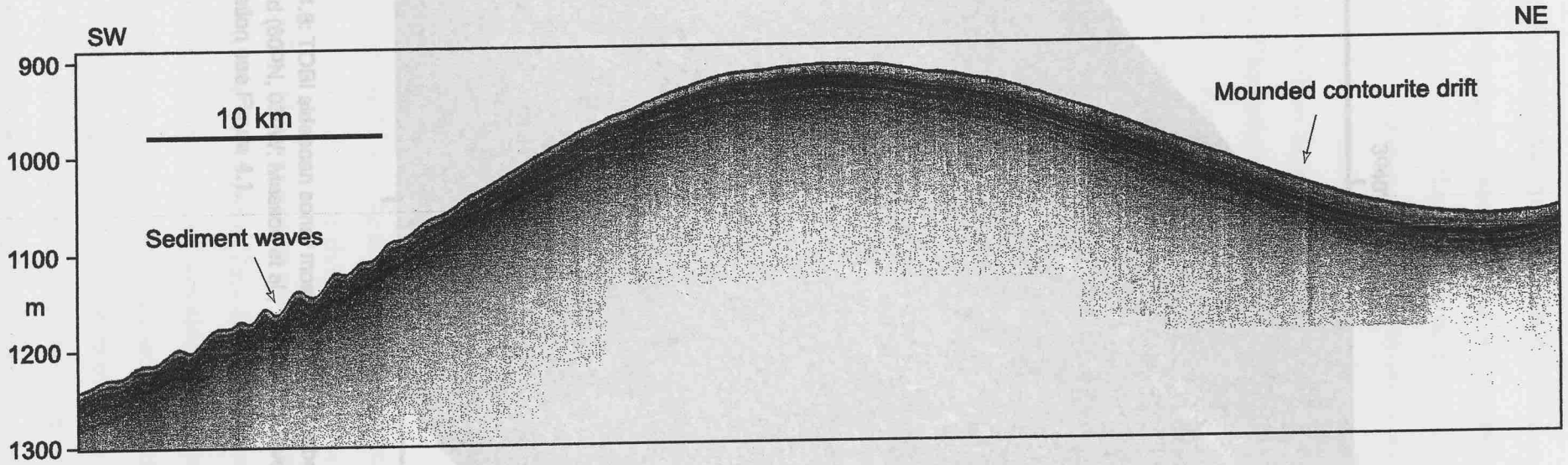

Figure 4.7: 3.5kHz profile showing sediment waves on the flank of a sediment drift in the northeast Rockall Trough (59°45'N, 07°40'W). For location see Figure 4.

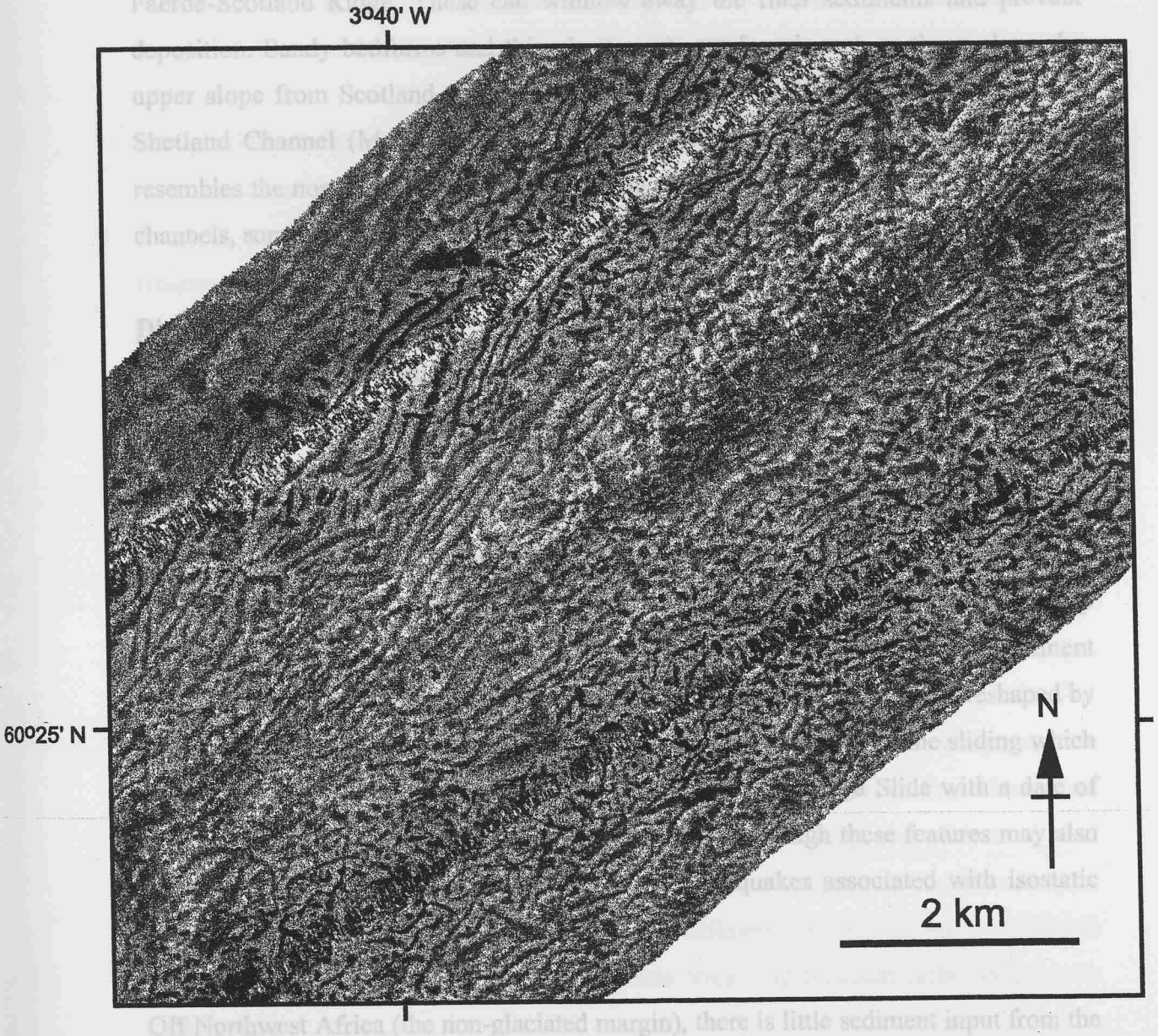

Figure 4.8: TOBI sidescan sonar mosaic showing iceberg ploughmarks on the upper slope west of Scotland (60°N, 03°W; Masson et al., 1997). High levels of backscatter are shown as light tones. For location see Figure 4.1.

Relatively strong currents are found both bounding the drifts and in other areas where topography enhances flow speeds, such as the outflow of NSDW across the Iceland-Faeroe-Scotland Ridge. These can winnow away the finer sediments and prevent deposition. Sandy bedforms and thin sheet sands are found, such as those along the upper slope from Scotland to northern Norway (Kenyon, 1986), and in the Faeroe-Shetland Channel (Masson et al., 1997). The exit from the Faeroe Bank Channel resembles the northern Gulf of Cadiz in having small drifts bounded by coarse floored channels, some of which appear to be aggradational (Kenyon et al., 1998).

Discussion

Variations in sedimentation pattern along the margin

The map (Figure 4.1) and the above description show that sedimentary processes vary along the length of the continental margin. There are three primary margin types: non-glaciated, glacially influenced, and glaciated. Mass movements are common on the non-glaciated margin south of about 26°N. From here to 56°N, on the glacially-influenced margin, there are few mass movements but canyons are common, cutting into a steep continental slope. North of 56°N, on the glaciated margin, most of the prominent seafloor features were generated during the last Ice Age and are now being reshaped by alongslope currents. An exception to this simple model is the submarine sliding which has occurred off Norway during the Holocene (e.g. the Storegga Slide with a date of emplacement of 7,100 years; Bondevik et al., 1997), although these features may also be related to climate change, for example via earthquakes associated with isostatic rebound initiating the sliding.

Off Northwest Africa (the non-glaciated margin), there is little sediment input from the continent, but high productivity along the upper slope produces accumulation rates of up to 147 m/Myr, in contrast to mid- and lower slope accumulation rates of 20 m/Myr (Ruddiman et al., 1988). This leads to oversteepening of the slope and potential instability. Sediment sequences along the upper part of this margin therefore show a series of hiatuses each representing tens to hundreds of metres of missing sediment, and a duration of hundreds of thousands of years (Weaver, 1994). Further downslope the sediment sequence contains a number of debris flow deposits, and at the base of the slope the abyssal plain fills gradually with a series of megaturbidites. The large sediment slides off Norway operate in a similar fashion, but in this area there are also

substantial deposits derived from ice sheet transport. The rate of accumulation of these ice-derived sediments is very high and they rapidly build large fan-like bodies. Although presently inactive, Holocene sedimentation has added only a thin veneer over the glacial fans and thus they still make prominent seafloor features.

The glacially influenced margin is characterised by a steep continental slope and relatively large abyssal plains, which almost coalesce in places. Off the Iberian margin, frequent earthquakes are correlated with frequent turbidite deposition, though the frequency seems to have been higher during glacial periods (Lebreiro et al., 1997). Although there is limited information on the canyons and abyssal plains in the Bay of Biscay, the density of canyons is striking. This may be due to the large amounts of sediment that would have been transported across this margin during ice ages, and particularly during ice retreat. There was no ice sheet near the shelf edge in this area during the ice ages, but the inland drainage basins of the UK, France and Iberia would have been much more active in transporting sediment eroded by ice at these times. South of the Atlas Mountains there would have been no influence of ice, and north of southern Ireland grounded ice processes would have operated near the shelf edge, especially in front of cross-shelf troughs, producing stacked debris flow deposits. The high sediment input on the glacially influenced margin, and the steep, narrow continental slope, has led to most deposition being on the abyssal plains, which have thus grown to a very large size. To summarise, therefore, the large size of these abyssal plains is due to a combination of: (1) high sediment supply from glacial outwash, (2) a narrow, steep slope and rise which sheds most sediment downslope, and (3) the high seismicity of the margin off south-west Iberia triggering frequent turbidity currents (Figure 4.9).

One consequence of the different margin physiographies is the distribution of sand from the numerous turbidity currents. For basins at the base of steep continental slopes, e.g. the Tagus and Horseshoe Basins off Portugal (Lebreiro et al., 1997) and the Bay of Biscay (Droz et al., 1999), turbidity currents have enough velocity to carry large volumes of sand to the abyssal plain. The sand is then dumped across a large area centred around the point of entry. On the Tagus Abyssal Plain this sandy area forms a very low relief fan with shallow channels, and covers approximately 20% of the total plain area. At the other extreme, the Madeira Abyssal Plain lies at the base of a very low

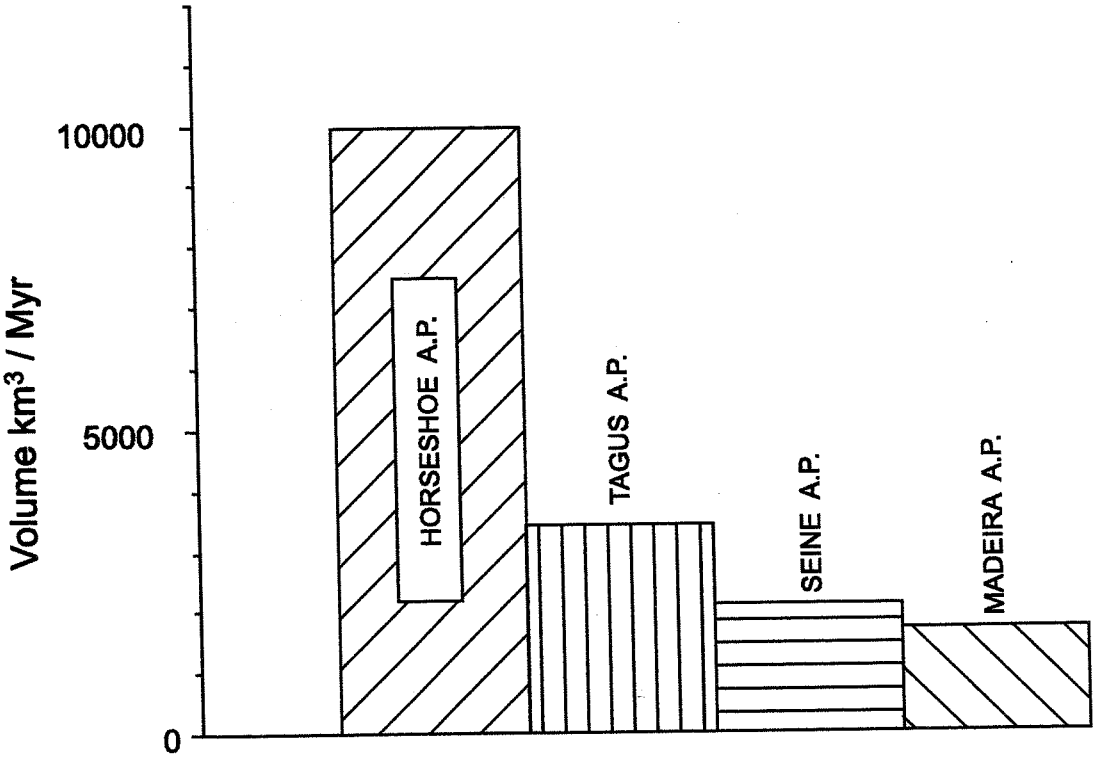

Figure 4.9: Graph showing how the volume of turbidites per million years varies on four different abyssal plains. The volume of material contributed to the abyssal plains increases as one goes northwards, as the margin is both more tectonically active and has a greater sediment supply in this area.

angle continental slope (1:300), and in this case the ratio of mud to sand is much higher (in the order of just a few % sand). The sand component in these turbidity currents may be deposited in channels and intraslope basins on the continental slope and rise. Sands deposited on the plain are concentrated around distributary channel terminations (Wynn et al., 2000a). This concentration of sand in one part of the plain produces laterally as well as vertically graded sediment units.

Turbidity currents can be generated by hyperpycnal discharge at the mouths of "dirty" rivers. The flows will follow the basin floor if the plume density is greater than that of the surrounding salty water. Such flows rarely occur off large rivers but they may occur off small rivers with a high suspended sediment load (Mulder & Syvitski, 1995). Such rivers may have been common on the steep, narrow land surrounding the Iberian Peninsula and, during periods of high glacial meltwater drainage, on the shelf to the north.

It is interesting to note that the spectacular meandering channels which are so common on the West African margin to the south of the study area, are absent from the Northwest African and West European margin. This is probably due to a combination of gradient and sediment composition. On the Northwest African and West European margin the outer shelf is dominated by coarse-grained sediments, and consequently most canyons and channels are formed by sand-rich turbidity currents.

Long term history of the margin

The abyssal plain turbidites provide an excellent record of large-scale mass wasting events in the Canary Basin, since each major event here seems to produce both a debris flow deposited on the continental slope and rise, and a turbidity current which deposits on the abyssal plain. Drillholes through the abyssal plain sequence can therefore provide a record of the largest mass wasting events, which have occurred at a variety of locations on the basin margins. In this way ODP Legs 157 (Schmincke et al., 1995) and 149 (Whitmarsh et al., 1996) which drilled the Madeira and Iberia Abyssal Plains respectively, each provided a history of their basin. In the case of the Iberia Abyssal Plain, the turbidite input, and hence basin filling, began at about 2.4 Ma, coincident with the onset of Northern Hemisphere glaciations (Milkert & Weaver, 1996). In the Madeira

Abyssal Plain turbidite sedimentation began abruptly in the middle Miocene, at a time when ice began to build up rapidly on Antarctica (Weaver et al., 1998). This external climatic change could have caused significant reorganisation of sedimentation along the world's continental margins. It would have initiated a time of lowered sea level, which may have allowed sediments to be deposited beyond the shelf edge on the upper slope for the first time. In addition, the build up of ice would have led to the production of cold bottom waters in Antarctica, which would in turn have caused a reorganisation of ocean circulation. This may have led to increased upwelling and associated sedimentation along the West African margin (see Sarnthein et al., 1982). Both of these processes would have caused an oversteepening of the upper continental slope, possibly leading to mass wasting and initiation of organic-rich turbidites that reached the abyssal plains.

Conclusions

A variety of sedimentary processes affect the Northeast Atlantic continental margin from Northwest Africa to northern Norway. Processes vary considerably along the margin, with some areas being dominated by downslope and others by alongslope transport and deposition. In the more northern areas there are also significant differences between the processes that operated during glacial periods and those that operate today. The main sectors of the margin and their respective dominant processes are:

1) *The non-glaciated margin south of 26°N*: High rates of upwelling here produce elevated accumulation rates along the upper slope, although there is little fluvial input and canyons are rare. This sediment is subject to mass movements involving dislocation of hundreds to thousands of km^3 of sediment, on time scales of a few tens of thousands of years. The resultant debris flows are deposited across the continental slope and rise, and large-scale turbidity currents transport hundreds of km^3 of sediment to the abyssal plains.

2) *The glacially influenced margin from 26°N to 56°N*: In this area there is more fluvial input and the margin is less prone to mass movements. A number of canyons funnel turbidity currents down the steep slopes to the extensive abyssal plains. Some canyons, such as the Agadir Canyon, have built high levees. The presence of a

lithospheric plate boundary off Southwest Iberia is associated with frequent earthquakes and has led to high rates of sediment transport to the deep sea via the canyon systems. In addition, there is a high sediment supply to the shelf edge, as much sediment was transported by glacial melt wash following glacial periods. The Mediterranean outflow has built a series of sediment drifts in the Gulf of Cadiz and off Southwest Portugal, although the alongslope transport is interrupted by a number of large canyons, some of which cut back into river mouths.

3) *The glaciated margin north of 56°N*: Here the margin is heavily influenced by glaciomarine processes, which build fans composed largely of stacked debris flows. These occur in front of the fast flowing ice streams that have cut cross-shelf troughs. There are iceberg plough marks on most of the upper slope and outer shelf. During interglacials this section of the margin has been influenced by alongslope currents. Giant submarine slides are again a prominent feature, particularly off Norway and the Faeroe Islands. Some of these slides have occurred during the Holocene, although high glacial sedimentation rates and failure at melting gas hydrate layers may have contributed to the instability.

Acknowledgements

This work was carried out as part of the EU-supported STEAM programme (contract MAS2-CT94-0083) and ENAM 2 programme (contract MAS3-CT95-0003). RBW would like to acknowledge PhD funding from the University of Southampton and the Southampton Oceanography Centre (Challenger Division). Tim le Bas is thanked for providing technical assistance. Finally, the manuscript benefited greatly from the detailed reviews of David Piper, William Morris and Ian Jarvis.

4.3: Summary

This paper has revealed that the Northeast Atlantic margin can be broadly subdivided into three main margin types, and that the sedimentary processes operating on each type of margin are largely controlled by climate, and more specifically the degree of glacial influence. The non-glaciated margin, off Northwest Africa has low terrigenous input but high upwelling, and is dominated by mass movements. Further north, the glacially influenced margin off Iberia and southern France is fed by a large amount of terrigenous sediment, especially from glacial melt waters, and is dominated by canyons and bottom current features. The glaciated margin off Northwest Europe is largely dominated by glacial and glaciomarine processes, including large-scale mass movements. However, during interglacial periods, bottom currents become the dominant process.

The next target is to look at the non-glaciated, Northwest African margin in more detail, and attempt to understand the key controls on sedimentary processes in an area with low terrigenous input and no glacial influence.

CHAPTER 5

SEDIMENTARY PROCESSES ON THE NORTHWEST AFRICAN MARGIN

5.1: Introduction and aims

In Chapter 4 it was proposed that the Northeast Atlantic margin could be subdivided into *non-glaciated*, *glacially influenced* and *glaciated* margins. In this chapter, the aim is to focus on the Northwest African (non-glaciated) margin, which is to be achieved with the production of a new sediment process map covering the entire margin, from the continental shelf to the deep abyssal plains. The key issues to be investigated in this study are:

1) What are the controls on sedimentary processes operating on a non-glaciated margin?

2) Can the Northwest African margin be classified as a slope apron, or is it dominated by turbidite fans?

3) How does complex seafloor morphology affect sedimentation processes and deposits?

5.2: Paper 2

The Northwest African slope apron: a modern analogue for deep-water systems with complex seafloor topography

Russell B Wynn, Douglas G Masson, Dorrik A V Stow and Philip P E Weaver

SOES/Challenger Division, Southampton Oceanography Centre, European Way, Southampton, SO14 3ZH, UK

This paper was submitted to Marine and Petroleum Geology in July 1998. It was reviewed by Mike Mayall and two anonymous reviewers, and was accepted for publication in March 1999. It was published in Marine and Petroleum Geology in February 2000, v.17, p.253-265.

Abstract

The Northwest African slope apron is an interesting modern analogue for deep-water systems with complex seafloor topography. A sediment process map of the Northwest African continental margin illustrates the relative roles of different sedimentary processes acting across the entire margin. Fine-grained pelagic and hemipelagic sedimentation is dominant across a large area of the margin, and is considered to result from background sedimentary processes. Alongslope bottom currents smooth and mould the seafloor sediments, and produce bedforms such as erosional furrows, sediment waves and contourite drifts. Downslope gravity flows (debris avalanches, debris flows and turbidity currents) are infrequent but important events on the margin, and are the dominant processes shaping the morphology of the slope and rise. The overall distribution of sedimentary facies and morphological elements on the Northwest African margin is characteristic of a fine-grained clastic slope apron. However, the presence of numerous volcanic islands and seamounts along the margin leads to a more complex distribution of sedimentary facies than is accounted for by slope apron models. In particular, the distribution and thickness of turbidite sands are controlled by the location of the break-of-slope, which is itself controlled by the pre-existing submarine topography.

Introduction

The Northwest African continental margin has been the focus of intensive research in the last thirty years. Early sediment facies maps, based on 3.5kHz-profiles, were produced for various sections of the margin (Embley, 1976; Jacobi, 1976; Embley and Jacobi, 1977; Jacobi and Hayes, 1982; 1984; 1992) and these have increased our understanding of the interaction between gravity flows, bottom currents and pelagic/hemipelagic sedimentation in continental slope and rise settings.

More recent studies have concentrated on the mapping of turbidity current pathways, debris flows and debris avalanches around the Canary Islands, with increasing use of the GLORIA and TOBI sidescan sonar systems. This work has led to a greater understanding of the sedimentary processes across the margin, such as debris flows (e.g. Masson, Huggett and Brunsden, 1993; Masson *et al.*, 1997; Weaver *et al.*, 1995; Gee *et al.*, 1999), the character and distribution of turbidity current pathways (Masson, 1994),

and the recognition of catastrophic landslides on the flanks of the western Canary Islands (Masson, 1996; Watts and Masson, 1995).

In this study we review the seafloor sedimentary processes of the Northwest African continental margin, and investigate the applicability of slope apron models to this system. Our understanding of the interplay between different sedimentary processes has benefited from the production of a new sediment distribution and process map (Figure 5.1, see foldout 2) which covers the entire margin, from the continental shelf to the deep abyssal plains. This paper builds upon previous studies of the area by 1) describing the sedimentary processes operating across the entire Northwest African margin, 2) attempting to classify the Northwest African margin as a fine-grained clastic slope apron, and 3) discussing the controls on sand distribution within the system.

Methods

The sediment process map has been compiled by the authors using data collected on a number of research cruises on board the RRS Discovery and the RRS Charles Darwin (e.g. Masson, 1994, 1996; Masson et al., 1992; Weaver et al., 1992, 1995). Many of the cruises were undertaken as part of the multi-national STEAM project (Sediment Transport on Eastern Atlantic Margins). A variety of data collection techniques were employed during these research cruises, and they have been grouped into four main categories:

Bathymetric data for the majority of the study area were collected by 12kHz-profiling. Some parts of the study area, in particular the flanks of the Canary Islands, have high-resolution bathymetric coverage collected using the Simrad EM12 multibeam echo-sounder. This has been particularly useful in the recognition of debris avalanche scars (e.g. Watts and Masson, 1995).

3.5kHz-profiles have been collected across a large area of the margin and are used to characterise a wide variety of seafloor acoustic facies. These range from turbidity current channels and debris flows, to volcanic seamounts and sediment wave fields. A review of the technique was presented by Damuth (1980), and echo-character definitions for the Northwest African margin are described in Embley (1982), Kidd *et*

al. (1985), and Masson *et al.* (1992). Table 5.1 summarises the echo-character definitions used in this study.

Swath imaging in the study area has been undertaken using the Geological Long-Range Inclined Asdic (GLORIA) and Towed Ocean Bottom Instrument (TOBI) side-scan sonar systems:

GLORIA is a 6.5kHz long-range side-scan sonar, with a swath width of up to 45 km. It is towed near the surface at speeds of up to 10 knots, allowing large areas of the seafloor to be mapped relatively quickly. A modified version of the GLORIA interpretation scheme given by Kidd *et al.* (1985) was presented by Masson *et al.* (1992). GLORIA has primarily been used in the mapping of debris flows and channel systems in the central part of the study area.

TOBI is a 30kHz high-resolution side-scan sonar, with a swath width of about 6 km (Murton *et al.*, 1992). It is deep-towed, and has primarily been used for detailed mapping of gravity flow deposits. These include the channel systems east of the Madeira Abyssal Plain (Masson, 1994), and the debris flows and debris avalanches around the Canary Islands (Masson *et al.* 1993; Masson, 1996; Watts and Masson, 1995). The sidescan character definitions used in this study are displayed in Table 5.1.

Sediment cores have been recovered from many areas of the Northwest African margin, for example, over 160 cores have been taken from the Madeira Abyssal Plain (Rothwell *et al.*, 1992). Piston, kasten, gravity and box corers have all been recovered, with the majority of cores being <10 m long. Core data have proved to be useful in confirming earlier interpretations of sediment facies, based purely on acoustic facies. In this study we also summarise the initial results from three cores recovered from the Agadir Basin during RRS Discovery cruise 225, and combine this with other core data to interpret sand distribution across the study area. Core character definitions used in this study are shown in Table 5.1.

No.	Echo-character	Sidescan character	Core character	Location	Interpretation
		PELAGIC AND HEMIPELAGIC SEDIMENTATION			
1	Continuous, flat, subbottom reflectors, > 50 m penetration	Low to intermediate backscatter, featureless or vaguely mottled/lineated	*On slope/rise* - interbedded marls, oozes and clays *On abyssal plains* - interbedded f-g turbidites and marls, oozes and clays	Found across large areas of the continental slope, rise and abyssal plains	Flat-lying pelagic/hemipelagic drape on slope/rise OR f-g turbidites and pelagic/ hemipelagic sediments on abyssal plain
2	Irregular, undulating > 50 m penetration	Very low backscatter patches	Marls, clays and oozes	Flanks of volcanic seamounts	Pelagic drape on seamounts
		BOTTOM CURRENT FEATURES AND DEPOSITS			
3	Very regular, overlapping hyperbolae, tangent to seafloor			Parallel to bathymetric contours, around seamounts	Erosional furrows
4	Regular, undulating, may show marked asymmetry. > 50 m penetration	Distinct, regular bands of low to intermediate backscatter	Interbedded fine-grained silts, clays, marls and oozes	Parallel to bathymetric contours, on continental rise and around seamounts	Bottom current sediment waves
		GRAVITY-FLOW FEATURES AND DEPOSITS			
5	Rough seabed with abundant large hyperbolae	Variable backscatter. Irregular, blocky texture		On, or adjacent to, slopes of volcanic islands	Debris avalanche deposits
6	Large hyperbolae with vertex elevation decreasing downslope. Rare subbottom reflectors			Continental slope/rise, slope and base of seamounts amd volcanic islands	Submarine slide deposits. Deposits grade from 'hummocky' near slide-scar to 'blocky' downslope
7	Prolonged echo with no penetration. Small-scale rough seabed with many hyperbolae	High backscatter, strongly lineated perpendicular to slope	Buried slide-scars show hiatus in sequence	Continental slope, slopes of volcanic islands and seamounts	Sediment-slide scars
8	Acoustically transparent, lens-shaped units with prolonged echo. Onlaps other facies	High backscatter lobate sheets, lineated with well-defined boundaries	Variable. Blocky unsorted material in f-g matrix OR deformed but coherent blocks of original sed sequence	Slope/rise and on slopes of volcanic islands and seamounts	Debris-flow deposits
9	Parallel-bedded with 10-30 m irregular penetration	Intermediate backscatter, lineated with variable backscatter lineations	Interbedded f-g turbidites and clays, marls, oozes. Low sand/shale ratio	Slope and rise, generally perpendicular to bathymetric contours	Turbidity current pathways and channel overbank deposits
10	Topographic lows on profiles, often with decreased penetration	Straight or curved narrow lineaments. High backscatter, or high with low central stripe	Interbedded c-g turbidites and clays, marls, oozes. High sand/shale ratio	Slope and rise, generally perpendicular to bathymetric contours	Turbidity current channels
11	Regular, undulating, often with marked asymmetry. penetration increases downslope, from < 10-> 50 m	Distinct, regular bands of low to intermediate backscatter. Spacing between bands decreases downslope.	Turbidites, interbedded with marls, clays and oozes	Slopes of volcanic islands and seamounts, levee backslopes, channel floors. Parallel to slope contours	Turbidity current sediment waves
		OTHER FEATURES AND DEPOSITS			
12	Sharp to prolonged echo with no penetration. Large-scale rough seabed with large hyperbolae	Very high backscatter, linear to irregular patches		Seamounts and volcanic island slopes. Canyon walls	Basement rock outcrop

Table 5.1: Character, location and interpretation of morphological features and sedimentary deposits on the Northwest African margin. Modified from Masson et al. (1992) and Jacobi and Hayes (1992).

A number of previously published studies have also been used in areas of the map not covered by the STEAM project. The echo-character maps of Jacobi and Hayes (1982, 1992) have been particularly useful for the mapping of submarine landslides, sediment waves, erosional furrows, and canyon and channel systems. In addition, the published maps of the Saharan Debris Flow (Embley, 1976), the Western Saharan Canyon System (von Rad and Wissman, 1982), the bedforms in the Gulf of Cadiz (Kenyon and Belderson, 1973), and the contourite drifts of the southern Portuguese margin (Stow *et al.*, 1986) have also been used in this study.

Morphology and oceanography of the Northwest African margin

The Northwest African margin is bordered by a flat continental shelf that is generally 40-60 km wide, although maximum shelf widths of >100 km occur off the Western Saharan coast. The shelf-break is at a water-depth of 100-200 m. Beyond the shelf-break, the continental slope has a width of 50-250 km, and displays slope angles of 1°-6°. In some areas, e.g. adjacent to the Western Sahara Canyon System, slope angles may reach 40°. The slope passes to the continental rise at water depths of 1500-4000 m, with gradients ranging from about 1° on the lower slope/upper rise, to 0.1° on the lower rise (Masson et al., 1992). The rise is generally 100-1500 km wide, and terminates in water depths of 4500-5400 m, beyond which lies the flat expanse of the abyssal plains. Large sections of the Northwest African slope and rise are punctuated by numerous volcanic islands and seamounts, and are dissected by canyons and channels (Figure 5.1). This creates a complex submarine topography that has greatly influenced the sedimentary processes operating upon this margin.

Deep-water bottom currents off the Northwest African margin include the North Atlantic Deep Water (NADW) and the Antarctic Bottom Water (AABW). The NADW occurs at a water-depth of 2000-3800 m and flows in a southerly direction, the AABW occurs below 3800 m and flows in a north-easterly direction. Bottom currents along the margin are thought to be fairly weak at the present day, with current velocities generally between 1-6 cm/sec (Sarnthein et al., 1982; Lonsdale, 1978; 1982).

Sedimentary processes on the Northwest African margin

Previous overviews of the Northwest African margin have largely concentrated on the description of seafloor features in terms of their echo-character (e.g. Embley, 1982;

Jacobi and Hayes, 1982; 1992) and sidescan sonar/core character (Masson et al., 1992). The descriptions of these features have therefore been well documented, and are summarised in Table 5.1. The present study has built upon this work by producing a map that is process-oriented (Figure 5.1), and the following section looks at the nature of these processes, and how they are distributed across the margin.

1 - Pelagic/hemipelagic sedimentation

Fine-grained pelagic and hemipelagic sediments are widespread throughout the study area, and are considered to result from background sedimentary processes (e.g. settling of dead planktonic organisms and wind-blown terrigenous dust). The sediments commonly occur in association with abyssal hills and seamounts, and across large areas of the continental slope and rise. Pelagic/hemipelagic sediments are also a significant component of the basin-fill on this margin. For example, on the Madeira Abyssal Plain, the sedimentary record for the last 300,000 years has revealed that 600 km^3 of turbiditic sediments have been deposited, together with 60 km^3 of pelagic/hemipelagic sediments (Rothwell et al., 1992).

2 - Alongslope processes (bottom currents)

The dominant deep-water bottom currents on the Northwest African margin are the south-flowing NADW (2000-3800 m), and the northeast-flowing AABW (below 3800 m). At the present-day these currents generally flow at velocities of <6 cm/s, although in areas where the current flow is affected by topographic forcing this figure may increase to 20 cm/s (Lonsdale 1978, 1982; Sarnthein *et al.*, 1982). These currents are responsible for smoothing the fine-grained seafloor sediments, and also produce a variety of bedforms. These include erosional bedforms such as furrows, and depositional bedforms such as sediment waves.

Erosional furrows

Erosional furrows are best developed in the area of the Saharan Seamounts (Figure 5.1), and are thought to have formed by intensified AABW flow around and between the seamounts. The lack of large turbidity current pathways in the Saharan Seamount region also promotes the formation of furrows as there is relatively low sediment input into this area. The furrows are aligned parallel to the regional bathymetric contours and display negative relief (Lonsdale, 1978, 1982; Jacobi and Hayes, 1992).

Sediment waves

Several fields of sediment waves also occur in the study area, some of which have been formed by AABW and NADW. However, as they are constructional bedforms, they only occur in areas that receive a regular sediment supply. The wave fields on the continental rise south of the Agadir Basin (Figure 5.1) occur at a water depth of 3500-4500 m, and may have been formed beneath AABW. The waves migrate upslope and display wavelengths up to 1.1 km and wave heights of up to 7 m. However, it should be noted that the relationship between bottom currents, turbidite systems and wave fields can be complex, and that the wave-forming process is often difficult to interpret with certainty.

3 - Downslope processes (gravity-flows)

Sediment gravity-flows are infrequent but important events on the Northwest African margin. They are the dominant process in shaping the morphology of the margin, as they often overprint pelagic/hemipelagic and bottom current deposits. There are four main types of gravity-flow deposit in the study area (Figure 5.2).

Submarine slides

Many slope failures on the Northwest African margin have been described using the general terms *submarine landslide* or *submarine slide* (e.g. Embley, 1976; 1982; Embley and Jacobi, 1977; Jacobi, 1976; Jacobi and Hayes, 1982; 1992). In particular, these terms have been applied to several large slope failures which appear to be complex events and include elements of slumping, sliding and debris flow.

A number of large submarine slides flank the Cape Verde Terrace (Jacobi and Hayes, 1982; 1992), and occur as part of a major gravity-flow complex, termed the Cape Verde Slide Complex. This has affected an area of 30,000 km^2, with individual slide masses reaching 500 km in length. The submarine slides interfinger with turbidity current pathways in a complex pattern, and in many of the slide zones multiple slide scars and a complicated depositional morphology indicate multiple slide movements (Jacobi, 1976). The submarine slide deposits typically display increasing deformation and evidence for mobilisation downslope, grading from hummocky and blocky material through to smoother debris flow material (Jacobi and Hayes, 1982).

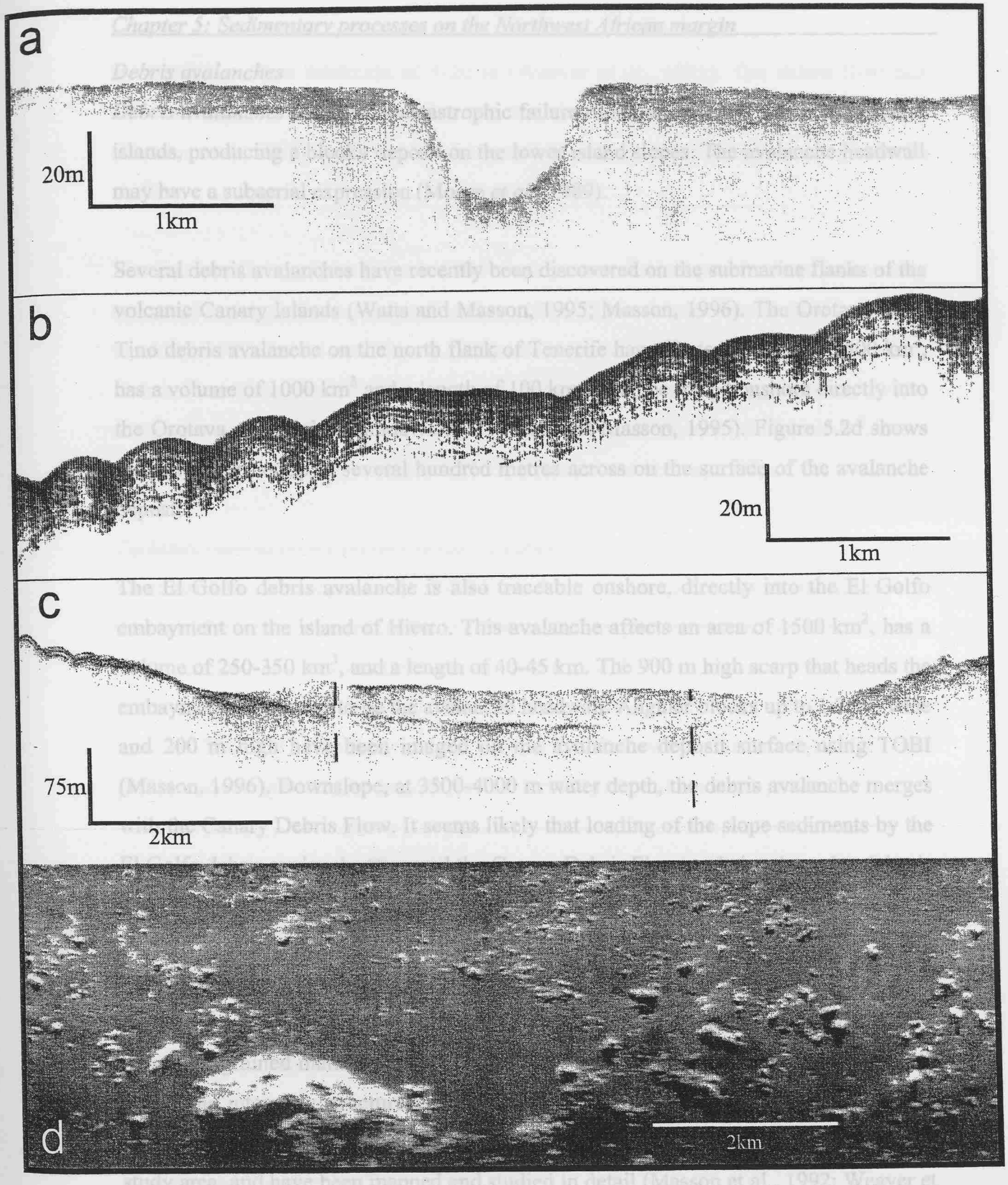

Figure 5.2: Gravity flow deposits on the Northwest African margin. Locations shown on Figure 5.1. (a) TOBI 7kHz profile across a channel on the lower rise (b) 3.5kHz profile showing turbidity current sediment waves on the flanks of La Palma (c) 3.5kHz profile through a section of the Saharan Debris Flow. The debris flow deposit is the thick acoustically transparent layer lying within the topographic low (d) TOBI image of a section of the Oratava-Icod-Tino debris avalanche complex north of Tenerife. Note the variation in size of avalanche blocks lying on the surface. Light shades indicate high backscatter, dark shades indicate low backscatter.

Debris avalanches

Debris avalanches result from catastrophic failure of the steep upper slopes of volcanic islands, producing a blocky deposit on the lower island slopes. The avalanche headwall may have a subaerial expression (Moore *et al.*, 1989).

Several debris avalanches have recently been discovered on the submarine flanks of the volcanic Canary Islands (Watts and Masson, 1995; Masson, 1996). The Orotava-Icod-Tino debris avalanche on the north flank of Tenerife has affected an area of 5500 km^2, has a volume of 1000 km^3 and a length of 100 km. It can be traced onshore directly into the Orotava and Icod landslide valleys (Watts and Masson, 1995). Figure 5.2d shows individual blocks up to several hundred metres across on the surface of the avalanche deposit.

The El Golfo debris avalanche is also traceable onshore, directly into the El Golfo embayment on the island of Hierro. This avalanche affects an area of 1500 km^2, has a volume of 250-350 km^3, and a length of 40-45 km. The 900 m high scarp that heads the embayment is believed to be the avalanche headwall. Angular blocks up to 1.2 km wide and 200 m high have been imaged on the avalanche deposit surface using TOBI (Masson, 1996). Downslope, at 3500-4000 m water depth, the debris avalanche merges with the Canary Debris Flow. It seems likely that loading of the slope sediments by the El Golfo debris avalanche triggered the Canary Debris Flow, and also the volcaniclastic b turbidite found on the Madeira Abyssal Plain, as discussed by Masson (1996).

Debris flows

Debris flows are gravity-flows that contain numerous large clasts supported and carried by a finer-grained matrix (Varnes, 1978; Stow, 1985). Debris flow deposits are poorly sorted and internally structureless, and typically have a pebbly mudstone texture. Two very large debris flows, the Canary and Saharan Debris Flows, occur in the centre of the study area, and have been mapped and studied in detail (Masson et al., 1992; Weaver et al., 1995).

The Canary Debris Flow extends all the way across the continental rise to the edge of the Madeira Abyssal Plain. It originated at 4000 m water depth on the western slopes of the Canary Islands, and is 100 km wide near the source, thinning to 60 km wide near its

termination, with a thickness of 5-20 m (Weaver *et al.*, 1995). The debris flow has affected an area of 40,000 km^2, has a volume of 400 km^3, and a length of 600 km (Masson *et al.*, 1992). Sediment blocks up to 300 m in diameter have been imaged on its surface.

The Saharan Debris Flow (Figure 5.2c) displays two distinct provinces, a source area scar, and a debris flow deposit (Embley, 1976). This debris flow is 20-50 m thick (Embley, 1982; Jacobi and Hayes, 1992) and stops on a steeper slope than the Canary Debris Flow (200 km ESE of the Madeira Abyssal Plain), which suggests that it was a more viscous flow (Masson *et al.*, 1992). It has affected an area of 48,000 km^2, has a volume of 1100 km^3, and a length of 700 km (Jacobi and Hayes, 1992).

Turbidity current pathways and sediment waves

Most *turbidity current pathways (TCP s)* on the Northwest African margin originate as a series of tributary canyons at the shelf break, before passing downslope into one main feeder canyon or channel. On the continental rise TCP s open out into a series of distributary channels (Figure 5.2a), and channel levees are very subdued or non-existent. The TCP s finally spread out to form distributary lobes at the edges of abyssal plains, and this is where the majority of the turbidity current load is deposited.

There are several major TCP s within the study area, through which sediments derived from the continental margins, islands and seamounts are transported downslope to the deep abyssal plains. The Madeira TCP is the largest on this margin and is described in detail in the next section. A number of smaller TCP s have also been mapped in the study area. A series of TCP s transport sediments from the Mauritanian and Senegalese margins to the Cape Verde Basin and Gambia Abyssal Plain (Jacobi and Hayes, 1982, 1992), while in the north of the study area a series of short TCP s pass onto the Seine, Tagus and Horseshoe Abyssal Plains (Davies *et al.*, 1997; Lebreiro, 1995; Lebreiro, McCave and Weaver, 1997).

Recent work undertaken on two *sediment wave fields* on the flanks of the western Canary Islands has revealed that they were formed by turbidity currents (Wynn et al., 2000b). The La Palma wave field covers some 20,000 km^2 of the continental slope and rise, and consists of waves that display wave heights of <5-70 m, and wavelengths of

0.4-2.4 km (Figure 5.2b). This wave field has been formed by unconfined turbidity currents originating on the northern slopes of La Palma. The El Julan wave field lies within a channel on the south-west flank of El Hierro. The sediment waves have an average wavelength of 0.8 km, wave heights of about 6 m, and have been formed by channelised turbidity currents.

The Madeira Turbidity Current Pathway (MTCP)

The MTCP is the largest in the study area with a total length of 1500 km. It transports sediments derived from the Moroccan margin and the Canary Islands, westwards to the Agadir Basin and the Madeira Abyssal Plain. In this section we summarise previously published data from this pathway and combine it with new data collected during RRS Discovery cruise 225. This has allowed us to investigate the key controls on sand distribution within the system (see Discussion).

The MTCP originates on the northern edge of the Morocco Shelf, as a series of straight tributary canyons at the shelf-break, offshore from the hinterland of the Atlas Mountains. These canyons merge into one major canyon, the Agadir Canyon, on the continental slope. The Agadir Canyon is about 460 km long, 5-15 km wide and 600-1500 m deep. It is slightly meandering (Jacobi and Hayes, 1992), and runs roughly perpendicular to the regional slope, its morphology being largely controlled by the adjacent salt diapirs and volcanic seamounts. Levees are well developed in its lower reaches, before it broadens out on the lower rise at a water depth of 4275 m. A channel system then runs onto the Agadir Basin below 4300 m (Ercilla *et al.*, 1998).

The Agadir Basin (Figure 5.3) is a large intraslope basin lying at a water depth of 4275-4450 m. It has an area of 22,000 km^2 and is almost flat, having a gradient of just 0.02°. Three cores recovered from the basin during RRS Discovery cruise 225 contain a sequence of turbidite sands, silts and muds, interbedded with pelagic/hemipelagic marls, oozes and clays (Figure 5.3). The results of an initial investigation of these cores are summarised as follows: *Core D13072* is 8 m long and was recovered from the north-east edge of the basin. It contains nine turbidites with a sand/mud ratio of 20:80, and a maximum sand-bed thickness of 56 cm. *Core D13070* is 10 m long and was recovered from the western basin floor. It contains nine turbidites with a sand/mud ratio of 10:90, and a maximum sand-bed thickness of 26 cm. *Core D13071* is 12 m long and was taken

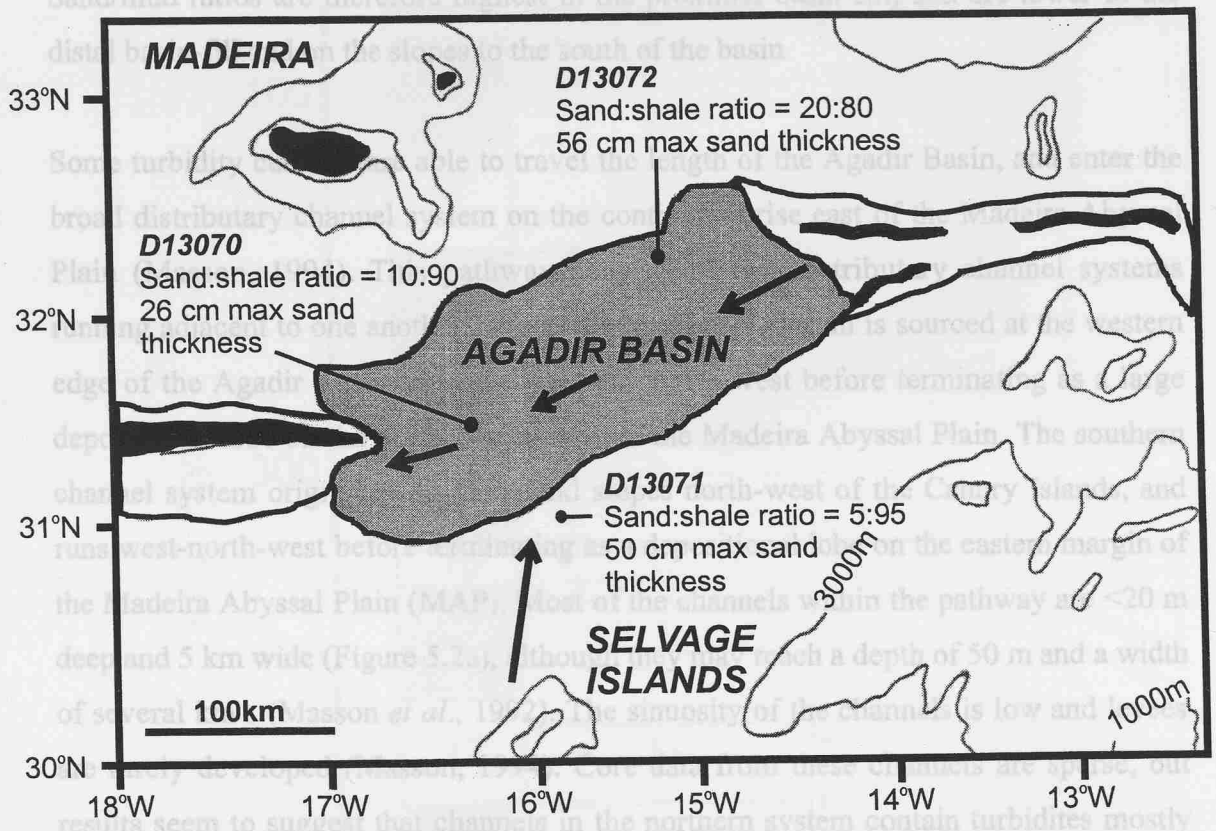

Figure 5.3: Turbidite sand distribution in the Agadir Basin. The sand/shale ratio for three cores are shown, together with the maximum sand-bed thickness in each core. Note that the core on the eastern plain, closest to the mouth of the Agadir Canyon, has the highest sand/shale ratio and the thickest sand. Stippled areas are turbidity current pathways. Channels shown in black. Arrows indicate main transport directions for turbidites on the plain.

through a sediment wave field on the lower rise, 100 m above the basin floor. This core contains 15 turbidites with a sand/mud ratio of 5:95, and a maximum sand-bed thickness of 50 cm. The provenance of these turbidites has yet to be determined. Sand/mud ratios are therefore highest in the proximal basin-fill, and are lower in the distal basin-fill and on the slopes to the south of the basin

Some turbidity currents are able to travel the length of the Agadir Basin, and enter the broad distributary channel system on the continental rise east of the Madeira Abyssal Plain (Masson, 1994). This pathway consists of two distributary channel systems running adjacent to one another. The northern channel system is sourced at the western edge of the Agadir Basin and runs west and north-west before terminating as a large depositional lobe on the north-east margin of the Madeira Abyssal Plain. The southern channel system originates on the island slopes north-west of the Canary Islands, and runs west-north-west before terminating as a depositional lobe on the eastern margin of the Madeira Abyssal Plain (MAP). Most of the channels within the pathway are <20 m deep and 5 km wide (Figure 5.2a), although they may reach a depth of 50 m and a width of several km s (Masson *et al.*, 1992). The sinuosity of the channels is low and levees are rarely developed (Masson, 1994). Core data from these channels are sparse, but results seem to suggest that channels in the northern system contain turbidites mostly derived from the Moroccan margin (via the Agadir Basin), and that the volcaniclastic turbidites in the southern channel system are derived from the Canary Islands. Overall, there appears to be increased sand deposition within the channels, as opposed to the interchannel areas (Masson, 1994). However, it should be noted that large turbidity currents (e.g. the 'b' turbidite of Masson, 1994) can flush out much of the sediment from within the channels on their passage downslope. At the present-day the channels therefore appear to be part of a bypassing system, and are dominantly acting as sediment conduits for turbidity currents travelling downslope to the Madeira Abyssal Plain.

The Madeira Abyssal Plain (MAP) is the largest abyssal plain in the study area, covering an area of 68,000 km^2 (Rothwell *et al.*, 1992). It is extremely flat, with a slope of less than 0.01°, and a surface relief varying by less than 10 m (Searle, 1987). Cores recovered from the plain have revealed that the ratio of turbiditic to pelagic sediments is approximately 10:1, with the sedimentary record over the last 300,000 years revealing

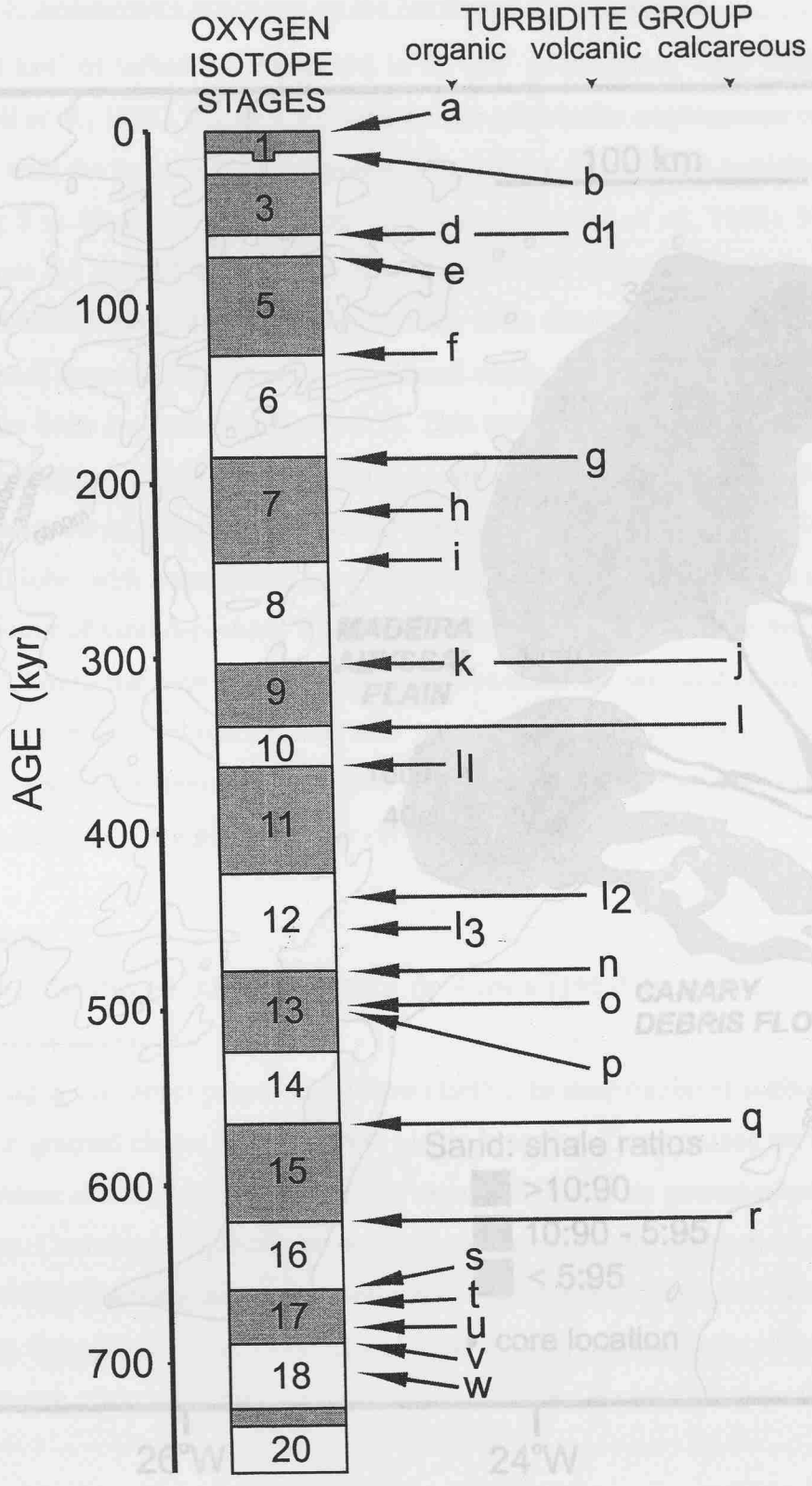

Figure 5.4: Schematic diagram showing the age of turbidite emplacement on the Madeira Abyssal Plain, in relation to the oxygen isotope timescale (from Weaver et al., 1992). Three distinct subgroups of turbidites can be recognised, derived from the Northwest African margin (organic), the Canary Islands (volcanic), and seamounts to the west of the plain (calcareous).

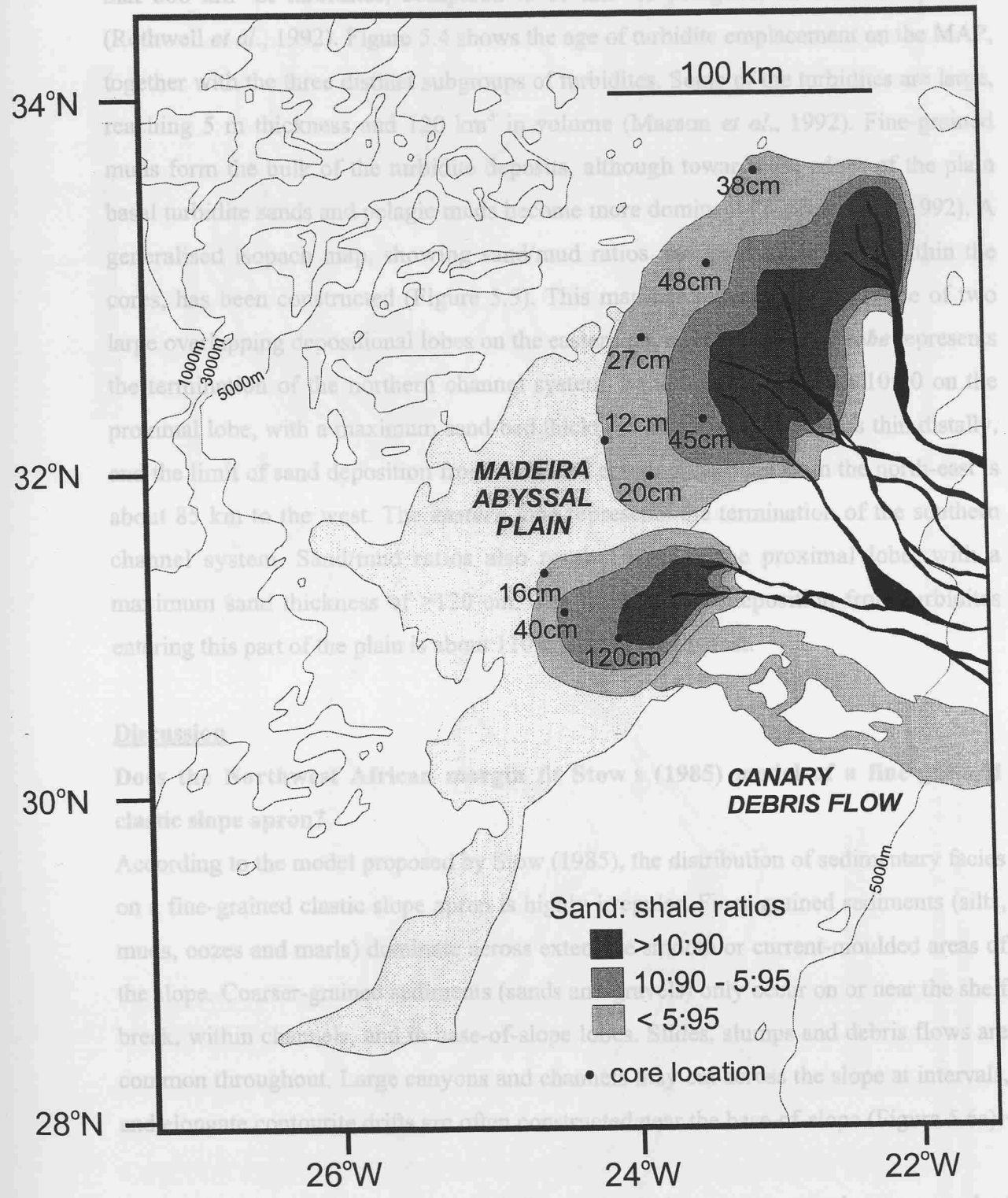

Figure 5.5: Turbidite sand distribution on the Madeira Abyssal Plain. Shaded contours show the overall turbidite sand/shale ratios in the cores shown. The thickness of the 'b' turbidite in these cores is also displayed. Note that the sand distribution is closely controlled by the break-of-slope at the base of the lower rise, and that the sands appear to form distinct lobes at the termination of the channel systems.

that 600 km^3 of turbidites, compared to 60 km^3 of pelagites, have been deposited (Rothwell *et al.*, 1992). Figure 5.4 shows the age of turbidite emplacement on the MAP, together with the three distinct subgroups of turbidites. Some of the turbidites are large, reaching 5 m thickness and 120 km^3 in volume (Masson *et al.*, 1992). Fine-grained muds form the bulk of the turbidite deposits, although towards the edges of the plain basal turbidite sands and pelagic muds become more dominant (Weaver *et al.*, 1992). A generalised isopach map, showing sand/mud ratios and sand thicknesses within the cores, has been constructed (Figure 5.5). This map has revealed the presence of two large overlapping depositional lobes on the eastern plain. The ***north-east lobe*** represents the termination of the northern channel system. Sand/mud ratios reach 10:90 on the proximal lobe, with a maximum sand-bed thickness of >50 cm. The sands thin distally, and the limit of sand deposition from turbidites entering the plain from the north-east is about 85 km to the west. The ***eastern lobe*** represents the termination of the southern channel system. Sand/mud ratios also reach 10:90 on the proximal lobe, with a maximum sand thickness of >120 cm. The limit of sand deposition from turbidites entering this part of the plain is about 110 km to the north-west.

Discussion

Does the Northwest African margin fit Stow s (1985) model of a fine-grained clastic slope apron?

According to the model proposed by Stow (1985), the distribution of sedimentary facies on a fine-grained clastic slope apron is highly irregular. Finer-grained sediments (silts, muds, oozes and marls) dominate across extensive smooth or current-moulded areas of the slope. Coarser-grained sediments (sands and gravels) only occur on or near the shelf break, within channels, and in base-of-slope lobes. Slides, slumps and debris flows are common throughout. Large canyons and channels may cut across the slope at intervals, and elongate contourite drifts are often constructed near the base-of-slope (Figure 5.6a).

The model also states that a typical fine-grained slope apron may be composed of constructional elements, erosional elements, or a combination of both. Constructional elements display a relatively smooth convex-concave profile, built upwards and outwards by slope progradation. Low-energy conditions dominate, and the slope tends to be smooth or current-moulded. Erosional elements are heavily affected by erosion (slumping, sliding, etc.) on the face of the slope, causing a steeper and more irregular

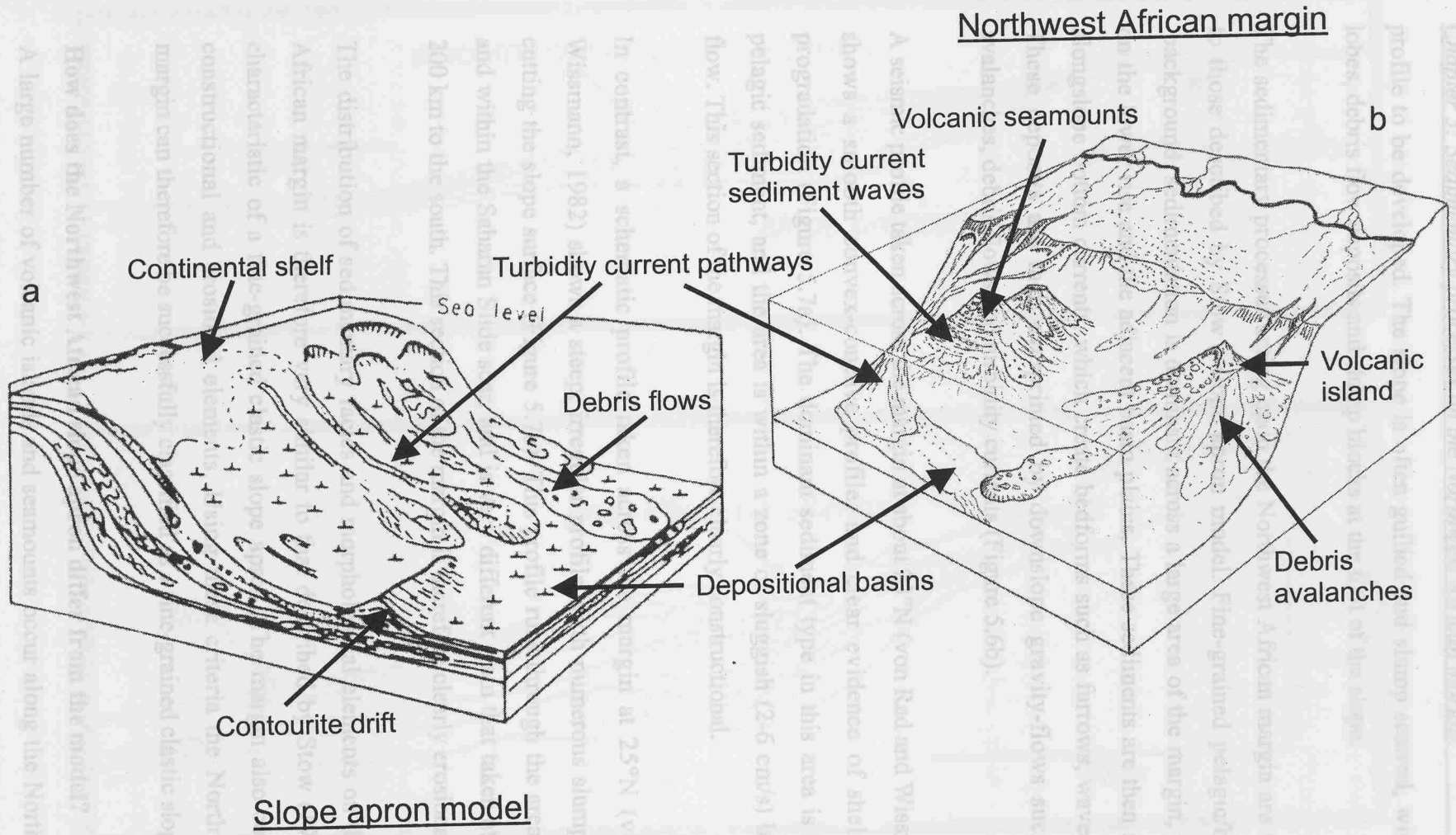

Figure 5.6: Sedimentary environment models showing the schematic distribution of sedimentary facies and morphological elements. (a) the Stow (1985) model of a fine-grained clastic slope apron (b) the Northwest African slope apron. Not to scale.

profile to be developed. The slope is often gullied and slump scarred, with sediment lobes, debris flow deposits and slump blocks at the foot of the slope.

The sedimentary processes acting upon the Northwest African margin are very similar to those described by Stow s slope apron model. Fine-grained pelagic/hemipelagic background sedimentation is dominant across a large area of the margin, particularly on the lower rise and the adjacent basin plains. These sediments are then modified by alongslope bottom currents, which create bedforms such as furrows, waves and drifts. These deposits are then overprinted by downslope gravity-flows such as debris avalanches, debris flows and turbidity currents (Figure 5.6b).

A seismic profile taken across the margin at about 23°N (von Rad and Wissmann, 1982) shows a smooth convex-concave profile, and clear evidence of shelf and slope progradation (Figure 5.7a). The dominant sediment type in this area is fine-grained pelagic sediment, and the area is within a zone of sluggish (2-6 cm/s) bottom water flow. This section of the margin is therefore clearly constructional.

In contrast, a schematic profile taken across the margin at 25°N (von Rad and Wissmann, 1982) shows a steep, irregular profile, with numerous slumps and slides cutting the slope surface (Figure 5.7b). This profile runs through the area lying above and within the Saharan Slide scar, and is very different from that taken at 23°N, some 200 km to the south. This section of the margin is therefore clearly erosional.

The distribution of sedimentary facies and morphological elements on the Northwest African margin is therefore very similar to that described by Stow (1985) as being characteristic of a fine-grained clastic slope apron. The margin also comprises both constructional and erosional elements. Using these criteria the Northwest African margin can therefore be successfully classified as a fine-grained clastic slope apron.

How does the Northwest African slope apron differ from the model?

A large number of volcanic islands and seamounts occur along the Northwest African margin, and in some areas this leads to a more complex distribution of sedimentary facies than is accounted for by Stow's slope apron model.

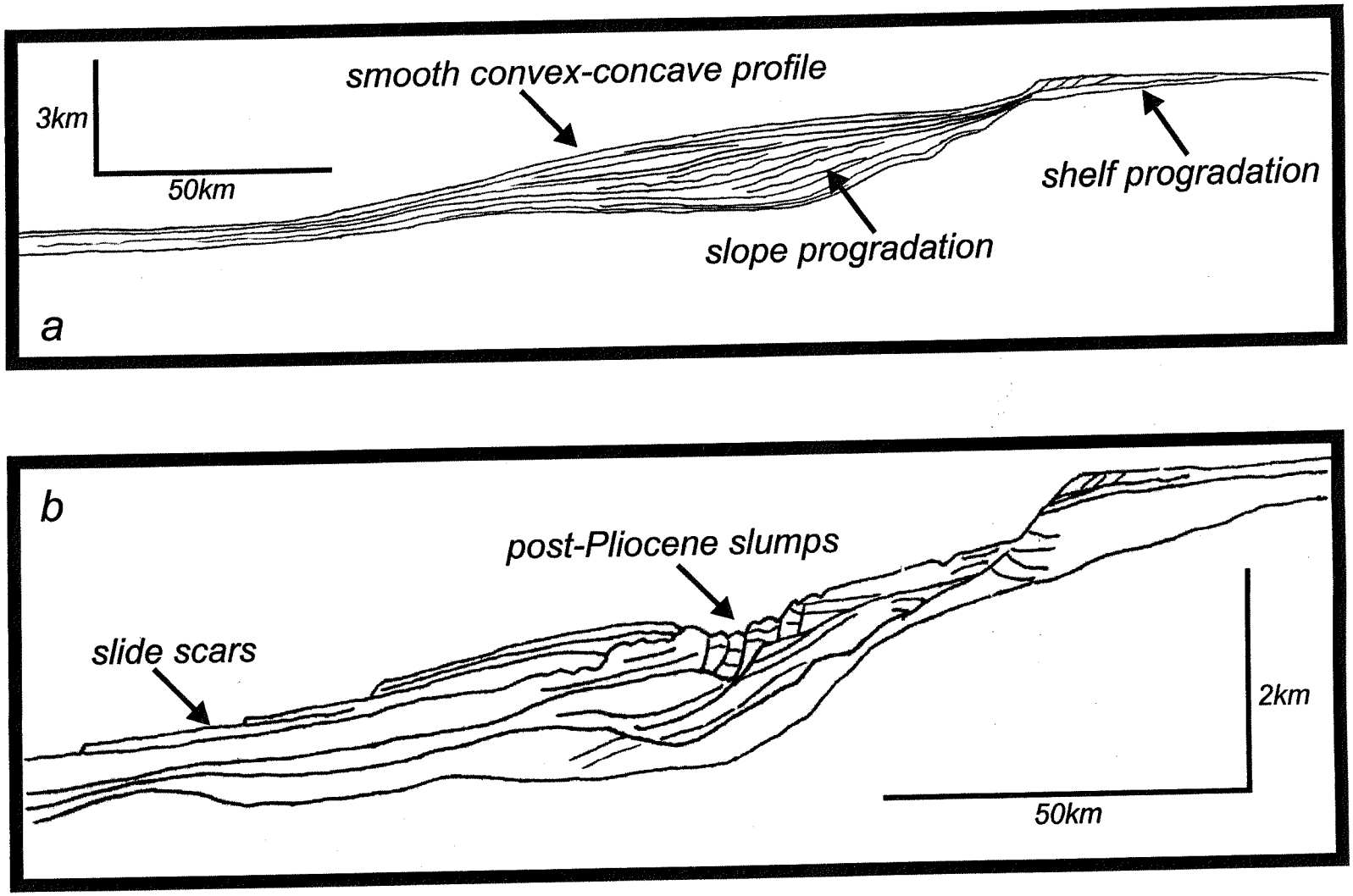

Figure 5.7: Schematic profiles of the continental margin off Western Sahara (modified from von Rad and Wissmann (1982)). (a) Profile from about 23°N showing a constructional section of the margin. Note the smooth convex-concave profile, and evidence of shelf and slope progradation (b) Profile from about 25°N showing an erosive section of the margin. Note the steep, irregular profile, and the numerous slumps and slides cutting the slope surface.

Most of the volcanic islands, and some of the larger seamounts, have a radial distribution of downslope flows around their flanks. The Canary Islands, for example, act as nuclei for a large number of gravity-flows (Figure 5.1). These include debris avalanches, debris flows, and turbidity current pathways. In some areas, the volcanic islands and seamounts are also responsible for disrupting and diverting the bottom water flow, leading to a more complex distribution of current-induced bedforms. For example, accelerated bottom water flow around and between the Saharan Seamounts has led to the development of erosional furrows (Jacobi and Hayes, 1992). In addition, the diversion of bottom currents around the Madeira archipelago has led to the development of sediment wave fields on the Madeira Rise (Jacobi and Hayes, 1992).

It is therefore important to note that seafloor topographic features, (e.g. volcanic islands and seamounts, salt diapirs, and tectonic features such as fault scarps) can have a significant effect on the distribution of sedimentary facies and morphological elements within a slope apron system (Figure 5.6b). This has important implications for hydrocarbon exploration in similar systems.

Sand distribution on the Northwest African slope apron

The Northwest African margin is dominated by fine-grained sediments, however, sands do occur above the shelf-break, in distributary channels on the slope and rise, and on flat basin floors. In this section we describe the key controls on sand distribution within the system, by linking onshore and offshore sediment transport pathways, and analysing core data from the Madeira Turbidity Current Pathway.

Onshore and offshore drainage systems

Sand distribution beyond the shelf break on the Northwest African margin is largely restricted to TCP s. In this section we investigate the relationship between fluvial input and canyon development along the margin, and discuss some of the other controls on the location of TCP s.

On the Moroccan margin a number of seasonal rivers transport sediments derived from the hinterland of the Atlas Mountains to the continental shelf. At the shelf break numerous canyons then transport this material to the Seine Abyssal Plain and the Agadir Basin/Madeira Abyssal Plain (Figure 5.1). A comparison of onshore river systems and

offshore bathymetry indicates a general spatial relationship between fluvial input points and the location of canyon heads at the shelf break. Therefore, the location of canyon heads on the Moroccan margin appears to be influenced by fluvial drainage. In deeper water, on the lower slope and rise, the location of canyons and channels tends to be controlled by the pre-existing topography (seamounts and volcanic islands).

Further south, on the Western Saharan margin, the fluvial input is greatly reduced. The only river systems that reach the sea are seasonal, and the majority of the margin has no fluvial input at all. This indicates that submarine canyon development on this margin, e.g. the Western Saharan Canyon System, is controlled by other factors, such as tectonic activity. The large Saharan Debris Flow is, however, sourced from this margin, and its location is controlled by a number of factors. A combination of low terrigenous sediment input and the location of the Saharan seamounts appear to inhibit development of linear turbidity current pathways. Seismicity on this margin is rare, so sediments have a long residence time on the shelf and slope. Therefore when a rare trigger event does occur it will lead to major slope failure, such as the Saharan Debris Flow.

On the Senegalese margin the fluvial input is dominated by the Senegal River, which transports sediment to the head of a major turbidity current pathway. Another large turbidity current pathway lies offshore of two seasonal rivers on the Mauritainian margin but little is known about this system (Figure 5.1).

There is therefore some evidence of a general spatial relationship between fluvial input points and TCP s on the Northwest African margin. However, other factors such as slope topography, slope angle, and shelf/slope width are also likely to influence the location of TCP s.

The Madeira Turbidity Current Pathway (MTCP)

Analysis of core data from the Agadir Basin (this study), the Madeira Abyssal Plain (Rothwell *et al.*, 1992; Weaver *et al.*, 1992), and the channel system linking the two (Masson, 1994), has allowed us to assess the major controls on sand deposition within the MTCP.

An initial investigation of cores recovered from the Agadir Basin (Figure 5.3) has revealed that sand/mud ratios are highest in the eastern (proximal) basin-fill, adjacent to the break-of-slope near the mouth of the Agadir Canyon. The sand/mud ratio decreases westwards in the more distal basin-fill, and is also lower on the slopes to the south of the basin. The Agadir Basin is particularly interesting, as it is an intraslope basin containing no channels. Turbidite sands within this system evolve from channelised sand bodies at the mouth of the Agadir Canyon, to sheet sands on the basin floor, and back to channel sands on the rise to the west.

Core data from the channel system to the west of the Agadir Basin is sparse. Channels in the northern system contain turbidites mostly derived from the Moroccan margin (via the Agadir Basin), and the southern channel system contains volcaniclastic turbidites derived from the Canary Islands. Overall, there is increased sand deposition within the channels, as opposed to interchannel areas (Masson, 1994). However, it should be noted that large turbidity currents (e.g. the 'b' turbidite of Masson, 1994) can flush out much of the sediment from within the channels on their passage downslope. At the present-day the channels appear to be part of a bypassing system, and are acting as sediment conduits for turbidity currents travelling downslope to the Madeira Abyssal Plain.

Core data from the Madeira Abyssal Plain (Figure 5.5) indicate that sand deposition is concentrated at the break-of-slope where the distributary channel systems of the lower rise run onto the flat basin floor. The sandy bases of the turbidites die out within 110 km of the break-of-slope. It is possible to calculate the frequency of turbidites reaching the MAP. In the last 750,000 years the deposition rate has averaged one turbidite every 30,000 years (Weaver *et al.*, 1992). Further investigation reveals that only one turbidite every 150,000 years has reached the MAP from the Moroccan margin via the Madeira TCP. This compares with one turbidite every 14,000 years for the Seine Abyssal Plain (Davies *et al.*, 1997), and 1 - 3 turbidites every 1000 years for the Horseshoe Abyssal Plain (Lebreiro *et al.*, 1997). Turbidites on the MAP are generally deposited at times of climate/sea-level change at isotope stage boundaries (Figure 5.4), and are therefore not linked to lowstands or highstands of sea level (Weaver *et al.*, 1992).

To summarise, major turbidity current events within the MTCP are relatively infrequent, and tend to occur during periods of climate/sea-level change. Sand/mud

ratios within the system are highest adjacent to the break-of-slope, the location of which is controlled by the position of volcanic islands and seamounts. Sand bodies pass distally from channel sands to sheet sands and back to channel sands again, in response to variations in topography. Under these topographic conditions, substantial sand depocentres can occur far from the continental slope.

Conclusions

The Northwest African continental margin is a typical fine-grained clastic slope apron, with pelagic/hemipelagic background sedimentation overprinted by downslope gravity flows and modified by alongslope bottom currents. The slope apron is made up of various architectural elements, and consists of both constructional and erosional sections. The pattern of sedimentation on this margin is made more complex by the presence of numerous volcanic islands and seamounts. These act as nuclei for gravity flows, and as a diversion for bottom currents.

Turbidity currents are relatively infrequent on this margin, and occur during periods of climate/sea-level change. Turbidite sand deposition is largely controlled by the position of the break-of-slope, which in turn is often controlled by the location of adjacent volcanic islands and seamounts. Under the appropriate topographic conditions, substantial sand depocentres can occur far from the continental slope. The Northwest African slope apron may be a useful modern analogue for deep-water hydrocarbon prospects with complex seafloor topography.

Acknowledgements

The data used in this paper were collected on a number of research cruises of the RRS Discovery and the RRS Charles Darwin, and we gratefully acknowledge the contributions of their respective masters and crews. RBW would like to acknowledge the provision of PhD. funding from the University of Southampton and the Southampton Oceanography Centre Challenger Division. The two anonymous reviewers and Mike Mayall are thanked for their comments, which helped to improve this paper.

5.3: Summary

This study has revealed that the Northwest African margin shows many characteristics that are typical of a slope apron system. However, it has also shown that complex seafloor topography can have a significant effect upon the distribution of sedimentary processes, and distorts the idealised pattern suggested by the slope apron model. The importance of downslope gravity flows has also been highlighted, as have some of the controls on sand body distribution and morphology.

The next chapter will build upon this work by focussing on the turbidite systems of the Northwest African margin, in an attempt to understand further the controls on the distribution, dimensions and timing of deposition of turbidite sand bodies on a non-glaciated margin.

CHAPTER 6

TURBIDITE DEPOSITIONAL ARCHITECTURE ON THE NORTHWEST AFRICAN MARGIN

6.1: Introduction and aims

A large number of studies have concentrated on turbidity current pathways and deposits on the Northwest African margin, but as yet none have focussed on the controls on sand body distribution and dimensions. In this study, the Moroccan Turbidite System (referred to as the MTCP in the previous chapter) is described in detail from source-to-sink. This has been made possible by the extensive coring undertaken on this system, which contains two abyssal plains and an intraslope basin connected by distributary channels. The principal aims of this chapter are to correlate individual turbidites across the whole system, and look at the controls on sand body characteristics, turbidite provenance and timing of trigger events.

6.2: Paper 3

Turbidite depositional architecture across three interconnected deep-water basins on the Northwest African margin

Russell B Wynn, Philip P E Weaver, Dorrik A V Stow and Douglas G Masson

SOES/Challenger Division, Southampton Oceanography Centre, European Way, Southampton, SO14 3ZH, UK

This paper was submitted to Sedimentology in May 2000.

Abstract

The Moroccan Turbidite System (MTS) on the Northwest African margin extends 1500 km from the head of the Agadir Canyon to the Madeira Abyssal Plain, making it one of the longest turbidite systems in the world. The MTS consists of three interconnected deep-water basins, the Seine Abyssal Plain, the intraslope Agadir Basin, and the Madeira Abyssal Plain, connected by a network of distributary channel systems. Excellent core control has enabled individual turbidites to be correlated between all three basins, giving a detailed insight into the turbidite depositional architecture of a system with multiple source areas and complex morphology. Large-volume (>100 km^3) turbidites, sourced from the Morocco Shelf, show a relatively simple architecture in the two deepest basins, the Madeira and Seine Abyssal Plains. Sandy bases form distinct lobes or wedges that thin rapidly away from the break-of-slope, and are overlain by extensive basin-wide muds. However, in the intraslope Agadir Basin the turbidite fill is more complex, due to a combination of multiple source areas (Morocco Shelf, Canary Islands, Western Sahara slope, and the Casablanca Seamount) and large variations in turbidite volume. Very large turbidity currents (>250km^3 of sediment) deposit most of their sandy bedload within the intraslope basin but still have sufficient energy to carry most of the mud fraction 500 km further downslope to the Madeira Abyssal Plain (MAP). Large turbidity currents (100-150 km^3 of sediment) deposit most of the sand and mud fraction within the intraslope basin, but still have sufficient energy to transport some of their load westwards to the MAP. Small turbidity currents (<30 km^3 of sediment) are wholly confined within the intraslope basin and pinch out on the basin floor.

Turbidity currents flowing beyond the Agadir Basin pass through a large distributary channel system. Individual turbidites correlated along this channel system show major variations in sand fraction mineralogy, whereas the mud fraction geochemistry and micropalaeontology remain similar. This is interpreted as evidence for flow separation, with a sand-rich basal layer confined within the channel system, overlain by an unconfined layer of suspended mud.

Large-volume turbidites within the MTS were deposited at oxygen isotope stage boundaries, during periods of rapid sea-level change. This contrasts with the classic fan model, which suggests that most turbidites are deposited during lowstands of sea level.

In addition, the three largest turbidites on the MAP were deposited during the largest fluctuations in sea level, suggesting a link between the volume of sediment input and the magnitude of sea level change.

Introduction and aims

The Northwest African continental margin has for many years been the focus of intensive research into modern deep-water sedimentary processes. For example, on the Madeira Abyssal Plain (MAP) a total of over 160 sediment cores have been recovered, allowing detailed correlation of the late Quaternary turbidite sequence (Rothwell at al., 1992; Weaver & Rothwell, 1987; Weaver et al., 1992). In addition, the timing and source area of turbidites on the MAP has been investigated in detail, revealing that turbidites deposited since the mid-Miocene are sourced from three main areas: the Northwest African margin, the volcanic Canary Islands, and seamounts to the west of the plain (Figure 6.1) (Weaver & Kuijpers, 1983; de Lange et al., 1987; Pearce & Jarvis, 1992; Weaver et al., 1998). Further research by Masson (1994), Davies et al. (1997), and Ercilla et al. (1998) has given some insight into the transport direction of turbidites derived from the Moroccan margin and Canary Islands. However, a more detailed knowledge of turbidity current pathways onto the MAP from these source areas has only recently been established (Wynn et al., 2000a). A major pathway for turbidites derived from the Moroccan margin and Canary Islands can now be traced from source to sink, and has been termed the Moroccan Turbidite System (MTS).

Long runout turbidite systems, in which turbidity currents travel over distances >1000 km, have only rarely been documented by previous research (e.g. Bengal Fan, Emmel & Curray, 1985; Indus Fan, Kolla & Coumes, 1985; Northwest Atlantic Mid-Ocean Channel, Hesse et al., 1987; 1996). In the MTS, turbidity currents transport sediments derived from the Atlas Mountains up to 1500 km before deposition on the MAP, making this one of the longest turbidite systems in the world (Wynn et al., 2000a). However, unlike most other long runout systems, the MTS has been extensively cored, and individual turbidites can be correlated across its entire length. This gives an unprecedented insight into the proximal-to-distal variations in depositional architecture of turbidites within a long runout system. The MTS is also unique because in this topographically complex area turbidity currents derived from one source can deposit a single turbidite across three different interconnected basins. The excellent core control

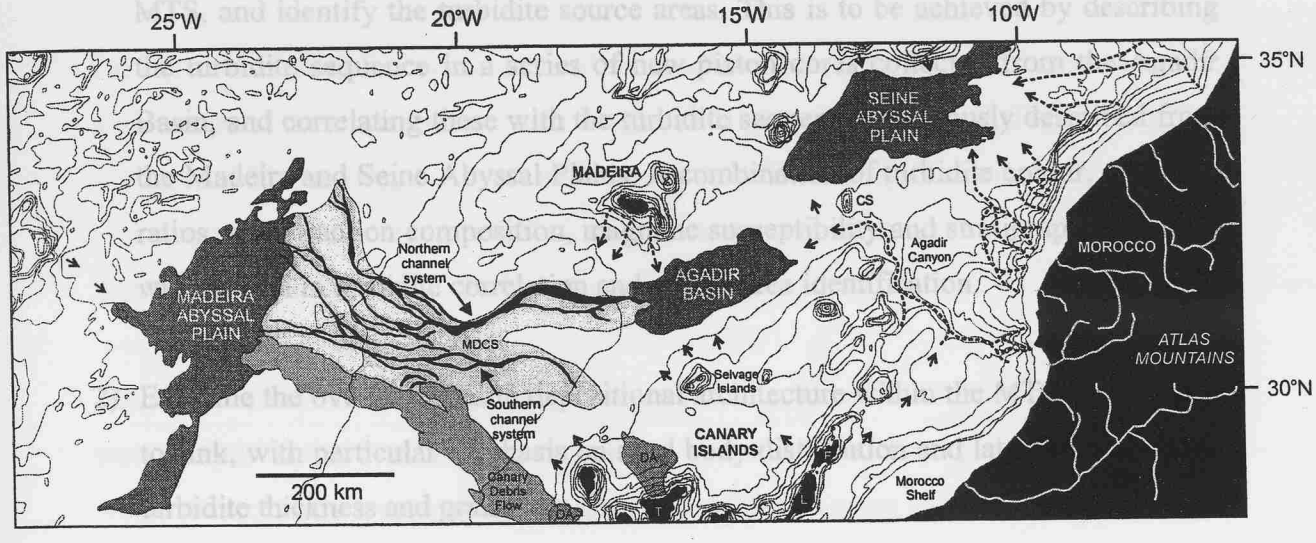

Figure 6.1: Location map showing the main features of the Moroccan Turbidite System. Principal transport directions for turbidity currents are shown by arrows and dashed lines. CS = Casablanca Seamount, DA = Debris Avalanche, MDCS = Madeira Distributary Channel System, T = Tenerife, L = Lanzarote, F = Fuerteventura.

in this area therefore also provides new insights into the distribution and thickness of sand bodies in a turbidite system with complex seafloor topography.

Therefore, the principal aims of this study are to:

1) Correlate individual turbidites between three different depositional basins within the MTS, and identify the turbidite source areas. This is to be achieved by describing the turbidite sequence in a series of new piston cores collected from the Agadir Basin, and correlating these with the turbidite sequences previously described from the Madeira and Seine Abyssal Plains. A combination of turbidite colour, coccolith ratios, sand fraction composition, magnetic susceptibility and stratigraphic position will be used in turbidite correlation and source area identification.

2) Examine the overall turbidite depositional architecture within the MTS from source to sink, with particular emphasis on sand body distribution and lateral variations in turbidite thickness and grain-size.

3) Interpret turbidity current flow processes using a combination of sedimentary structures and mineralogical data.

4) Investigate the controls on the timing of turbidite deposition and attempt to identify possible trigger mechanisms.

Morphology of the Moroccan Turbidite System (MTS)

The MTS originates on the Moroccan margin, before running westwards between the Canary and Madeira archipelagos and terminating on the MAP (Figure 6.1). It has a total length of 1500 km, and its morphology is largely controlled by the position of volcanic islands, seamounts and salt diapirs (Wynn et al., 2000a). The MTS has been classified as a turbidity current pathway (Wynn et al., 2000a), although it could also be argued that it is a morphologically complex form of elongate fan (e.g. Stow, 1985; Reading and Richards, 1994). It is longitudinally extended perpendicular to the margin, has a broad head region at the top of the main Agadir Canyon, a complex distributary channel system, and large terminal lobes constructed at channel terminations on the MAP. The complex morphology of the MTS is responsible for additional features not

accounted for by standard fan models, such as the intraslope Agadir Basin and the multiple input points.

The MTS can be subdivided into five main morphological segments: the Agadir Canyon, the Agadir Basin, the Seine Abyssal Plain, the Madeira Distributary Channel System, and the Madeira Abyssal Plain:

The Agadir Canyon lies at the edge of the northern Morocco Shelf, offshore from the termination of the Sous River, which drains the High Atlas hinterland (Figure 6.1). The canyon is 460 km long, 5-15 km wide and 600-1500 m deep, and opens out onto the lower rise at a water depth of 4250 m before passing westwards into the flat-lying Agadir Basin (Ercilla et al., 1998).

The Agadir Basin is a large intraslope basin with an area of 38,000 km^2 and a maximum water depth of 4450 m (Figure 6.1). From the mouth of the Agadir Canyon to the western basin margin the average gradient is just 0.02° (Figure 6.2). The Agadir Basin is separated from the *Seine Abyssal Plain (SAP)* to the north-east by an intrabasinal sill. This sill varies in height from 40-130 m, and is composed of interbedded turbidites and pelagic/hemipelagic sediments lying upon flat acoustic basement (Davies et al., 1997). To the north and south it is bordered by the volcanic archipelagos of the Madeira and Canary/Selvage Islands. At the western edge of the basin the head of a broad distributary channel system correlates with a small increase in slope gradient.

The Madeira Distributary Channel System (MDCS) on the continental rise east of the MAP can be subdivided into two major channel systems. The northern channel system runs west and then north-west from the edge of the Agadir Basin before terminating on the north-east margin of the MAP. The southern channel system runs west-north-west from the submarine slopes of the Canary Islands before terminating on the eastern margin of the MAP (Masson, 1994) (Figure 6.1). Channel dimensions and spacing are strongly controlled by gradient (Figure 6.2). Broad, shallow channels occur in the central braided section of the channel system, on slopes of 0.05°. The deepest channels, which are up to 50 m deep, occur in the adjacent deeply incised sections, on steeper slopes of 0.11° - 0.14° (Masson, 1994).

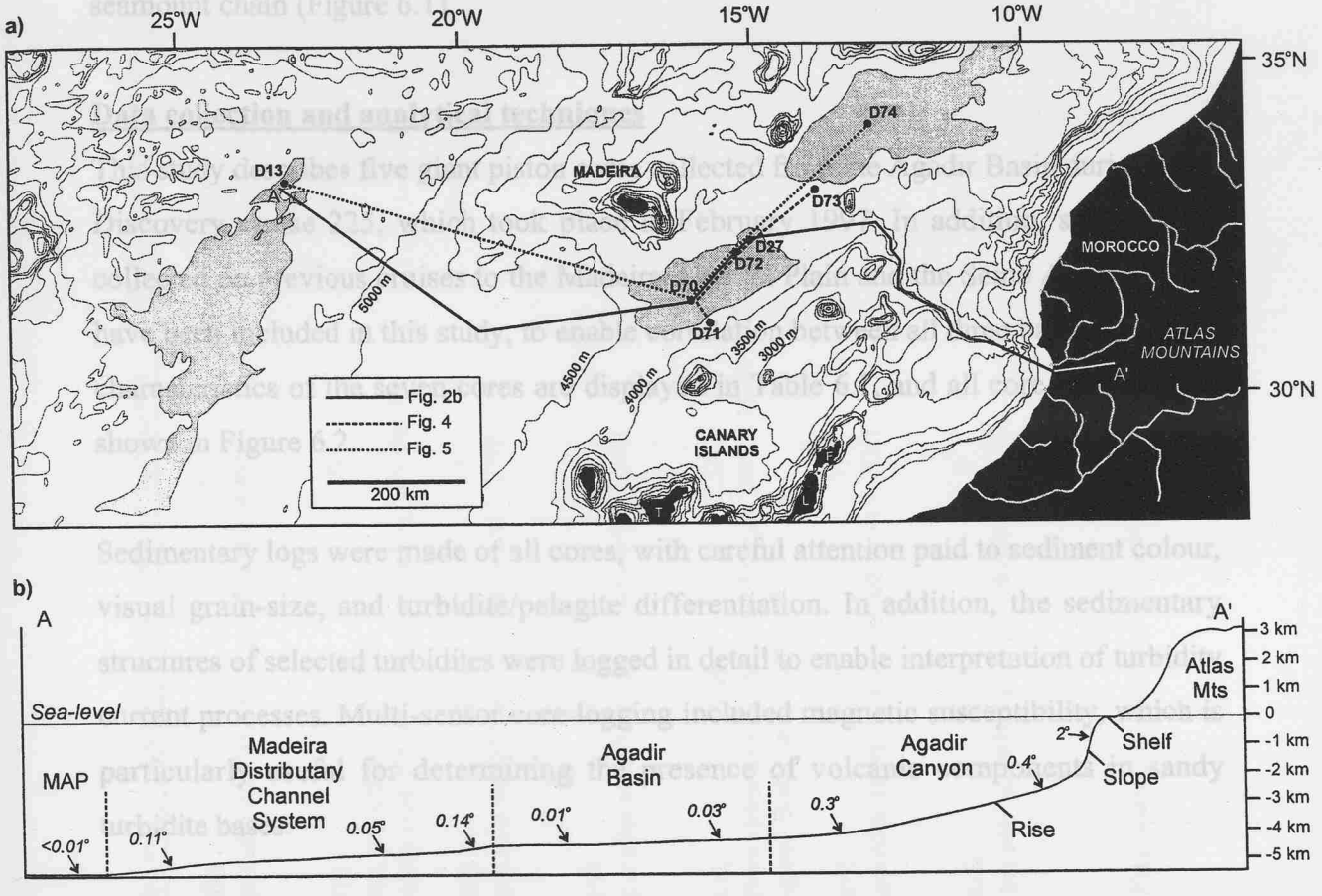

Figure 6.2: (a) Location map showing core locations (D74 etc.), lines of cross-section and core correlation, and bathymetry of the study area. Bathymetric contours spaced at 500 m intervals (b) Cross-section A-A' showing the variations in slope angle across the Moroccan Turbidite System. Note the change in gradient between the almost flat Agadir Basin and the head of the Madeira Distributary Channel System.

The Madeira Abyssal Plain (MAP) covers an area of 68,000 km^2, lies at a water depth of 5400 m, and has an overall gradient of less than 0.01° (Rothwell et al., 1992, Searle, 1987). The MAP marks the western limit for turbidites transported downslope along the MTS, as its western boundary is bordered by the Great Meteor-Hyeres-Cruiser seamount chain (Figure 6.1).

Data collection and analytical techniques

This study describes five giant piston cores collected from the Agadir Basin during RRS Discovery cruise 225, which took place in February 1997. In addition, single cores collected on previous cruises to the Madeira Abyssal Plain and the Seine Abyssal Plain have been included in this study, to enable correlation between all three basins. The key characteristics of the seven cores are displayed in Table 6.1, and all core locations are shown in Figure 6.2.

Sedimentary logs were made of all cores, with careful attention paid to sediment colour, visual grain-size, and turbidite/pelagite differentiation. In addition, the sedimentary structures of selected turbidites were logged in detail to enable interpretation of turbidity current processes. Multi-sensor core logging included magnetic susceptibility, which is particularly useful for determining the presence of volcanic components in sandy turbidite bases.

Analysis of turbidite sand mineralogy was carried out in an attempt to understand more about the provenance of individual turbidites, and as an aid to correlation. Approximately one cm^3 of sediment was sampled from each sandy turbidite base and bathed in 10% acetic acid. This removed the majority of the carbonate fraction as only terrigenous clastic sediments were to be analysed. All samples were then wet sieved and divided into seven grain size classes from 63 μm to >500 μm. The main mineral constituents in every grain size class were recorded, and 300 individual grains point-counted and identified for the following grain size classes: very fine sand (63-90 μm), fine sand (125-180 μm), medium sand (250-355 μm) and coarse sand (> 500 μm).

A micropalaeontological technique developed by Weaver (1994) has been used for dating and correlation of turbidites in the cores. In this technique, the ratios of different

Core no.	Core location (lat + long)	Depth (m)	Length (cm)	No. of turbidites	Turbidite/pelagite ratio	Sand/mud ratio
D70	31°30'N/16°12'W	4404	1061	13	71:29	16:84
Echofacies: Continuous flat subbottom reflectors, parallel stratification, penetration = 40m						
Environment: Western Agadir Basin floor						
D71	31°07'N/15°51'W	4311	1201	16	29:71	5:95
Echofacies: Regular undulating subbottom reflectors, penetration = 27m						
Environment: Sediment wave field on lower continental rise 100m above floor of Agadir Basin						
D72	32°23'N/15°17'W	4365	801	11	51:49	19:81
Echofacies: Continuous flat subbottom reflectors, parallel stratification, penetration = 25m						
Environment: Northeast Agadir Basin floor						
D27	32°36'N/15°00'W	4358	376	8	44:56	16:84
Echofacies: Continuous flat subbottom reflectors, parallel stratification, penetration = 25m						
Environment: Northeast Agadir Basin floor						
D73	32°59'N/13°57'W	4315	998	38	57:43	11:89
Echofacies: Slightly undulating, continuous subbottom reflectors on sediment ridge, penetration = 25m						
Environment: Shallow turbiditic levee separating Agadir Basin and Seine AP						
D74	34°00'N/13°00'W	4411	858	17	66:34	13:87
Echofacies: Continuous flat subbottom reflectors, parallel stratification, penetration = 30m						
Environment: Central Seine AP						
D13	33°12'N/23°30'W	5420	1000	9	92:8	13:87
Echofacies: Continuous flat subbottom reflectors, parallel stratification, penetration = 50m						
Environment: Northern Madeira AP						

Table 6.1: Key characteristics of cores used in this study

species of coccoliths (calcareous algae) are analysed in both pelagic layers and the mud fraction of turbidites. This provides a stratigraphic framework and a method of correlating turbidites between cores. The stratigraphic scheme uses both first and last appearance datum levels (FAD's and LAD's), and species abundance data (acmes). Coccoliths show a turnover of dominant species through the Quaternary, with a single species outnumbering all others for a few tens or hundreds of thousands of years before giving way to another dominant species (Thierstein et al., 1977; Weaver 1983). A combination of FAD's, LAD's, and dominance intervals therefore provides a large number of coccolith datum levels in the late Quaternary. For example, within the Brunhes palaeomagnetic interval there are six recognisable coccolith intervals (Weaver, 1993).

The turbidites contain mixtures of coccoliths from more than one isotope stage, since the landslide that caused the turbidity current would have eroded some depth into the seabed. Weaver (1994) showed that this mixture was relatively constant for each turbidite in a range of cores from across the whole Madeira Abyssal Plain, and furthermore that different turbidites had different coccolith mixtures. In this study, individual turbidites have firstly been correlated by their relative stratigraphic positions in each core, and this has then been confirmed by examining the coccolith stratigraphy of the pelagic layers. In addition, the coccolith mixtures within the turbidites themselves have also been analysed.

3.5kHz profiles across several core locations have been included to give an indication of the acoustic facies (Figure 6.3). These profiles are the most important dataset for the description of regional sediment facies distribution. A review of the echofacies characteristics on the Northwest African margin is presented by Masson et al. (1992) and Wynn et al. (2000a).

The turbidite sequence in the Agadir Basin

Detailed correlation of turbidites in the Agadir Basin has allowed a numbering system for individual turbidites to be established. Each turbidite is numbered on the basis of its position within the sedimentary sequence, with *AB1* being at the top and *AB17* at the base. Correlation of individual turbidites between cores is achieved using a combination of turbidite colour, sand composition, magnetic susceptibility, coccolith ratios and

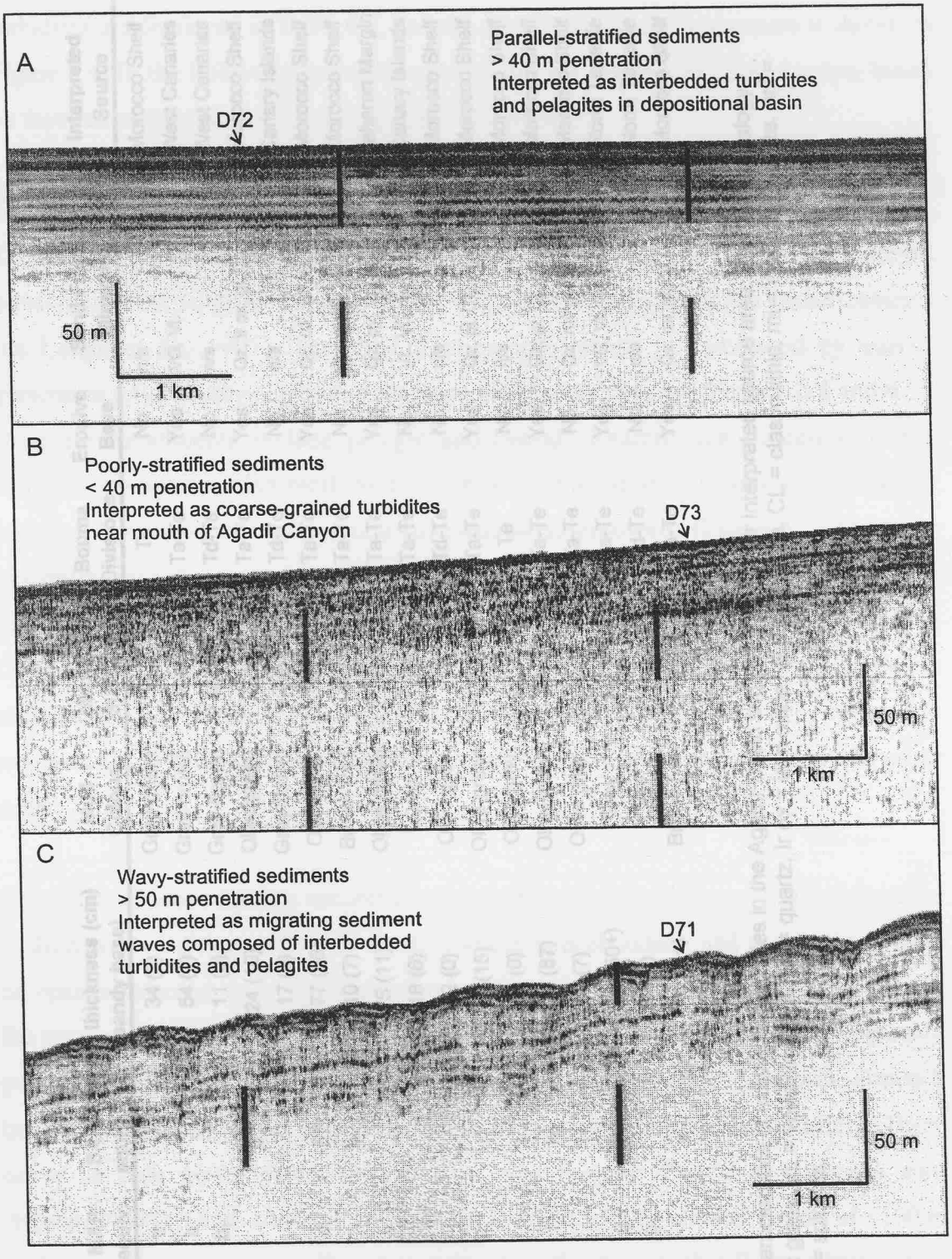

Figure 6.3: 3.5kHz profiles showing the acoustic character of the sea floor at various core localities. A = typical basin-fill facies in the vicinity of core D72, and also typical of cores D13, D70, D27 and D74. B = proximal levee facies in the vicinity of core D73. Note the increase in acoustic stratification, interpreted as due to decreasing sand content, towards the right of the profile. C = migrating sediment wave facies in the vicinity of core D71.

Turbidite number	MAP equiv.	SAP equiv.	Max thickness (cm) (sandy base)	Mud Colour	Magnetic Susc. (SI)	Bouma Divisions	Erosive Base	Sand Fraction Mineralogy	Interpreted Source
1	a		34 (0)	Grey-green	15	Te	No	n/a	Morocco Shelf
2	b		54 (1)	Grey-brown	40-240	Ta-Te	Yes	VG, VL	West Canaries
3	b_1		11 (0)	Grey-brown	40-100	Td-Te	No	n/a	West Canaries
4		d	24 (10)	Olive green	15-20	Ta-Te	Yes	Qz, ir ox, gl, CL, mi	Morocco Shelf
5			17 (0)	Grey-brown	20-30	Td-Te	No	n/a	Canary Islands
6	d	e	177 (66)	Olive grey	15-60	Ta-Te	Yes	Qz, CL, gl, py, dol	Morocco Shelf
7		h	10 (7)	Brown (ox)	15-35	Ta-Te	No	Qz, gl, CL, mi	Morocco Shelf
8	e		75 (11)	Olive green	0-15	Ta-Te	Yes	Qz, py, VG, spi, mi	Saharan Margin
9			18 (6)	Grey	>200	Ta-Te	No	VL, VG, qz	Canary Islands
10			12 (0)	Olive grey	15	Td-Te	No	n/a	Morocco Shelf
11	e_1	i	46 (15)	Olive green	5-20	Ta-Te	Yes	Qz, gl, CL, mi, dol	Morocco Shelf
12		j	34 (0)	Olive grey	0-15	Te	No	n/a	Morocco Shelf
13	f	k	135 (87)	Olive green	15-50	Ta-Te	Yes	Qz, gl, CL, mi, spi	Morocco Shelf
14		l	30 (7)	Olive grey	10-15	Ta-Te	No	Qz, mi, gl, CL	Morocco Shelf
15	g	m	151+ (50+)	Grey	60-290	Ta-Te	Yes	VG, VL, qz, mi, spi	North Tenerife
16	g_1		6 (0)	Grey	>200	Td-Te	No	n/a	North Tenerife
17		n	32+ (3+)	Brown (ox)	15-40	Ta-Te	Yes	Qz, mi, gl, CL, py	Morocco Shelf

Table 6.2: Characteristics of individual turbidites in the Agadir Basin sequence, and their interpreted source area. Key for mineralogy - VG = volcanic glass, VL = volcanic lithics, Qz = quartz, Ir ox = iron oxide, gl = glauconite, CL = clastic lithic, mi = mica, py = pyrite, dol = dolomite, spi = spicules.

position within the stratigraphic sequence. The key characteristics of the Agadir Basin turbidites are displayed in Table 6.2, and the correlated basin-fill sequence is shown in Figure 6.4. In the following description, turbidites are divided into four groups, based on their mineralogy, colour, and magnetic susceptibility:

Group 1 (Morocco Shelf source)

Turbidites *AB1, AB4, AB6, AB7, AB10, AB11, AB12, AB13, AB14* and *AB17* are all olive-green to olive-grey in colour (Table 6.2), indicating high organic matter contents (de Lange et al., 1987). The sand fraction mineralogy is dominated by quartz, glauconite, clastic lithics, pyrite, mica, iron oxide and dolomite (Figures 6.6 and 6.7). Biogenic constituents include pelagic and benthic foraminifera, siliceous sponge spicules, phosphatic fish teeth and vertebrae, echinoid spines, and shallow-water bivalves. Fragments of lignitic wood have also been discovered (Figure 6.7). Magnetic susceptibility values are low, being in the range of 0-50 SI units (Figure 6.5). In addition, a number of turbidites seen in core D73 below *AB15* are also believed to be Group 1 turbidites (Figure 6.4). They are all <40 cm thick and display similar characteristics to the Group 1 turbidites seen higher in the sequence, however, they are not included in the correlated sequence as they are not penetrated by any of the other cores.

Group 1 turbidites contain a number of indicators that suggest they are sourced from the shallow waters of the continental shelf. Glauconite is abundant, and is thought to form on open continental shelves at water depths of 15-500 m (Rothwell, 1989). In addition, the presence of clastic lithic fragments, shallow-water bivalves and lignitic wood also point to a nearshore origin. Further evidence of a shallow-water source for Group 1 turbidites is shown by the presence of certain species of benthic foraminifera. These occur as pale green glauconitized casts, and include *Elphidium crispum* and *Amphistigina sp.*, both of which are found at the present-day in water depths of <150 m (J.W.Murray, pers. comm.). However, it is interesting to note that Summerhayes et al. (1976) suggest that the majority of glauconite and pyrite present on the Morocco Shelf has been derived from Miocene strata outcropping on the outer shelf. Therefore, it seems likely that not all of the shallow-water indicators are representative of modern shelf conditions. Despite this, they still provide good evidence for a Morocco Shelf source for Group 1 turbidites, even if they are derived from outcropping strata on the

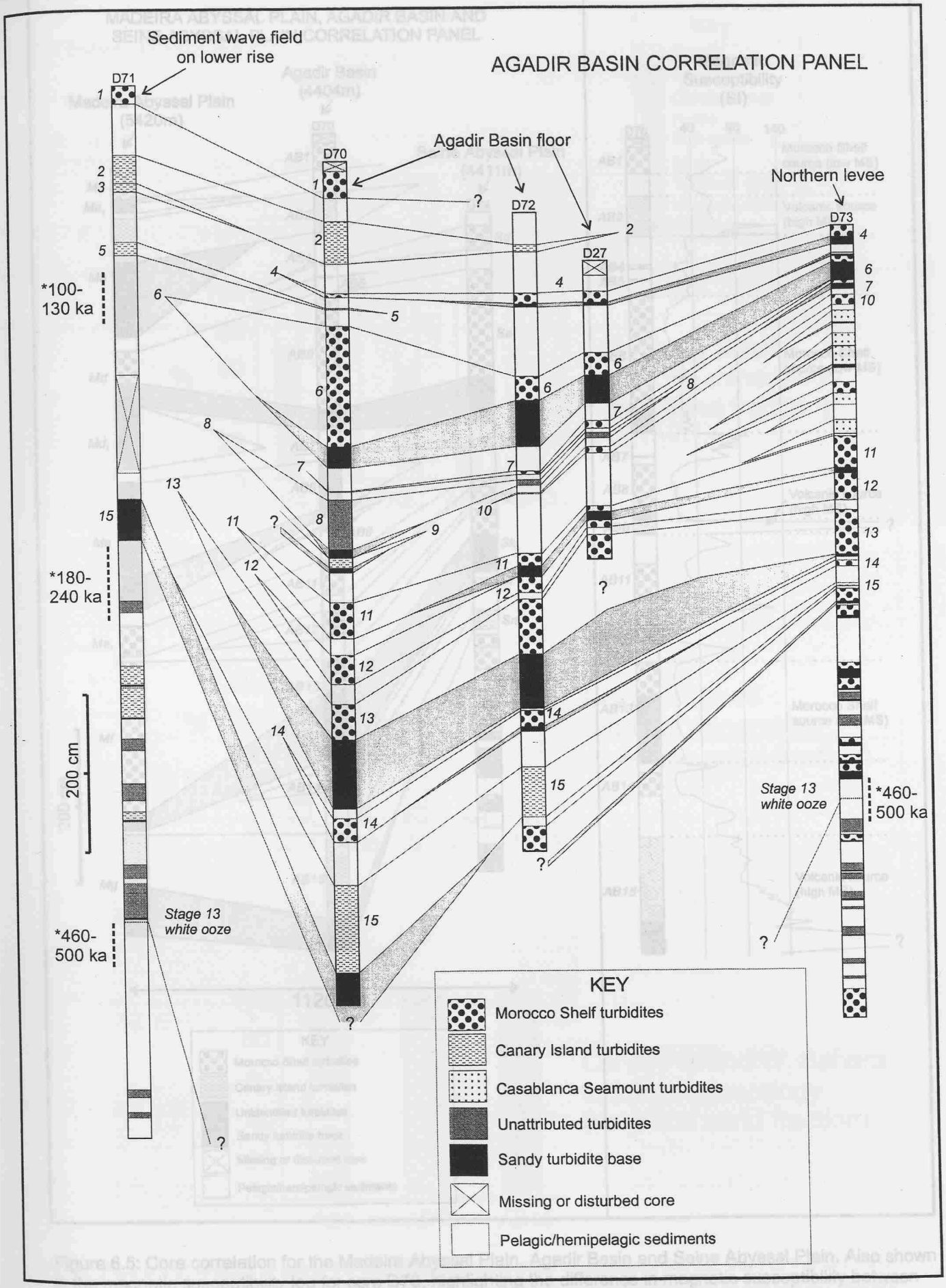

Figure 6.4: Core correlation for the Agadir Basin sequence showing the turbidite fill. Numbers shown in italics indicate the turbidite number within the sequence. Dates marked with an asterisk (*) indicate age of pelagic sediments based on coccolith dating. Sand bodies are highlighted with black/grey shading. Location of correlation line is shown on Figure 6.2.

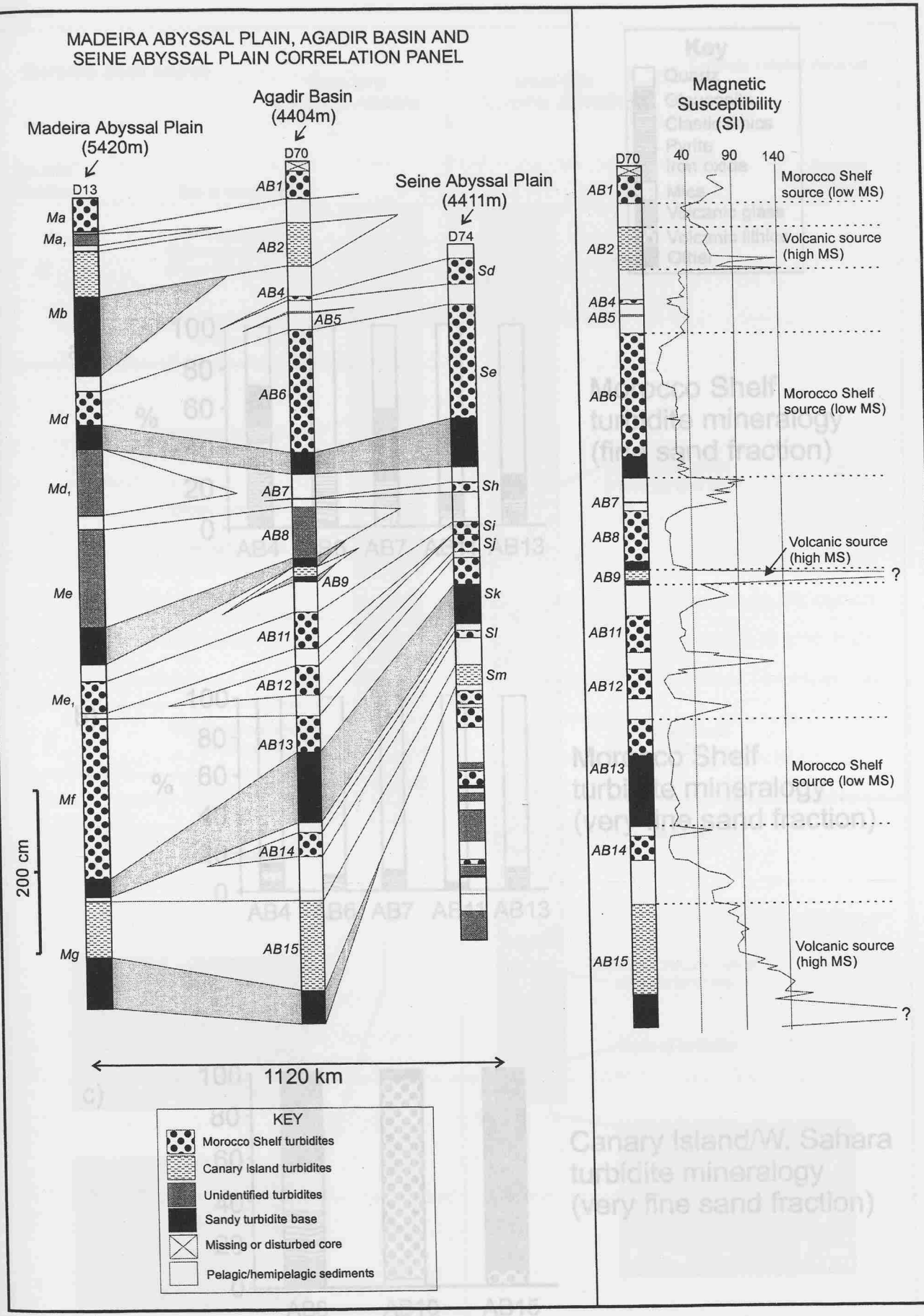

Figure 6.5: Core correlation for the Madeira Abyssal Plain, Agadir Basin and Seine Abyssal Plain. Also shown is the magnetic susceptibility log for core D70, highlighting the difference in magnetic susceptibility between turbidites derived from the Morocco Shelf and the volcanic Canary Islands. Numbers shown in italics indicate the turbidite number within the MAP sequence (Weaver and Kuijpers, 1983), the Agadir Basin sequence (this study) and the SAP sequence (Davies et al., 1997). Sand bodies are highlighted with black/grey shading. Location of correlation line shown in Figure 6.2.

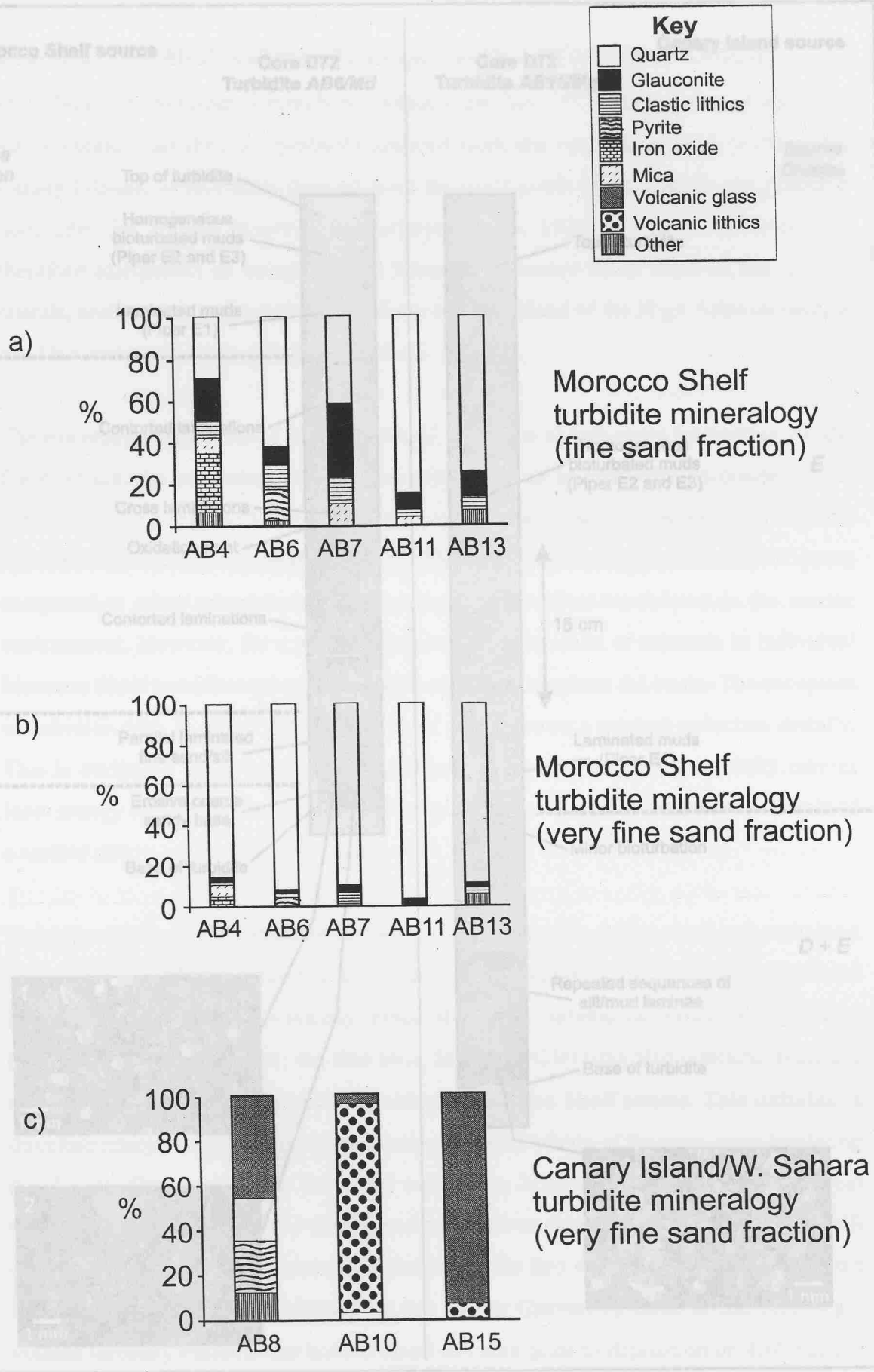

Figure 6.6: Graphs showing the percentage composition of turbidites derived from a) the Morocco Shelf (fine sand fraction), b) the Morocco Shelf (very fine sand fraction), and c) the Canary Islands/ Western Sahara shelf (very fine sand fraction). Note the high percentage of quartz in the very fine sand fraction of turbidites derived from the Morocco Shelf, and the absence of glauconite and clastic lithics in turbidites derived from the Canary Islands/Western Sahara shelf.

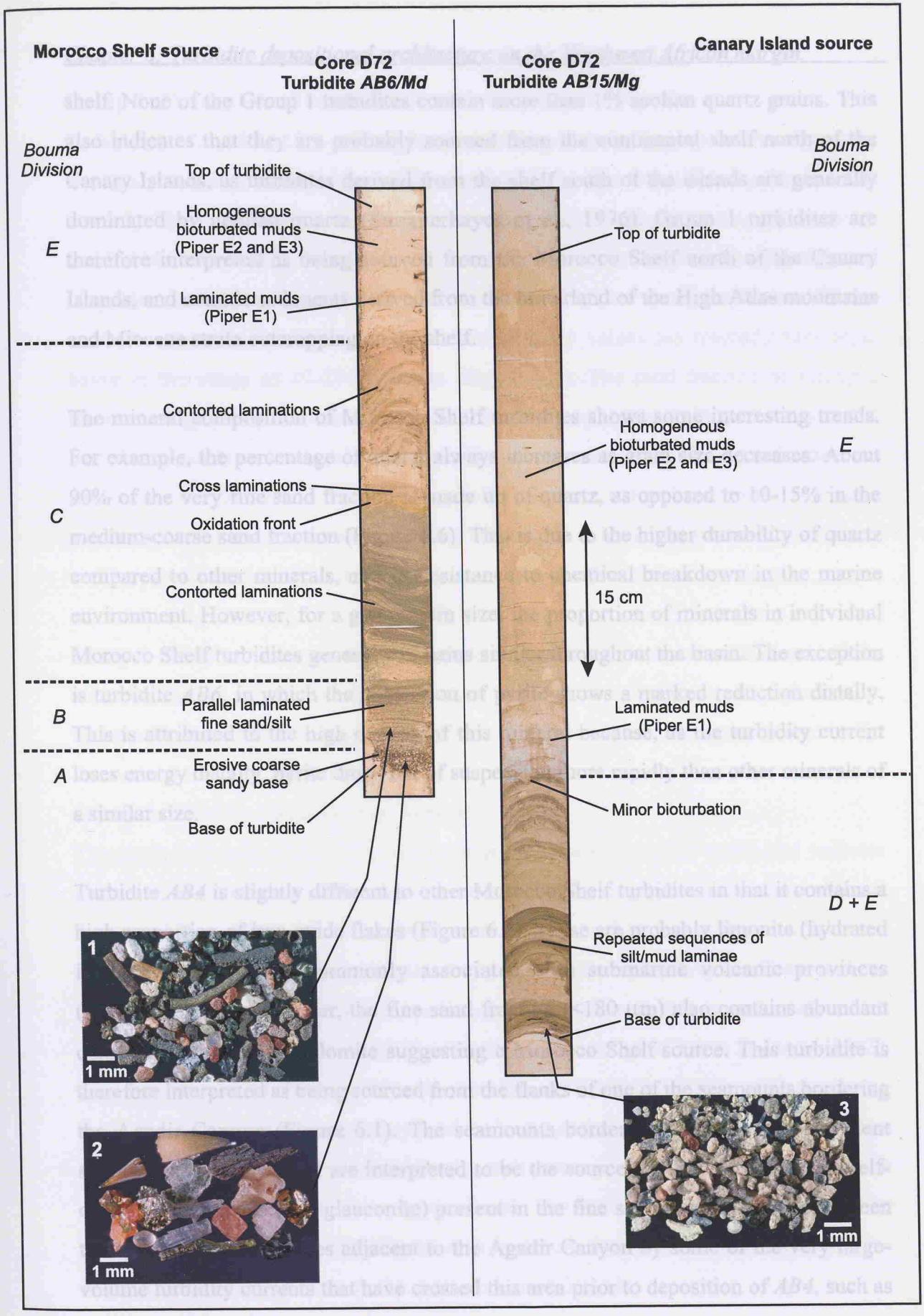

Figure 6.7: Core photographs showing the sedimentary structures of two turbidites in the Agadir Basin. Turbidite AB6/Md is sourced from the Morocco Shelf and turbidite AB15/Mg is sourced from the volcanic Canary Islands. Examples of the sand fraction mineralogy are also shown: (1) is a typical sample from the sandy base of a Morocco Shelf turbidite containing abundant quartz, glauconite, clastic lithics and pyritized burrows/fossils (2) is a selection of grains from Morocco Shelf turbidite bases including fish teethand vertebrae, lignified wood, dolomite, mica and pyrite (3) is a typical sample from a Canary Island turbidite base, containing altered volcanic glass and lithic fragments.

shelf. None of the Group 1 turbidites contain more than 1% aeolian quartz grains. This also indicates that they are probably sourced from the continental shelf north of the Canary Islands, as turbidites derived from the shelf south of the islands are generally dominated by aeolian quartz (Summerhayes et al., 1976). Group 1 turbidites are therefore interpreted as being sourced from the Morocco Shelf north of the Canary Islands, and contain sediments derived from the hinterland of the High Atlas mountains and Miocene strata outcropping on the shelf.

The mineral composition of Morocco Shelf turbidites shows some interesting trends. For example, the percentage of quartz always increases as grain size decreases. About 90% of the very fine sand fraction is made up of quartz, as opposed to 10-15% in the medium-coarse sand fraction (Figure 6.6). This is due to the higher durability of quartz compared to other minerals, and its resistance to chemical breakdown in the marine environment. However, for a given grain size, the proportion of minerals in individual Morocco Shelf turbidites generally remains similar throughout the basin. The exception is turbidite *AB6*, in which the proportion of pyrite shows a marked reduction distally. This is attributed to the high density of this mineral because, as the turbidity current loses energy distally, pyrite drops out of suspension more rapidly than other minerals of a similar size.

Turbidite *AB4* is slightly different to other Morocco Shelf turbidites in that it contains a high proportion of iron oxide flakes (Figure 6.6). These are probably limonite (hydrated iron oxide), which is commonly associated with submarine volcanic provinces (Rothwell, 1989). However, the fine sand fraction (<180 μm) also contains abundant quartz, glauconite and dolomite suggesting a Morocco Shelf source. This turbidite is therefore interpreted as being sourced from the flanks of one of the seamounts bordering the Agadir Canyon (Figure 6.1). The seamounts bordering the canyon are ancient submarine volcanoes, and are interpreted to be the source for the limonite. The shelf-derived components (e.g. glauconite) present in the fine sand fraction, may have been transported onto the slopes adjacent to the Agadir Canyon by some of the very large-volume turbidity currents that have crossed this area prior to deposition of *AB4*, such as turbidite *AB6*. Turbidite *AB4* is therefore sourced in deeper water beyond the shelf-break, but for the purposes of this study it has been included within the Morocco Shelf group of turbidites.

Group 2 (Canary Island source)

Turbidites *AB2, AB3, AB5, AB9, AB15* and *AB16* generally display a distinctive sand fraction mineralogy, with volcanic glass and volcanic lithics dominating (Figures 6.6 and 6.7). The volcanic glass occurs in a variety of morphologies, including pipe vesicles and bubble wall shards. Small amounts of pyrite and mica may also be present, and biogenic constituents include foraminifera and siliceous sponge spicules. Quartz contents are generally <2 %. Magnetic susceptibility values are typically very high, being in the range of 40-290 SI units (Figure 6.5). The mud fraction of Group 2 turbidites is grey or grey-brown in colour, with dark grey or black silt/sand bases (Table 6.2). Three additional volcaniclastic turbidites, and several unattributed turbidites, are present in core D71 below *AB15* (Figure 6.4). These are not included in the correlated sequence as they are not penetrated by any other cores. All are <40 cm thick and display similar characteristics to the other volcanic turbidites higher in the sequence.

Group 2 turbidites are interpreted as being derived from the submarine slopes of the volcanic Canary Islands, as they contain no shallow-water indicators, e.g. glauconite, and are dominated by volcanic glass and volcanic lithic fragments (Figures 6.6 and 6.7).

Group 3 (Western Saharan slope source)

The sandy base of turbidite *AB8* is dominated by quartz, irregular pyrite and volcanic glass, and contains none of the shallow-water indicators (e.g. glauconite, clastic lithics) that would suggest a Morocco Shelf source (Figure 6.6). In addition, unlike the Morocco Shelf turbidites it is absent, or very thin, in the eastern Agadir Basin and the SAP. However, the mud fraction is olive-green in colour and is organic-rich, which does indicate a source area on the Northwest African margin (Pearce & Jarvis, 1992). The source area for this turbidite is therefore difficult to identify with certainty. Turbidite *AB8* is tentatively interpreted as being derived from the Western Saharan slope to the south of the Canary Islands, with some of the flow passing around the western Canary Islands into the Agadir Basin. The presence of volcanic glass in the sandy base of turbidite *AB8* (Figure 6.6) indicates that seafloor erosion may have occurred on its passage close to the volcanic Canary Islands.

Group 4 (Casablanca Seamount source)

Five turbidites in the top 3 m of core D73 (Figure 6.4) are not present in any other cores, and are therefore very local in extent. They are all <30 cm thick, with thin (<4 cm) foraminifera sand bases and orange/red-brown mud tops. Additional biogenic constituents include siliceous sponge spicules, echinoid spines and fish teeth. Magnetic susceptibilities are in the range of 10-30 SI units.

Group 4 turbidites are interpreted to have been derived from the flanks of the Casablanca Seamount, which reaches 650 m below sea level, some 3400 m above the basin floor (Figure 6.1). The seamount flanks are draped by pelagic/hemipelagic sediments, which explains the lack of mineral grains in the medium-coarse sand fraction of Group 3 turbidites. However, the fine sand fraction often contains shelf-derived sediments similar to that seen in Morocco Shelf turbidites. These sediments are probably transported onto the lower flanks of the seamount by earlier large-scale turbidity currents. A Morocco Shelf source for these turbidites can be eliminated due to their localised distribution near to the base of the seamount. They are probably linked to small-scale failures on the seamount flanks, which would explain their small volume and restricted distribution.

Correlation with the MAP and SAP sequence

Using the criteria discussed above, a number of turbidites in the Agadir Basin sequence have been correlated with the sequences described from the Madeira Abyssal Plain (MAP) (Weaver & Kuijpers, 1983) and the Seine Abyssal Plain (SAP) (Davies et al. 1997). Core D13 has been selected from the MAP, and core D74 from the SAP, and the results of the correlation are displayed in Figure 6.5 and Table 6.3. Turbidites *AB6, AB11, AB13* and *AB15* are the only turbidites to occur in all three basins. In the following discussion the correlated turbidites will occasionally have their abyssal plain correlations displayed in parentheses. Therefore turbidite *AB6* will be displayed as *AB6(Md/Se),* indicating that turbidite *AB6* in the Agadir Basin has been correlated with turbidite *Md* on the MAP and turbidite *Se* on the SAP.

Turbidite volumes

The estimated volumes of each turbidite have been calculated on the basis of their thickness and areal distribution in the Agadir Basin, SAP and MAP (Table 6.3). It

Madeira AP (68,000 km^2)			Agadir Basin (38,000 km^2)			Seine AP (37,500km^2)				
Letter	*Max thickness (cm)*	*Vol. (km3)*	*No.*	*Max thickness (cm)*	*Vol. (km3)*	*Letter*	*Max thickness (cm)*	*Vol. (km3)*	*Total volume*	*Age (ka)*
a	120	?	1	34	?				?	< 1
b	500	125	2	54	8				130	12
b_1	?	4	3	11	1				5	12
			4	24	4	d	75	11	15	24
			5	17	2				2	
d	150	30	6	177	37	e	445	59	125	59
			7	10	2	h	60	4	6	
e	300	110	8	75	14				125	71
			9	18	3				3	
			10	12	1				1	
e_1	60	8	11	46	13	i	35	7	28	120
			12	34	9	j	20	6	15	
f	500	190	13	135	37	k	115	34	260	128
			14	30	8	l	10	3	11	
g	250	70	15	151+	29+	m	45	13	110+	186
g_1	40	4	16	6	1				5	186
			17	32+	12+	n	20	6	20+	

Table 6.3: Correlation of turbidites in the MAP, Agadir Basin and SAP sequence, with volume, maximum thickness and ages shown for each turbidite. The five large-volume (100 km^3) turbidites are highlighted by grey shading.

should be noted that these values are only estimates, as it is not possible to quantify the volume of individual turbidites on the slope and rise due to lack of core control. Table 6.3 displays the maximum thickness and volume of each turbidite in the three basins, together with the estimated total volume and age. The data show an interesting pattern, with a wide range of total volumes. The largest turbidite is *AB13(Mf/Sk)* which, with a total volume of 260 km^3, is almost twice as large as any of the other turbidites. There are four additional large-volume turbidites (*AB2(Mb), AB6(Md/Se), AB8(Me),* and *AB15(Mg/Sm)),* which all have total volumes greater than 100 km^3. Then, the next largest turbidite is *AB11(Me1/Si)* which is just 30 km^3. The other 11 turbidites are all <20 km^3. Therefore, there appear to be three size groups, with the largest turbidite being 260 km^3, four others between 110—135 km^3, and the rest being <30 km^3.

Discussion

Basin connectivity in the Moroccan Turbidite System

Detailed correlation of individual turbidites has revealed that large-volume turbidites derived from the Morocco Shelf and the Canary Islands are present in three different depositional basins. Turbidites *AB6/Md* and *AB13/Mf* are both sourced from the Morocco Shelf, and are present in the SAP, the Agadir Basin, and the MAP basin-fill sequences (Figure 6.5). The turbidity currents that produced these deposits transported material from the Morocco Shelf through the Agadir Canyon (Figure 6.1). These flows must have divided at the canyon mouth as they became unconfined, and one part flowed northwards and entered the SAP via an intrabasinal sill (Davies et al., 1997). The remainder of the flow travelled westwards through the Agadir Basin, and then passed through the northern section of the Madeira Distributary Channel System before terminating on the MAP. Turbidite *AB15/Mg* is sourced from the Canary Islands, and is also present in all three basins. The major part of this turbidity current flowed north-west and passed through the southern section of the MDCS before terminating on the MAP. The remainder of the flow would have travelled northwards around the western slopes of the Selvage Islands, before entering the Agadir Basin from the west (Figure 6.1). This flow then travelled slightly upslope across the gentle gradients of the basin floor, and a small amount of the muddy suspended load passed over the intrabasinal sill into the SAP (Figure 6.5).

The analysis of turbidity current pathways discussed above has been made possible by having good-quality core control in all three basins, and highlights the unique nature of this turbidite system. Other studies have also described turbidity currents passing from one basin to another (e.g. Heezen et al., 1959; Laughton, 1960), and it has been suggested that turbidity currents can be rejuvenated by the increase in gradient and lateral constriction as they pass through intrabasinal passages (Laughton, 1960). However, this is the first example of a turbidite system where different flows, derived from sources 600 km apart, can deposit sediments in the same three depositional basins across a distance of at least 1200 km.

Turbidite mineralogy: implications for turbidity current flow processes

In a study of the Madeira Distributary Channel System, Masson (1994) commented on the presence of volcanic components in turbidites derived from the Moroccan margin, and suggested that some Morocco Shelf turbidity currents incorporate volcanic material picked up from the MDCS on their passage downslope. The volcanic material had been deposited within the MDCS by earlier volcaniclastic turbidity currents, indicating that both erosion and deposition can occur within this channel system. This study reveals that a number of turbidites correlated between the Agadir Basin and Madeira Abyssal Plain do show a significant lateral variation in mineralogy, and this is also interpreted as evidence for channel floor erosion.

Turbidites *AB2(Mb), AB6(Md), AB8(Me), AB13(Mf)* and *AB16(Mg)* in the Agadir Basin, can be divided by source area on the basis of their distinctive sand fraction mineralogy. However, when the same turbidites are sampled on the MAP, after having passed through the MDCS, the sand composition is generally very different to that seen upslope in the Agadir Basin. All of the turbidite sands in the MAP are dominated by pelagic foraminifera, sponge spicules, biotite and volcanic glass, with smaller amounts of quartz, glauconite and volcanic lithics. The dominance of forams, spicules, biotite and volcanic glass over the other grain types can in part be explained by their lower effective density. This affects transport potential, i.e. for a given grain size these components will be transported a greater distance. However, this does not explain why turbidites containing no volcanic material in the Agadir Basin are found to contain significant numbers of volcanic grains on the MAP. This is interpreted as being a result of flow evolution within the MDCS. Turbidites passing through this channel system

erode some of the previously deposited channel sands on the passage to the MAP, which explains why each turbidite has a mixed Morocco Shelf/Canary Island mineral assemblage on reaching the abyssal plain.

Masson (1994) also concluded that flow stripping probably occurs within the channel system, whereby the sandy bedload of the turbidites is transported within the confines of the channel, and the finer-grained suspended load is unconfined as it crosses the continental rise. The sandy turbidite bedload forms two distinct sandy lobes at the termination of the northern and southern sections of the Madeira Distributary Channel System (Wynn et al., 2000a), confirming that the passage of turbidite sands has been channelised. We can now also reinforce the finding that the fine-grained suspended load is unconfined. Geochemical analysis of turbidite muds on the MAP has shown that individual turbidites have retained their signature of source composition, i.e. as Canary Island or Morocco Shelf sourced (de Lange et al., 1987). In addition, the unique coccolith ratios in each turbidite remains essentially the same between the Agadir Basin and the MAP (Weaver, 1994). An example of this is shown in Figure 6.8, where turbidite *Mf* from the MAP has been correlated with turbidite *AB13* from the Agadir Basin and turbidite *Sk* from the Seine Abyssal Plain. In all three cores the coccolith ratios in the turbidite mud are very similar; the species *Gephyrocapsa caribbeanica* has between 50-60%, *Gephyrocapsa aperta* has 25-35% and *Gephyrocapsa muellerae* has 10-20% of the total. These results indicate that the mud fraction of individual turbidites on the MAP has not evolved significantly during transport between the Agadir Basin and the MAP, and is therefore unlikely to have interacted with previously deposited seafloor sediments on the passage downslope. This is in contrast with the findings discussed above relating to the turbidite sands, whereby turbidite source areas cannot be distinguished on the basis of sand fraction mineralogy due to flow evolution. To summarise, it is interpreted that the sand fraction of turbidity currents is channelised as it passes through the MDCS, and undergoes flow evolution due to channel floor erosion/deposition. In contrast, the mud fraction is unconfined and does not interact with seafloor sediments on the passage downslope.

Interpretation of turbidite sedimentary structures

A wide variety of sedimentary structures are present in the Agadir Basin turbidites, although only *AB6* and *AB13* display the complete Bouma sequence (Bouma, 1962)

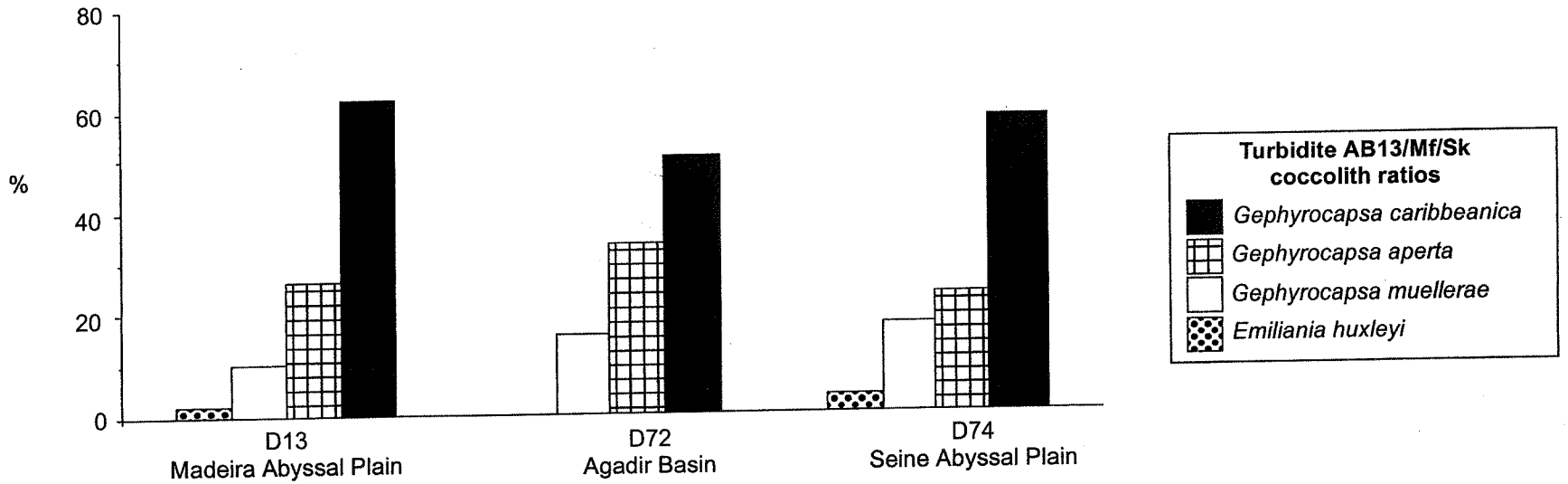

Figure 6.8: Diagram illustrating the coccolith ratios in the mud fraction of turbidite AB13/Mf/Sk in three different basins. Note how the ratios are similar in all three basins, indicating that the muddy suspended load of the turbidity current has not been involved in seafloor erosion

from Ta - Te. Many turbidites show a progressive base cut-out of the lower Bouma divisions (Ta - Tc) in the distal basin, while the smaller turbidites are often composed entirely of Td and Te silts and muds. The Bouma Tc division of contorted laminated and cross-laminated silts is commonly developed, although uncontorted cross-laminae are rare, as noted in turbidites on the MAP by Rothwell et al. (1992). Well-developed oxidation fronts are present in many turbidites, and some of the thin silt-mud turbidites display complete oxidation. Two of the largest turbidites in the Agadir Basin (*AB6/Md* and *AB15/Mg*) show a series of sedimentary structures that can be interpreted in terms of flow processes. These turbidites often have a complex coarse basal facies that can be correlated across the basin.

Turbidite *AB6* (Figure 6.7) has a thin, erosive, sandy base (Ta) overlain by laminated coarse to fine sands (Tb). The Tc division shows variable development; in the eastern basin it consists of contorted laminae and cross-laminae, occasionally containing small mud clasts. In the western basin it consists of fine sand/muddy silt laminae that are often contorted and lenticular, and contain irregular silty blebs. The contorted laminae are interpreted as being formed by shear deformation, whereby deposition of subsequent sub-flow surges results in the deformation of underlying unconsolidated laminated and cross-laminated silts (Rothwell et al., 1992). The mud clasts and silty blebs are also associated with disturbance and erosion of ripple- and convolute-laminae by subsequent sub-flow surges (Stow & Shanmugan, 1980). The top of turbidite *AB6* comprises Td division silt-mud laminae, and Te division muds. The Te division can be further subdivided according to the classification scheme of Piper, (1978). In turbidite *AB6*, E1 laminated muds are overlain by E2 and E3 structureless bioturbated muds.

Turbidite *AB15* (Figure 6.7) shows a basal sequence of multiple, often coarsening-upward packages, composed of silt-mud laminae. Overall, this laminated unit grades from coarse silt and silty mud at the base, to fine silt and mud at the top. This basal sequence is interpreted as being the result of deposition from a surging-type turbidity current with fluctuating flow velocities (Lowe, 1982; Rothwell et al., 1992; Kneller, 1995). Towards the top of this laminated unit, very regular alternations between slightly lenticular laminae and cross-laminae may represent the Tc division. The top of the turbidite consists of Te division muds, with E1 laminated muds overlain by a thick sequence of E2 and E3 structureless bioturbated muds.

Turbidite depositional architecture of the intraslope Agadir Basin

The complex topography of the Northwest African margin is responsible for creating an unusual turbidite system, with multiple, widely spaced source areas and an intraslope basin containing a complex turbidite fill. The turbidite architecture of the MAP and the SAP has already been covered in detail (Rothwell et al., 1992; Davies et al., 1997; Wynn et al., 2000a), and several types of turbidite sand body can been recognised. For example, on the MAP sands are concentrated around channel terminations at the break-of-slope and form distinct depositional lobes (Wynn et al., 2000a). On the SAP sands onlap the lower rise forming a linear wedge (Davies et al., 1997). In both cases, overlying turbidite muds tend to be ponded deposits, that fill in topographic lows on the plain. Linear, sand-rich turbidite deposits are present in the distal Agadir Canyon and the MDCS (e.g. Masson, 1994), but due to lack of core control these are poorly documented. However, the total volume of sand present within these channels is likely to be insignificant when compared to the large volumes present in the basin-fill sequences.

This discussion will now concentrate on the turbidite depositional architecture of the intraslope Agadir Basin, which contains turbidites derived from four main source areas: the Morocco Shelf, the volcanic Canary Islands, the Western Saharan slope, and the Casablanca Seamount. Turbidites from these different source areas show different patterns of bed thickness and sand/mud ratio, but even turbidites from the same source area have a highly variable distribution. For example, three turbidites derived from the Morocco Shelf all have a different architecture. Turbidite *AB4* is thickest in the eastern basin-fill (proximal to the Morocco Shelf) and thins distally (Figure 6.9). The sand/mud ratio is about 35:65 in the eastern basin, but decreases to 20:80 in the central basin and 0:100 in the western basin. The opposite is shown by turbidite *AB6*, which is thinnest in the eastern basin and thickens distally (Figure 6.9). The sand/mud ratio decreases from 75:25 in the eastern basin, to 60:40 in the central basin and 10:90 in the western basin, indicating that it is the mud fraction which forms the bulk of the thick deposit in the western basin. Turbidite *AB13* is different again, showing a fairly uniform thickness across the whole basin (Figure 6.9). However, the sand/mud ratio is only 10:90 in the eastern basin, but increases to 40:60 in the central basin, and 65:35 in the western basin.

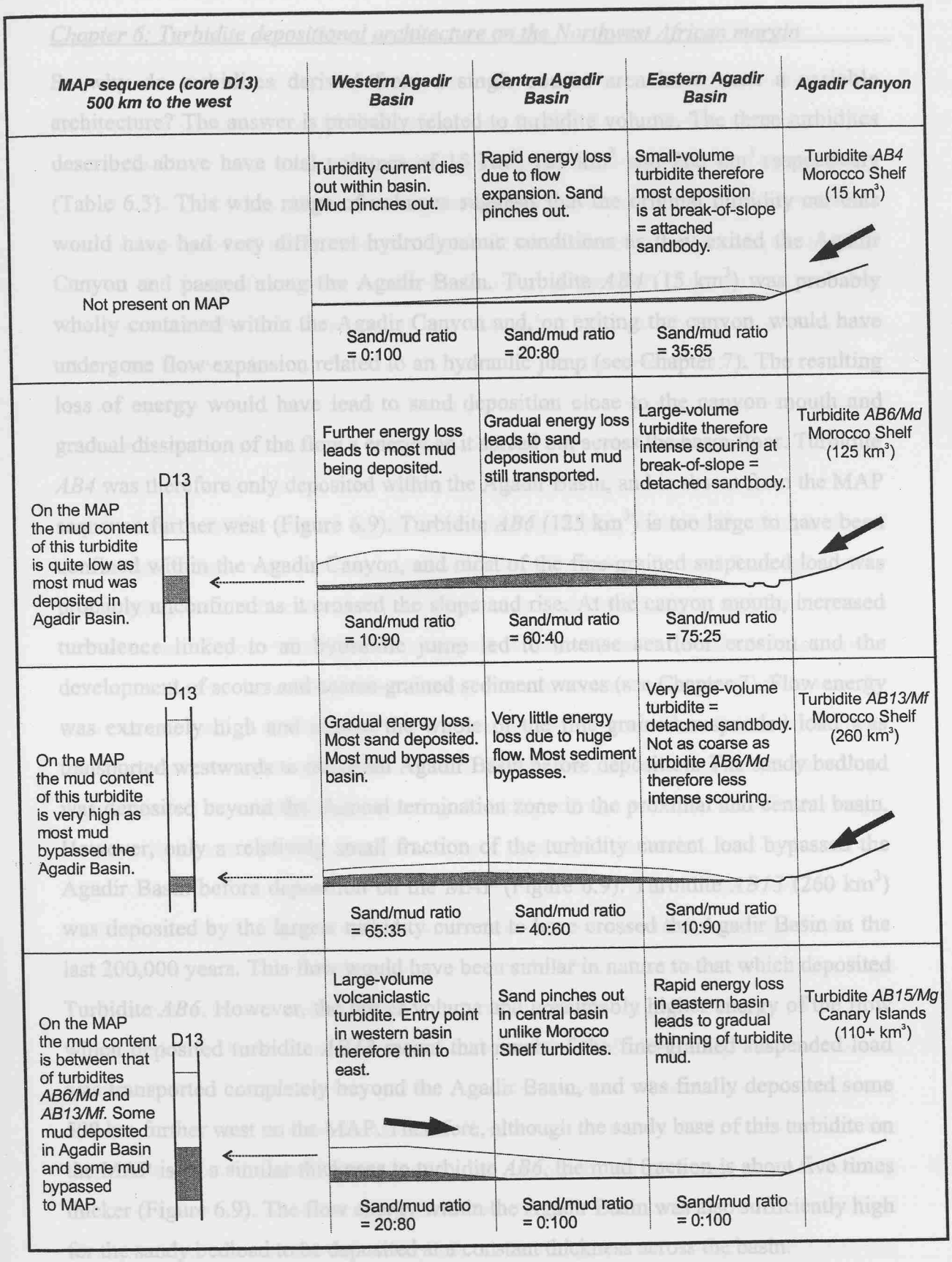

Figure 6.9: Schematic diagram showing the depositional architecture of four different turbidites in the Agadir Basin, together with a comparison of their appearance in core D13 from the MAP. Note how the architecture of the three Morocco Shelf turbidites varies as a result of their different volumes. Black arrows indicate turbidity current flow direction. Diagram not to scale.

So why do turbidites derived from a single source area have such a variable architecture? The answer is probably related to turbidite volume. The three turbidites described above have total volumes of 15 km^3, 125 km^3 and 260 km^3 respectively (Table 6.3). This wide range of volumes suggests that the original turbidity currents would have had very different hydrodynamic conditions as they exited the Agadir Canyon and passed along the Agadir Basin. Turbidite *AB4* (15 km^3) was probably wholly contained within the Agadir Canyon and, on exiting the canyon, would have undergone flow expansion related to an hydraulic jump (see Chapter 7). The resulting loss of energy would have lead to sand deposition close to the canyon mouth and gradual dissipation of the flow s energy as it spread out across the basin floor. Turbidite *AB4* was therefore only deposited within the Agadir Basin, and is absent from the MAP sequence further west (Figure 6.9). Turbidite *AB6* (125 km^3) is too large to have been confined within the Agadir Canyon, and most of the fine-grained suspended load was probably unconfined as it crossed the slope and rise. At the canyon mouth, increased turbulence linked to an hydraulic jump led to intense seafloor erosion and the development of scours and coarse-grained sediment waves (see Chapter 7). Flow energy was extremely high and almost the whole of the fine-grained suspended load was transported westwards to the distal Agadir Basin before deposition. The sandy bedload was deposited beyond the channel termination zone in the proximal and central basin. However, only a relatively small fraction of the turbidity current load bypassed the Agadir Basin before deposition on the MAP (Figure 6.9). Turbidite *AB13* (260 km^3) was deposited by the largest turbidity current to have crossed the Agadir Basin in the last 200,000 years. This flow would have been similar in nature to that which deposited Turbidite *AB6*. However, the larger volume and presumably higher energy of the flow which deposited turbidite *AB13* meant that much of the fine-grained suspended load was transported completely beyond the Agadir Basin, and was finally deposited some 500 km further west on the MAP. Therefore, although the sandy base of this turbidite on the MAP is of a similar thickness to turbidite *AB6*, the mud fraction is about five times thicker (Figure 6.9). The flow energy within the Agadir Basin was also sufficiently high for the sandy bedload to be deposited at a constant thickness across the basin.

It is interesting to note that none of the Morocco Shelf turbidites discussed above are present in core D71, recovered from the lower rise at a height of 100 m above the basin floor (Figure 6.2). This indicates that none of these flows were >100 m in thickness as

they crossed the central Agadir Basin, probably due to intense flow thinning as the flows expanded across the 100 km width of the Agadir Basin. However, several flows were sufficiently large to cross the broad intrabasinal sill separating the Agadir Basin from the SAP, which is about 40 m high at its lowest point. Core D73 recovered from near the high point of the sill shows a highly condensed turbidite fill compared to that seen on the floor of the adjacent Agadir Basin and the SAP (Figures 6.4 and 6.5). However, all of the turbidites present on either side of the sill display sand continuity across this barrier, although the sandy bases are generally coarser and thinner, and are capped by thin Te division muds. This is partly due to erosional processes, as many turbidite bases on the levee crest have eroded down into underlying turbidite muds.

Variations in turbidite volume appear to be one contributing factor to the complexity of the basin-fill, and another is multiple source areas. Turbidites derived from the Canary Islands are generally thickest in the western and central Agadir Basin, and thin or pinch-out to the east (Figure 6.9). This is the opposite of most Morocco Shelf turbidites, and is due to the Canary Island turbidites having a south or south-west entry point into the basin, as opposed to the Morocco Shelf turbidites which enter from the east and south-east. To summarise, the complex turbidite depositional architecture of the intraslope Agadir Basin is a function of varying turbidity current volume and flow energy, combined with multiple source areas and input points into the basin.

Controls on the timing of turbidite deposition and possible trigger mechanisms

Previous studies of the turbidite sequence on the MAP has revealed that all of the large (>100 km^3) turbidites were deposited at oxygen isotope stage boundaries (Weaver & Kuijpers, 1983; Rothwell et al., 1992; Weaver et al., 1992). These represent periods of global climate change between glacial and interglacial conditions, when eustatic sea level was changing rapidly. In addition, Weaver & Kuijpers (1983) revealed that the three largest turbidites on the MAP (*AB2/Mb, AB8/Me*, and *AB13/Mf*) occurred during the largest fluctuations in sea level (based on the rate and relative amount of sea-level change). They also noted that nearly all of the oxygen isotope stage boundaries are represented by a single large-volume turbidite on the MAP. These findings contrast with many studies of submarine fans, which suggest that most turbidites are deposited during lowstands of sea level (e.g. Shanmugan & Moiola, 1981; Stow et al., 1984). The timing

and possible trigger mechanisms for four of the largest turbidites are now discussed in more detail:

Turbidite *AB2/Mb* was deposited at about 12 ka (between oxygen isotope stages 1 and 2) during a period of rising sea level following the last glacial (Rothwell et al., 1992). This turbidite was deposited at the same time as the Canary Debris Flow (Masson et al., 1992; 1998), and both events are believed to have been triggered by the El Golfo debris avalanche on the flanks of El Hierro in the western Canary Islands (Masson, 1996; Masson et al., 1998). The initial trigger for the debris avalanche is unknown, but probably involved volcanic processes in addition to possible loading and subsequent destabilisation of the island flanks due to rising sea level.

Turbidite *AB6/Md* was deposited at 59 ka (between oxygen isotope stages 3 and 4) during a period of rising sea level following the stage 4 glacial. This turbidite originated on the Morocco Shelf north of the Canary Islands, but appears to have occurred at the same time as the Saharan Debris Flow, south of the islands (Gee et al., 1999). The source area of the Saharan Debris Flow is at a water depth of about 2000 m (Embley, 1982) and is therefore much deeper than the shelf. It is possible that an earthquake on the Moroccan/Western Saharan margin is the trigger for both turbidite *AB6/Md* and the Saharan Debris Flow, which would explain why they occurred at the same time, but in different water depths. In addition, there would have been a large amount of sediment on the Morocco Shelf at this time, supplied by meltwater discharge from the Atlas Mountains at the end of the Stage 4 glacial. This in itself could have destabilised the shelf sediments, and left them susceptible to failure following an earthquake (e.g. Einsele et al., 1996). Although the final trigger mechanism is uncertain, the sand fraction of turbidite *AB6/Md* does contain good evidence to suggest the sediment had a relatively short residence time on the shelf. The fine sand fraction displays very low textural and compositional maturity (Figure 6.6 and 6.7), which indicates rapid transport from source to sink.

Turbidite *AB13/Mf* was deposited at around 128 ka (between oxygen isotope stages 5 and 6) during a period of rising sea level. This turbidite is particularly interesting, as it seems to have been derived from two different source areas, and may therefore have been deposited by two different turbidity currents triggered at the same time. On the

MAP, Rothwell et al. (1992) concluded that turbidite *AB13/Mf* was probably derived from the margin north and south of the Canary Islands. Evidence presented in this paper confirms the northern source as being the Morocco Shelf. In addition, studies conducted on this turbidite in the MAP sequence reveal that it also has a significant proportion of aeolian quartz and feldspar (Pearce & Jarvis, 1992), which is absent in the same turbidite in the Agadir Basin. The presence of aeolian quartz and feldspar confirms that turbidite *AB13/Mf* also has a Western Sahara Shelf source (Summerhayes et al., 1976). Turbidity currents that travel along different pathways before deposition on one abyssal plain are likely to be seismically triggered (Normark and Piper, 1991).

Turbidite *AB15/Mg* was deposited at around 186 ka (between oxygen isotope stages 6 and 7) during a period of falling sea level. This turbidite was derived from the central Canary Islands (Pearce & Jarvis, 1992), and appears to be linked to the Icod debris avalanche on the north flank of Tenerife (Watts & Masson, 1995). The debris avalanche is dated at roughly the same time as turbidite *AB15/Mg*, and may have triggered the turbidite in a similar fashion to the El Golfo debris avalanche and turbidite *AB2/Mb*.

In the last 750,000 years, turbidite frequency on the MAP has averaged one every 30,000 years (Weaver et al., 1992). This compares with one turbidite every 14,000 years for the Seine Abyssal Plain (Davies et al., 1997), indicating that turbidite frequency generally decreases with distance from the continental margin. In the Agadir Basin turbidite frequency has averaged about one every 10,000 years, although there appears to be a major change in turbidite frequency at about 200 ka, which marks the start of the Stage 6 glacial. A total of 12 Morocco Shelf turbidites were deposited between 200 ka and the present day, but only 7 were deposited in the preceding 300,000 years. This change was also noted by Rothwell et al. (1992) on the MAP, where there was a major switch in turbidite source areas at 200 ka. At this time the dominant turbidite source area changed from the Western Sahara margin, to the Morocco Shelf and Canary Islands. Unfortunately, the reasons for this switch in turbidite frequency and source area are still poorly understood.

Conclusions

This study has revealed that turbidites in the Moroccan Turbidite System are derived from several source areas, including the Morocco Shelf, the Western Sahara Shelf, the

volcanic Canary Islands, and adjacent seamounts. Excellent core control has enabled the turbidite sequence for the last 200,000 years to be correlated between the Agadir Basin, the MAP and the SAP, giving us new insights into turbidite depositional architecture across interconnected deep-water basins. Turbidite sand bodies on the MAP and SAP are generally concentrated at the break-of-slope, and form radial lobes or longitudinal wedges aligned parallel-to-slope. However, within the intraslope Agadir Basin, extensive basin-wide sheet sands are developed. The thickness and lateral extent of these sheet sands is largely controlled by turbidite source area and volume. Turbidites derived from the Morocco Shelf all enter the Agadir Basin from the east or south-east, but show a highly variable architecture related to differences in volume. Very large-volume turbidity currents (>250 km^3 of sediment) deposit most of their sand in the central and distal basin, but have enough energy to transport most of the mud fraction out of the basin and a further 500 km west before deposition on the MAP. They form large sand bodies that are separated from the Agadir Canyon mouth by a zone of erosional scours. Large-volume turbidity currents (100-150 km^3 of sediment) also deposit most of their sandy load in the central and distal basin, but lose sufficient energy to also deposit most of the mud fraction in the distal basin. Small-volume turbidity currents (<30 km^3 of sediment) are totally confined within the Agadir Basin, and pinch out in the distal basin. They form small, thin sand bodies that are attached to the Agadir Canyon mouth. Turbidites derived from the Canary Islands enter the Agadir Basin from the south or south-west, and therefore show a different pattern of thickness and grain-size to the Morocco Shelf turbidites. To summarise, the turbidite fill of intraslope basins can be highly complex in areas with multiple source areas and large variations in turbidity current volume.

Acknowledgements

We would like to acknowledge the effort and expertise of the Master, officers and crew during RRS Discovery cruise 225. RBW would like to acknowledge the provision of PhD funding from the University of Southampton and the SOC Challenger Division. DAVS acknowledges tenure of a RS Industry Fellowship and support from BP Amoco. Mr Barry Marsh (University of Southampton) is thanked for technical assistance.

6.3: Summary

This study has revealed that turbidite depositional architecture on the Northwest African margin is largely controlled by turbidity current volume, basin morphology and turbidite source area. Sand body distribution and dimensions are highly variable, particularly within the intraslope Agadir Basin where the overall basin-fill is highly complex. The largest turbidite are deposited during periods of rapid sea-level change, although the exact trigger mechanisms for individual events are still poorly understood.

In the next chapter, the links between the Agadir Basin and the Agadir Canyon will be investigated, in an attempt to understand how sand body continuity is affected by the erosional processes that operate within the channel-lobe transition zone.

CHAPTER 7

CHANNEL-LOBE TRANSITION ZONES

7.1: Introduction and aims

A combination of core data and seismic profiles have allowed detailed analysis of the turbidite depositional architecture within the basin-fill sequences of the Moroccan Turbidite System. However, the channel-lobe transition zone beyond the mouth of the Agadir Canyon, and its links with the turbidite fill of the Agadir Basin, is still poorly understood as the sediments in this area are generally too coarse-grained to be penetrated using conventional coring techniques. During Discovery Cruise 225, TOBI sidescan sonar data was collected across the Agadir channel-lobe transition zone in an attempt to understand how this area is connected to its feeder canyon and the basin fill. In addition, new TOBI data from the mouth of the Lisbon Canyon, and MAK1 data from the Rhone Fan, are also presented. These new data are combined with previously published results so that a new model can be developed that characterises the location, morphology and dimensions of the channel-lobe transition zone. An additional target is to understand how the channel-lobe transition zone may be recognised during hydrocarbon exploration, and how it may affect continuity between channel and proximal lobe sands.

7.2: Paper 4

A new model for deep-water channel-lobe transition zones based on high-resolution seafloor mapping and modern and ancient analogues

Russell B Wynn, Dorrik A V Stow, Neil H Kenyon, Douglas G Masson and Philip P E Weaver

SOES/Challenger Division, Southampton Oceanography Centre, European Way, Southampton, SO14 3ZH, UK.

This paper was submitted to AAPG Bulletin in May 2000.

Abstract

The channel-lobe transition zone (CLTZ) is an important element of many large-scale turbidite systems, however, our knowledge of the distribution, morphology and dimensions of architectural elements within this zone is very limited. Three case studies of modern CLTZ s are presented, from the Agadir and Lisbon Canyons, and the Rhone Fan. These data are then compared with modern and ancient analogues in an attempt to produce a new model highlighting the characteristics of the CLTZ, and the controls on their formation.

CLTZ s are associated with canyon/channel mouths, often with an associated break-in-slope. They occur in highly efficient turbidite systems swept by large-volume, sand-laden flows with a high mud content, and lead to formation of a depositional lobe that is detached from its feeder canyon/channel. Erosional features in the CLTZ include giant individual scours up to 60 m deep, 2 km wide and 2 km long. In areas of intense erosion these merge to form amalgamated scours several kilometres wide. Associated bedforms include coarse-grained sediment waves with wavelengths up to 2 km and wave heights of several metres. Recognition and understanding of CLTZ s in the subsurface is vital during hydrocarbon exploration, as they often contain a highly complex sequence of sedimentary facies that will affect fluid flow between good-quality channel and proximal lobe sands.

Introduction

Our understanding of deep-water turbidite systems has increased considerably in recent years, with high-quality datasets from modern and ancient systems giving us new insights into the processes and deposits occurring within this environment. For example, the use of side-scan sonar in seafloor mapping, and the development of 3-D seismic technology, has revealed the complex morphology of deep-sea channels and fans in unprecedented detail. However, there are still large gaps in our knowledge of sea-floor processes. In particular, our knowledge of the sedimentary processes operating in the region of channel terminations is very limited, especially as it is often difficult to recognise this zone in modern and ancient systems (Mutti and Normark, 1991). Most existing submarine fan models, largely based on ancient analogues, suggest that depositional lobes will be attached to their feeder channels (e.g. Bouma, 2000). However, there is a growing body of evidence from modern and ancient datasets

showing that in many turbidite systems this is not the case, and that erosional scours and detached lobes are developed in a channel-lobe transition zone (CLTZ). The recognition of channel-lobe transition zones is particularly important during hydrocarbon exploration, as they may separate good-quality reservoir targets such as channel-fill and proximal lobe sands.

Normark (1970) and Normark et al. (1979) were the first to discover large-scale erosional features associated with channel terminations. Mutti (1985), and Mutti and Normark (1987, 1991), then developed a model based largely on outcrop data, which recognised that in systems swept by *large-volume, sand-laden turbidity currents with a high mud content*, a range of large-scale erosional features occur within a channel-lobe transition zone (CLTZ). The model revealed that sand bodies in these systems usually form as detached lobes, separated from the channel mouth by the CLTZ. Recently, the recognition of erosional scours and associated bedforms in modern CLTZ s has been aided by the increased use of deep-towed side-scan sonar imagery (e.g. O Connell et al., 1991; Kenyon et al., 1995; Kenyon and Millington, 1995; Palanques et al., 1995; Morris et al., 1998). However, no model has yet been developed which describes the systematic distribution, morphology and dimensions of architectural elements within CLTZ s. In addition, there have been few attempts to underline how an increased understanding of this zone has important applications to hydrocarbon exploration in deep-water systems.

In this study we present three high-quality datasets of modern CLTZ s, based on high-resolution seafloor mapping using the TOBI and MAK1 sidescan-sonar instruments. These new data are then combined with previously published examples of modern and ancient CLTZ s, in an attempt to produce a new model that characterises the location, morphology and dimensions of the CLTZ and the features within it. The application of this model to hydrocarbon exploration is then investigated, including: 1) the dimensions of erosional features and depositional bedforms within the CLTZ, 2) the problem of separating large-scale erosional scours from channels, 3) sand body distribution and continuity across the CLTZ, 4) the recognition of CLTZ s in the subsurface, and 5) the linkage with 3-D seismic time-slice imagery from deep-water channel and lobe systems.

Definition of a channel-lobe transition zone

Mutti and Normark (1987; 1991) termed the area between turbidite channels and depositional lobes as the *channel-lobe transition zone*, and defined this zone as the region that, within any turbidite system, separates well-defined channels or channel-fill deposits from well-defined lobes or lobe facies . However, it is important to note that in a small number of cases, morphologically recognisable depositional lobes are not developed downstream of the CLTZ. For example, sheet-like deposition can occur as on the Agadir Basin and Tagus Abyssal Plain (Case Studies 1 and 2). It is also important to note that CLTZ s separating channel and lobe facies are not present in all turbidite systems, and therefore one of the aims of this study is to investigate the key controls on their formation.

In this study, transition zones at both canyon and channel mouths are described as CLTZ s as, in reality, canyons and channels represent a morphologic continuum. However, the higher energy of flows exiting canyon mouths means that the characteristics of canyon-lobe transition zones differ to those of channel-lobe transition zones, and these differences are discussed in this paper.

In addition, it is important to recognise that large-scale erosional scours and associated bedforms are not just confined to CLTZ s, but are also found on channel levee backslopes (Normark et al., 1979; Masson et al., 1995; Elliott, 2000) and channel floors (Shor et al., 1990; Kidd et al., 1998). However, this paper will only describe in detail those features associated with the CLTZ.

Data

This study is largely based on high-resolution side-scan sonar imagery, using the Towed Ocean Bottom Instrument (TOBI) and MAK-1 side-scan sonar instruments. TOBI is a 30kHz deep-towed side-scan sonar with a swath width of about 6 km. It has been developed at Southampton Oceanography Centre in the UK. The TOBI unit also operates a 7kHz high-resolution sub-bottom profiler. The MAK-1 is also a 30kHz, deep-towed side-scan sonar, with a swath width of 2 km. This system has been developed by Yuzhmorgeologiya, Russia. A 5kHz high-resolution sub-bottom profile is collected simultaneously with the MAK-1 images.

The Agadir and Lisbon Canyon datasets comprise TOBI images and 7kHz profiles that were collected during RRS Discovery cruise 225 in 1997. In addition, the Agadir Canyon dataset contains a 3.5kHz profile obtained during RRS Discovery cruise 144. The Rhone Fan dataset comprises MAK-1 images and 5kHz profiles, and was collected during the 1992 Training Through Research cruise on the RV Gelendzhik.

Case study 1: The Agadir Canyon mouth

The Agadir Canyon is a major pathway for turbidity currents transporting sediment from the Moroccan Shelf to the intraslope Agadir Basin and the Madeira Abyssal Plain. The canyon is about 200 km long, and extends downslope from the shelf-break at 150 m to the continental rise at 4250 m (Figure 7.1). The canyon is 5-15 km wide and 600-1500 m deep. Below 4250 m the canyon mouth opens into a broad channel between the Agadir and Casablanca Seamounts that is some 25 km wide (Ercilla et al., 1998). TOBI images in this area beyond the canyon mouth show a zone of erosional scours and depositional bedforms extending basinwards in a well-developed CLTZ (Figure 7.2). The main zone of erosion is some 30 km long, and the whole CLTZ extends at least 60 km from the canyon mouth. The scours occur immediately downslope of a change in slope gradient, from 0.2° to 0.08° (Figure 7.3). The proximal region of the CLTZ contains several isolated erosional scours that resemble giant flute marks, as well as areas of amalgamated scours. Isolated erosional scours are up to 500 m long and 250-500 m wide. In plan view they are typically crescentic and widen downslope (Figure 7.4). TOBI profiles through the scours show they are up to 10 m deep, with steeper upslope walls (Figure 7.4b). One of the erosional scours appears to be truncated by an amalgamated scour, indicating that erosion has occurred in successive events. In the centre of the CLTZ is a large amalgamated scour that is at least 9 km wide and up to 10 m deep (Figure 7.5). The seafloor within this scoured area is highly irregular and appears to represent an area of intense seafloor erosion. Further downslope, beyond the amalgamated scour, the seafloor becomes more regular and scours are absent or poorly developed. The TOBI mosaic shows highly variable backscatter in this area, which is interpreted as being a mixture of sediment erosion and deposition, possibly with sediment wave development (Figure 7.2). A single 3.5kHz profile running across the proximal CLTZ shows that turbidity currents have eroded through a sequence of stratified sediments (Figure 7.6). These sediments were deposited on the lower rise, and

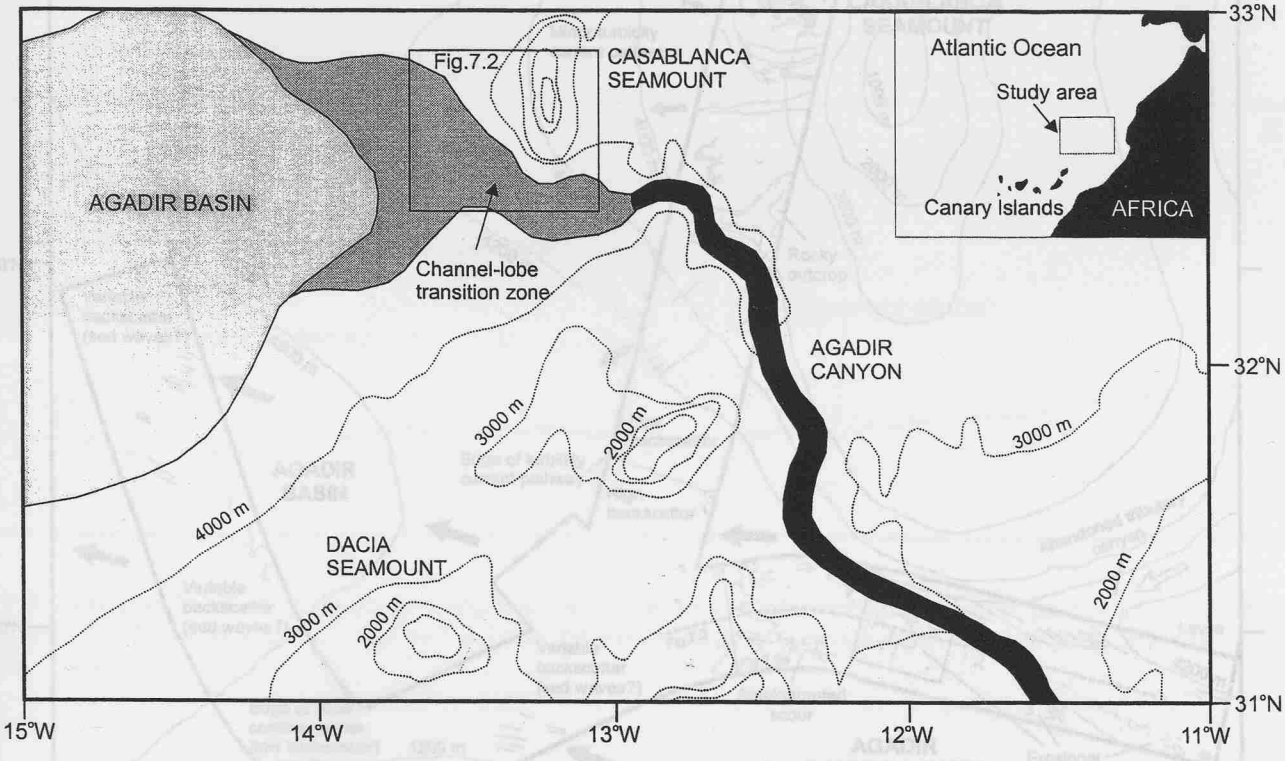

Figure 7.1: Location map of the CLTZ at the mouth of the Agadir Canyon on the Moroccan margin. Box indicates location of Figure 7.2.

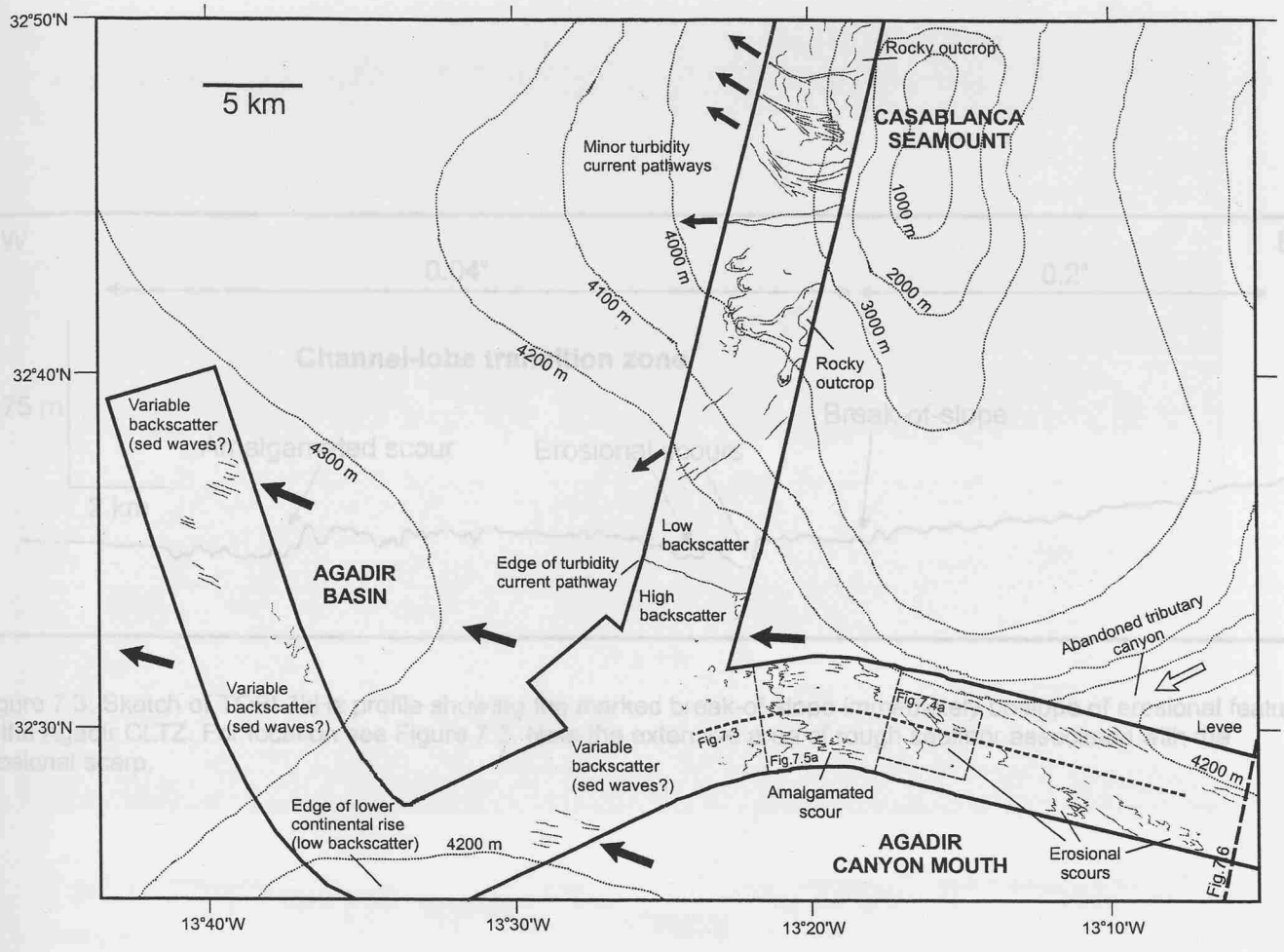

Figure 7.2: Interpretation of TOBI mosaic across the Agadir CLTZ. For location see Figure 7.1. Locations of Figures 7.3-7.6 are shown.

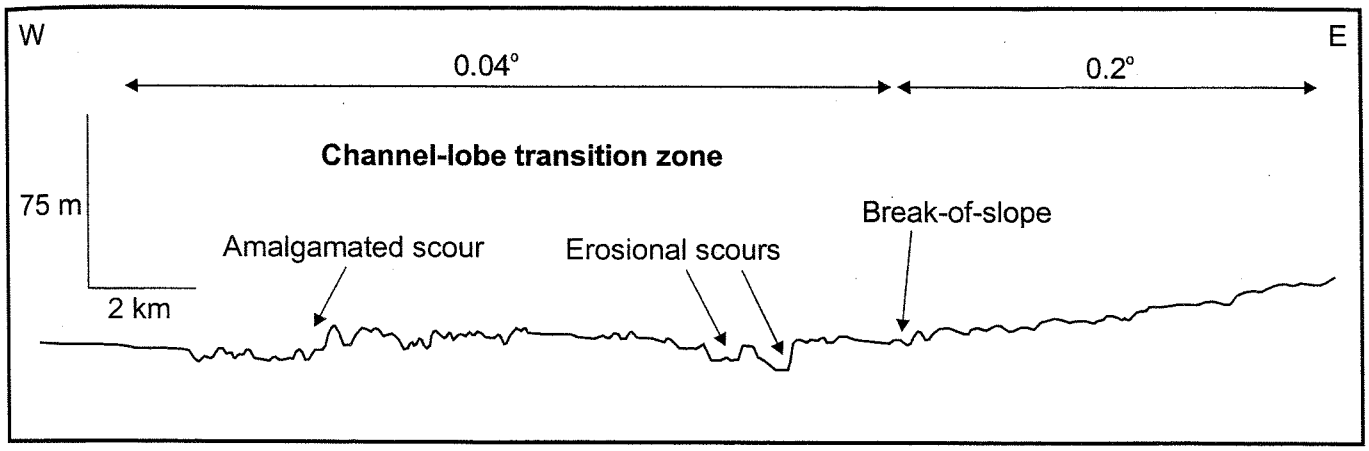

Figure 7.3: Sketch of TOBI 7kHz profile showing the marked break-of-slope immediately upslope of erosional features in the Agadir CLTZ. For location see Figure 7.2. Note the extensive area of rough seafloor associated with the erosional scarp.

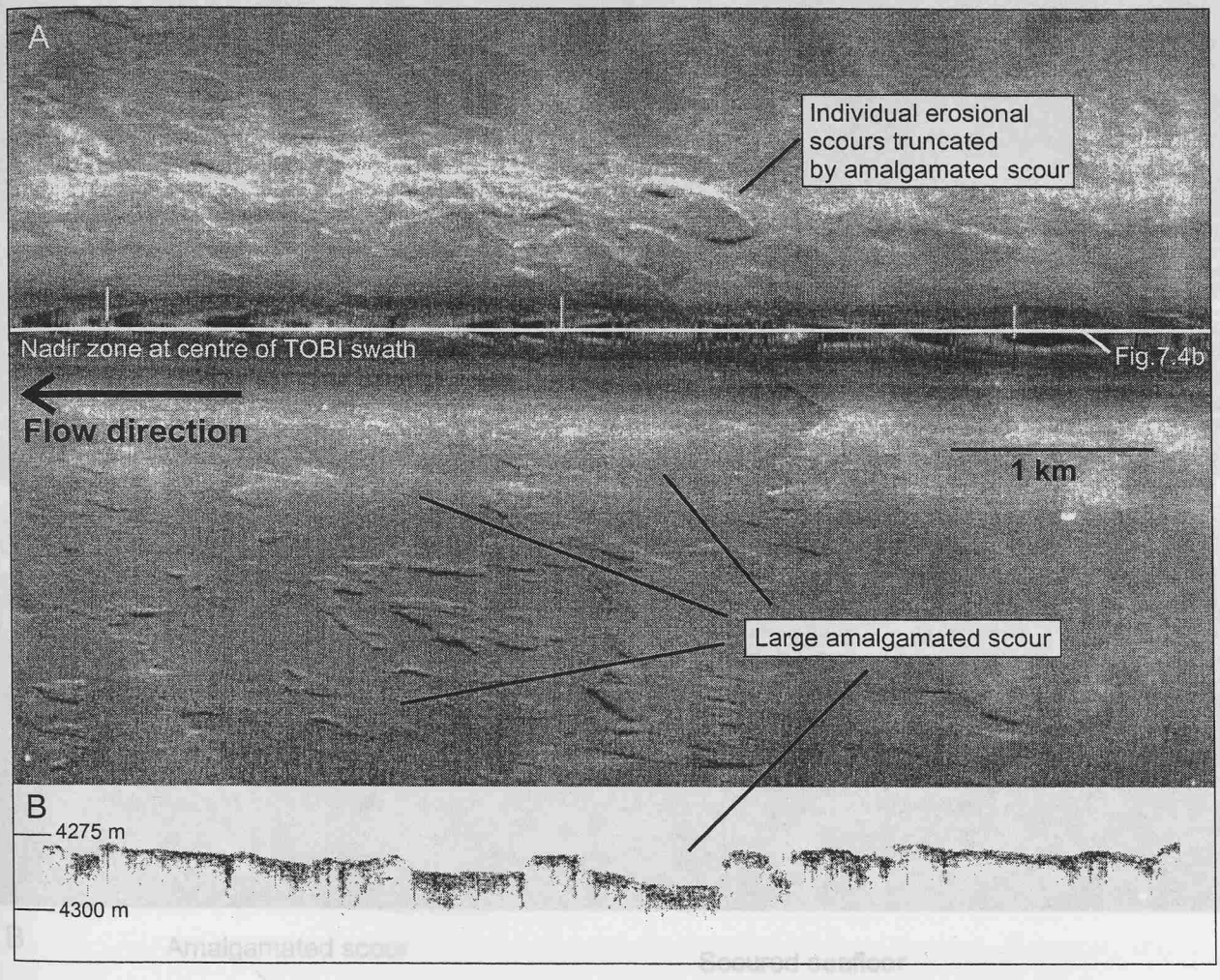

Figure 7.4: (A) TOBI image showing a large amalgamated scour and two spoon-shaped individual scours within the Agadir CLTZ. Note how one of the individual scours appears to be truncated by the amalgamated scour, possibly indicating multiple erosive events. Illumination is outwards from the centre of the TOBI swath. Light tones = high backscatter and dark tones = low backscatter. For location see Figure 7.2. (B) TOBI 7kHz profile showing the morphology of scours in longitudinal section. For location see Figure 7.4a

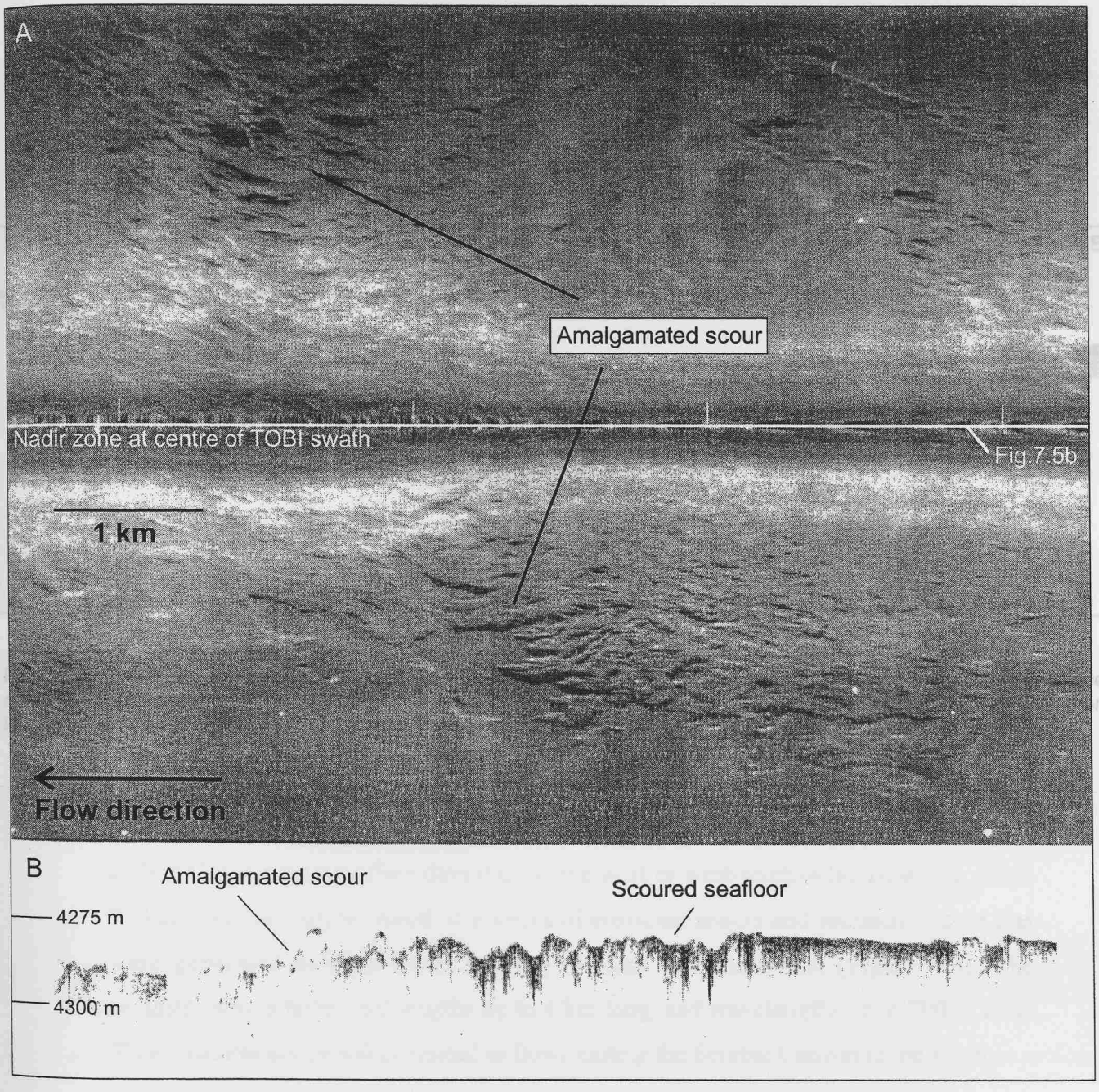

Figure 7.5: (A) TOBI image showing an extensive amalgamated scour within the Agadir CLTZ. Note the irregularity of the scoured surface. Illumination is outwards from the centre of the TOBI swath. Light tones = high backscatter and dark tones = low backscatter. For location see Figure 7.2. (B) TOBI 7kHz profile showing the irregular topography of the scoured seafloor associated with the amalgamated scour. For location see Figure 7.5a.

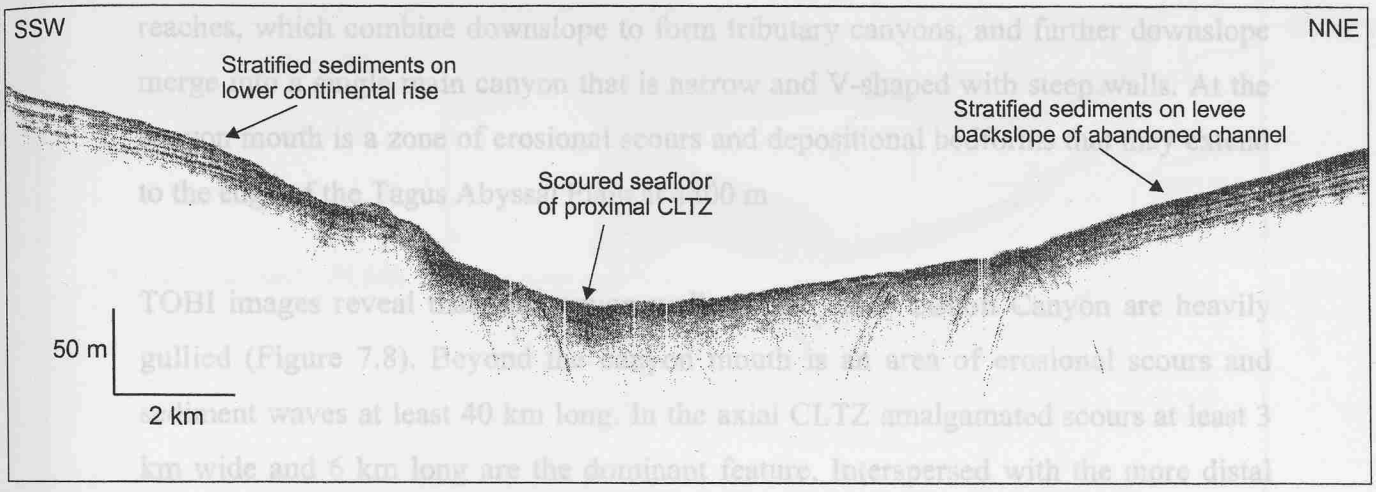

Figure 7.6: 3.5kHz profile across the proximal Agadir CLTZ, highlighting how the erosion has truncated a sequence of stratified sediments, and the lack of acoustic penetration on the scoured surface indicating a hard substrate. For location see Figure 7.2.

also on the backslope of a levee bordering an abandoned canyon to the north (Figure 7.2).

Case study 2: The Lisbon Canyon mouth

The Lisbon Canyon is located offshore of the Tagus River on the west Portugese margin (Figure 7.7). The canyon is some 90 km long and extends from the shelf-break at 200 m to the base of the lower rise at 4600 m. There is a complex system of gullies in its upper reaches, which combine downslope to form tributary canyons, and further downslope merge into a single main canyon that is narrow and V-shaped with steep walls. At the canyon mouth is a zone of erosional scours and depositional bedforms that may extend to the edge of the Tagus Abyssal Plain at 4800 m.

TOBI images reveal that the canyon walls of the outer Lisbon Canyon are heavily gullied (Figure 7.8). Beyond the canyon mouth is an area of erosional scours and sediment waves at least 40 km long. In the axial CLTZ amalgamated scours at least 3 km wide and 6 km long are the dominant feature. Interspersed with the more distal amalgamated scours are sediment waves with wavelengths of 1-2 km. At the edge of the CLTZ, slightly south from the main flow pathway, is an area of chevron-shaped features (Figure 7.9). These features are V-shaped and open out downslope. They are up to 1 km long and 800 m across, and in places appear to coalesce to form small amalgamated scours. Generally, the alignment of bedforms and scours in the CLTZ beyond the Lisbon Canyon indicate flow directions to the west or west-south-west. However, about 75 km from the canyon mouth is a series of erosional scours and sediment waves that were generated beneath flows moving towards the north-west (Figure 7.8). The sediment waves have crest lengths up to 4 km long, and wavelengths up to 700 m long. These features are probably related to flows exiting the Setubal Canyon to the south.

Case study 3: The Rhone Fan

A well-developed CLTZ occurs on the upper Rhone Fan, immediately downslope of a major channel mouth (Figure 7.10). This recently avulsed channel has deposited a sandy lobe (termed the neofan by Droz and Bellaiche, 1985) on top of an earlier levee sequence and slump deposit. This lobe has an areal extent of about 750 km^2, and a thickness of less than 100 m. The channel feeding the lobe decreases in depth downslope from 80 m to less than 10 m, and widens from 500 m to 800 m. A major

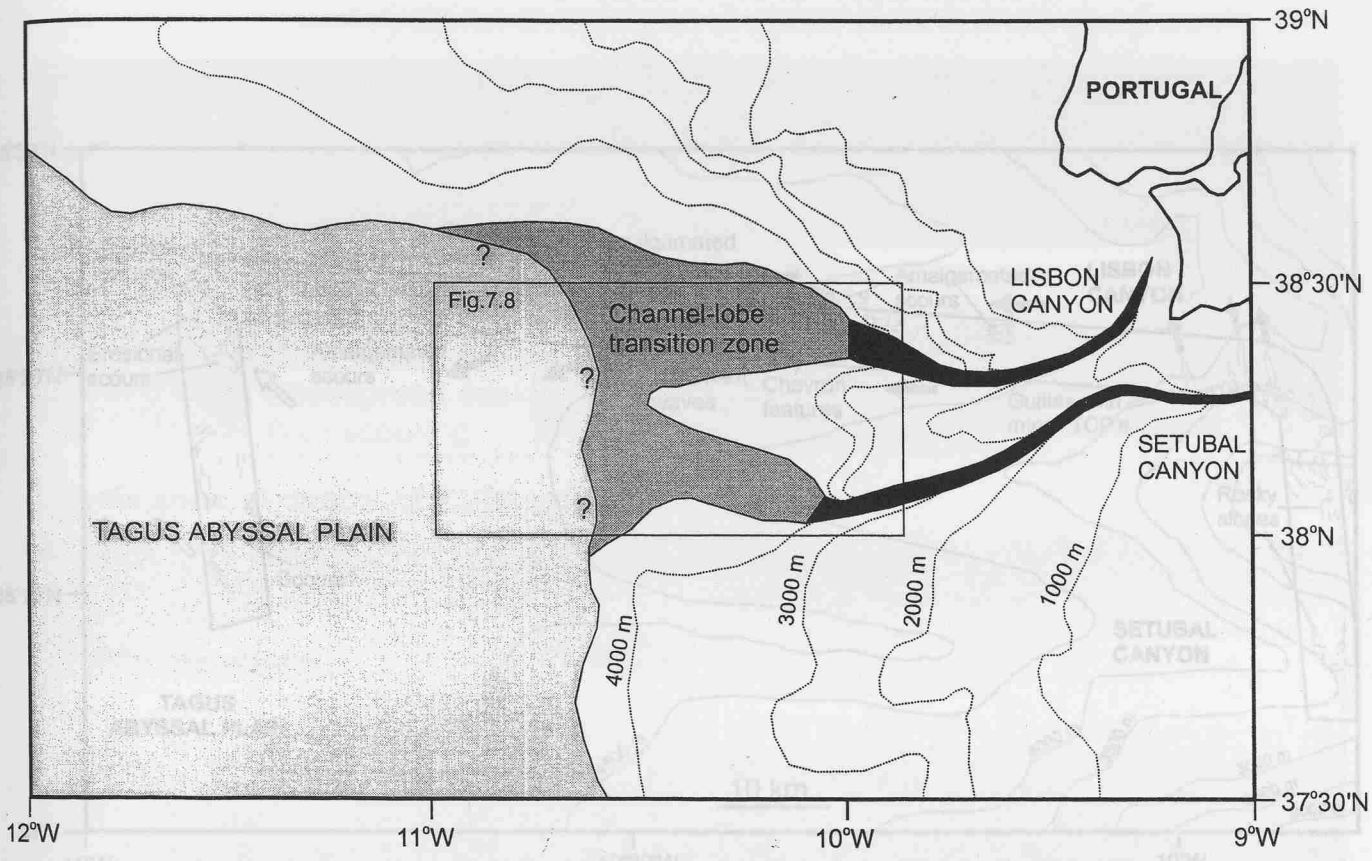

Figure 7.7: Location map of the CLTZ at the mouth of the Lisbon and Setubal Canyons on the Portugese margin. Box indicates location of Figure 7.8.

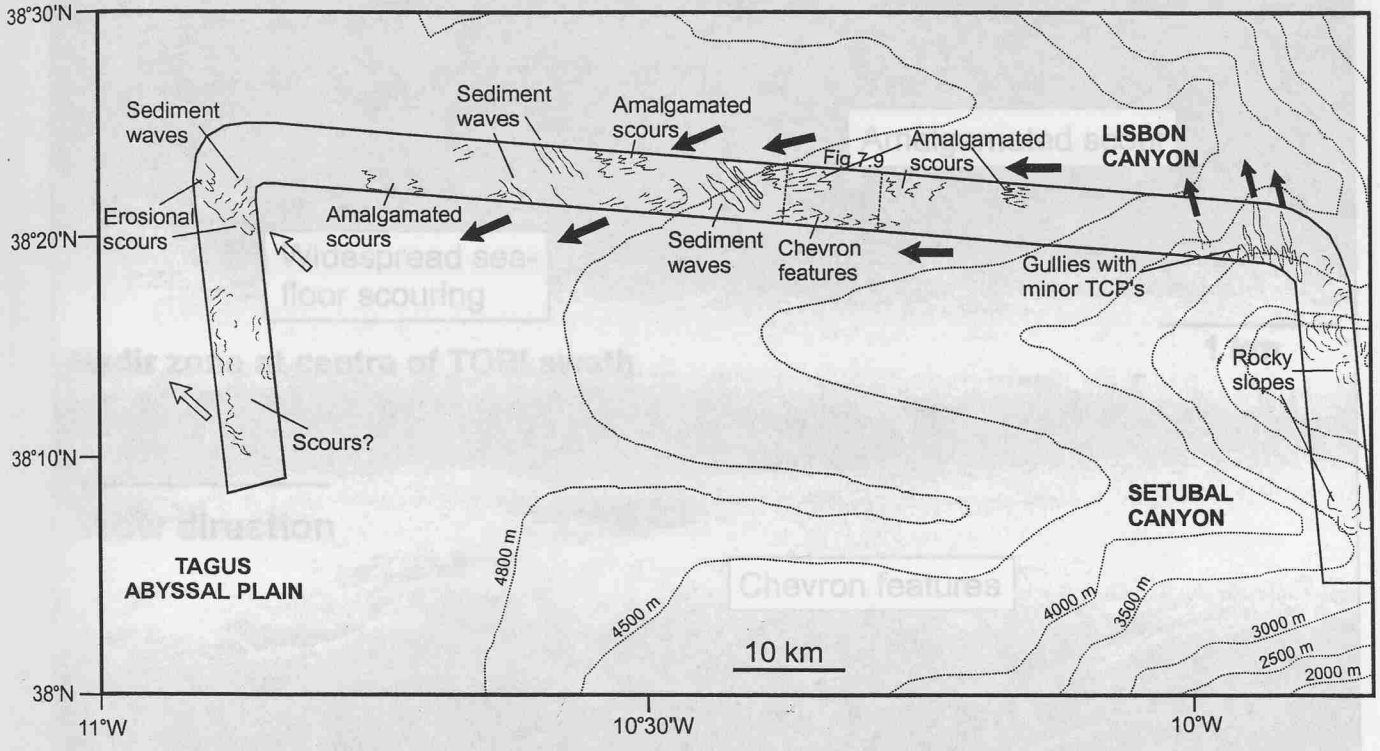

Figure 7.8: Interpretation of TOBI mosaic across the Lisbon and Setubal CLTZ's. Note how the orientation of erosional scours and bedforms in the Lisbon CLTZ (black arrows) is different to that in the Setubal CLTZ (white arrows), and the complex arrangement of erosional scours and sediment waves. For location see Figure 7.7. Location of Figure 7.9 is indicated.

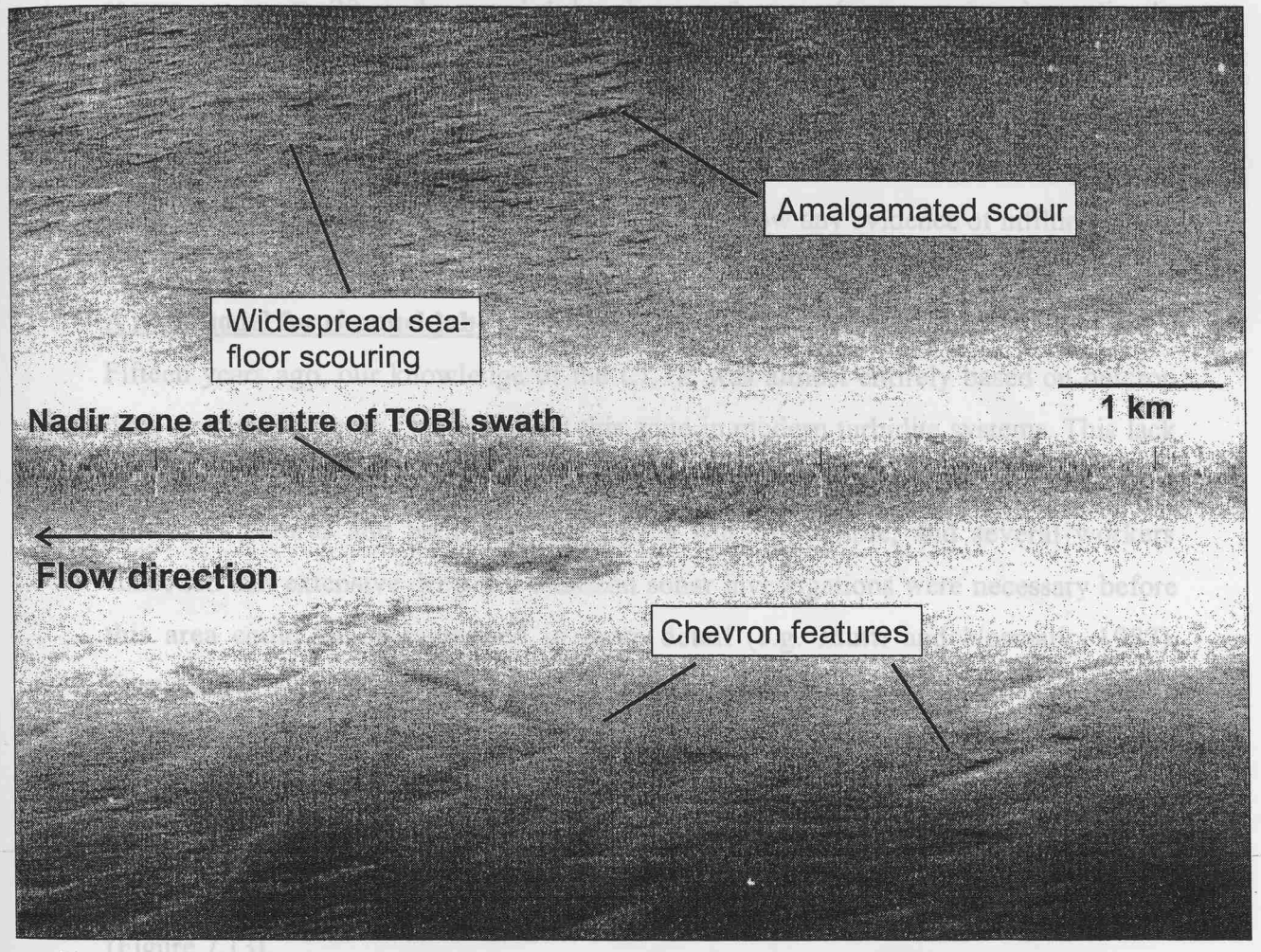

Figure 7.9: TOBI image showing an area of widespread seafloor erosion associated with an amalgamated scour, and a zone of chevron-shaped features within the Lisbon CLTZ. Illumination is outwards from the centre of the TOBI swath. Light tones = high backscatter and dark tones = low backscatter. For location see Figure 7.8.

break-in-slope occurs just upslope from the channel mouth, with a gradient decrease from 0.57° to 0.29° (Kenyon et al., 1995). Beyond the channel mouth, the CLTZ is characterised by a series of erosional scours of various sizes (Figure 7.11). The largest scours are up to 20 m deep and 1 km long and occur in the region immediately downslope from the channel termination (Figure 7.12). They are asymmetrical, with a steeper upslope wall, and have cut through a large proportion of the sandy lobe and underlying transparent facies. A series of smaller scours occur further downslope, up to 30 km from the channel mouth. None of the scours show any evidence of infilling.

A new model for channel-lobe transition zones

Fifteen years ago, our knowledge of the CLTZ was almost entirely based on outcrop data, and very little was known about this zone in modern turbidite systems. This lack of modern data meant that detailed analysis of the distribution and dimensions of erosional features and bedforms in CLTZ s was impossible, and several workers conceded that extensive deep-tow sidescan sonar investigations were necessary before this area could be characterised in more detail (e.g. Mutti and Normark, 1987). Fortunately, in the last few years the required upsurge in deep-tow studies of modern turbidite systems has taken place, and it is now possible to characterise the features of the CLTZ with more confidence. The three case studies presented in this paper are now combined with other published studies in an attempt to produce a more comprehensive, up-to-date model for the distribution and dimensions of seafloor features in CLTZ s (Figure 7.13).

Controls on the location and size of CLTZ s

1) Seafloor topography

CLTZ s are located immediately downslope of channel/canyon mouths, and are typically associated with a significant break-in-slope (e.g. Figure 7.3). Turbidity currents are likely to undergo a hydraulic jump in this area, during the transformation from confined to unconfined flow (Komar, 1971). This leads to rapid flow expansion and increased turbulence, which in turn leads to seafloor erosion. However, although several studies conclude that hydraulic jumps probably are responsible for the formation of erosional scours in CLTZ s (e.g. Mutti and Normark, 1987; 1991; Normark and Piper, 1991; Kenyon et al., 1995; Millington and Clark, 1995, and Palanques et al., 1996), only the work of Komar (1971) has a numerical basis for this theory. He

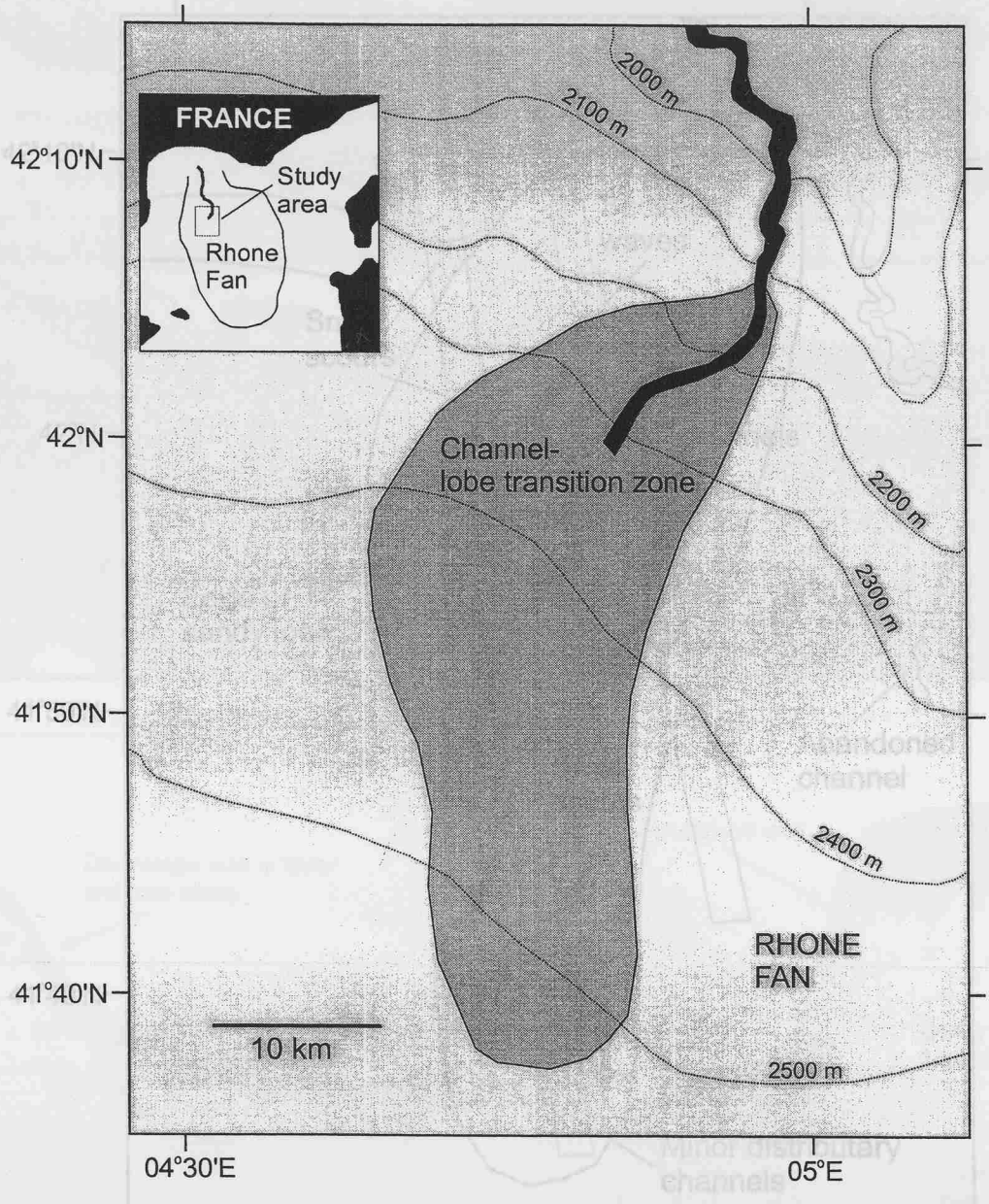

Figure 7.10: Location map of the CLTZ on the Rhone Fan (modified from Kenyon et al., 1995).

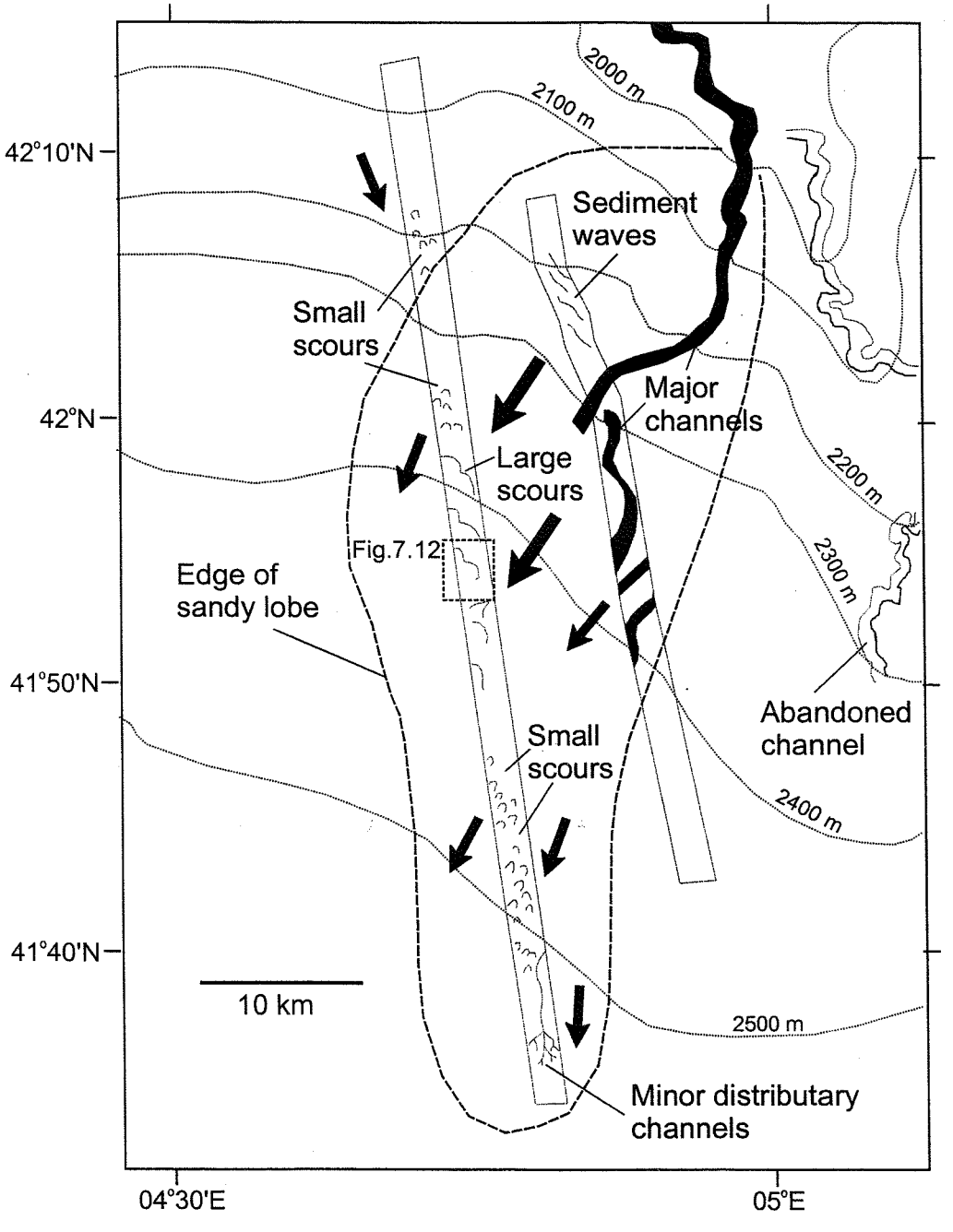

Figure 7.11: Interpretation of MAK1 images across the Rhone CLTZ. Rectangles indicate MAK1 swath coverage. Note the gradation from large scours near the channel mouth to small scours further downslope. For location see Figure 7.10.

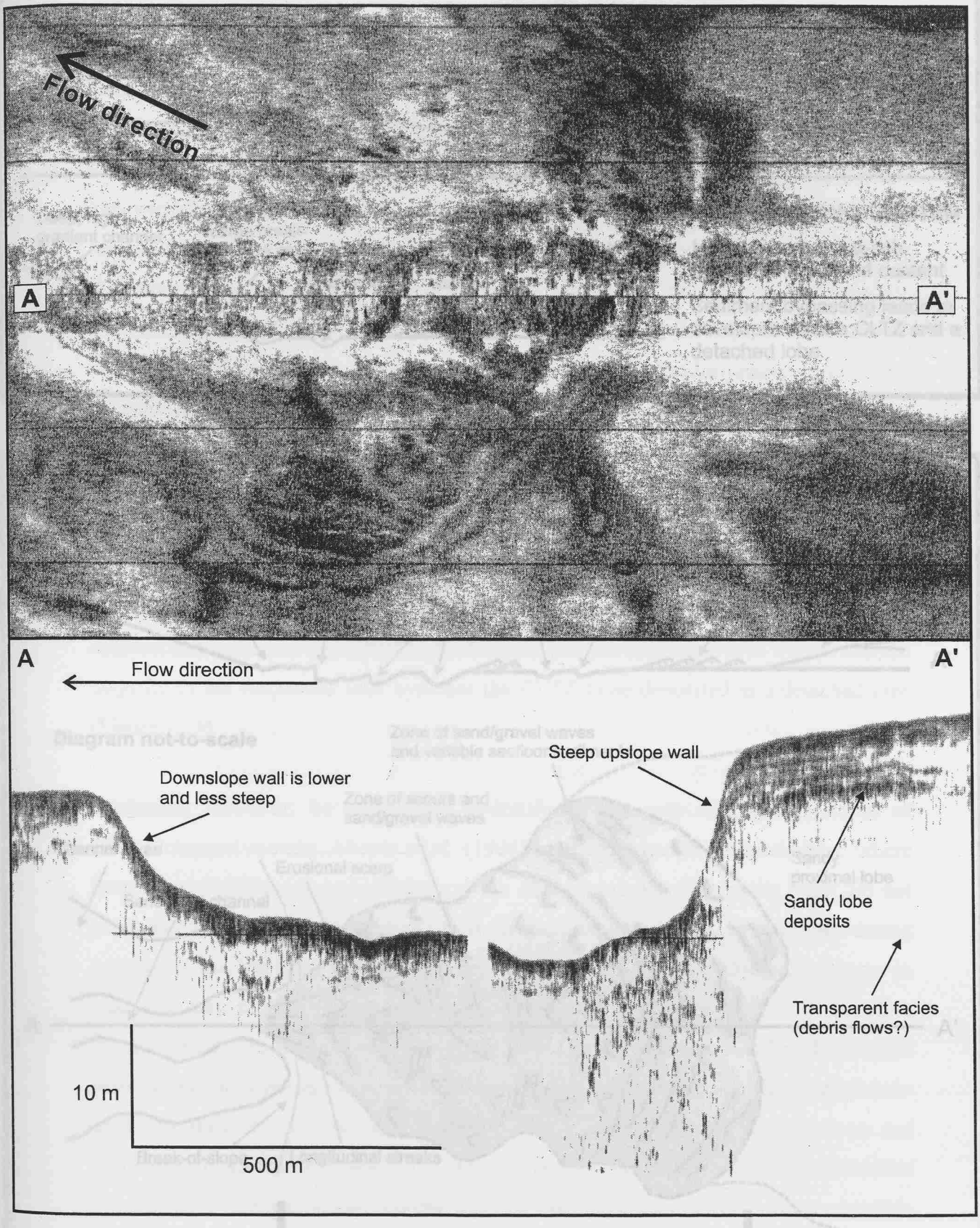

Figure 7.12: MAK1 image showing a large erosional scour within the Rhone CLTZ. Dark tones = high backscatter and light tones = low backscatter. For location see Figure 7.11. Also shown is a 5kHz profile (line A-A') showing the scour in longitudinal section.

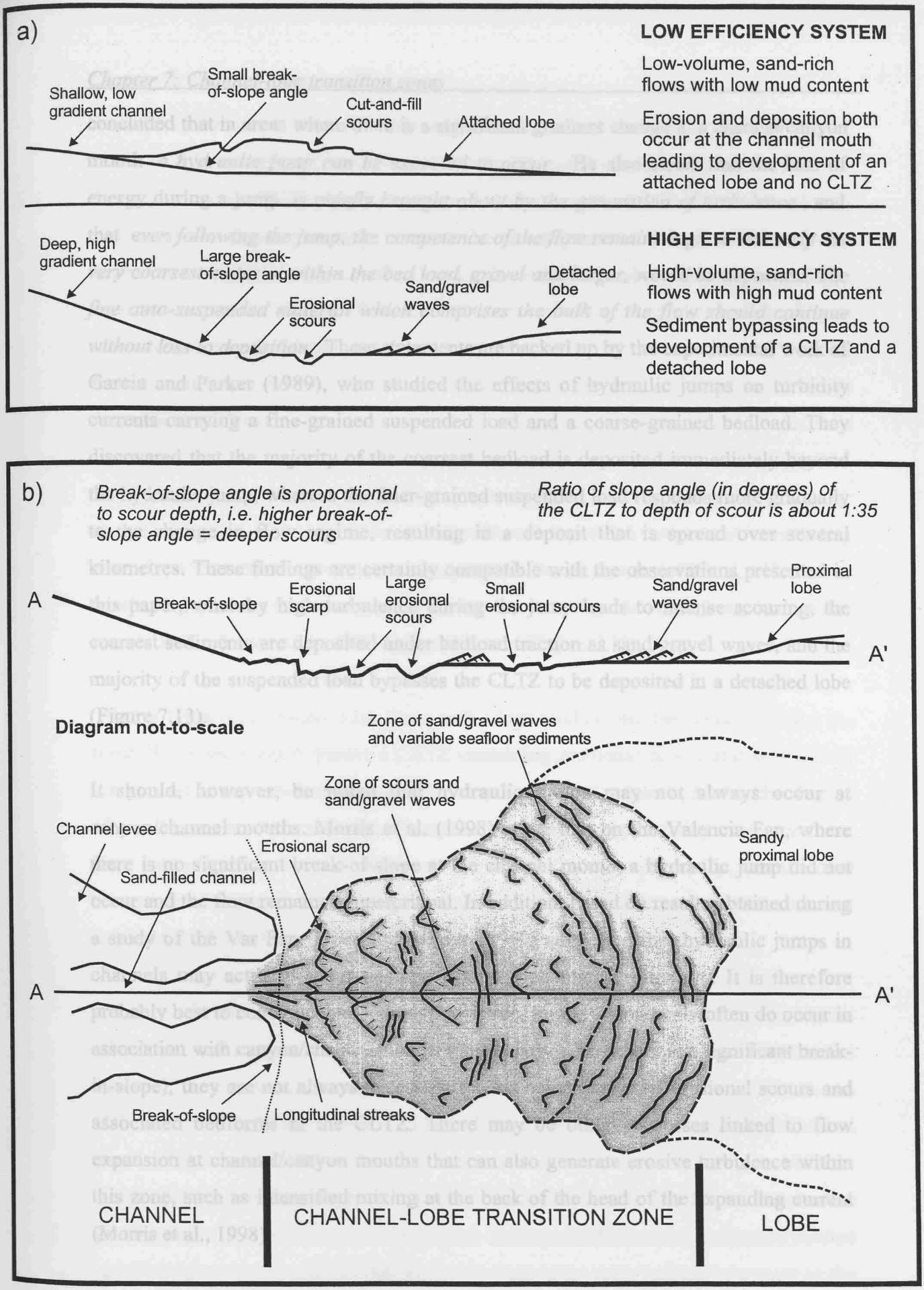

Figure 713: (A) Summary diagram showing typical cross-sections through a low efficiency system with an attached lobe, and a high efficiency system with a detached lobe. (B) Schematic model showing the spatial distribution of erosional scours and depositional bedforms within a CLTZ in a high efficiency system.

concluded that in areas where there is a significant gradient change at a channel/canyon mouth *a hydraulic jump can be expected to occur.* He also states that the loss of energy during a jump *is chiefly brought about by the generation of turbulence* , and that *even following the jump, the competence of the flow remains high so that only the very coarsest material within the bed load, gravel and larger, would be deposited. The fine auto-suspended material which comprises the bulk of the flow should continue without loss to deposition.* These statements are backed up by the experimental work of Garcia and Parker (1989), who studied the effects of hydraulic jumps on turbidity currents carrying a fine-grained suspended load and a coarse-grained bedload. They discovered that the majority of the coarsest bedload is deposited immediately beyond the hydraulic jump, whereas the finer-grained suspended load responds more gradually to the change in flow regime, resulting in a deposit that is spread over several kilometres. These findings are certainly compatible with the observations presented in this paper, whereby high turbulence during the jump leads to intense scouring, the coarsest sediments are deposited under bedload traction as sand/gravel waves, and the majority of the suspended load bypasses the CLTZ to be deposited in a detached lobe (Figure 7.13).

It should, however, be noted that hydraulic jumps may not always occur at canyon/channel mouths. Morris et al. (1998) argue that on the Valencia Fan, where there is no significant break-of-slope at the channel mouth, a hydraulic jump did not occur and the flow remained supercritical. In addition, based on results obtained during a study of the Var Fan, Piper and Savoye (1993) suggested that hydraulic jumps in channels may actually occur upslope from the channel termination. It is therefore probably best to conclude that, although hydraulic jumps undoubtedly often do occur in association with canyon/channel mouths (particularly where there is a significant break-in-slope), they are not always necessary for the development of erosional scours and associated bedforms in the CLTZ. There may be other processes linked to flow expansion at channel/canyon mouths that can also generate erosive turbulence within this zone, such as intensified mixing at the back of the head of the expanding current (Morris et al., 1998).

2) Turbidity current volume and composition

Mutti (1985) recognised that the volume of turbidity currents will determine the development of a CLTZ and the location of sand deposition. He concluded that large-volume flows will excavate huge erosional features beyond the channel mouth, and will deposit the majority of their load as basinwide unchannelised sandstone lobes. Under these circumstances, the CLTZ is generally bypassed by most of the sand, leading to formation of detached lobes. Mutti and Normark (1987; 1991) developed this concept further, and presented two general models for deposition beyond the channel mouth from sand-rich flows:

1) For relatively low-volume, sand-laden flows with a low mud content they suggested the area of erosional scour and sediment deposition both occur immediately downslope from the channel mouth (the poorly efficient system of Mutti, 1979). This results in deposition of a wedge of sediment that downlaps downfan from the channel mouth, and includes cut and fill erosional scours (Figure 7.13).

2) For large-volume sand-laden flows with a high mud content they concluded that most of the sediment bypasses a CLTZ containing erosional scours and sand/gravel waves, and is deposited away from the channel mouth as a detached lobe (the highly efficient system of Mutti, 1979). Therefore it seems that the turbidity current volume must be sufficiently large to create enough energy for scour formation, and the mud content must be high enough to enable continued transport of the turbidity current load beyond the CLTZ (Figure 7.13).

Analysis of modern data indicates that the areal extent of erosional features within the CLTZ is closely related to the size of the turbidite system and the turbidity current volume. For example, the main erosional zones in the Agadir, Lisbon, Rhone and Valencia systems extend between 25 and 45 km downcurrent from the canyon/channel mouth. The whole CLTZ in these systems may extend basinwards for up to 100 km. These systems are very large, for example, the areal extent of the Rhone Fan is over 10,000 km^2 (Bellaiche et al., 1981), and the Agadir Basin is filled with ponded turbidites that cover some 20,000 km^2. Although large-scale turbidity currents in the Agadir Basin are infrequent (1 every 30,000 years), they often have volumes >100 km^3 and are consequently very powerful (see Chapter 6). In contrast, the erosional zones on

the smaller Navy and San Lucas Fans extend only 3-5 km downcurrent, and the whole CLTZ may be just 6 km long (Normark, 1970; Normark et al., 1979). This is because these fans are on a much smaller scale than those described above, for example, the Navy Fan has an area of just 560 km^2 (Normark and Piper, 1983). As a consequence the size and energy of turbidity currents in these systems is much lower, and therefore the erosion zone is smaller.

3) Canyon/channel size and gradient

The dimensions and maximum gradient of a canyon/channel may give an indirect indication of other parameters controlling the development of a CLTZ, e.g. flow volume. For example, a study of two modern turbidite systems in the Bering Sea found that only one, the Umnak system, has a well-developed CLTZ and a detached lobe (Kenyon and Millington, 1995). This system is fed by a channel which has a maximum gradient of 5.7°, is up to 350 m deep, and has well-developed levees. In the smaller Pochnoi system an attached lobe occurs adjacent to the channel mouth and a CLTZ is not developed. This system is fed by a channel that has a maximum gradient of 2.9°, is up to 60 m deep, and has poorly-developed levees. These results suggest that the Umnak system is fed by larger, higher velocity flows, and the steeper channel gradient may lead to a more abrupt break-of-slope. This combination leads to development of a CLTZ.

Distribution and dimensions of erosional features and bedforms in CLTZ s

1) Erosional features

Erosional features in CLTZ s can take on a variety of forms, including individual spoon- and chevron-shaped scours. All the data collected indicate that individual erosional scours in CLTZ s range from 2-60 m deep, 50-2000 m wide, and 350-2000 m long (Table 7.1). Smaller scours are probably widespread but are beyond the resolution of most seafloor imaging tools. In plan view scours are typically elongated parallel to flow direction, and become wider and shallower downcurrent. In profile, they are asymmetrical, with a steeper, higher upcurrent face and a shallower downcurrent face (e.g. Figure 7.12). Individual scours may be cut by later scours, suggesting multiphase erosion by several turbidity currents (Figure 7.4). Several studies have recognised distinctive mounds immediately downcurrent from erosional scours, for example, Normark et al. (1979) recognised a low bulge downslope of the two largest depressions

Location and environment	Maximum dimensions			Slope angle (°)	Reference
	Depth (m)	Width (m)	Length (m)		
Modern channel-lobe transition zones					
Agadir Canyon	10.5	?	500	0.2 - 0.04	this study
Lisbon Canyon	?	600	1200	?	this study
Rhone Fan	20	?	1000	0.57 - 0.29	Kenyon et al., 1995
Valencia Fan	8	80	?	?	Morris et al., 1998
Mississippi Fan	2	?	2000	0.14	O'Connell et al., 1990
San Lucas Fan	60	?	600	1.6	Normark, 1970
Hueneme Fan	2	?	?	?	Piper et al., 1999
Navy Fan	20	400	350	0.97	Normark et al., 1979
Bering Sea	5	2000	?	?	Kenyon and Millington, 1995
Ancient channel-lobe transition zones					
Annot Basin	20	?	?	?	Hilton, 1995
Albian Flysch, Spain	5	50	?	?	Vicente Bravo and Robles, 1995
Other turbiditic environments					
Stromboli Canyon: inner bend of canyon	?	400	?	?	Kidd et al., 1998
Laurentian Fan: flow expansion in fan-valley	100	?	1000	1.43 - 0.97	Shor et al., 1990
Monterey Fan: levee-overbank	10	1000	?	1.3	Masson et al., 1995
Var Fan: levee-overbank	90	?	2000	0.68	Malinverno et al., 1988
West Ireland: ancient levee-overbank	3	45	25	?	Elliott, 2000

Table 7.1: Dimensions of erosional scours in modern and ancient CLTZ's, compared to other turbiditic environments. The slope angle on which the scours were developed is included where known.

on the Navy Fan, and Vicente Bravo and Robles (1995) described a series of hummocky-like bedforms beyond scour mouths in outcrop. They found that the hummocks were up to 40 m long, 1.5 m high, and composed of gravel and pebbly sand. These mounds are probably deposited downcurrent of scours because of interaction between the main flow of the turbidity current and turbulent eddies within the scour hollows.

At the mouths of the Agadir and Lisbon Canyons, large amalgamated scours have been imaged that appear to be formed of coalescing individual scours (Figures 7.5 and 7.8). These amalgamated scours display a similar depth range to individual scours, but may be up to 9 km wide and 6 km long, indicating widespread seafloor erosion. Similar features consisting of laterally coalesced individual scours have also been described from channel levee backslopes (Masson et al., 1995; Elliott, 2000). These amalgamated scours probably represent areas affected by more intense erosive turbulence than individual scours.

Based on the limited amount of quantitative data available, there appears to be a relationship between slope angle and depth of scour in CLTZ s (Figure 7.14). Higher slope angles lead to deeper scours, and the overall ratio of slope angle (in degrees) to depth of deepest scour in a CLTZ (in metres) is about 1:35. Therefore, for a slope of 1°, the depth of scour can be expected to be approximately 30-40 m, while for a slope of 0.5°, the depth of scour will be about 15-20 m. This relationship may also be used in reverse, i.e. where the depth of scour is known it may be used to predict slope angles in the region of the CLTZ. It is interesting to note that the three values for scours in channel floor and levee overbank environments differ substantially to those obtained from CLTZ s, and may be due to differences in flow velocity and/or seafloor sediment composition in these areas.

A similar relationship can be recognised between depth of scour and the change of slope angle at the break-of-slope, although quantitative data are again sparse. For example, in the Eastern Valley of the Laurentian Fan the change of slope angle is 0.5° and the depth of scour is 100 m (Shor et al., 1990). On the Rhone Fan and the Agadir Canyon mouth the change of slope angles are lower at 0.3° and 0.16°, and the depth of scour is only 20

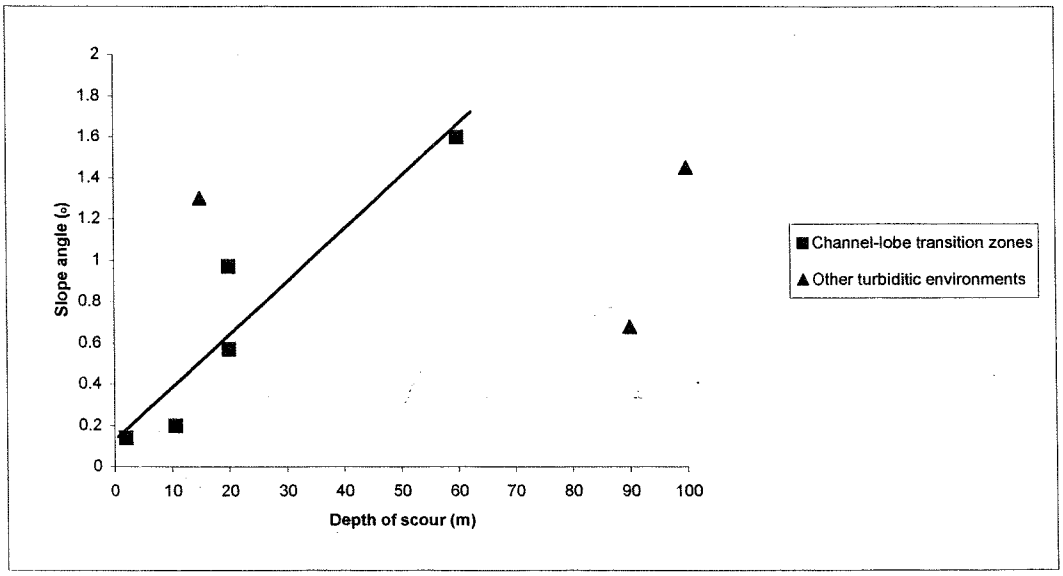

Figure 7.14: Chart showing the relationship between slope angle and depth of scour in CLTZ's and other turbiditic environments. Note that there appears to be a strong positive correlation for the relationship between scour depth and slope angle in CLTZ's, and that the values from other turbiditic environments are more scattered.

m and 10.5 m respectively. This relationship, where the change of slope angle is proportional to scour depth, has also been noted by Millington and Clark (1995).

The distribution of erosional features in CLTZ s appears to show some regularity (Figure 7.13). Generally, amalgamated scours and the largest individual spoon-shaped scours occur immediately downslope from canyon/channel mouths. Further downslope, smaller spoon-shaped scours are found. Chevron-shaped features have only been described from the Valencia and Lisbon CLTZ s (Figure 7.9), but in both cases they occur downslope of, or adjacent to, the axial zone of large scours and erosional scarps. However, it is unclear as to whether these features are erosional or depositional, or a combination of both.

2) Sand/gravel waves

Sand/gravel waves are commonly developed in CLTZ s (e.g. Morris et al., 1998) but are rarely recognised in outcrop due to their large scale and subtle morphology. Examples from modern datasets indicate that they have wave lengths up to 1-2 km, wave heights up to 4 m and crest lengths up to 4 km. Sand/gravel waves in CLTZ s are generally absent from the proximal CLTZ, and are more commonly developed in association with small erosional scours in the central and distal CLTZ (Figure 7.13). They may show evidence of reworking and erosion by later turbidity currents, and are generally formed by tractional processes, unlike the large-scale (up to 70 m high), fine-grained sediment waves found on levee backslopes which are dominantly formed by sediment falling out of suspension (e.g. Normark et al., 1980, Wynn et al., 2000b).

3) Other bedforms

Other bedforms developed in CLTZ s include longitudinal streaks aligned parallel to the flow direction. These have been described from the Umnak and Valencia CLTZ s (Kenyon and Millington, 1995; Morris et al., 1998), and are up to 15 km long and have a spacing of about 2 km. They are commonly developed within, or immediately downslope from the channel/canyon mouth (Figure 7.13), and are believed to be erosional features that occur in areas of flow expansion.

Sediment distribution in CLTZ s

The lateral distribution of sediments in CLTZ s, and the internal architecture of erosional scours and sand/gravel waves is poorly documented. This is partly because of the problems associated with recovering cores from modern CLTZ s, as generally the sediments are too coarse-grained to allow core penetration (Mutti and Normark, 1987; 1991). For example, Morris et al. (1998) reported poor recovery of gravity cores from a survey undertaken on the Valencia CLTZ, which was thought to be due to the presence of impenetrable sand layers.

Some idea of lateral sediment distribution within the CLTZ can be derived from side-scan sonar images, which often show a highly variable pattern of backscatter within this region. For example, Normark et al. (1979) described areas of variable backscatter from channel terminations on the Navy Fan, and interpreted them as areas of abundant fine-scale relief such as small bedforms, or textural changes such as grain-size. Similar patterns of variable backscatter are visible on TOBI images from the Agadir Canyon mouth (Figure 7.2), and are interpreted as being coarse-grained sediment waves, some of which appear to have been partly eroded or reworked during later flows.

The sediment fill of erosional scours in CLTZ s is highly variable, and is probably representative of the decreasing activity of the feeder system, rather than the activity of the flows which cut the scours. For example, scours that are totally filled with muddy pelagic/hemipelagic sediments probably represent complete abandonment of a turbidite system (Shanmugan and Moiola, 1988), whereas mud-draped scours with a thin-bedded, fine-grained turbidite fill probably indicate a gradual reduction in flow volume and energy. Scours within active turbidite systems will probably remain unfilled, as successive large flows remove the fine sediments accumulated since the preceding flow. However, in active systems with fluctuating flow volumes, a complex pattern of scour filling and infilling will be expected. Most scours within ancient CLTZ s are cut through pre-existing sand-mud turbidites, contain abundant rip-up mud clasts, and may show evidence of multiphase scouring (Mutti, 1985; Mutti et al., 1989; Millington and Clark, 1995; Vicente Bravo and Robles, 1995). In these examples the scour fill consists of a thin mud drape overlain by interbedded thin turbidite sands and muds, with a high sand-mud ratio (Figure 7.15). Mud-dominated scour-fills have been described from other turbiditic environments (e.g. Elliott, 2000), but may also occur in CLTZ s

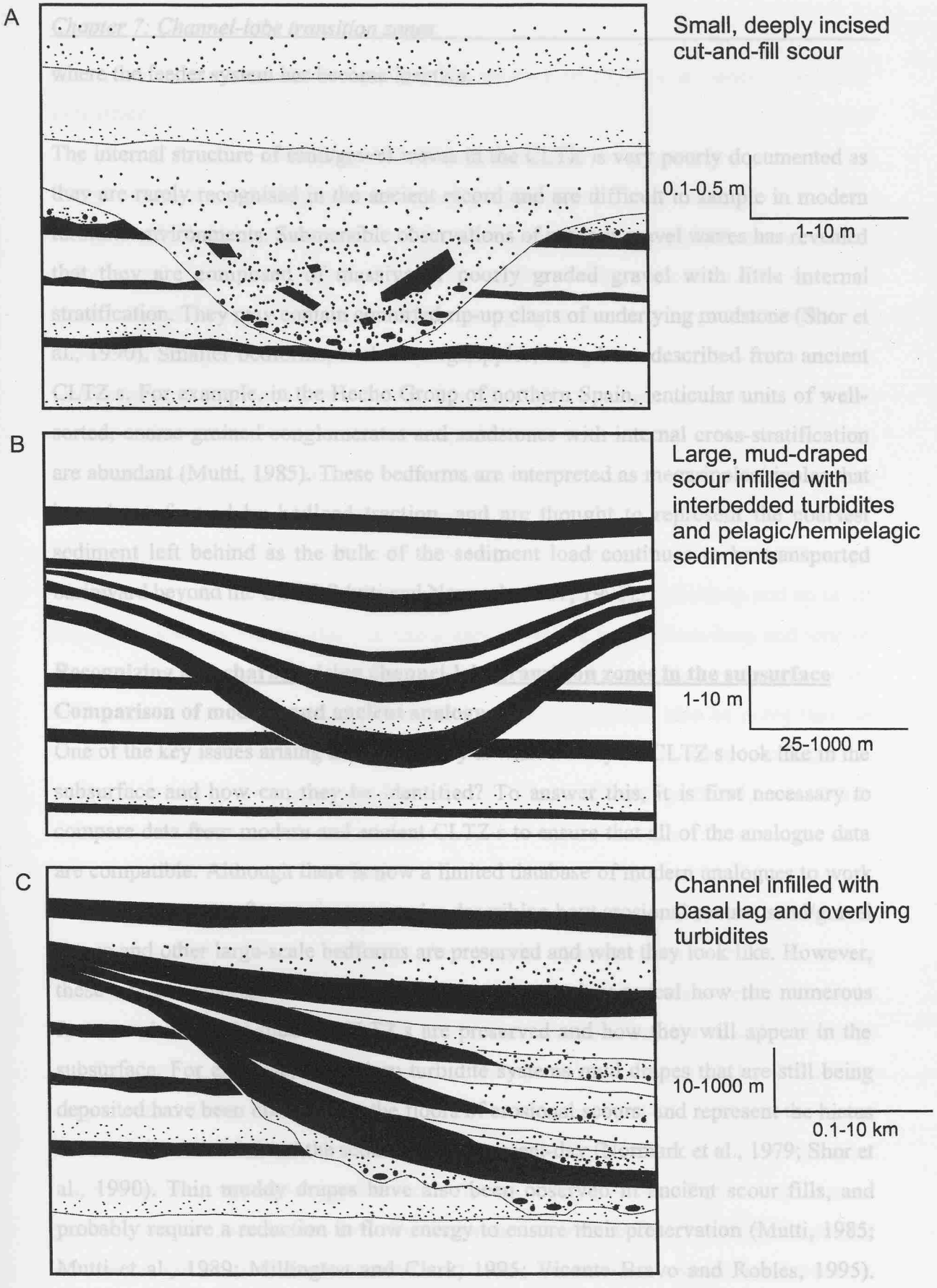

Figure 7.15: Schematic diagrams illustrating the typical fill of A) small cut-and-fill scours B) large mud-draped scours and C) turbidite channels. Note the variation in dimensions, in particular the larger size of channels compared to both types of scour.

where the feeder system has become inactive.

The internal structure of sand/gravel waves in the CLTZ is very poorly documented as they are rarely recognised in the ancient record and are difficult to sample in modern turbidite environments. Submersible observations of modern gravel waves has revealed that they are composed of massive or poorly graded gravel with little internal stratification. They may contain contorted rip-up clasts of underlying mudstone (Shor et al., 1990). Smaller bedforms, such as megaripples, have been described from ancient CLTZ s. For example, in the Hecho Group of northern Spain, lenticular units of well-sorted, coarse-grained conglomerates and sandstones with internal cross-stratification are abundant (Mutti, 1985). These bedforms are interpreted as megaripples/ripples that have been formed by bedload traction, and are thought to represent the coarsest sediment left behind as the bulk of the sediment load continues to be transported basinward beyond the CLTZ (Mutti and Normark, 1987; 1991).

Recognizing and characterising channel-lobe transition zones in the subsurface

Comparison of modern and ancient analogues

One of the key issues arising from this study is what exactly do CLTZ s look like in the subsurface and how can they be identified? To answer this, it is first necessary to compare data from modern and ancient CLTZ s to ensure that all of the analogue data are compatible. Although there is now a limited database of modern analogues to work with, there are very few ancient examples describing how erosional scours, sand/gravel waves and other large-scale bedforms are preserved and what they look like. However, these ancient analogues are extremely important as they reveal how the numerous features observed in modern CLTZ s are preserved and how they will appear in the subsurface. For example, in modern turbidite systems mud drapes that are still being deposited have been observed on the floors of erosional scours, and represent the hiatus between the event that cut the scours and the present-day (Normark et al., 1979; Shor et al., 1990). Thin muddy drapes have also been observed in ancient scour fills, and probably require a reduction in flow energy to ensure their preservation (Mutti, 1985; Mutti et al., 1989; Millington and Clark, 1995; Vicente Bravo and Robles, 1995). Bedforms such as sand/gravel waves and megaripples that are abundant in modern CLTZ s have also been recognized in ancient CLTZ s as coarse, lenticular, cross-stratified units (e.g. Mutti, 1985). Therefore, it seems that it is possible to apply modern

analogues to the characterisation and recognition of CLTZ s in outcrop and the subsurface.

The problem of separating scours from channels

A key problem arising from studies of the CLTZ is how to distinguish between scours and channels, both in outcrop and in the subsurface. In the modern environment, the increased use of high-resolution seafloor mapping means that large-scale erosional scours are being identified more frequently and with greater confidence. However, large-scale scours have been rarely described from ancient sequences and are undoubtedly misidentified in outcrop, especially when viewed in cross-section only (Normark et al,. 1979). Scours vary widely in their size and geometry, although nearly all measured scours are <100 m deep and most are <20 m deep (Table 7.1). In addition, they are generally <1000 m wide and <2000 m long. Channels also display a wide range of dimensions, the largest fan valleys can be several hundred metres deep and up to 10 km wide, whereas the smallest channels may be only a few metres deep and tens of metres wide. Most ancient channels are <250 m wide, although this largely reflects the difficulties of recognising larger channels in outcrop. It should also be noted that the term channel with respect to ancient turbidite studies has a very loose meaning as it refers to anything from small-scale scours to large-scale amalgamated channel-fills (Mutti and Normark, 1991).

It is sometimes possible to distinguish between scours and channels on the basis of their fill. Scours *within* channels generally show similar characteristics to the small scours associated with coarse sediment wedges, which occur at channel terminations in systems swept by sandy, high-density turbidity currents. They are usually relatively small (<3 m deep), deeply incised, and are interpreted as being eroded and filled by single events (Normark et al., 1979; Mutti and Normark, 1987; 1991). In contrast, scours in CLTZ s are typically larger and may show complex patterns of coalescence or multiphase scouring indicating formation during multiple events (Figure 7.4). In most turbidite systems, successive flows have varying volumes, leading to a complex pattern of erosion and deposition across the CLTZ while the turbidite system remains active. Once the system becomes inactive, scours are draped by beds that are typically continuous across the scour axis and only show limited thinning towards the margin (Mutti and Normark, 1987; 1991). Channels differ from scours in that they are relatively

stable, long-term conduits for turbidity current transport. They are characterised by successive episodes of erosion and infilling that are largely contained within the channel margins. This means that most channel-fill sequences display lateral pinch-out of coarse-grained units, and therefore show a thin-bedded, mud-dominated, channel-margin facies compared to a thick-bedded, sand-dominated channel-axis facies (Figure 7.15).

Continuity between channel and lobe sandstones across the CLTZ

An understanding of how lateral continuity between channel and lobe sands will be affected by the fill of the CLTZ is of major significance to hydrocarbon exploration. Upstream of the CLTZ, good-quality sands and gravels are developed as channel-fill deposits. These include 1) the fill of downcutting (erosional) channels where a coarse-grained basal lag is overlain by a fine-grained plug representing channel abandonment, 2) aggradational channel-fill deposits composed of either thick-bedded, coarse-grained, amalgamated axial facies or alternating thin-bedded sands and muds, and 3) mixed channel-fill deposits containing a mixture of these two types (Mutti and Normark, 1991). It is important to note that some channels and channel-fills may display very similar characteristics to CLTZ s, for example, the Eastern Valley on Laurentian Fan contains large erosional scours and is floored by gravel waves (Shor et al., 1990). However, these features are only found in areas of the channel where major flow expansion occurs due to the channel widening, and also around bends in channels where flow velocity increases (e.g. Kidd et al., 1998).

Downstream of the CLTZ, good-quality, parallel-stratified sands are also developed within the proximal lobe facies (Shanmugan and Moiola, 1988). However, not all depositional lobes in this setting show a marked relief. For example, basin-wide, sheet-like sand deposition occurs beyond the CLTZ in the Agadir Basin and Tagus Abyssal Plain (Figures 7.1 and 7.7). In these cases, it may be very difficult to pick out any kind of lobe morphology, and the lobe deposits are likely to onlap adjacent slope facies. Broad, shallow, tabular scours containing abundant rip-up mud clasts are also rarely developed within the lobe facies, and are produced by the impact of dense flows on a soft substratum (Mutti and Normark, 1987; 1991). However, these features have not been observed downstream of modern CLTZ s and are more likely to occur in areas

swept by high-density, sand-rich turbidity currents, where the CLTZ is replaced by an attached lobe.

Lateral continuity across the CLTZ is largely dependent on the nature of the turbidite system. In most cases it is likely that turbidity current volume within a system will vary through time, and that eventually the system will gradually become inactive. This scenario will lead to deposition of a highly heterogeneous CLTZ facies, with development of thin mud drapes in scour-fills, overlain by increasingly thin-bedded turbidites. Coarse-grained, internally stratified bedforms will be preserved, further contributing to the heterogeneity. However, although the CLTZ facies in this setting is likely to be highly heterogeneous the overall pattern is likely to be of dominantly coarse-grained sediments separated by thin, laterally discontinuous muds. In this case, the lateral continuity between channel and proximal lobe facies may be quite high. If the system is supplied by very infrequent, large-scale, sand- and mud-rich turbidity currents then it is likely that due to sediment bypassing a substantial hiatus may occur in the CLTZ, as each successive turbidity current will remove the mud drape deposited since the previous flow. If the turbidity currents are then switched off the CLTZ will eventually be infilled with fine-grained pelagic/hemipelagic sediments, leading to a potential permeability barrier between the channel-fill and proximal lobe sands, and a complete lack of continuity (Shanmugan and Moiola, 1988).

Recognising CLTZ s in the subsurface

It is probably difficult to distinguish CLTZ facies from channel-fill and proximal lobe facies using core data alone. However, there are a number of features, which if seen together, may be an aid to the recognition of this zone. The most obvious features are erosional, with scoured bases, gravel lags, top-cut-out facies and significant hiatuses all observed in ancient CLTZ facies. Depositional bedforms such as sand/gravel waves and megaripples/ripples can be recognised as large-scale lenses with highly variable bed thickness, internal cross-stratification and abundant mud rip-up clasts. Overall, the CLTZ facies is very heterogeneous, making core correlation across this zone almost impossible.

Time-slice attribute analysis of three-dimensional seismic data is now a routine method of determining likely reservoir distribution in the subsurface. In a number of current

exploration areas, for example offshore West Africa, west of Norway and in the Campos Basin offshore Brazil, seismic attribute patterns that show elongate, sinuous reservoir trends are readily interpreted as parts of slope or fan channels (Souza et al., 1989; Gregerson, 1998; Wonham et al., 2000). Other patterns imaged in these papers show more sheet-like distributions that may be interpreted as lobe or basin fill, as well as more irregular, scattered reservoir geometries that are less easily interpreted. We suggest that this pattern type might represent CLTZ s, and therefore be extremely useful in predictive model development. Clearly, more work is required on this topic.

Conclusions

CLTZ s are an important, but largely overlooked, element of deep-water turbidite systems, and this study has attempted to highlight some of their key characteristics and the controls on their development. CLTZ s occur in the vicinity of canyon/channel mouths and are often associated with a break-in-slope. In these areas significant flow expansion and increased turbulence associated with a hydraulic jump are expected, leading to extensive seafloor erosion. CLTZ s are found in areas swept by large-volume, sand-laden, highly efficient flows with a high mud content, leading to sediment bypassing and formation of a detached lobe. The scale of erosion within this zone is controlled by turbidity current volume, canyon/channel size and gradient, and the change of slope angle.

Erosional scours in CLTZ s are up to 60 m deep, 2 km wide and 2 km long. Amalgamated scours up to 9 km wide and 6 km long are also found in larger systems. Generally, amalgamated scours and the largest individual scours are found immediately downslope of canyon/channel mouths, with smaller spoon- and chevron-shaped scours found further downslope. Sand/gravel waves with wavelengths up to 2 km and wave heights up to 4 m are found adjacent to scours throughout the CLTZ, and smaller bedforms such as megaripples are also widespread. Erosional scours described from ancient CLTZ s often display a mud drape overlain by an increasingly thin-bedded turbidite fill, representing gradual abandonment of the turbidite system. Sand/gravel waves and megaripples are preserved as lenticular units of coarse sandstone and conglomerate with internal cross-stratification and abundant rip-up mud clasts.

It seems likely that many outcrops previously identified as channel-fills actually refer to CLTZ s (Mutti and Normark, 1991), so revisiting outcrops where CLTZ s are expected to occur may reveal new information, and lead to reinterpretation of certain systems. Further outcrop studies of the CLTZ are necessary to increase our knowledge of how this element may be recognised in the subsurface, and how it affects continuity between channel-fill and proximal lobe sandstones.

Acknowledgements

The authors would like to thank the Masters, officers and crew of the RRS Discovery and RV Gelendzhik for their efforts and expertise during data collection. RBW acknowledges PhD funding from the University of Southampton and the Southampton Oceanography Centre Challenger Division. DAVS acknowledges tenure of a Royal Society Industry Fellowship.

7.3: Summary

Channel-lobe transition zones are an important part of most high-efficiency turbidite systems, and this study highlights some of the key controls on their development. In particular, it has been demonstrated that there is a recognisable gradation of bedforms and erosional features with distance from the channel/canyon mouth. In addition, this study has revealed that channel-lobe transition zones are likely to effect sand body continuity between high-quality channel and proximal lobe sandstones. This makes their recognition in the subsurface a prime concern, and several criteria have been recognised to aid this.

The following three chapters now concentrate on the recognition and process of formation of deep-water sediment waves, which are one of the key features of channel-lobe transition zones and many other turbiditic environments.

CHAPTER 8

TURBIDITY CURRENT SEDIMENT WAVES (1)

8.1: Introduction and aims

The investigation of channel-lobe transition zones presented in the previous chapter revealed that coarse-grained sediment waves are a common feature of this turbidite-dominated environment. The following three chapters will now attempt to further challenge the notion that deep-water sediment waves are mostly deposited beneath bottom currents.

In this chapter two sediment-wave fields on the submarine slope of the Canary Islands are investigated. These sediment waves have previously been interpreted as being formed beneath bottom currents (Jacobi and Hayes, 1992; Masson et al., 1992). In this study a combination of high-quality data is presented and the wave-forming process re-evaluated in detail.

8.2: Paper 5

Turbidity current sediment waves on the submarine slopes of the western Canary Islands

Russell B Wynn, Douglas G Masson, Dorrik A V Stow and Philip P E Weaver

SOES/Challenger Division, Southampton Oceanography Centre, European Way, Southampton, SO14 3ZH, UK

This paper was submitted to Marine Geology in April 1999. It was reviewed by David Piper, Lionel Carter and John Howe, and accepted for publication in August 1999. It was published in Marine Geology in February 2000, v.163, p.185-198.

Abstract

Two sediment wave fields have been identified on the flanks of the western Canary Islands of La Palma and El Hierro, using a high-quality 2-D and 3-D dataset that includes GEOSEA and TOBI imagery, 3.5kHz-profiles, and short sediment cores.

The La Palma sediment wave field covers some 20,000 km^2 of the continental slope and rise, and consists of sediment waves with wave heights of up to 70 m and wavelengths of up to 2.4 km. The wave crestlines have a complex morphology, with common bifurcation and a clear sinuosity. Waves have migrated upslope through time. Cores recovered from the wave field contain volcaniclastic turbidites interbedded with pelagic/hemipelagic layers. The wave field is interpreted as having formed beneath unconfined turbidity currents. A simple, previously published, two-layer model is applied to the waves, revealing that they formed beneath turbidity currents flowing at 10-100 cm/s^{-1}, with a flow thickness of 60-400 m and a sediment concentration of 26-427 mg/l.

The El Julan sediment wave field lies within a turbidity current channel on the south-west flank of El Hierro. The sediment waves display wave heights of about 6 m and wavelengths of up to 1.2 km. The waves are migrating upslope, and migration is most rapid in the centre of the channel where the flow velocity is highest. This wave field has been formed by channelised turbidity currents originating on the flanks of El Hierro.

Introduction

Sediment waves formed by turbidity currents have been described from a number of deep-water environments, including channel levees (Damuth, 1979; Normark et al., 1980; Carter et al., 1990; Piper and Savoye, 1993; McCave and Carter, 1997; Nakajima et al., 1998), channel floors (Malinverno et al., 1988; Kidd et al., 1998), and the margins of submarine fans (Howe, 1996). These sediment waves display wave heights of 1-70 m and wavelengths of 0.1-6 km, and generally occur on slopes of <1°. Wave crests may reach 60 km in length and are aligned roughly perpendicular to the turbidity current flow direction. 3.5kHz-profiles indicate that the waves are often asymmetric, with a thicker upslope flank suggesting upslope migration. Wave dimensions generally decrease downslope.

Single-channel seismic reflection profiles have revealed that sediment wave sequences on levees may reach 400 m in thickness (Carter et al., 1990). Sediments are dominantly fine-grained, although some waves are composed of numerous thin-bedded sand/silt turbidites. A study of channel-levee overbank waves on the Amazon Fan revealed that on the upslope (upstream) flanks of the waves, turbidite beds were thicker and more numerous than on the downslope (downstream) flank (Shipboard Scientific Party, 1995). Previous hydrodynamic interpretations of turbidity current waves suggest they form as giant antidunes beneath low-velocity, low-concentration turbidity currents (Normark et al., 1980).

This study describes two sediment wave fields on the submarine slopes of the Canary Islands (Figure 8.1), using a high-quality dataset obtained during RRS Charles Darwin cruise 108. Examination of the wave distribution and morphology, combined with detailed sedimentological analysis, has allowed the wave-forming processes to be interpreted.

Methodology

Many previous studies of turbidity current sediment waves have been restricted by a lack of core data and 3-D imagery. This limits the opportunity to interpret the wave-forming process with any certainty. The present study comprises TOBI and GEOSEA 3-D data collected during RRS Charles Darwin cruise 108, which took place in the autumn of 1997. In addition, a GLORIA mosaic and three sediment cores collected during earlier cruises have also been incorporated into this study (Masson et al., 1992). The six main types of data have been grouped as follows:

1: Multibeam Bathymetry

The La Palma and El Julan sediment wave fields have been imaged by the Simrad EM12 multibeam echo-sounder. These bathymetric data have been processed with GEOSEA modelling software, which produces high-resolution 3-D images of the seafloor (Figures 8.2, 8.3 and 8.7).

2: 3.5kHz-profiles

Most of the quantitative data from the La Palma wave field were obtained from a series of 3.5kHz-profiles that run perpendicular to the wave crests (Figures 8.1 and 8.4). These

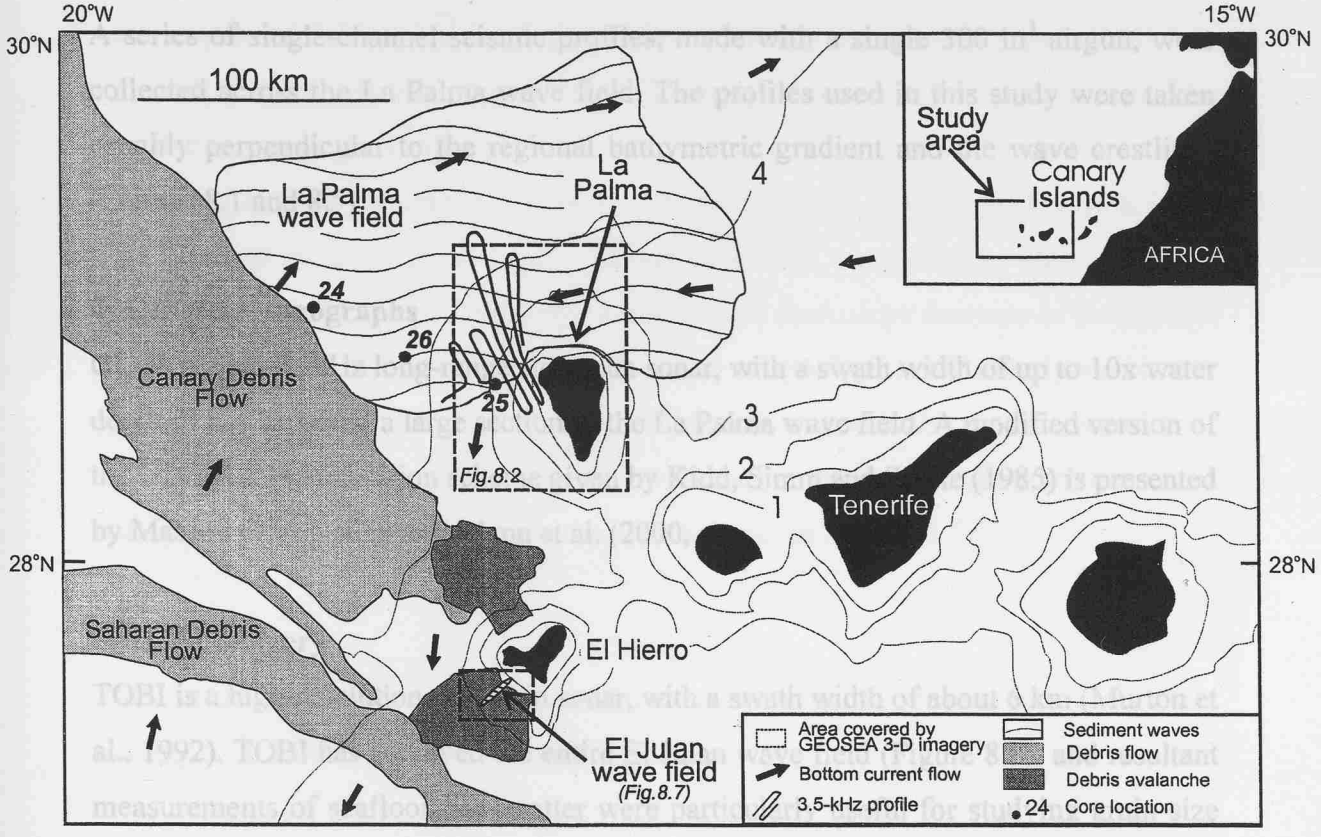

Figure 8.1: Location map showing the regional setting and bathymetry of the sediment wave fields around the western Canary Islands. Boxes indicate the location of the GEOSEA images shown in Figures 8.2 and 8.7. Bathymetric contours in kilometres.

data provided information on wavelength, wave height, thicknesses and migration direction. A review of the 3.5kHz echo-character definitions applied to the Northwest African margin is presented in Wynn et al. (2000, a).

3: Airgun seismic profiles

A series of single-channel seismic profiles, made with a single 300 in^3 airgun, were collected across the La Palma wave field. The profiles used in this study were taken roughly perpendicular to the regional bathymetric gradient and the wave crestlines (Figures 8.1 and 8.5).

4: GLORIA sonographs

GLORIA is a 6.5kHz long-range side-scan sonar, with a swath width of up to 10x water depth. It has surveyed a large section of the La Palma wave field. A modified version of the GLORIA interpretation scheme given by Kidd, Simm and Searle (1985) is presented by Masson et al. (1992) and Wynn et al. (2000, a).

5: TOBI imagery

TOBI is a high-resolution side-scan sonar, with a swath width of about 6 km (Murton et al., 1992). TOBI has surveyed the entire El Julan wave field (Figure 8.8), and resultant measurements of seafloor backscatter were particularly useful for studying grain-size variations across the wave crests.

6: Sediment Cores

Three short (max. length 2.05 m) kasten cores were recovered from the southern margin of the La Palma wave field (Figures 8.1 and 8.6). These cores confirm earlier interpretations of sediment facies, based on 3.5kHz data, and have been a key factor in determining the wave-forming process.

The La Palma sediment-wave field

Distribution and Morphology

The La Palma wave field lies upon the northern slopes of La Palma at a water depth of 3600-4500 m, and covers approximately 20,000 km^2 (Figure 8.1). The waves extend upslope to the boundary between the rocky island flanks and the slope sediments, and downslope onto the continental rise. To the west, the wave field is bordered by the

Canary Debris Flow, which is believed to post-date the sediment waves (Masson et al., 1992). Sediment waves are not present on the southern flanks of La Palma, probably due to the dominance of mass movements in this area (Figure 8.2).

The sediment waves display wave heights of <5-70 m (averaging 21 m), and wavelengths of 0.4-2.4 km (averaging 1.2 km). Wave crests are aligned parallel or subparallel to the regional slope, and are laterally continuous for up to 40 km. The crestline morphology is often complex, with common bifurcation and a clear sinuosity, although the crests become less sinuous and more regular downslope (Figure 8.3). In profile, most of the waves display an asymmetrical morphology, with a steeper downslope flank. The waves also show a progressive downslope decrease in dimensions (Figure 8.4). On airgun seismic profiles the wave morphology is still clearly visible to a depth of at least 200 m (assuming a sediment velocity of 1600 m/s), and the wave crests and troughs consistently shift downslope with increased penetration depth, indicating upslope migration throughout deposition of the sequence (Figure 8.5).

Sediments

Three short kasten cores have been recovered from the study area, in water depths ranging from 3364-4377 m (Figures 8.1 and 8.6):

Core CD56-25 is 185 cm long and was taken from an area of hummocky topography at a water depth of 3364 m, just within the upper limit of the wave field. This core contains two bioturbated silty clay units, and an 80 cm thick volcaniclastic debris flow. The debris flow is poorly developed, and appears to be a 'grain-flow' deposit. It contains clasts of sediment similar to those seen in the underlying and overlying beds, as well as volcanic debris and shell fragments. It is not seen in other cores recovered from the area and is therefore interpreted as a small-scale failure on the island flanks.

Core CD56-26 is 148 cm long and was taken from an area of migrating sediment waves in a water depth of 4103 m. This core contains seven volcaniclastic turbidites, interbedded with bioturbated pelagic marls and oozes. The turbidites are up to 20 cm thick, and generally consist of normally graded, fine-grained silts and muds. One turbidite has a thin (5 cm) sandy base. Parallel and cross lamination is present in some of the silty units.

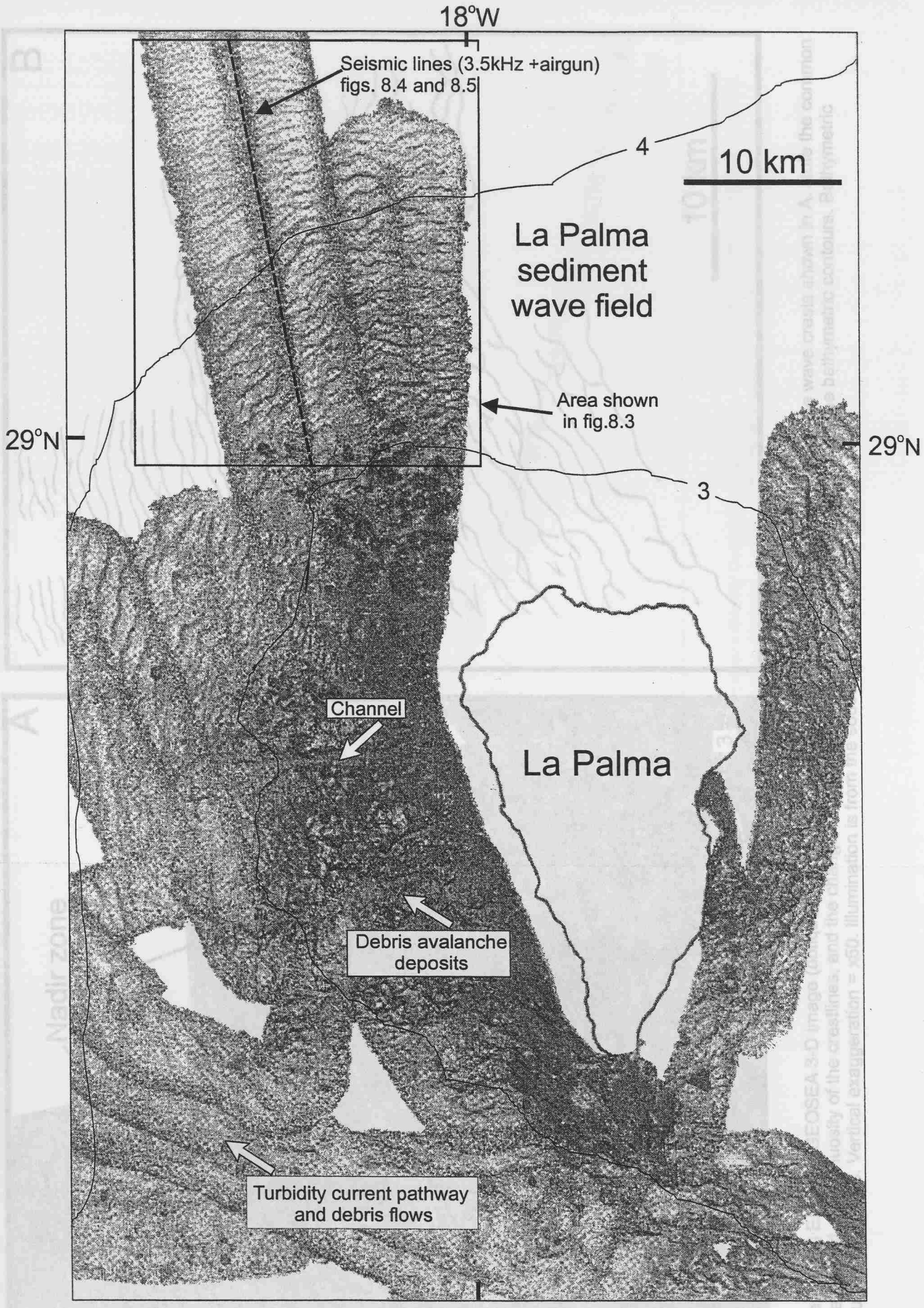

Figure 8.2: GEOSEA 3-D image (plan view) of the La Palma sediment wave field. Note that wave crests are aligned roughly parallel to the bathymetric contours, and that the waves are not present on the southern flanks of La Palma. Bathymetric contours in kilometres. Box locates Figure 8.3. Dashed line shows location of 3.5kHz profile in Figure 4 and airgun seismic profile in Figure 8.5. Vertical exaggeration = x10. Illumination is from the north.

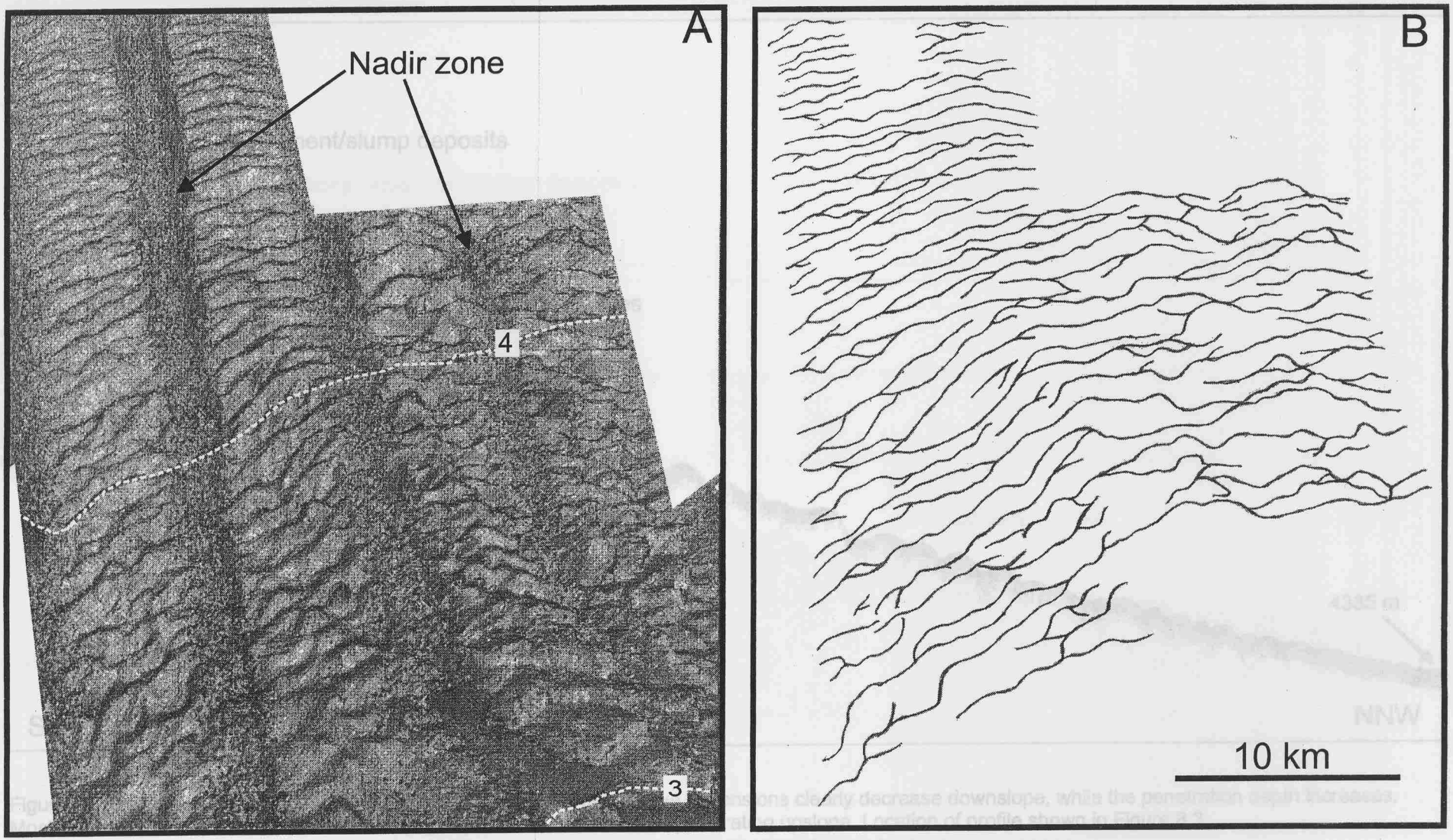

Figure 8.3: (A) Enlarged GEOSEA 3-D image (oblique plan view) of the La Palma sediment waves (B) Tracing of the wave crests shown in A. Note the common bifurcation and clear sinuosity of the crestlines, and the change in crestline orientation in response to the curve of the bathymetric contours. Bathymetric contours in kilometres. Vertical exaggeration = x50. Illumination is from the south.

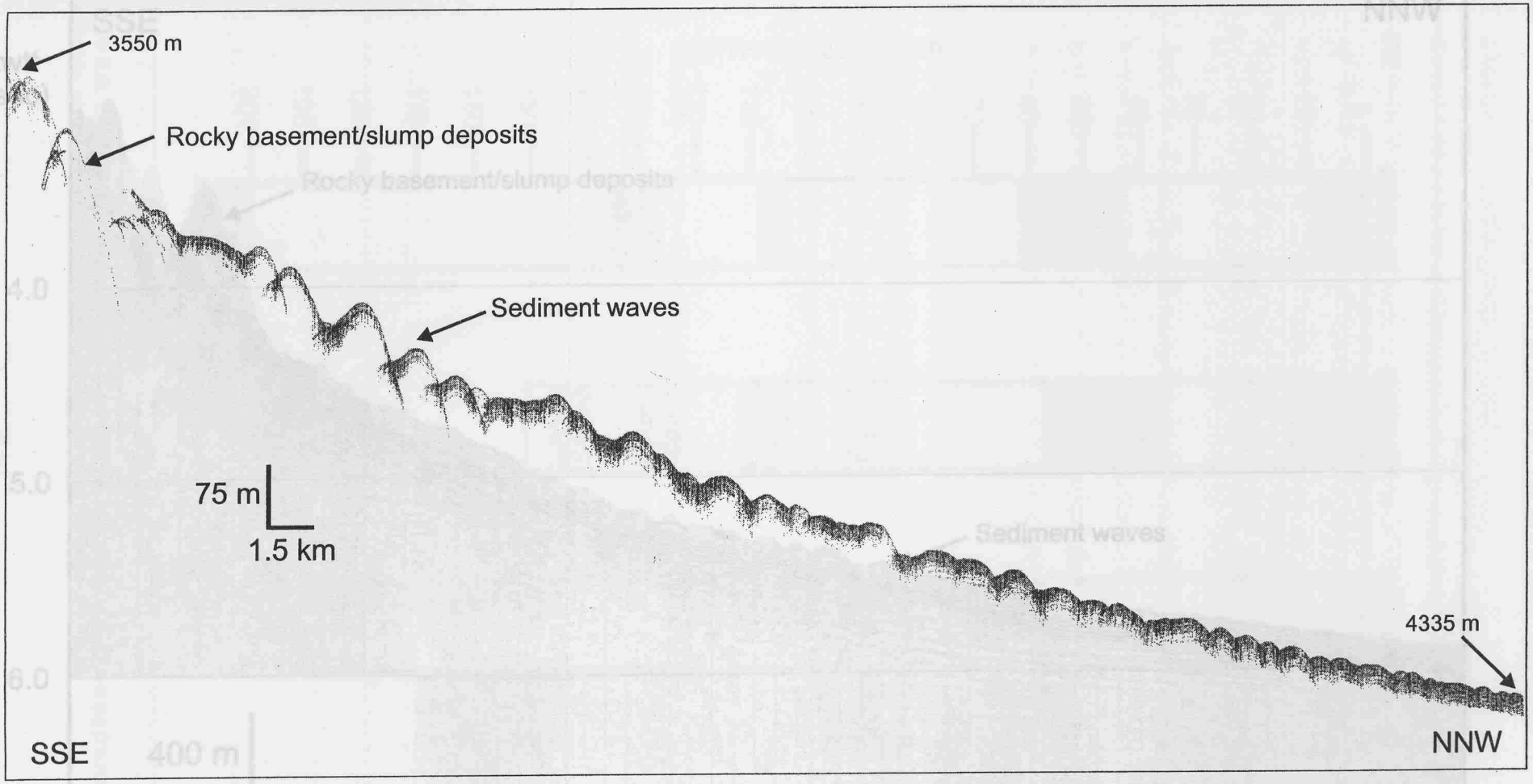

Figure 8.4: 3.5kHz profile through the La Palma sediment wave field. Wave dimensions clearly decrease downslope, while the penetration depth increases. Most of the waves have thicker beds on their upslope faces, and are clearly migrating upslope. Location of profile shown in Figure 8.2.

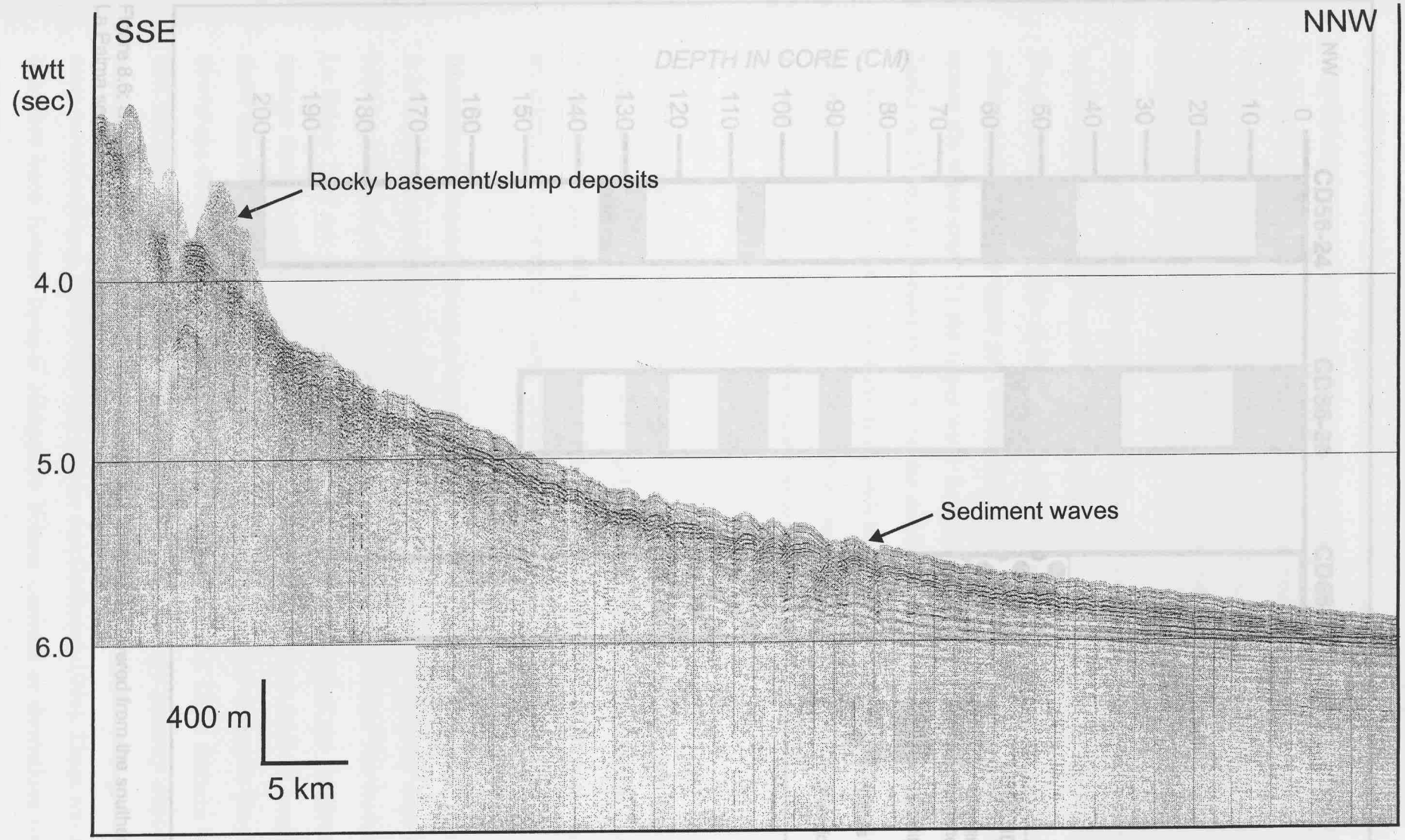

Figure 8.5: Airgun seismic profile through the La Palma sediment wave field. Note the sharp contrast in seismic expression between the rocky island flanks (top left) and the sediment wave field. Location of profile shown in Figure 8.2.

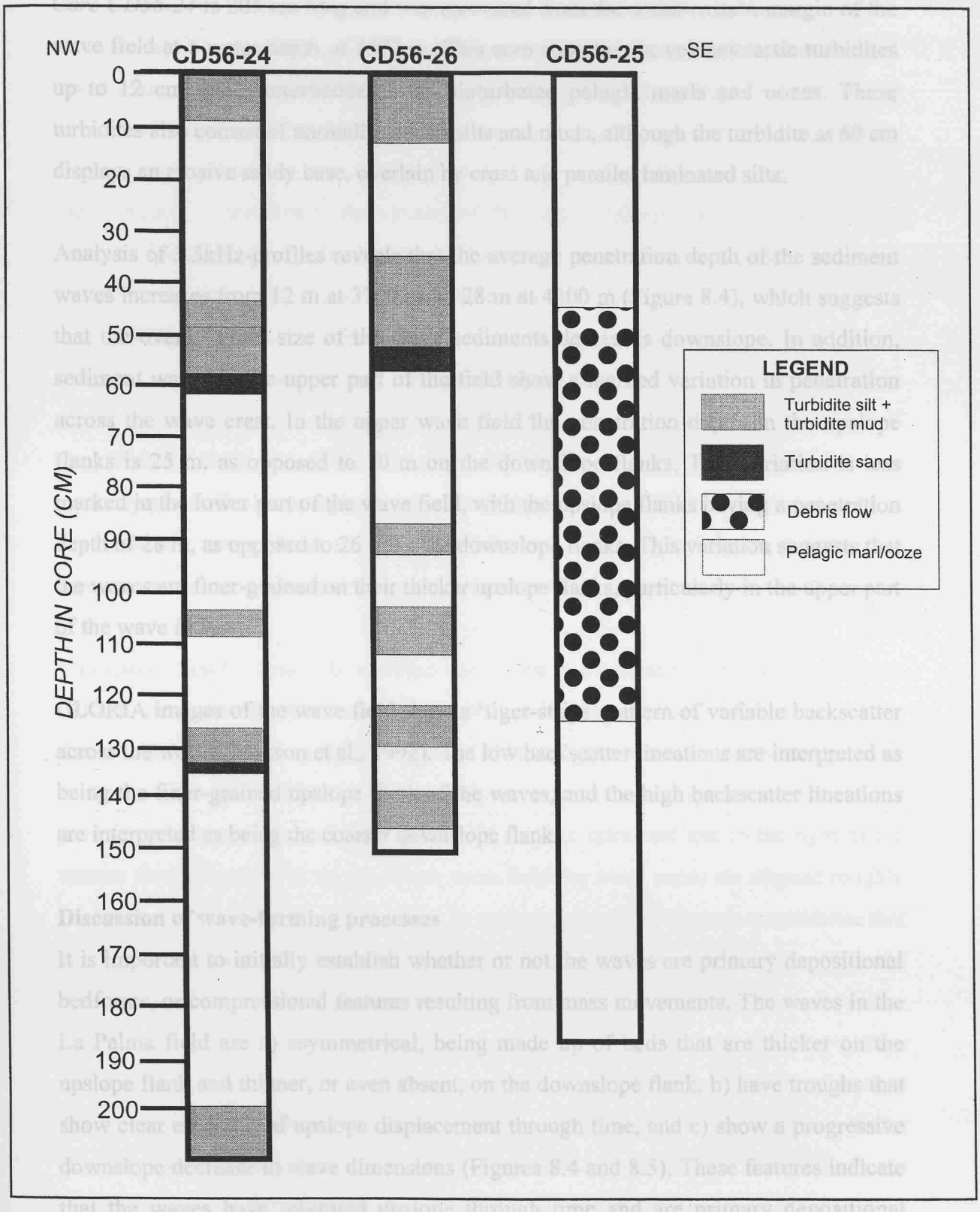

Figure 8.6: Simplified sedimentary logs of three short kasten cores recovered from the southern margin of the La Palma sediment wave field. Core locations shown in Figure 8.1.

Core CD56-24 is 205 cm long and was recovered from the south-eastern margin of the wave field at a water depth of 4377 m. This core contains six volcaniclastic turbidites up to 12 cm thick, interbedded with bioturbated pelagic marls and oozes. These turbidites also consist of normally graded silts and muds, although the turbidite at 60 cm displays an erosive sandy base, overlain by cross and parallel laminated silts.

Analysis of 3.5kHz-profiles reveals that the average penetration depth of the sediment waves increases from 12 m at 3700 m, to 28 m at 4300 m (Figure 8.4), which suggests that the overall grain size of the wave sediments decreases downslope. In addition, sediment waves in the upper part of the field show a marked variation in penetration across the wave crest. In the upper wave field the penetration depth on the upslope flanks is 25 m, as opposed to 10 m on the downslope flanks. This variation is less marked in the lower part of the wave field, with the upslope flanks having a penetration depth of 28 m, as opposed to 26 m on the downslope flanks. This variation suggests that the waves are finer-grained on their thicker upslope flanks, particularly in the upper part of the wave field.

GLORIA images of the wave field show a 'tiger-stripe' pattern of variable backscatter across the waves (Masson et al., 1992). The low backscatter lineations are interpreted as being the finer-grained upslope flank of the waves, and the high backscatter lineations are interpreted as being the coarser downslope flanks.

Discussion of wave-forming processes

It is important to initially establish whether or not the waves are primary depositional bedforms, or compressional features resulting from mass movements. The waves in the La Palma field are a) asymmetrical, being made up of beds that are thicker on the upslope flank and thinner, or even absent, on the downslope flank, b) have troughs that show clear evidence of upslope displacement through time, and c) show a progressive downslope decrease in wave dimensions (Figures 8.4 and 8.5). These features indicate that the waves have migrated upslope through time and are primary depositional bedforms. They are clearly not compressional features associated with gravitational mass movements (e.g. Hill et al., 1982; Mulder and Cochonat, 1996). These waves have therefore been formed beneath alongslope bottom currents or downslope turbidity currents.

The La Palma wave field lies within a zone of north-eastward-flowing Antarctic Bottom Water (AABW), and it is possible that this current has been responsible for forming and maintaining the waves (Figure 8.1). Jacobi and Hayes (1992) and Masson et al. (1992) have previously described the sediment waves in this area, and both favour a bottom current origin. However, the AABW flow is fairly weak at the present-day. Current meter studies undertaken in the vicinity of the Canary Islands have recorded bottom currents flowing to the north-east at velocities of <5 cm/s^{-1} (Lonsdale, 1982; Saunders, 1988). In addition, bottom photographs taken from the slope and rise north-east of the Canary Islands show a tranquil seafloor, with no evidence of significant bottom current activity (Jacobi, Rabinowitz and Embley, 1975; Embley, 1976). Generally, sediment waves maintained by bottom currents believed to occur under velocities of 9-50 cm s^{-1} (e.g. Flood, 1988), therefore the present-day bottom current regime in the area is probably not sufficient to maintain the waves. However, AABW was believed to have been stronger during glacial periods (Sarnthein et al., 1982), therefore it is possible that bottom currents may have had a more significant role in wave development in the past.

It is also difficult to relate the crestline orientation to a bottom current origin, as recent models of mudwave dynamics (Blumsack and Weatherly, 1989; Blumsack, 1993), derived from the lee-wave model of Flood (1988), suggest that sediment waves growing in the northern hemisphere will generally propagate at an angle clockwise to the prevailing bottom current direction, and will migrate upcurrent and to the right of the current flow direction. In the La Palma wave field the wave crests are aligned roughly parallel to the bottom current flow, with an upslope migration. There is no evidence that wave migration has an *upcurrent* component, and overall it is difficult to relate the distribution of the sediment wave crestlines to current models of bottom current waves.

Finally, the upper part of the wave field lies within a zone of mixing at 3800 m, between the north-east flowing AABW and the south-west flowing North Atlantic Deep Water (Sarnthein et al., 1982). Zones of mixing between two opposing major water masses are commonly zones of "no motion" and are therefore unlikely to generate significant bottom currents (L. Carter, pers. comm.). In addition, there is no change in the wave migration direction and crestline orientation across this zone of mixing, which also suggests that bottom currents are having little effect on sediment wave processes.

It seems unlikely from these observations and arguments that bottom currents are responsible for forming and maintaining the La Palma wave field. They are certainly not being maintained by the present-day current regime, although the possibility that increased AABW flow in the past had a greater influence on wave formation cannot be dismissed.

An alternative explanation is that the waves have formed beneath downslope turbidity currents. Evidence of turbidity current flow across the wave field is shown by the presence of numerous fine-grained volcaniclastic turbidites in cores taken from the southern edge of the field (Figure 8.6). In addition, the wave crests are aligned roughly parallel to the regional slope (and are therefore perpendicular to downslope flows), and the waves migrate upslope. These features are all compatible with a turbidity current origin for the waves (e.g., Damuth, 1979; Normark et al., 1980; Carter et al., 1990; Piper and Savoye, 1993; Nakajima et al., 1998). The progressive downslope decrease in wave dimensions can be attributed to a reduction in turbidity current velocity as the slope gradient decreases. Further evidence for recent turbidity current activity in the area is given by Urgeles et al. (1999). They describe the channels on the western flanks of La Palma, which occur adjacent to debris avalanche lobes (Figure 8.2). Several of the channels contain scattered debris avalanche blocks, and haloes of fine-grained sediment in the lee of the blocks are interpreted as being deposited by turbidity currents.

Within the La Palma wave field channels are absent, and the wave field is generally out of range of turbidity current overspills from the channel systems to the north and south (Masson, 1994; Urgeles et al., 1999). We therefore interpret the waves as being formed by unconfined turbidity currents originating on the island flanks. These flows are initially constrained within feeder canyons, but rapidly become unconfined downslope and therefore spread out over an extensive area. The lateral extent of the La Palma wave field suggests that turbidity currents are sourced from several input points along the island flanks, rather than from a single canyon. The bifurcation and clear sinuosity of the wave crests may be a function of different turbidity currents from different input points interacting. This is backed up by the core data, which show a marked heterogeneity in sediment deposition across the wave field.

Howe (1996) attempted to apply the lee-wave model of Flood (1988) to turbidity current sediment waves in the Rockall Trough area. However, the lee-wave model is dependent upon a weakly stratified water column and a steady, continuous current flow. This model is therefore not wholly appropriate to sediment waves that form beneath an episodic, dense turbid underflow (McCave and Carter, 1997). Instead, we propose that the sediment waves described in this study form as antidunes, which develop beneath a flow with a Froude number close to one. Normark et al. (1980) used measured wave dimensions and an estimate of flow velocity to construct a simple two-layer model applicable to unconfined turbidity currents flowing over sediment waves on the Monterey Fan levee. This two-layer model accounts for the excess density of a turbulent sediment/water mix flowing beneath stationary sea water. Normark et al. (1980) assumed a flow velocity of 10 cm/s^{-1} (equivalent to deposition of silt-sized material) and used a wavelength value of 0.5-5 km in the following equation, derived from the antidune model of Allen (1970):

$$C \cong \frac{2\pi}{1.6g}\frac{U^2}{L} = (4\times10^{-3})\frac{U^2}{L}$$

The concentration C is dimensionless, velocity U is expressed in cm/s, g is acceleration of gravity (980 cm/sec^2), and wavelength L in cm. The specific gravity of suspended sediment in the flow is assumed to be 2.6.

For the Monterey Fan waves, this produces an estimated flow concentration between 8×10^{-7} and 8×10^{-6}. A concentration of 8×10^{-6} is approximately equivalent to 20mg/l, assuming a sediment density of 2.6 g/cm^3.

This procedure can be repeated for the La Palma sediment waves. For the upper part of the wave field, comparison with other turbidity current data suggests that a flow velocity of 100 cm/s^{-1} is reasonable (e.g. Bowen et al., 1984). For the lower part of the wave field a flow velocity of 10 cm/s^{-1} is assumed (e.g. Stow and Bowen, 1980; Normark et al., 1980). The wavelength value averages 2.4 km for the upper wave field, and 0.4 km for the lower wave field. These values produce a sediment concentration of

$1.7x10^{-4}$ (427 mg/l) for a turbidity current crossing the upper wave field, decreasing to $1x10^{-5}$ (26mg/l) as it reaches the lower wave field.

Normark et al. (1980) then combined the antidune model with Ellison and Turner's (1959) results, which showed that flow in the centre of a turbidity current approaches Fr ≅ 1. They formulated the following equation to calculate the depth of flow:

$L \cong 2\pi h$ (Fr ≅ 1)

so that the depth of flow h is approximately one-sixth of the wavelength.

The maximum wavelength of the La Palma sediment waves is 2.4 km in the upper wave field, giving an estimated flow thickness of 400 m. The minimum wavelength of 0.4 km in the lower wave field gives a flow thickness of 60 m. This compares to Normark et al's estimated flow thickness of 80-800 m for the Monterey Fan waves.

To summarise, on the basis of this simple two-layer model we can estimate the flow conditions of turbidity currents passing over the La Palma wave field. At the top of the wave field, turbidity currents flowed at $100cm/s^{-1}$, had a thickness of 400 m, and a sediment concentration of 427 mg/l. The flow velocity decreased to around $10cm/s^{-1}$ at the bottom of the wave field, and the flow thickness and sediment concentration decreased to 60 m and 26 mg/l respectively. It should, however, be remembered that this antidune model has a number of limitations. For example, there are obvious problems with applying a model derived in laboratory flumes and fluvial systems to kilometre-scale bedforms in the deep ocean. In addition, antidunes are generally recognised as being short-lived, unstable bedforms and are rarely described from the geological record (Allen, 1984). It is therefore difficult to understand how extensive sediment wave fields can build up over millions of years by this process. We therefore need to obtain a greater understanding of the processes that generate and maintain turbidity current sediment waves if we are to use predictive models with any certainty.

The El Julan sediment-wave field

Distribution and Morphology

The El Julan wave field lies within a low relief turbidity current channel, some 8 km long and 2 km wide, on the south-west flank of El Hierro. The wave field covers 14

km^2, and lies at a water depth of 2400-3000 m (Figures 8.1 and 8.7). The waves are confined to the floor of the channel, and no waves are visible on the adjacent slopes.

There are ten sediment waves within the channel, with wavelengths of 0.4-1.2 km (averaging 0.8 km), and wave heights of around 6 m. The wave crests are aligned parallel to the bathymetric contours and are therefore perpendicular to downslope flows, although they show a roughly crescentic outline with the 'arms' pointing downslope (Figures 8.7 and 8.8). There is no downslope variation in wavelength.

Sediments

Unfortunately the lack of core and good-quality profile data through the wave field limits any interpretation of sediment type. Backscatter patterns on the TOBI image, however, provide some indication of the grain-size distribution across the wave (Figure 8.8). There appears to be a series of high backscatter streaks on the downslope flanks of the waves, which are interpreted to be coarse sediments. These contrast with the low backscatter areas on the upslope flanks and in the wave troughs, which are interpreted to be fine-grained sediments.

Discussion of wave-forming processes

Sediment waves within channels have previously been assigned to a turbidity current origin (e.g. Normark and Piper, 1991; Kidd et al., 1998). Most of these channel floor waves have wavelengths of <300 m, wave heights of <6 m, and are composed of gravel or sand. For example, gravel-rich sediment waves in channels on the Var Fan (Malinverno et al., 1988) and in the Corinth Graben, Greece (Piper and Kontopoulos, 1990) display wavelengths of 35-100 m and wave heights of 1.5-6 m. Sand-rich waves in channels on the Laurentian Fan (Piper et al., 1988) and in the Stromboli Canyon (Kidd et al., 1998) have similar dimensions, with wavelengths reaching 300 m and wave heights up to 4 m. The location of the El Julan wave field within a channel also points towards a turbidity current origin for the waves. However, the El Julan waves are different from the above examples in that they display wavelengths up to 1.2 km, and this makes them substantially longer than previously published examples of sediment waves in channels.

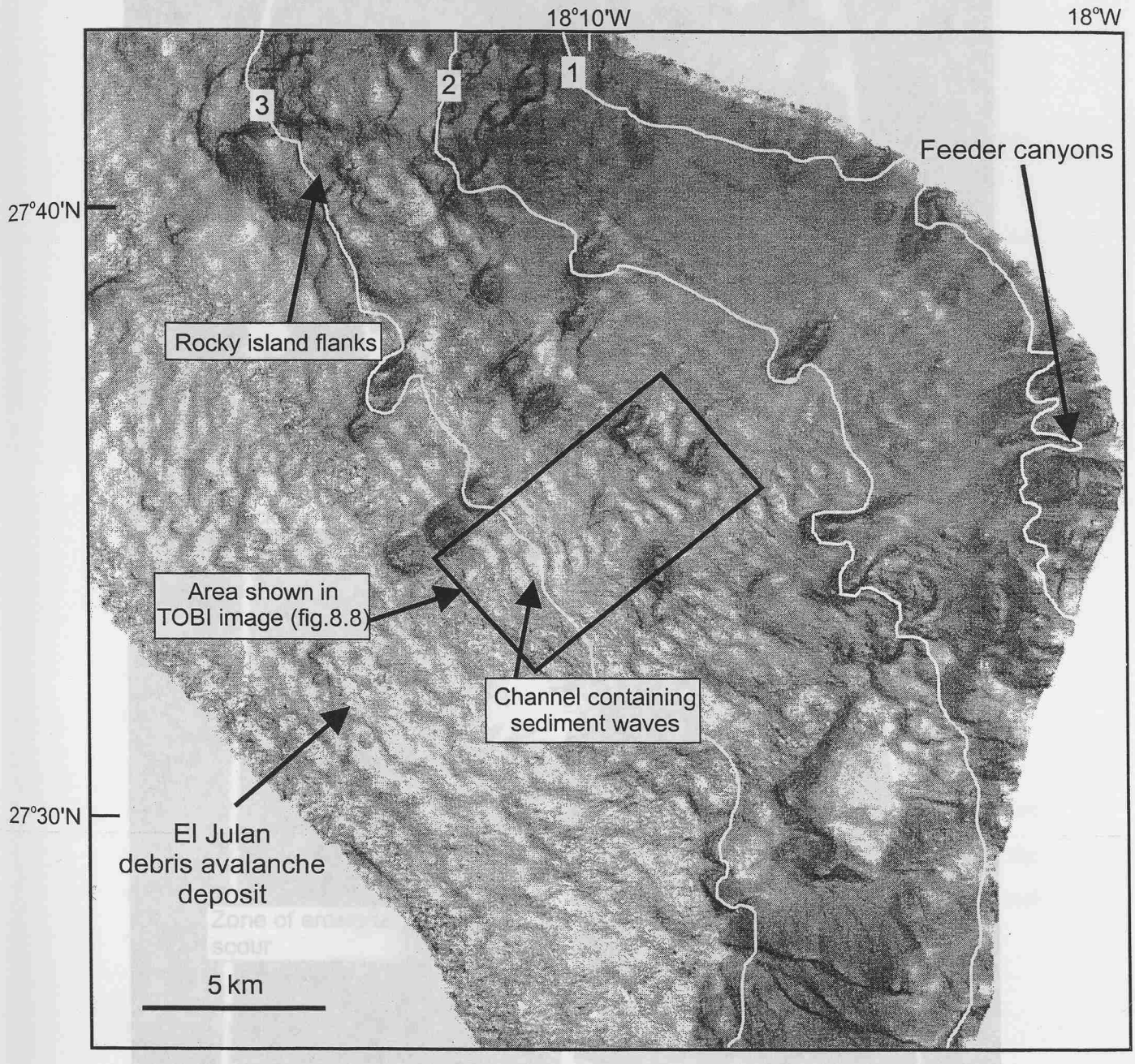

Figure 8.7: GEOSEA 3-D image (plan view) of the El Julan sediment wave field within the scar of the El Julan debris avalanche. Box indicates location of TOBI image in Figure 8.8. Bathymetric contours in kilometres. Vertical exaggeration = x10. Illumination is from the north-east.

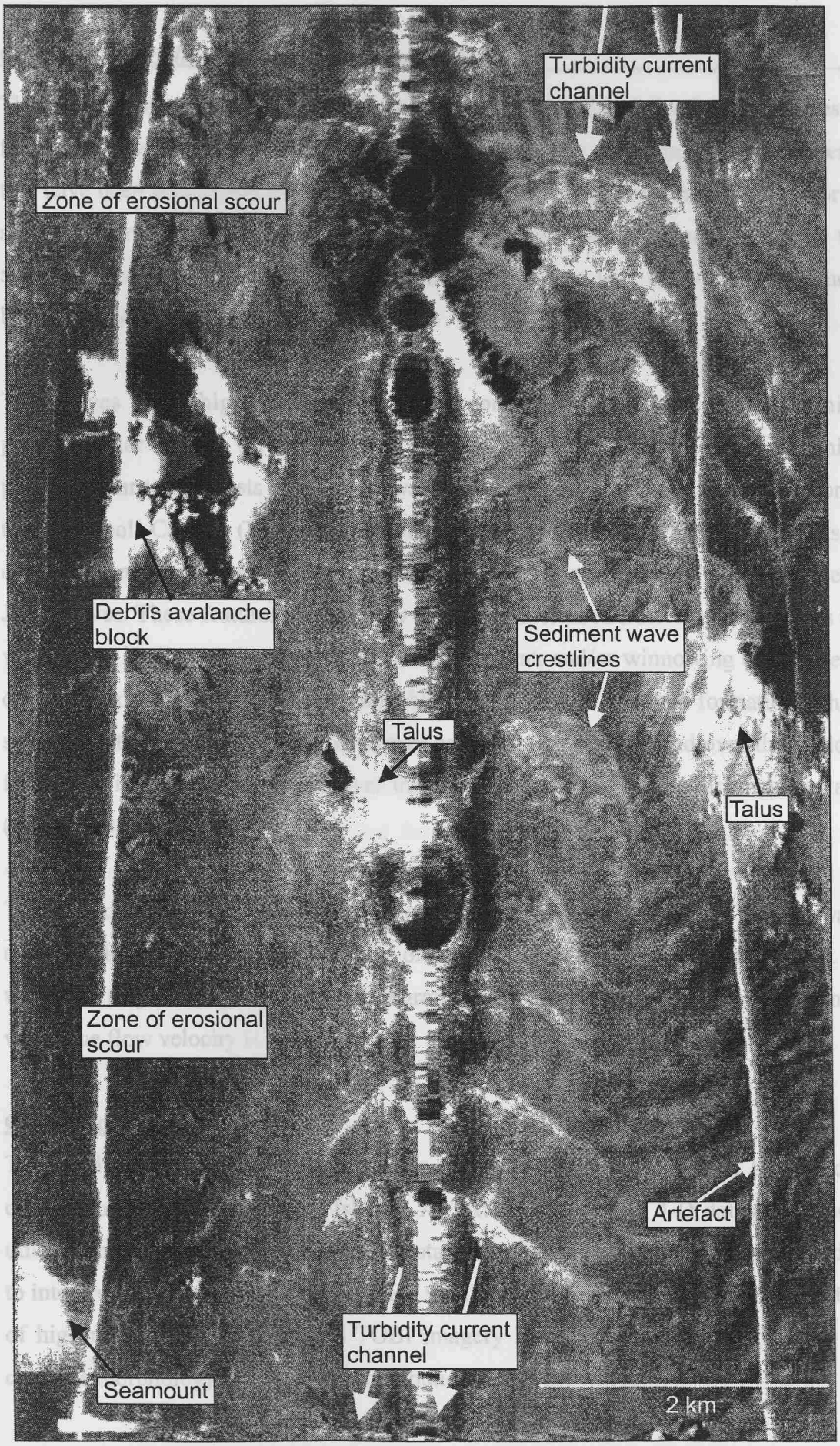

Figure 8.8: TOBI image of the El Julan sediment wave field. High backscatter area are pale, low backscatter areas are dark. Note the high backscatter streaks on the lee faces of the waves. For location, see Figure 8.7.

The El Julan channel lies within a debris avalanche scar, and is downslope of a series of feeder canyons (Figure 8.7). It seems likely that the waves are composed of sediments that have been transported through these canyons and deposited on the channel floor as sediment waves. It is interesting to note that sediment waves are not present on the slopes adjacent to the channel. This is probably due to a lack of available sediment being transported to these areas.

The waves have high backscatter streaks on their downslope flanks running perpendicular to the wave crest (Figure 8.8). High backscatter streaks running perpendicular to the crests of sediment waves have also been recorded from the floor of the Stromboli Canyon (Kidd et al., 1998). These have been interpreted as streaks of coarse sediment, and it seems likely that this interpretation can also be applied to the El Julan waves. These features are probably a result of increased flow velocities across the wave crest, leading to deposition of coarser sediment, and/or winnowing of sediments on the downslope flank. This is compatible with models of antidune formation, which suggest that the current velocity decreases as the flow travels up and over the upslope flank, and increases as it passes over the wave crest and across the downslope flank (Allen, 1984).

The curved crestlines of the waves are concave downslope, which means that the wave crests are furthest upslope in the middle of the channel. It therefore seems likely that the waves are migrating upslope, and are migrating most rapidly in the centre of the channel where the flow velocity is highest.

Conclusions

This study describes two sediment wave fields that have been formed by turbidity currents in the western Canary Islands. An extensive 2-D and 3-D dataset has been utilised and this, combined with an understanding of regional processes, has enabled us to interpret the process of wave formation with confidence. In particular, the application of high-resolution GEOSEA and TOBI imagery has given us new insights into the crestline morphology and sediment distribution across the waves.

The La Palma wave field was formed by unconfined turbidity currents originating on the flanks of La Palma. An attempt at modelling the flow characteristics suggests that

this wave field formed beneath flows similar to those that form sediment waves on channel-levee backslopes.

The El Julan wave field was formed by channelised turbidity currents originating on the flanks of El Hierro. These waves are migrating upslope, and migration is most rapid in the centre of the channel where flow velocity is highest. The backscatter pattern across the waves suggests that the flow velocity increases on the downslope flanks of the waves, leading to deposition of coarse sediment streaks.

Future work should be directed towards obtaining a greater understanding of the flow conditions that initiate and maintain the waves. In particular some attempt should be made to formulate a new model for turbidity current wave formation.

Acknowledgements

The data used in this study were collected during cruises of the RRS Charles Darwin and the RRS Discovery. The authors gratefully acknowledge the contributions of their respective masters and crews. Particular thanks go to Rod Pearce for his help in processing the GEOSEA images, and Barry Marsh for technical assistance. We also thank David Piper and Andy Pulham for their comments on various aspects of sediment waves. The manuscript benefited greatly from reviews by John Howe, Lionel Carter and David Piper. RBW would like to acknowledge PhD funding from the University of Southampton and the SOC Challenger Division.

8.3: Summary

This study has shown that a high-quality dataset combining core, seismic and geophysical data is essential in identifying the mode of formation of sediment waves in areas swept by both turbidity currents and bottom currents. The La Palma and Selvage sediment-wave fields are both interpreted to have been formed by turbidity currents, although they occur in different turbidite environments. This study has also shown that although models of turbidity current sediment wave generation do exist, they are limited in scope and contain numerous flaws.

In the next chapter a sediment-wave field on the lower rise north of the Canary Islands is investigated in detail, and the mechanisms for sediment wave generation beneath turbidity currents are discussed in more detail.

CHAPTER 9

TURBIDITY CURRENT SEDIMENT WAVES (2)

9.1: Introduction and aims

The previous chapter revealed that sediment waves on the continental rise can be formed by unconfined turbidity currents, but highlighted the need for a high-quality integrated dataset. In this chapter another sediment-wave field on the lower rise is investigated, and a 13 m long core through the waves is combined with high-resolution seismic profiles to enable the wave-forming process to be identified with confidence.

Micropalaeontological dating of the core sediments will be attempted to enable sedimentation and wave migration rates to be calculated. In addition, existing models of sediment wave generation will be discussed in detail, and the one most suitable for turbidity current waves identified.

9.2: Paper 6

Sedimentary processes in the Selvage sediment-wave field, Northeast Atlantic: New insights into the formation of sediment waves by turbidity currents

Russell B Wynn[1], Philip P E Weaver[1], Gemma Ercilla[2], Dorrik A V Stow[1] and Douglas G Masson[1]

1) SOES/Challenger Division, Southampton Oceanography Centre, European Way, Southampton, SO14 3ZH, UK

2) Instituto Ciencias del Mar, CSIC, Paseo Juan de Borbon s/n, 08039 Barcelona, Spain

This paper was submitted to Sedimentology in September 1999. It was reviewed by John Damuth, Stephen Morris and Jim Best, and was accepted in October 2000. It is due to be published in December 2000.

Abstract

An integrated geophysical and sedimentological investigation of the Selvage sediment-wave field has revealed that the sediment waves are formed beneath unconfined turbidity currents. The sediment waves occur on the lower continental rise, and display wavelengths of up to 1 km, and wave heights of up to 6 m. Wave sediments consist of interbedded turbidites and pelagic/hemipelagic marls and oozes. Nannofossil-based dating of the sediments indicates a bulk sedimentation rate of 2.4 cm/1000 yrs, and the waves are migrating upslope at a rate of 0.28 m/1000 yrs. Sediment provenance studies reveal that the turbidity currents maintaining the waves are largely sourced from volcanic islands to the south.

Investigation of existing models for sediment-wave formation leads to the conclusion that the Selvage sediment waves form as giant antidunes. Simple numerical modelling reveals that turbidity currents crossing the wave field have internal Froude numbers of 0.5-1.9, which is very close to the antidune existence limits. Depositional flow velocities range from <6-125 cms^{-1}. There is a rapid increase in wavelength and flow thickness in the upper 10 km of the wave field, which is unexpected as the slope angle remains relatively constant. This anomaly is possibly linked to a topographic obstacle just upslope of the sediment waves. Flows passing over the obstacle may undergo a hydraulic jump at its boundary, leading to an increase in flow thickness. In the lower 15 km of the wave field, flow thickness decreases downslope by 60%, which is comparable to results obtained for other unconfined turbidity currents undergoing flow expansion.

Introduction

Deep-water sediment waves are a type of large-scale depositional bedform that may be generated beneath alongslope-flowing bottom currents or downslope-flowing turbidity currents. Sediment waves have previously been referred to as gravel waves (Shor *et al.*, 1990), sand waves (Kenyon & Belderson, 1973), mud waves (e.g. Lewis *et al.*, 1998), lower continental rise hills (Rona, 1969), abyssal antidunes (Fox *et al.*, 1968), giant ripples (Ewing *et al.*, 1968) and depositional ridges (Johnson & Schneider, 1969). Although most of the recent published literature correctly refers to them as sediment waves, this variety of terms can still create confusion. In the present study, a sediment wave is defined as a large-scale (generally tens of metres to a few kilometres wavelength and several metres high), sinusoidal, depositional bedform that is generated

beneath a current flowing at the seafloor. Sediment waves may be composed of sediment of any grain-size, from gravel to mud. It is recommended that the basic definition of 'coarse-grained sediment waves' (sand- and gravel-dominated) and 'fine-grained sediment waves' (mud-dominated) is applied to future studies to avoid further confusion.

Turbidity-current (TC) sediment waves generally occur on the backslopes of channel levees (Damuth, 1979; Normark *et al.*, 1980; Carter *et al.*, 1990; Piper & Savoye, 1993; Droz *et al.*, 1996; McCave & Carter, 1997; Lewis *et al.*, 1998; Nakajima *et al.*, 1998; Piper *et al.*, 1999) and in turbidity-current channels (Malinverno *et al.*, 1988; Shor *et al.*, 1990; Kidd *et al.*, 1998; Lewis *et al.*, 1998; Morris *et al.*, 1998; Wynn *et al.*, 2000*a*). TC sediment waves have also been described from submarine fans (Kenyon *et al.*, 1995; Howe, 1996) and open slopes flanking volcanic islands (Wynn *et al.*, 2000*a*). TC sediment waves display wavelengths of up to 6 km and wave heights of up to 70 m, commonly show a downslope decrease in dimensions (Table 9.1), and typically occur on slopes of $<2^{\circ}$. Wave crests are aligned parallel or subparallel to the slope, and are therefore perpendicular to turbidity current flow. Cores taken through sediment wave sequences on levees and open slopes contain interbedded thin turbidites and pelagic/hemipelagic sediments. Sediment waves within channels are generally dominated by coarse-grained turbidites rich in sand and gravel.

Although TC sediment waves display very similar characteristics to sediment waves formed beneath bottom currents, previous hydrodynamic interpretations of TC sediment waves have favoured the 'antidune' model, suggesting the waves form as giant antidunes beneath flows with a Froude number close to unity (Normark *et al.*, 1980; Howe, 1996; McCave & Carter, 1997; Wynn *et al.*, 2000*a*).

In the present study, a sediment-wave field on the lower continental rise north of the volcanic Selvage and Canary Islands (Figure 9.1) is described, using a dataset containing high-resolution TOPAS (TOpographic PArametric Sonar) profiles and a single giant piston core. The wave field is referred to as the Selvage sediment-wave field, because of its close proximity to the Selvage Islands. Nannofossil-based dating of the sediments has allowed sedimentation and wave migration rates to be calculated. The

Wave field setting	Max WH (m)	Max WL (km)	Slope angle (°)	Comments	Reference
Selvage wave field: lower continental rise	5	1.1	0.13-0.22	WL + WH decrease downslope, crests parallel to slope	this study
La Palma wave field: continental slope/rise	70	2.4	0.4-1.8	WL + WH decrease downslope, crests sinuous and parallel to slope	Wynn *et al.*, 2000b
Bounty Channel: levee backslope	17	6	0.3-0.7	WL + WH decrease downslope, crests parallel to slope	Carter *et al.*, 1990
Toyama Channel: levee backslope	70	3	0.4-1.4	WL + WH decrease downslope, crests sinuous and parallel to slope	Nakajima *et al.*, 1998
Hikurangi Channel: levee backslope	15	3	?	WL + WH decrease downslope, crests subparallel to slope	Lewis *et al.*, 1998
Monterey Fan: levee backslope	37	2.1	0.8	WL + WH decrease downslope, sinuous crests subparallel to slope	Normark *et al.*, 1980
Hueneme Fan: levee backslope	10	0.6	0.8	WL + WH decrease downslope	Piper *et al.*, 1999
Var Fan: levee backslope	50	7	0.5-1.7	WL+ WH increase downslope (slope steepens), crests oblique to slope	Piper and Savoye, 1993
Barra Fan: distal fan slope	5	1.75	?	Crests possibly oblique to slope	Howe, 1996

Table 9.1: Examples of sediment-wave fields formed beneath unconfined turbidity currents. Note that all of the wave fields occur on slopes of 0.1°-1.7°, wave dimensions generally decrease downslope, and wave crests are aligned parallel/subparallel to the slope. WH = wave height, WL = wavelength.

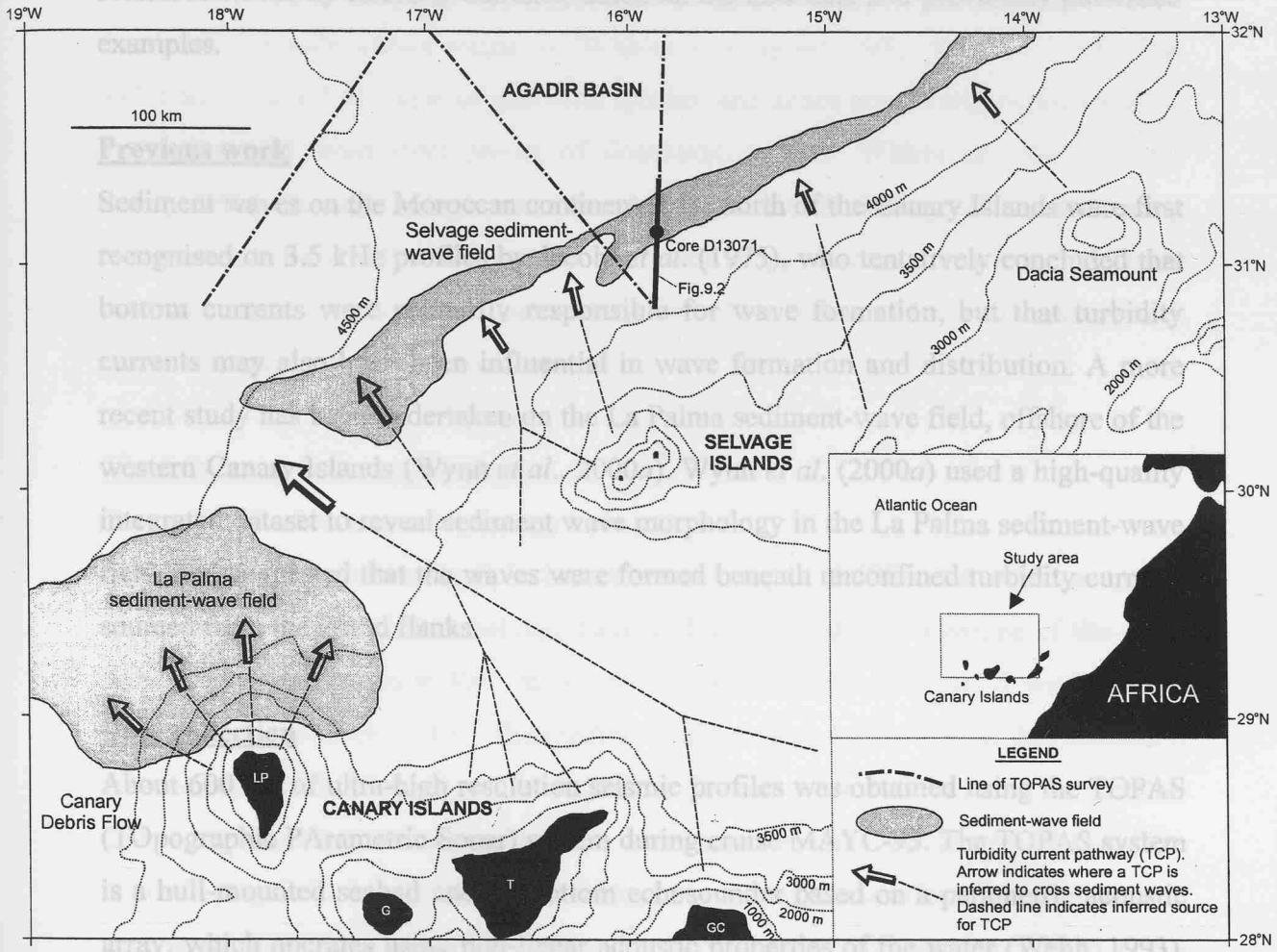

Figure 9.1: Location map showing the position of sediment-wave fields and turbidity current pathways on the continental slope and rise north of the Canary Islands. The location of TOPAS lines and Core D13071 are also indicated. Island names are as follows: LP = La Palma, G = Gomera, T = Tenerife, GC = Gran Canaria. The boundary of the Selvage sediment-wave field has been modified from Jacobi et al. (1975). The boundary of the La Palma sediment-wave field is based on a map by Wynn et al. (2000b).

principal objectives of the present study are to: 1) interpret the wave-forming processes in the Selvage wave field, and 2) present some new insights into the formation of sediment waves by turbidity currents, based on the new data and previously published examples.

Previous work

Sediment waves on the Moroccan continental rise north of the Canary Islands were first recognised on 3.5 kHz profiles by Jacobi *et al.* (1975), who tentatively concluded that bottom currents were primarily responsible for wave formation, but that turbidity currents may also have been influential in wave formation and distribution. A more recent study has been undertaken on the La Palma sediment-wave field, offshore of the western Canary Islands (Wynn *et al.*, 2000*a*). Wynn *et al.* (2000*a*) used a high-quality integrated dataset to reveal sediment wave morphology in the La Palma sediment-wave field, and suggested that the waves were formed beneath unconfined turbidity currents sourced from the island flanks.

Data collection

About 600 km of ultra-high resolution seismic profiles was obtained using the TOPAS (TOpographic PArametric Sonar) system during cruise MAYC-95. The TOPAS system is a hull-mounted seabed and subbottom echosounder based on a parametric acoustic array, which operates using non-linear acoustic properties of the water (Webb, 1993). The TOPAS system transmits two acoustic signals of 15 and 18 kHz that interact within the water column to generate a secondary signal of lower frequency (1.5 to 4 kHz) in the form of a narrow beam. This produces a vertical resolution of <30-40 cm within the upper 50-80 m of the sediment column at any water depth. The absolute position of any TOPAS reflection is accurate to within 10 cm (Webb, 1993).

A single giant piston core (Core D13071) was recovered from the Selvage sediment-wave field during RRS Discovery cruise 225 in February 1997 (Fig. 9.1). This 13 m core has been logged with the multi-sensor core logger developed at Southampton Oceanography Centre (Best & Gunn, 1999), which records the P-wave velocity (ms^{-1}), wet bulk density using gamma ray attenuation (gcc^{-1}), and magnetic susceptibility (SI) of the core sediments. Core D13071 has also been logged visually, and all sand-sized sediments sampled for mineralogical analysis.

A microfossil stratigraphy has been established for Core D13071 based on coccolith ratios. The distribution of coccoliths has previously been tied to the oxygen isotope stratigraphy (e.g. Weaver, 1983), and provides a rapid, inexpensive and reliable method for dating the sedimentary sequence (Weaver & Kuijpers, 1983; Weaver, 1994). The technique is based on ratios of coccolith species, and zones are defined by appearance, extinction and cross over points of dominant species. Within any zone, linear extrapolation through pelagic units is used to determine the age of a sedimentary horizon. Zones are only a few tens of thousands of years long so potential errors are relatively small. This technique has enabled the sedimentation and wave migration rates in the Selvage wave field to be calculated.

The Selvage sediment-wave field

Wave distribution and morphology

The Selvage sediment-wave field lies at a water depth of 4285 m to 4350 m on the continental rise north of the Selvage Islands (Figs 9.1 and 9.2). Upslope of the wave field is a break-of-slope at 4045 m, where a steep rock outcrop passes downslope into stratified sediments (Fig. 9.2). The gradient changes from 1.8° to 0.3° at this boundary. Between the break-of-slope and the top of the Selvage wave field is a zone of parallel- and wavy-stratified sediments that are interrupted by two transparent debris-flow deposits (Fig. 9.3). Small (<2 m high), irregular, non-migrating sediment waves occur in this zone. The well-developed sediment waves in the Selvage wave field occur immediately downslope from the lower debris-flow deposit, and extend northwards for more than 20 km before dying out on the edge of the intraslope Agadir Basin (Fig. 9.4). Slope angles are between 0.22°-0.21° (+/-0.05°) up to 20 km downslope from the top of the wave field, decreasing to 0.16°-0.13° (+/-0.05°) beyond 20 km, where the sediment waves gradually merge into flat seafloor (Fig. 9.2). Wave heights (WH) reach a maximum of 6.2 m, and wavelengths (WL) vary from 0.4 km to 1.0 km (average 0.7 km). Wave dimensions vary with distance downslope from the top of the wave field (Fig. 9.5). Sediment waves in the upper 10 km of the wave field show an overall increase in size downslope, and the largest sediment waves generally occur between 10 and 15 km downslope from the top of the wave field. Beyond 15 km downslope, the sediment waves show a progressive downslope decrease in size. WL:WH ratios show a similar pattern, with the lowest values of 100-150 all occurring in the upper 10 km of the wave field. Between 10 and 25 km downslope the waves show progressively higher

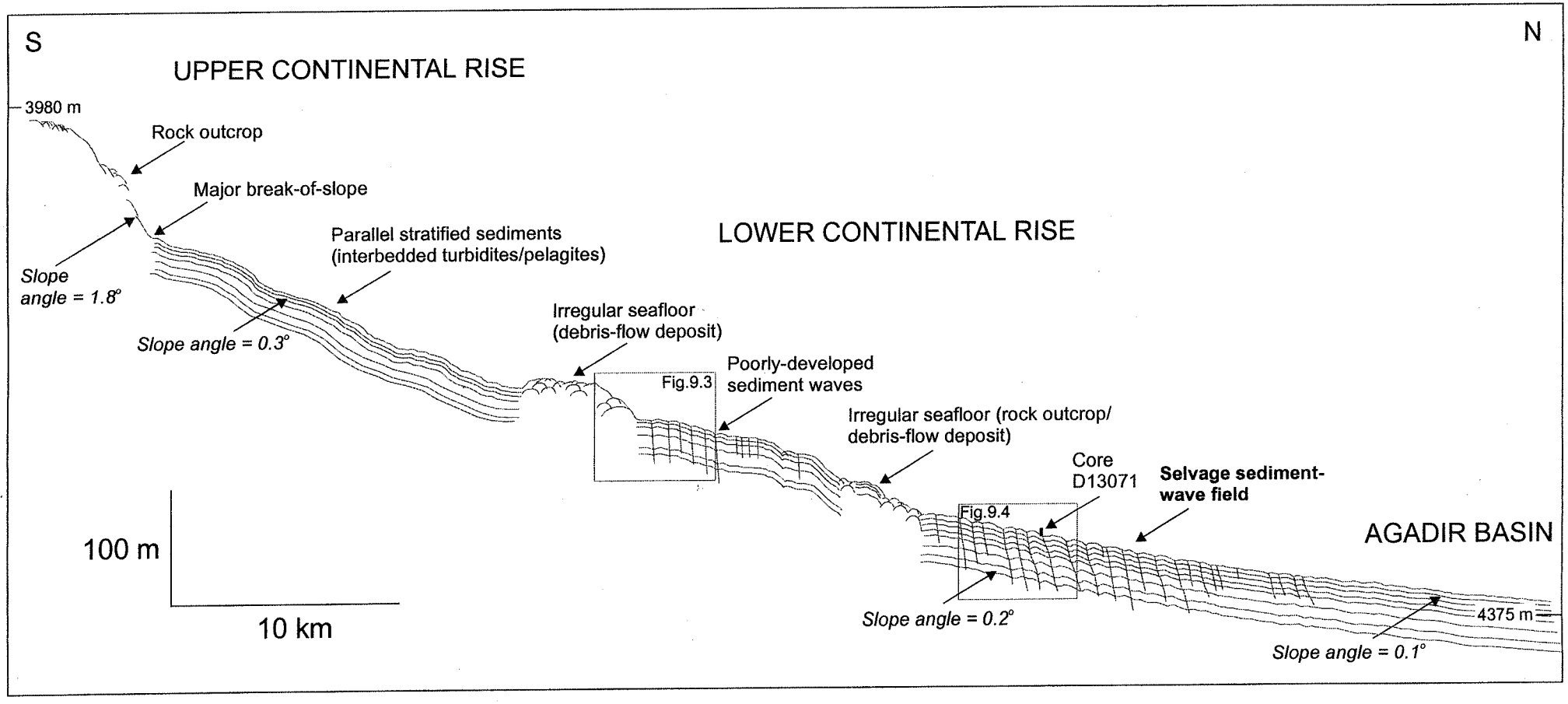

Figure 9.2: Interpretative line drawing of TOPAS profile taken across the continental rise north of the Selvage Islands. Note the position of the Selvage sediment-wave field immediately downslope of the lower zone of irregular seafloor. Location of TOPAS profile is shown in Figure 9.1. Dashed boxes indicate locations of Figures 9.3 and 9.4.

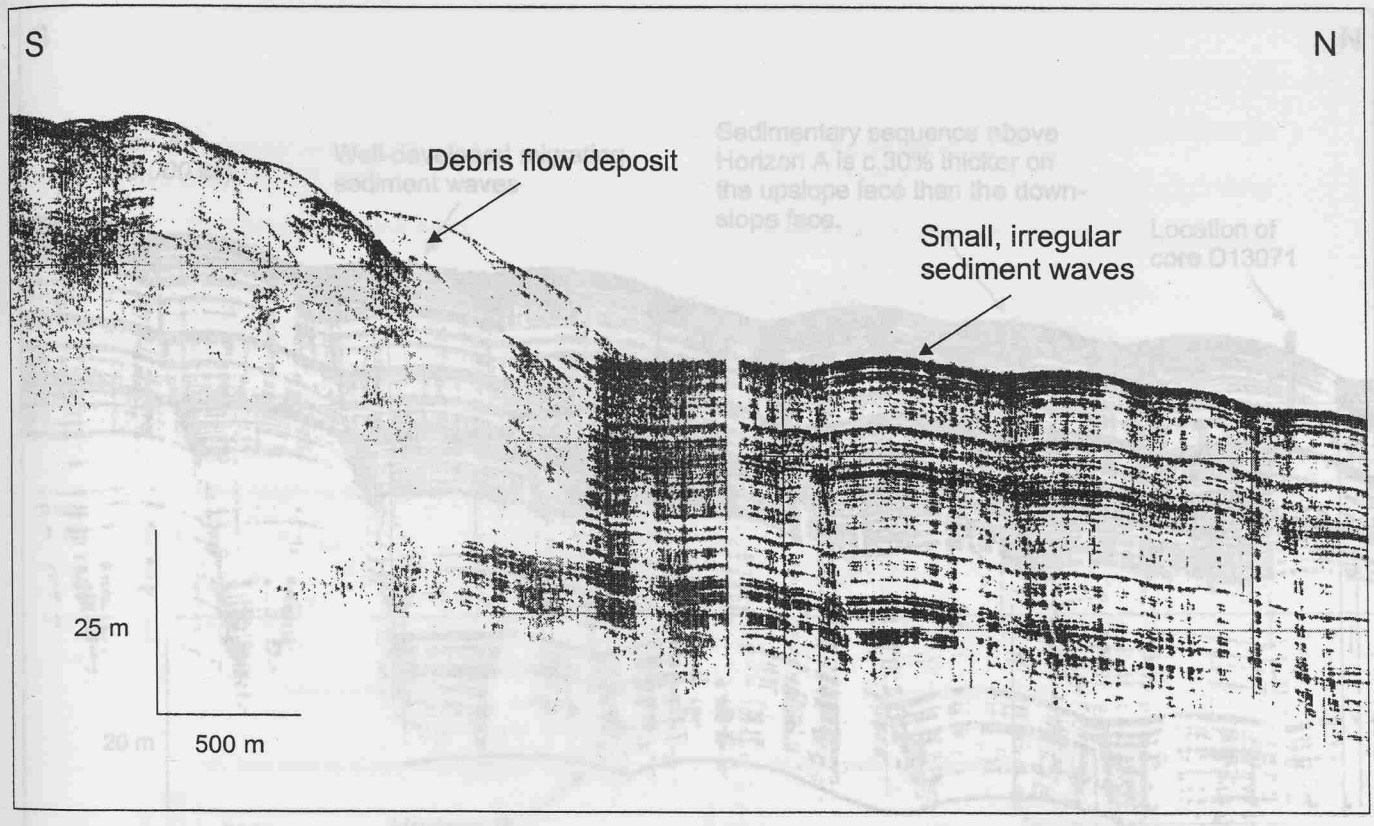

Figure 9.3: TOPAS profile showing poorly developed sediment waves downslope of a transparent debris-flow deposit. Location of profile shown on Figure 9.2.

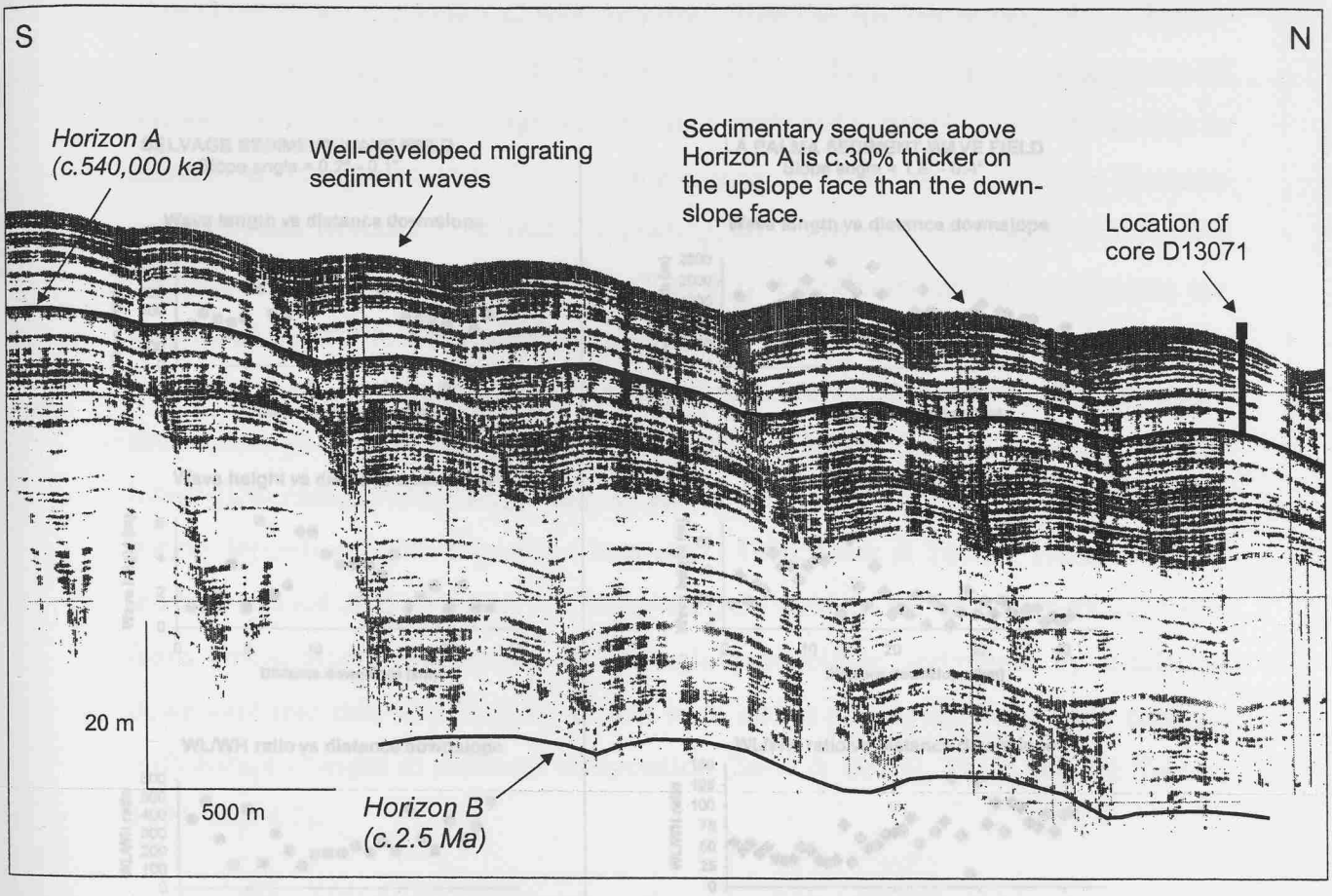

Figure 9.4: TOPAS profile showing well-developed sediment waves in the Selvage sediment-wave field. Note the clear upslope migration of the waves. Position of Core D13071 is indicated. Location of profile shown on Figure 9.2.

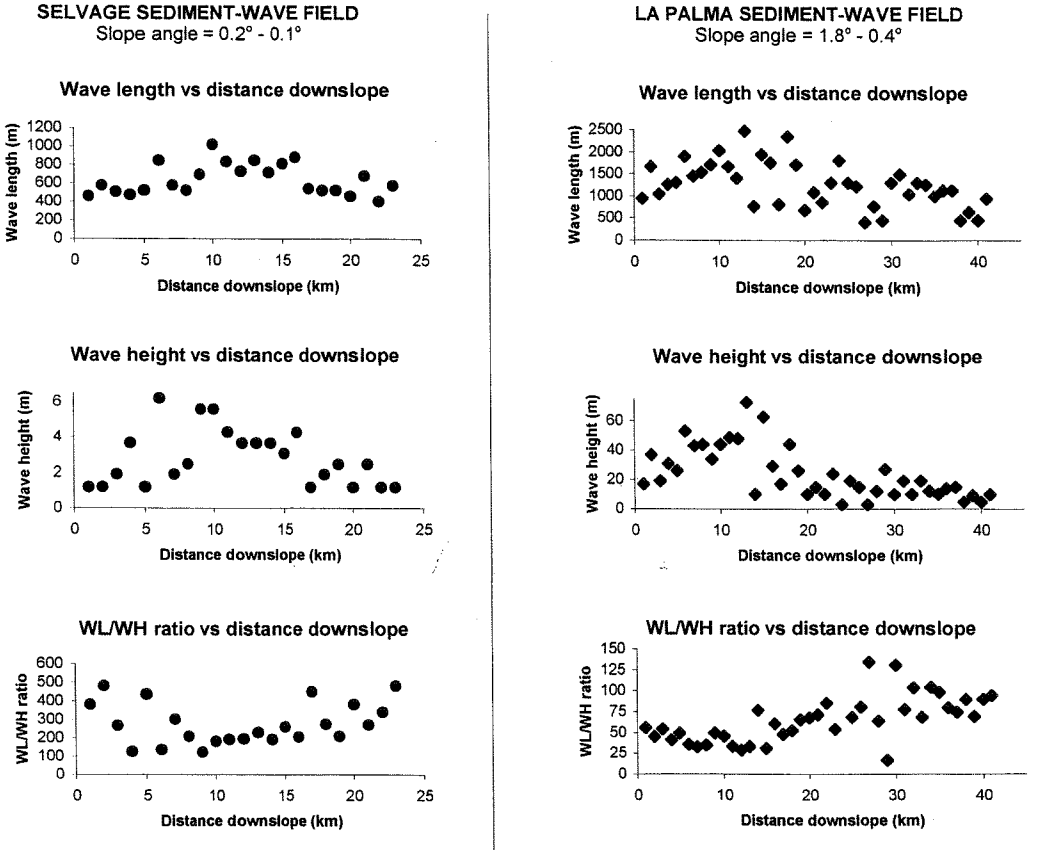

Figure 9.5: Graphs showing variations in wave height (WH), wavelength (WL) and WL/WH ratio in the Selvage and La Palma sediment-wave fields (data for La Palma from Wynn et al., 2000b). Note how WH + WL peak about 10 km downslope in both wave fields, and then gradually decrease downslope. The relatively small size of the Selvage sediment waves, compared with those off La Palma, is due to the shallower slope angle, and consequently lower turbidity current flow velocity, in the Selvage area.

values (Fig. 9.5). The sediment waves are migrating upslope, and the sedimentary sequence on the upslope faces of the sediment waves, above Horizon A, is about 30% thicker (+/-5%) than that on the downslope faces (Fig. 9.4).

Wave sediments

Core D13071 is 13 m long and was recovered from the downslope face of a sediment wave at a water depth of 4311 m (Figs 9.1 and 9.4). The core contains a sequence of interbedded turbidites and pelagic/hemipelagic marls and oozes (Fig. 9.6). Turbidites in this core are recognised using the following criteria: 1) a sharp or erosive base, 2) coarse sand/silt basal laminae, 3) normal size grading, and 4) reduced (or absent) bioturbation towards the base (Stow *et al.*, 1996) (Fig. 9.7). Pelagic/hemipelagic sediments are dominated by white, foram-rich, calcareous oozes, and brown marls and clays. There are no indications of primary sedimentary structures within the pelagic/hemipelagic sediments, (e.g. discontinuous laminae, lenses, sharp erosive contacts, abrupt lithological changes etc.), suggesting an absence of significant bottom-current activity during deposition of the sequence (Stow *et al.*, 1996; Stow & Tabrez, 1998). Some of the fine-grained mud turbidites are bioturbated throughout, but are still distinguishable from fine-grained contourites and pelagic/hemipelagic sediments by gradation downward into thin silty laminae at their base, and/or displaying sharp basal contacts with abrupt changes in sediment composition (Stow & Lovell, 1979; Stow & Tabrez, 1998; Fig. 9.7).

Four turbidites have sandy bases that have been sampled for mineralogical analysis. Generally, the mineralogical assemblages of these turbidites are dominated by volcanic glass and volcanic lithic fragments, with minor amounts of quartz and biotite (Fig. 9.6). Volcanic minerals in turbidite bases commonly show a distinctive magnetic susceptibility 'spike' (Fig. 9.7). Biogenic constituents of turbidite sands include pelagic foraminifera (commonly present as siliceous casts), siliceous sponge spicules and fish teeth.

Dating of the pelagic intervals in Core D13071, based on coccolith ratios, gives a date of approximately 540 (+/-10) ka for the base of the core. This is based on linear extrapolation from a data point at 1175 cm which represents the extinction of *Pseudoemiliania lacunosa* at 450 ka (Weaver, 1994). The overall sedimentation rate for

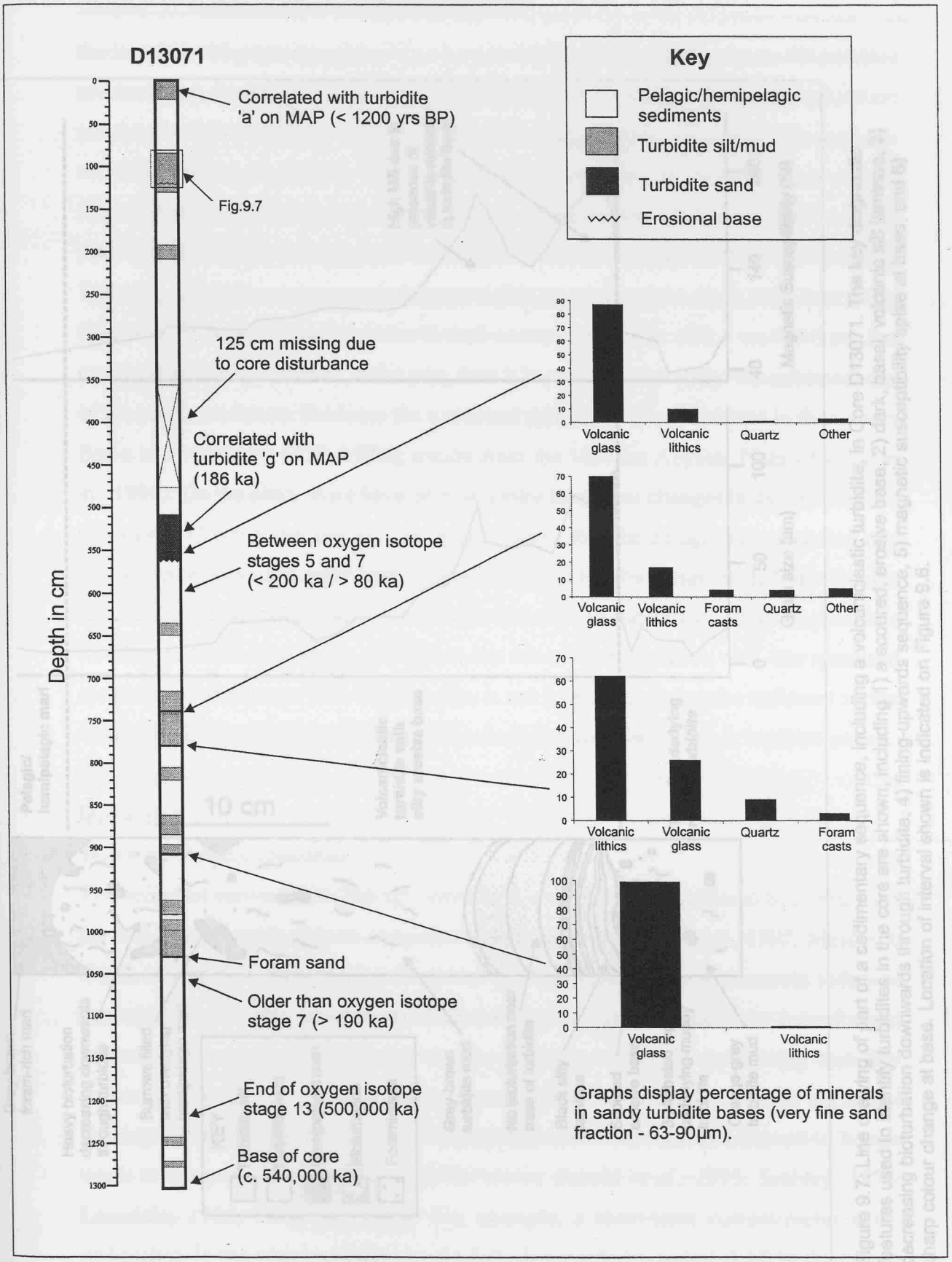

Figure 9.6: Description of Core D13071 recovered from the Selvage sediment-wave field, with graphs displaying the composition of sandy turbidite bases. Location of close-up interval in Figure 9.7 is shown. Core location is shown on Figures 9.1 and 9.2.

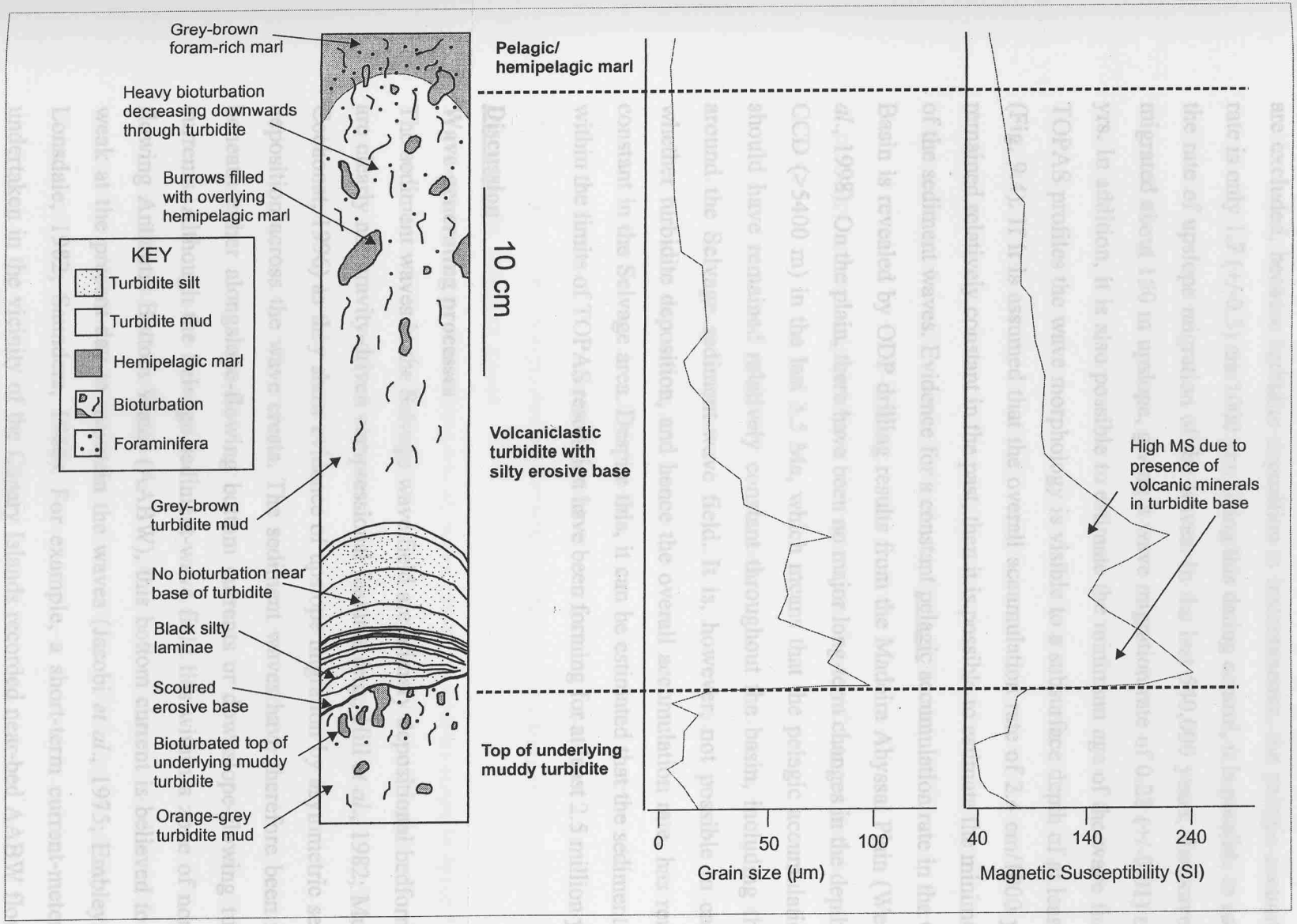

Figure 9.7: Line drawing of part of a sedimentary sequence, including a volcaniclastic turbidite, in Core D13071. The key diagnostic features used to identify turbidites in the core are shown, including 1) a scoured, erosive base, 2) dark, basal, volcanic silt laminae, 3) decreasing bioturbation downwards through turbidite, 4) fining-upwards sequence, 5) magnetic susceptibility spike at base, and 6) sharp colour change at base. Location of interval shown is indicated on Figure 9.6.

the last 540,000 years is estimated at 2.4 (+/-0.3) cm/1000 yrs. However, if turbidites are excluded, because turbidite deposition is instantaneous, the pelagic accumulation rate is only 1.7 (+/-0.3) cm/1000 yrs. Using this dating control, it is possible to calculate the rate of upslope migration of the waves. In the last 540,000 years, the waves have migrated about 150 m upslope, giving a wave migration rate of 0.28 (+/-0.01) m/1000 yrs. In addition, it is also possible to estimate the minimum age of the wave field. On TOPAS profiles the wave morphology is visible to a subsurface depth of at least 60 m (Fig. 9.4). If it is assumed that the overall accumulation rate of 2.4 cm/1000 yrs has remained relatively constant in the past, then it is possible to estimate the minimum age of the sediment waves. Evidence for a constant pelagic accumulation rate in the Canary Basin is revealed by ODP drilling results from the Madeira Abyssal Plain (Weaver *et al.*, 1998). On the plain, there have been no major long-term changes in the depth of the CCD (>5400 m) in the last 3.5 Ma, which means that the pelagic accumulation rate should have remained relatively constant throughout the basin, including the area around the Selvage sediment-wave field. It is, however, not possible to calculate whether turbidite deposition, and hence the overall accumulation rate, has remained constant in the Selvage area. Despite this, it can be estimated that the sediment waves within the limits of TOPAS resolution have been forming for at least 2.5 million years.

Discussion

Wave-generating processes

The sediment waves in the Selvage wave field are primary depositional bedforms, and are clearly not gravity-driven compressional features (e.g., Hill *et al.*, 1982; Mulder & Cochonat, 1996) as they show evidence of upslope migration by asymmetric sediment deposition across the wave crests. The sediment waves have therefore been formed beneath either alongslope-flowing bottom currents or downslope-flowing turbidity currents. Although the Selvage sediment-wave field lies within a zone of north-east flowing Antarctic Bottom Water (AABW), this bottom current is believed to be too weak at the present-day to maintain the waves (Jacobi *et al.*, 1975; Embley, 1976; Lonsdale, 1982; Saunders, 1988). For example, a short-term current-meter study undertaken in the vicinity of the Canary Islands recorded near-bed AABW flowing to the north-east at velocities of just 3-6 cms^{-1} (Lonsdale, 1982). Generally, sediment waves formed beneath bottom currents only occur at current velocities of 9-50 cms^{-1} (e.g. Flood, 1988). Although it is possible that AABW flow across the Selvage wave

field was stronger in the past, there is no evidence of significant bottom-current sedimentation or reworking in Core D13071. Detailed examination of pelagic/hemipelagic sediments in the core has revealed no indication of the primary sedimentary structures (e.g. discontinuous laminae, lenses, sharp erosive contacts, abrupt lithological changes etc.) that would be expected to occur under bottom currents with sufficient velocity to generate sediment waves. In addition, Jacobi *et al.* (1975) discovered that the wave crests are aligned parallel to the slope. This alignment is not compatible with existing models of bottom-current sediment waves on slopes, which predict that the wave crests will be oblique to the bottom-current flow and the regional bathymetric gradient (Blumsack & Weatherly, 1989; Blumsack, 1993).

A turbidity current origin for the Selvage wave field is favoured for the following reasons:

1) *Core sediments* - Core D13071 contains a total of 15 turbidites (Fig. 9.6) that are recognised by a sharp or erosive base, coarse sand/silt basal laminae, normal size grading, and reduced (or absent) bioturbation towards the base (Fig. 9.7). The presence of several turbidites in Core D13071 indicates regular turbidity-current flow across the wave field. In addition, there is no evidence of significant bottom-current sedimentation or reworking in the fine-grained sediments, and this strongly suggests a turbidity current origin for the sediment waves.

2) *Crest alignment* - The alignment of wave crests parallel-to-slope is typical of TC sediment waves (Table 9.1). Sediment waves generated by bottom currents flowing parallel-to-slope generally show an oblique crest alignment (Blumsack & Weatherly, 1989; Blumsack, 1993).

3) *Wave dimensions* - The sediment waves show a progressive downslope decrease in wave height and wavelength in the lower section of the wave field (Fig. 9.5). This pattern is a response to decreasing slope gradient and flow velocity, and is a common feature of TC sediment waves (Table 9.1). Sediment waves generated beneath bottom currents typically display more irregular dimensions (e.g. Cunningham & Barker, 1996; Howe *et al.*, 1998).

The Selvage sediment-wave field is therefore interpreted as having formed beneath unconfined turbidity currents, in a similar fashion to that described from the La Palma sediment-wave field in the western Canary Islands (Wynn *et al.*, 2000*a*). There is no

evidence for the existence of turbidity current channels in the area of the Selvage wave field, so turbidity currents are believed to flow as unconfined sheet flows across the continental rise. This setting is very similar to that described for sediment waves on channel-levee backslopes (e.g. Normark *et al.*, 1980; Carter *et al.*, 1990; Piper & Savoye, 1993; Lewis *et al.*, 1998; Nakajima *et al.*, 1998; Piper *et al.*, 1999). The upslope migration direction of the waves, and the dominantly volcanic mineral assemblage, indicates formation beneath turbidity currents originating from the flanks of volcanic islands to the south (Fig. 9.1). The Selvage Islands may be the source for some of the smaller flows, but are probably too stable and eroded to provide enough sediment to feed the larger flows. Good evidence of a Canary Island source for at least some of the flows is given in a recent study of turbidite deposition in the Agadir Basin (Wynn *et al.*, 2000*b*), which demonstrates that the turbidite in core D13071 between 520-570 cm (Fig. 9.6) can be correlated with turbidite *15* in the Agadir Basin and turbidite '*g*' on the Madeira Abyssal Plain. Turbidite '*g*' is dated at 186 ka and is sourced from the north flank of Tenerife (Rothwell *et al.*, 1992; Masson, 1994).

Wave migration

The migration rates of waves estimated for the Selvage sediment-wave field can be compared with those recorded in sediment-wave sequences elsewhere, and appear to demonstrate a clear link between sedimentation rate, especially the frequency of turbidity currents, and wave migration rate. Carter *et al.*, (1990) described a sediment-wave field on the backslope of the Bounty Channel levee that was formed beneath unconfined turbidity currents. The overall sedimentation rate was estimated at 13-26 cm/1000 yrs and the wave migration rate was between 2.8-5.6 m/1000 years. Sediment waves generated beneath bottom currents on the Feni Ridge were found to have a sedimentation rate of 2.7-4.5 cm/1000 yrs and a wave migration rate of 0.25 m/1000 yrs (Lonsdale & Hollister, 1979). The Selvage sediment waves have a sedimentation rate of 2.4 cm/1000 yrs and a wave migration rate of 0.28 m/1000 yrs, and are therefore more comparable to the sediment waves generated beneath bottom currents on the Feni Ridge. This is because turbidity currents are relatively infrequent on the continental rise south of the Canary Islands (Wynn *et al.*, 2000*b*) leading to a low sedimentation rate, and consequently a low wave migration rate.

It is important to note that on TOPAS profiles (Fig. 9.4), the sediment waves appear to be migrating upslope at a regular rate. This seems unusual as nearly three-quarters of the sediments in Core D13071 are pelagic and hemipelagic sediments, which would be expected to evenly drape the wave morphology through vertical settling. Wave migration should therefore only occur during deposition of turbidites, which make up just 28% of the core. A possible solution is that irregular wave migration will not be resolvable on TOPAS profiles, as any small-scale irregularities in the migration profile will probably be smoothed over, making upslope migration appear regular over time. Another possibility is that, although large-scale, instantaneous turbidity currents are undoubtedly the key process in controlling wave morphology and migration, other processes may also be involved. For example, fine-grained terrigenous sediment can be transported downslope by slow, dilute, 'continuous' turbidity currents (Damuth, 1977; Damuth *et al.*, 1988), and may contribute to wave formation and migration. In addition, although bottom currents are clearly not responsible for generation of the Selvage sediment waves (as shown by the wave orientation and sedimentology), a weak bottom current may redistribute pelagic/hemipelagic sediments unevenly across the wave crest, also contributing to the overall upslope migration. Therefore, although large, infrequent turbidity currents are the dominant force shaping and maintaining the waves, the possibility that slow, dilute, continuous, turbidity/bottom currents are contributing to upslope wave migration cannot be ruled out.

Turbidity current flow characteristics

The flow characteristics for turbidity currents can be constrained by simple numerical modelling, and this is attempted for flows crossing the Selvage sediment-wave field. First, an attempt is made to calculate the internal Froude number, and this value is combined with wave length to estimate flow thickness; flow velocity is calculated using two different methods, one based on grain size and the other on internal Froude number and sediment concentration.

Internal Froude number

The internal Froude number (Fi) for a turbidity current can be calculated using a combination of slope gradient ($sin\beta$), drag coefficient at the bed (C_f), and entrainment coefficient at the upper interface (E). Generally, Fi decreases with a reduction in slope gradient, and is lower in less turbulent flows (Bowen *et al.*, 1984). At $Fi = 1$, also

known as critical flow, the turbidity current is in a relatively steady state, and the head and body travel at a similar speed (Middleton, 1966). The following calculations of *Fi* are based on Equation (1), from Bowen *et al.* (1984):

$$Fi^2 = \frac{\sin\beta}{Cf + E} \qquad (1)$$

where *Fi* = internal Froude number, $\sin\beta$ = slope angle, *Cf* = drag coefficient, and *E* = entrainment coefficient.

In the Selvage sediment-wave field, the slope angle varies from 0.22°-0.13°. Suggested values for the drag coefficient (C_f) in channelised turbidity currents are in the range of 3-5 x 10^{-3} (e.g. Komar, 1975; Bowen *et al.*, 1984). However, in the case of unconfined flows crossing the slope and rise a lower figure may be more applicable. Therefore a range of C_f values are used, varying from the minimum possible value of 5 x 10^{-4} for a smooth, artificial bed, to a maximum of 5 x 10^{-3} for channelised flows crossing a gravel bed. The entrainment coefficient (*E*) for most turbidity currents varies between 5 x 10^{-4} and 6 x 10^{-3} (Bowen *et al.*, 1984). Using Equation (1), these figures give a range of Froude numbers, from *Fi* = 1.9-0.6 on the maximum slope of 0.22° in the upper wave field, to *Fi* = 1.5-0.5 on the minimum slope of 0.13° in the lower wave field. Taking the mean values, *Fi* decreases from 1.25 to 1 downslope. These figures are in agreement with previous research of unconfined turbidity currents (e.g. Normark *et al.*, 1980), and suggest that the turbidity currents may have passed from supercritical to subcritical flow on their passage across the wave field.

Flow thickness

Equation (2) illustrates the relationship between sediment wavelength (*L*), flow thickness (*h*) and internal Froude number (*Fi*), and has been modified from Normark *et al.* (1980):

$$h = \frac{L}{2\pi Fi^2} \qquad (2)$$

where *h* = flow thickness and *L* = wavelength

In the Selvage sediment-wave field L reaches a maximum of 1 km about 10 km downslope from the top of the wave field, before showing a gradual decrease to a minimum of 0.4 km about 25 km downslope. Using Equation (2), and accounting for variations in Fi as demonstrated by Equation (1), it can be shown that from 0-10 km downslope, flow thickness increases from 20-200 m to 45-450 m. Flow thickness then gradually decreases downslope to a minimum of 30-260 m at 25 km downslope. These values are comparable to those estimated in previous studies (e.g. Normark *et al.*, 1980; Wynn *et al.*, 2000*a*). Between 10-25 km, flow thickness decreases downslope by about 60% over a total distance of 15 km. This compares to a downslope decrease in flow thickness of 83% over 25 km for turbidity currents crossing the La Palma sediment-wave field (Wynn *et al.*, 2000*a*) and 86% over 15 km for turbidity currents crossing the Monterey Fan levee backslope (Normark *et al.*, 1980). This relatively rapid reduction in flow thickness is expected for unconfined, spreading flows on open slopes (Komar, 1975). It should be noted that the wide range of flow thicknesses obtained using Equation (2) highlights the sensitivity of this equation to relatively minor changes in Fi, and leads to variations in flow thickness of an order of magnitude.

Flow velocity based on maximum settling velocity

An indication of flow velocity can be obtained by estimating the maximum settling velocity (w), which is a function of the turbidite grain size. Generally, turbidites in Core D13071 contain thin sandy bases with a maximum grain size of about 200 μm (2.3 ϕ). Above these bases, silt laminae of modal grain size 30 to 60 μm (4-5 ϕ) are often developed, and the top of the turbidite is composed of fine silts and muds (<30 μm or 5 ϕ). Assuming that these relatively fine-grained sediments are carried in the flow as suspended load, then b = 1.25 in the following equation (Bowen *et al.*, 1984):

$$u = \frac{bw}{\sqrt{C_f}} \qquad (3)$$

where u = flow velocity, b = parameter linking settling velocity to frictional velocity, w = settling velocity of the suspended sediment, and Cf = drag coefficient.

A range of predicted flow velocities are obtained if variations in C_f, are accounted for, as discussed above. For the sandy turbidite bases, the maximum flow velocity attainable

at the time of deposition is between 42-125 cms^{-1}. For deposition of the overlying silty laminae, velocities range from 6-38 cms^{-1}. Finally, the fine-grained turbidite tops are deposited at velocities of <6-38 cms^{-1}. These figures are very similar to those obtained by Stow & Bowen (1980), Normark *et al.* (1980) and Bowen *et al.* (1984) for turbidity currents on submarine fans.

Flow velocity based on internal Froude number and sediment concentration

Estimates of flow velocity can also be obtained using the following equation (Piper & Savoye, 1993):

$$u^2 = \Delta pCghFi^2 \qquad (4)$$

where Δp = grain density – TC density/seawater density, C = volume concentration, and g = gravitational acceleration.

C is a dimensionless number that represents the sediment concentration. For fine-grained, unconfined turbidity currents, previous research has shown that C is in the range of 10^{-5} to 10^{-6} (Normark *et al.*, 1980). However, it should be noted that Equation (4) is very sensitive to changes in C, which is one of the most poorly constrained variables in turbidity current modelling. Existing data indicate that C can vary by several orders of magnitude depending on the type of flow involved (e.g. Normark *et al.*, 1980; Bowen *et al.*, 1984; Piper & Savoye, 1993). Flow thickness (h) has been shown to vary between 20-450 m, and Fi^2 ranges from 3.61-0.25. When these variables are entered into Equation (4), it can be shown that velocities in the upper wave field range from 3-130 cms^{-1}, and in the lower wave field range from 2-80 cms^{-1}. The maximum value of 130 cms^{-1} is very similar to that of 125 cms^{-1}, obtained from grain size data using Equation (3). These maximum values probably represent the velocity at the head of the turbidity current, as this is where sediment concentration and flow thickness are highest. The lower values probably represent the slower moving tail of the turbidity current, where sediment concentration and flow thickness are much reduced.

New insights into the formation of deep-water sediment waves

Having established that the Selvage sediment-wave field has formed beneath unconfined turbidity currents, the discussion will now focus on the two existing models

for sediment-wave formation, and investigate which model is most applicable to the Selvage sediment waves. The applicability of each model to the formation of both bottom-current and turbidity-current sediment waves is discussed in turn.

1a: The lee-wave model and bottom-current sediment waves

The link between internal lee-waves and sediment-wave formation was first described by Allen (1984), with respect to sediment waves generated beneath bottom currents. The lee-wave model was further developed by Flood (1988), but was only applicable to situations where wave crests were oriented perpendicular to the flow. Blumsack & Weatherly (1989) and Blumsack (1993) adapted the model to account for sediment waves on slopes with crests aligned oblique to bottom-current flow direction. The lee-wave model is dependent upon a weakly stratified water column and an initial seafloor perturbation to initiate the development of lee-waves within a bottom-current flow. The model predicts that the formation of bottom current sediment waves will generally only occur at current velocities of 9-50 cms^{-1} (Flood, 1988). At these velocities, internal lee-waves are generated within the bottom current, leading to increased flow velocities on the downstream face of a sediment wave. This causes reduced deposition, non-deposition or erosion on the downstream flank. As the current slows on the upstream face of the wave, deposition occurs, leading to an overall upcurrent wave migration. When tested against observations in the Argentine Basin, the lee-wave model appeared to show good agreement with real datasets (Flood, 1988; Blumsack & Weatherly, 1989). However, this model is not applicable to the Selvage sediment-wave field because, as previously discussed, the crest orientation is parallel to the slope and the bottom current flow (Jacobi *et al.*, 1975). This crest alignment is not compatible with the lee-wave model of Flood (1988), which is only applicable to sediment waves with crests aligned perpendicular to the flow direction. It is also incompatible with the advanced lee-wave model of Blumsack & Weatherly (1989) and Blumsack (1993), which predicts that most sediment waves on slopes will develop crest orientations that are oblique to the flow direction.

1b: The lee-wave model and turbidity-current sediment waves

The lee-wave model of Flood (1988) has also been applied to TC sediment waves (Lewis, 1994; Howe, 1996). This application seems logical given that the morphology and internal architecture of sediment waves generated beneath bottom and turbidity

currents are very similar, suggesting a common process of formation. In addition, the present study has revealed that the relationship between sedimentation rate and wave migration rate in the Selvage sediment-wave field is very similar to that described for a field of bottom-current sediment waves on the Feni Ridge (Lonsdale & Hollister, 1979). Since lee-waves are generated when a density stratified current flows over an irregular seafloor (Flood, 1988), it may be possible that under certain conditions turbidity currents flowing over uneven topography will achieve sufficient internal density stratification to allow lee-wave formation (e.g. Stacey & Bowen, 1988; Normark & Piper, 1991; Kneller & Branney, 1995). However, Allen (1984), clearly states that "lee waves exist only if the densiometric Froude number is smaller than $1/\pi$ (approximately 0.318), a result that must exclude many turbidity currents as causes of lee waves". Turbidity currents responsible for generating the Selvage sediment waves are calculated to have Fi = 0.5-1.9, and are therefore not suitable for lee-wave generation. In addition, the slope angles of seven other TC sediment-wave fields have been measured, and the values all fall between 0.1° and 1.8° (Table 9.1). According to Equation (1), turbidity currents flowing across these slopes will have $Fi \approx$ 0.4-2.4, and are therefore also unsuitable for lee-wave generation. These results suggest that lee-waves cannot be generated within the types of turbidity currents responsible for creating and maintaining the Selvage and other TC sediment-wave fields.

2a: The antidune model and bottom-current sediment waves

Several studies have discussed the possible application of the antidune model to sediment waves generated beneath bottom currents (Hand, 1974; Kolla *et al.*, 1980; McCave & Tucholke, 1986). However, evidence presented by Allen (1984) and Piper & Savoye (1993) indicates that this is impossible, as for most bottom currents Fi <0.3 (based on observed flow thickness, density and density differences). This is well below the lower limit of Fi = 0.844 required for antidune formation, and shows that antidune conditions cannot be generated within most bottom currents. Unfortunately, there is no information available on flow thickness or concentration for bottom currents flowing over the Selvage sediment waves, and it is therefore not possible to estimate Fi for these flows. However, as most bottom currents generally display similar characteristics (Allen, 1984), it is unlikely that the bottom currents crossing the Selvage sediment waves will have Froude numbers within the antidune existence limits.

2b: The antidune model and turbidity-current sediment waves

There is better agreement in the literature that TC sediment waves can form as antidunes. Hand *et al.* (1972) first noted that large-scale antidunes (with wavelengths in the order of tens to hundreds of metres), could occur as a result of the formation of surface waves at the interface between a turbidity current and seawater. Normark *et al.* (1980) then developed a two-layer antidune model for sediment waves formed beneath unconfined turbidity currents on channel levees. This model accounts for the condition where a dense turbid underflow moves beneath stationary seawater, and reveals several features that are compatible with actual observations. For example, the calculated values of sediment concentration and flow thickness, derived from the antidune model, are very similar to those taken from first-hand observations in similar settings (e.g. Stow & Bowen, 1980; Piper & Savoye, 1993). In addition, Normark *et al.* (1980) state that "the depth of flow is approximately one-sixth of the wavelength", implying that as flow thickness decreases, wavelength also decreases (see Equation (2)). This appears to be the case in reality, whereby the majority of TC sediment waves display an overall decrease in wavelength downslope (Table 9.1), and is compatible with the observations of Komar (1975), who argued that levee overbank (unconfined) flows will become thinner downslope as they expand laterally. Observed and calculated occurrences of antidunes suggest they form beneath flows where Fi = 0.844-1.77 (Allen, 1984). For turbidity currents crossing the Selvage sediment-wave field, Fi = 0.5-1.9, which is in good agreement with the antidune existence limits. The minimum value of Fi = 0.5 is just below the lower limit of antidune formation (Allen, 1984) and may explain why the Selvage sediment waves die out downslope on slope angles <0.1°. A number of other TC sediment-wave fields (Table 9.1) are crossed by turbidity currents with $Fi \approx$ 0.4-2.4, and are therefore also close to the antidune existence limits.

The pattern of wave dimensions in the Selvage sediment-wave field may give some indication of how turbidity currents interacting with seafloor topography can inhibit sediment-wave development. The largest sediment waves occur about 10 km downslope from the top of the wave field (Fig. 9.5), and then show a progressive downslope decrease in dimensions. However, in the upper 10 km of the wave field the sediment waves show an overall downslope increase in dimensions, which is unexpected as the slope angle in this area remains fairly constant at 0.2°. A possible explanation may be linked to the fact that sediment waves in the upper 10 km of the wave field occur

immediately downslope of a buried rock outcrop/debris flow deposit (Fig. 9.2). Turbidity currents will have flowed over or around this obstacle, although as its lateral extent is unknown this cannot be qualified with certainty. However, Alexander and Morris (1994) found that for experimental unconfined flows, where obstacle height is significantly smaller than flow thickness, the flow will continue over the obstacle without being deflected. As the height of the topographic obstacle upslope of the Selvage wave field is only about 20% of the flow thickness, it seems likely that the flow will pass over the obstacle in this instance. Alexander and Morris (1994) also suggested that flow over even relatively small obstacles can influence bedform character and distribution. Flows travelling over the top of the deposit may have undergone a hydraulic jump on leaving the obstacle, as there is a distinct break of slope at its downslope boundary. The slope angle changes from 0.6° to 0.2° at this boundary, leading to a change in *Fi* of 1.0-3.2 to 0.6-1.9 (based on Equation (1)). This may therefore correspond to a change from super- to subcritical conditions, and development of a hydraulic jump. During a hydraulic jump, turbidity currents increase in thickness and generate intense turbulence (Komar, 1971). Speculatively, this increase in turbulent energy could prevent development of the optimum conditions necessary for antidune formation. Allen (1984) states that near stationary bed and surface waves are necessary for the development of antidunes, and that in turbidity currents the surface waves are probably developed on interfaces within the flow. Therefore, if these interfaces are disrupted by the increased turbulence of a hydraulic jump, antidune development may be affected. In addition, experimental work by Garcia and Parker (1989) revealed that the maximum deposition of sediment carried as suspended load occurred downstream of the jump. This may also explain why the largest waves are 10 km downslope of the topographic obstacle, as this is probably where the zone of maximum sediment deposition occurs.

A similar pattern of wave dimensions is observed in the La Palma sediment-wave field (Fig. 9.5), with the largest waves occurring between 10 and 20 km downslope from an area of steep rock outcrop/slump deposits (Wynn *et al.*, 2000*a*). This pattern is probably also related to the factors discussed above. However, in both examples, the 10-20 km 'lag' between the edge of the obstacle and the maximum wave dimensions has yet to be satisfactorily explained, and further data need to be collected on the exact nature and

orientation of these topographic obstacles before this interpretation can be developed further.

Wider implications of this study

The interpretation that the Selvage sediment-wave field is formed beneath unconfined turbidity currents has important implications for studies of other sediment-wave fields in the deep ocean. The Selvage sediment waves occur in a linear belt that runs along the lower continental rise parallel to the bathymetric gradient, in a setting that was previously seen as being typical of bottom current dominated settings (e.g. Embley & Langseth, 1977). However, this study has revealed that in areas where the lower rise is crossed by unconfined sheet flows, a linear band of TC sediment waves can occur. A similar situation occurs on channel-levee backslopes, where sediment waves generated by unconfined sheet flows are generally confined to a narrow band oriented parallel to the bathymetric gradient (e.g. Normark *et al.*, 1980; Carter *et al.*, 1990; Nakajima *et al.*, 1998). It is therefore important to recognise that sediment waves generated by turbidity currents are not just confined to channels and their levees, but may also occur in other deep-water settings with turbidity current input.

Conclusions

Sediment waves in the Selvage wave field display characteristics similar to those described from channel levee-backslopes, and are interpreted as having formed beneath unconfined turbidity currents. Sedimentological analysis of sandy turbidite bases indicates that the flows were probably sourced from the flanks of the volcanic Canary Islands to the south. The wave migration rate in the Selvage wave field is similar to that estimated for bottom-current sediment waves on the Feni Ridge, but is considerably lower than the wave migration rate on the Bounty Channel levees. This is compatible with the relatively low sedimentation rate and turbidity current frequency in the vicinity of the Selvage sediment-wave field.

Application of existing models for sediment-wave formation indicates that the antidune model is most applicable to sediment waves formed beneath unconfined turbidity currents, including the Selvage sediment waves. Slope angles across the Selvage sediment-wave field are very close to the lower limit for antidune formation (based on the relationship between Froude number and slope angle), and this may explain the

relatively small size of the waves, and their disappearance downslope as the slope angle decreases. Estimates of flow thickness, based on wavelength and Froude number, suggest that turbidity currents initially increase in thickness downslope of an obstacle, and reach a maximum flow thickness of 45-450 m about 10 km from the top of the wave field. Between 10-25 km downslope, there is a gradual decrease in flow thickness to a minimum flow of 30-260 m.

Several key questions regarding turbidity-current flow processes need to be answered before models of sediment-wave formation can be further developed. For example, is the relationship between Froude number and slope angle accurate and is it applicable to unconfined turbidity currents? Can the antidune model be applied to coarse-grained sediment waves in channels? How is sediment wave formation affected by flow over obstacles? Unfortunately, because of the nature, environment and unpredictability of natural turbidity currents, field observation of flow processes is generally impossible. However, carefully constructed laboratory experiments could lead to an increased understanding of the controls on sediment wave formation, and may help prediction of their occurrence in subsurface turbidite systems.

Acknowledgements

The authors would like to acknowledge the expertise and enthusiasm of the Masters, officers and crew present on RRS Discovery cruise 225 and RV Hesperides cruise MAYC-95. The RV Hesperides cruise was carried out within the framework of project AMB-95-0196. RBW acknowledges the provision of PhD funding from the University of Southampton and the Southampton Oceanography Centre Challenger Division. B. Alonso and J. Baraza are thanked for their contribution to collection and interpretation of the TOPAS profiles. Dave Gunn provided technical assistance with core logging. This paper benefited greatly from the constructive reviews provided by John Damuth and Stephen Morris, and the thorough editing of Jim Best.

Notation

WH = Wave Height (m)

WL = Wavelength (km)

L = Wavelength (m) (in equations)

Fi = internal Froude number

$\sin\beta$ = slope angle

Cf = drag coefficient

E = entrainment coefficient

h = flow thickness (m)

u = flow velocity (ms^{-1})

b = parameter linking settling velocity to frictional velocity

w = settling velocity of the suspended sediment (ms^{-1})

Δp = grain density – TC density/seawater density (kgm^{-3})

C = volume concentration

g = gravitational acceleration (ms^{-2})

ϕ = Phi

9.3: Summary

The two papers presented in this and the previous chapter, have revealed that sediment waves on the continental rise can be formed by unconfined turbidity currents. They have also been shown that the antidune model is most applicable to sediment waves generated beneath unconfined flows. Cores taken through the sediment waves show sequences of interbedded turbidites and pelagic/hemipelagic sediments, with many turbidites having sandy bases.

In the following chapter the effects of wave morphology on the thickness and spatial distribution of these turbidite sands are investigated, and the implications for deep-water hydrocarbon exploration are discussed. In addition, an attempt will be made to understand how sequences of migrating sediment waves in turbidite-dominated environments can be identified in the subsurface.

CHAPTER 10

TURBIDITY CURRENT SEDIMENT WAVES (3)

10.1: Introduction and aims

Deep-water sediment waves are a common feature of turbiditic environments, being commonly found in channels and on levee backslopes. The previous two chapters have revealed how sediment waves on open slopes can be generated by unconfined turbidity currents, in a similar fashion to sediment waves on levee backslopes. In this chapter the application of these studies to deep-water hydrocarbon exploration in turbidite systems is presented. In particular, methods of recognising migrating sediment waves in the subsurface are investigated, and sandbody continuity and fluid flow through buried wave sequences are discussed.

10.2: Paper 7

Turbidity current sediment waves in subsurface sequences

Russell B. Wynn, Douglas G. Masson, Dorrik A. V. Stow and Philip P. E. Weaver

SOES/Challenger Division, Southampton Oceanography Centre, European Way, Southampton, SO14 3ZH, UK

This paper was submitted for inclusion in an AAPG/SEPM special publication in October 1998. It was reviewed by Arnold Bouma, John Southard and John Bratton, and was accepted for publication in May 1999. It was published in April 2000, as Chapter 26 of '*Fine-Grained Turbidite Systems (Ed. by A.H. Bouma, C.E. Stelting and C.G. Stone), AAPG Memoir 72/SEPM Spec. Publ.68*'.

Abstract

Two sediment wave fields on the submarine slopes of the Canary Islands display wave heights up to 70 m and wavelengths up to 2.4 km. Wave sediments consist of fine-grained turbidites and pelagic/hemipelagic sediments. The sediment waves are formed beneath unconfined turbidity currents, and are similar to sediment waves found on channel-levee backslopes.

Sediment wave morphology is resolvable on high-resolution seismic profiles. In areas lacking high-resolution seismic data, analysis of dipmeter readings may provide a useful tool for recognising buried sequences of migrating waves. Thick sequences of sediment waves will impart a marked heterogeneity to a potential reservoir, leading to complications during reservoir production.

Introduction

Sediment waves formed beneath turbidity currents are large-scale depositional bedforms that occur in a variety of deepwater turbiditic environments. They can be broadly subdivided into two groups, on the basis of their grain size, environment, and type of depositional flow:

1) Gravel-rich sediment waves have been described from a number of modern fan valleys (see Normark and Piper, 1991, for a review) and are interpreted as having been formed beneath channelised turbidity currents. They typically display wavelengths of <100 m and wave heights of <10 m.

2) Fine-grained turbidity current waves occur on channel-levee backslopes and on the flanks of islands and seamounts (e.g., Normark et al., 1980; Carter et al., 1990; McCave and Carter, 1997; Nakajima et al., 1998). Wynn et al. (2000, a, b). They typically display wavelengths of 1-6 km and wave heights of 5-70 m, and are formed beneath unconfined turbidity currents. The wave crests are up to 60 km long, and are aligned parallel to the slope. There is generally a regular downslope decrease in wave dimensions and the waves often display upslope migration. Wave sediments consist of thin-bedded sand/silt turbidites interbedded with pelagic/hemipelagic sediments. Individual turbidites are thicker on the upslope face of the wave, and are thinner, or eroded, on the downslope face.

Many previous studies of turbidity current deposited sediment waves are restricted because of low-quality or sparse data. The present study uses a variety of high-quality data, including 3.5kHz-profiles, single-channel seismic profiles, GEOSEA 3-D imagery, and sediment cores. The principal objectives of this paper are to (1) summarise the data presented by Wynn et al. (2000, b), describing two sediment wave fields on the submarine slopes of the Canary Islands, (2) compare this data with other published data on fine-grained turbidity current waves, and (3) discuss how the results may be applied to hydrocarbon exploration, in particular the recognition and interpretation of sediment wave sequences in the subsurface.

Study area

The two sediment wave fields investigated are located on the submarine slopes of the Canary Islands (Figure 10.1). The La Palma wave field lies to the north-west of La Palma Island, and is centred on 18°30'W, 29°30'N. The Selvage wave field is situated on the lower rise south of the Agadir Basin, at 15°45'W, 31°10'N. The continental slope in this region is 100-200 km wide, and passes to the continental rise in water depths of 4000-4500 m. The rise is 400-600 km wide and displays gradients of about 1° on the lower slope/upper rise to 0.1° on the lower rise (Masson et al., 1992).

Previous work

The sediment waves on the submarine slopes of the northern Canary Islands were first described by Jacobi et al. (1975). They mapped a nearly continuous zone of sediment waves on the lower rise, lying parallel to the regional bathymetric trend. Those authors found that the present-day bottom current circulation in the area is too weak to have formed the waves, and suggested that relatively stronger bottom currents in the recent past may have been responsible for wave formation. However, they also discussed the possibility that turbidity currents may have influenced wave distribution. Masson et al. (1992) and Jacobi and Hayes (1992) mapped the La Palma wave field, and also concluded that bottom currents were probably responsible for wave formation. However, recent work by Wynn et al. (2000, b), using the newly obtained dataset, suggest that the sediment waves in this area have been formed and maintained by unconfined turbidity currents.

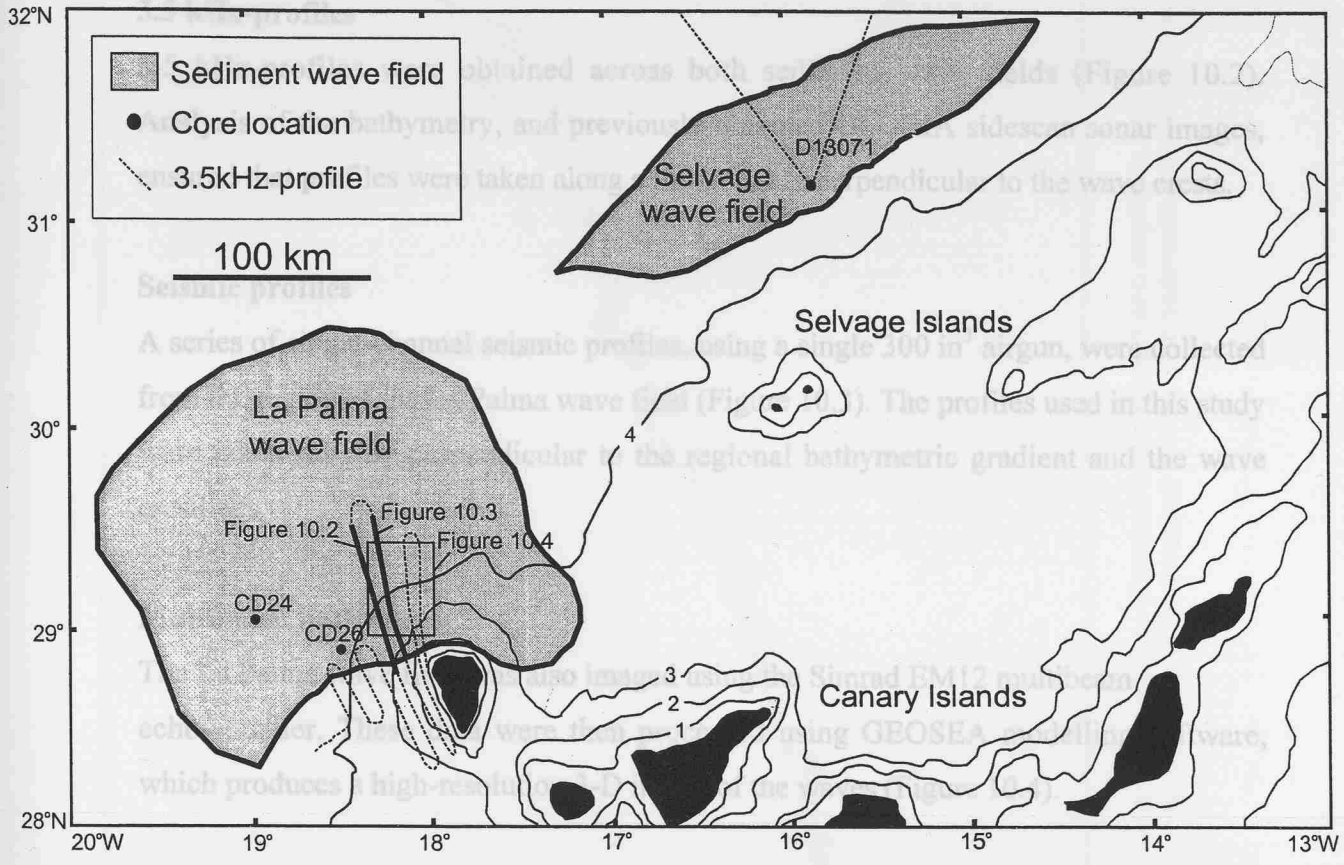

Figure 10.1: Location map of the study area, highlighting the position of the La Palma and Selvage wave fields. Locations of Figures 10.2-10.4 are indicated. Bathymetric contours in kilometres.

Data collection

The dataset used was collected during RRS Charles Darwin cruises 56 and 108, and RRS Discovery cruise 225. A variety of data were collected to facilitate detailed surface and subsurface characterisation of the waves:

3.5 kHz-profiles

3.5 kHz-profiles were obtained across both sediment wave fields (Figure 10.2). Analysis of the bathymetry, and previously obtained GLORIA sidescan sonar images, ensured that profiles were taken along a line roughly perpendicular to the wave crests.

Seismic profiles

A series of single-channel seismic profiles, using a single 300 in^3 airgun, were collected from the region of the La Palma wave field (Figure 10.3). The profiles used in this study were taken roughly perpendicular to the regional bathymetric gradient and the wave crestlines.

Multibeam bathymetry

The La Palma wave field was also imaged using the Simrad EM12 multibeam echo-sounder. These data were then processed using GEOSEA modelling software, which produces a high-resolution 3-D image of the waves (Figure 10.4).

Sediment cores

Cores were recovered from both wave fields. Three short (<2 m) kasten cores were obtained from the southern margin of the La Palma wave field, and a 12 m piston core from the Selvage wave field (Figure 10.5). The core locations are shown in Figure 10.1.

Results

The La Palma sediment-wave field

Surface morphology: 3.5kHz- and single-channel seismic profile data across the La Palma wave field reveal that the sediment waves at the surface display heights of <5-70 m and wavelengths of 0.4-2.4 km (Figures 10.2 and 10.3). There is generally a slight asymmetry across the waves, with a steeper downslope face. There is also a regular downslope decrease in wave dimensions (Figure 10.2). GEOSEA images of the waves indicate that the wave crests are aligned roughly parallel to the regional gradient, and

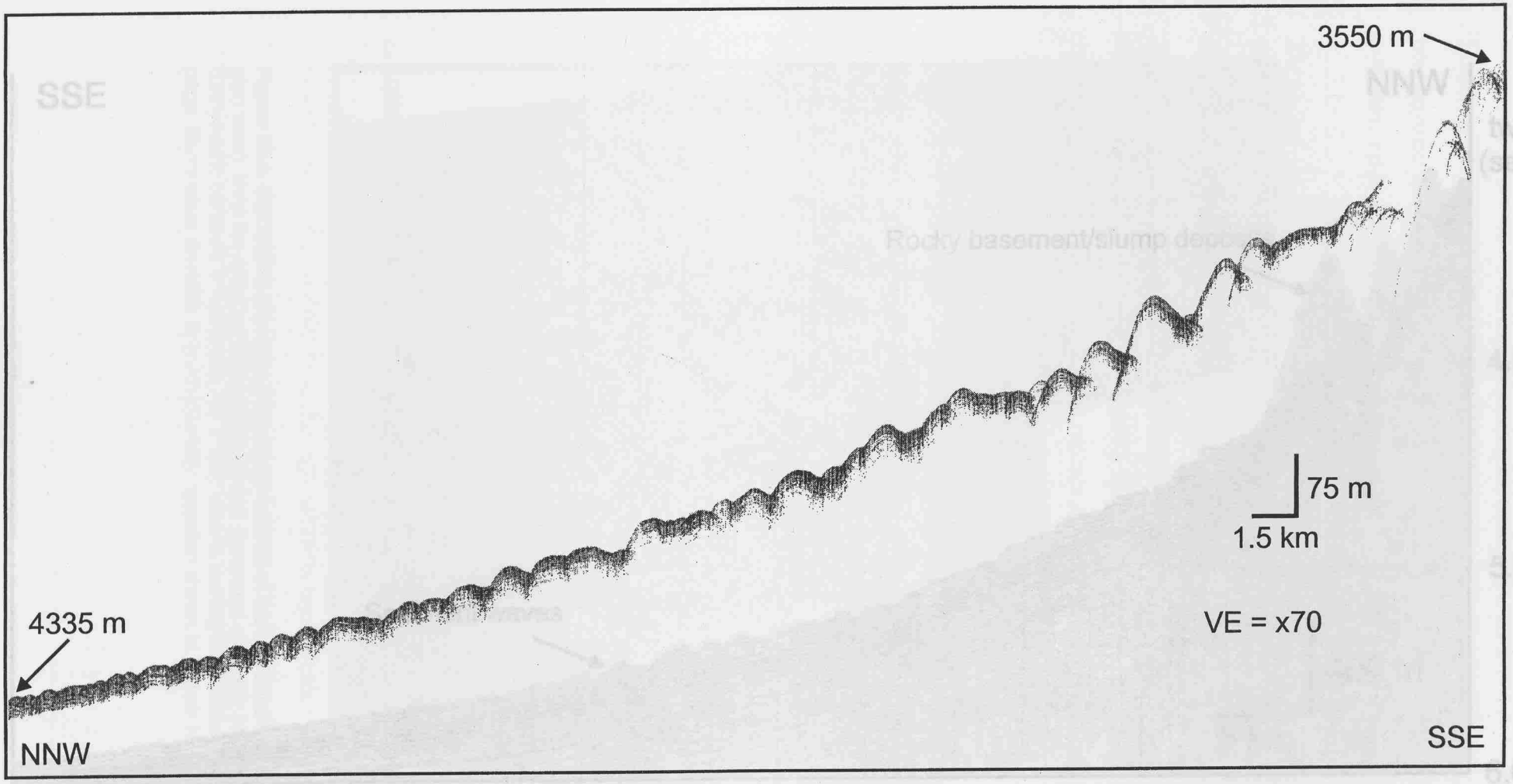

Figure 10.2: 3.5kHz profile through the La Palma wave field. Note the downslope decrease in wavelength and amplitude, and the gradual increase in penetration depth. Waves show clear evidence of upslope migration, and in some cases, show evidence of incerased sedimentation on the upslope face. Location of profile shown in Figure 10.1.

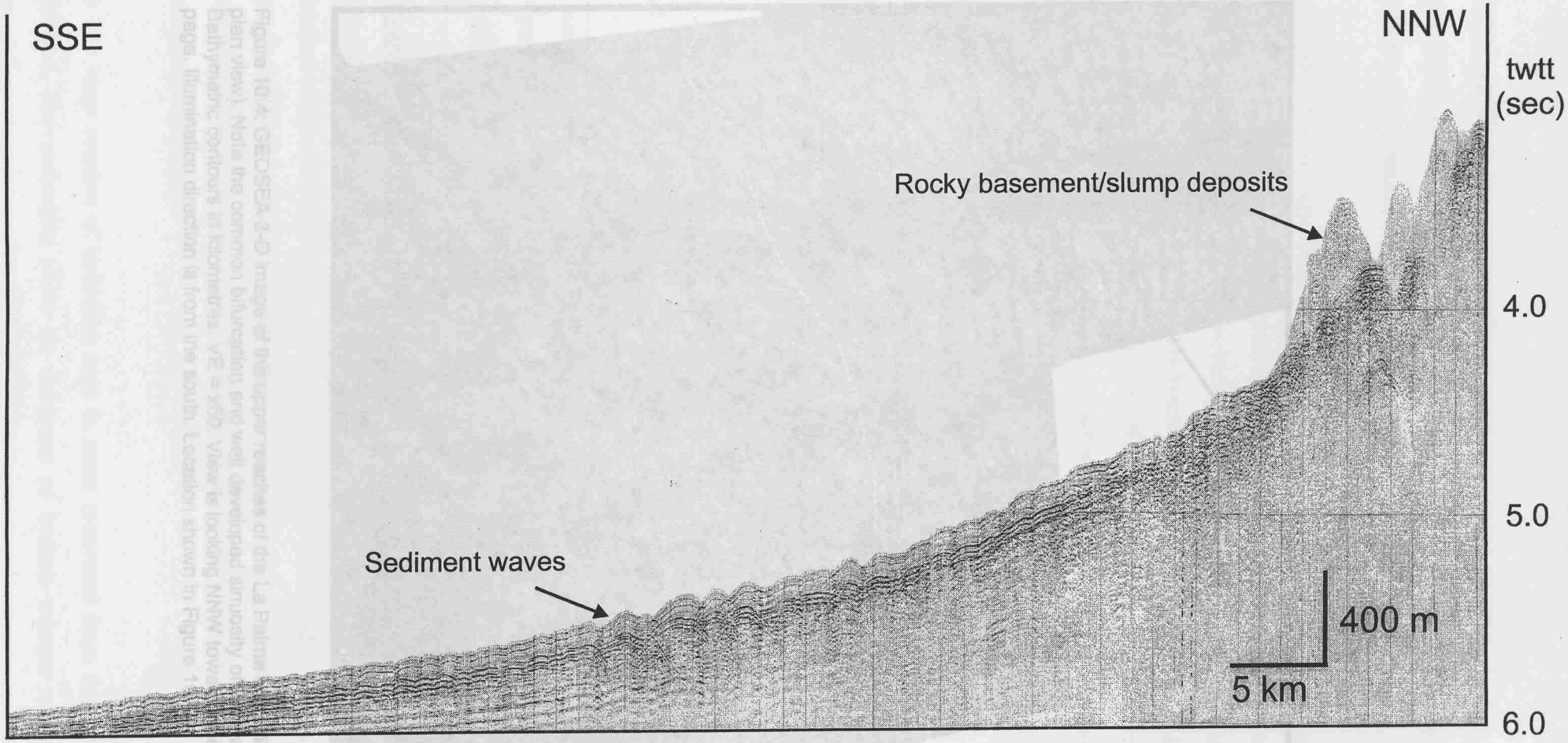

Figure 10.3: Single-channel seismic profile through the La Palma wave field. Location of profile is shown in Figure 10.1.

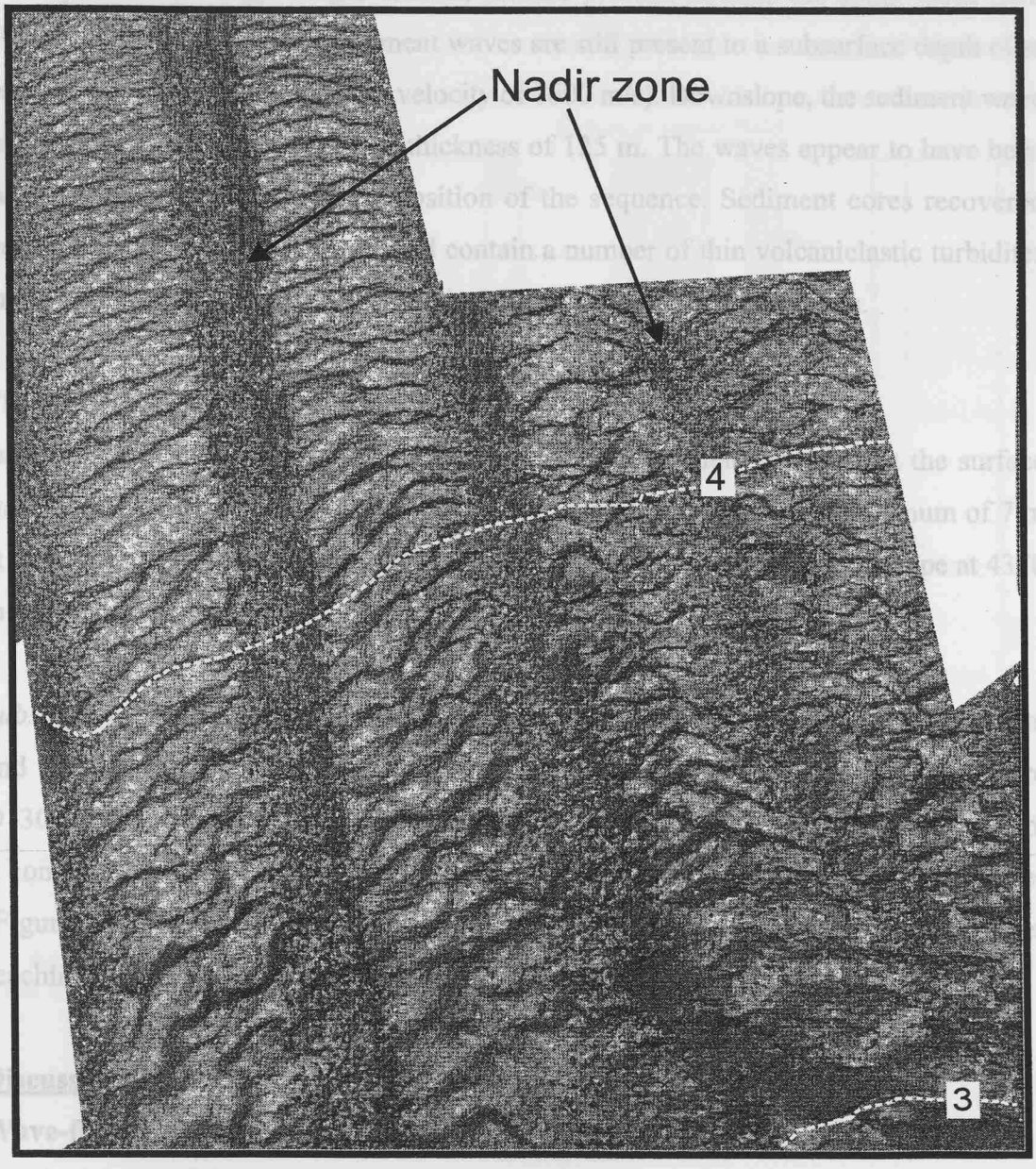

Figure 10.4: GEOSEA 3-D image of the upper reaches of the La Palma wave field (oblique plan view). Note the common bifurcation and well developed sinuosity of the wave crests. Bathymetric contours in kilometres. VE = x50. View is looking NNW towards the top of the page. Illumination direction is from the south. Location shown in Figure 10.1.

are laterally continuous for up to 40 km (Figure 10.4). The crestline morphology is complex, with common bifurcation and well-developed sinuosity.

Subsurface morphology: Single-channel seismic profiles through the upper wave field (Figure 10.3) reveal that the sediment waves are still present to a subsurface depth of at least 470 m (assuming a sediment velocity of 1600 m/s). Downslope, the sediment wave sequence gradually decreases to a thickness of 125 m. The waves appear to have been migrating upslope throughout deposition of the sequence. Sediment cores recovered from the upper 2 m of the wave field contain a number of thin volcaniclastic turbidites (up to 20 cm thick) interbedded with bioturbated pelagic marls and oozes.

The Selvage sediment-wave field

Surface morphology: A 3.5 kHz-profile across the wave field reveals that the surface waves have a wavelength of 0.4 - 1.1 km. The wave height reaches a maximum of 7 m at 4300 m water depth, and gradually decreases as the waves die out downslope at 4370 m.

Subsurface morphology: The wave morphology is present to a depth of at least 30 m, and the waves have migrated upslope throughout deposition of the sequence. Core D13071 is 12 m long and was collected from the wave field at a water depth of 4311 m. It contains a series of 12 turbidites interbedded with bioturbated pelagic marls and oozes (Figure 10.5). Some of the turbidites have thin sandy bases, with sand-bed thicknesses reaching 50 cm. Overall, the core contains 5% sand.

Discussion

Wave-forming processes

Detailed study of the La Palma and Selvage sediment wave fields (Wynn et al., 2000b) revealed that the sediment waves have been formed and maintained by unconfined turbidity currents originating on the flanks of the Canary Islands. Evidence for this interpretation includes:

1) The large number of turbidites seen in cores recovered from the wave fields. In addition, the sediments show no evidence of bottom current sedimentation or reworking.

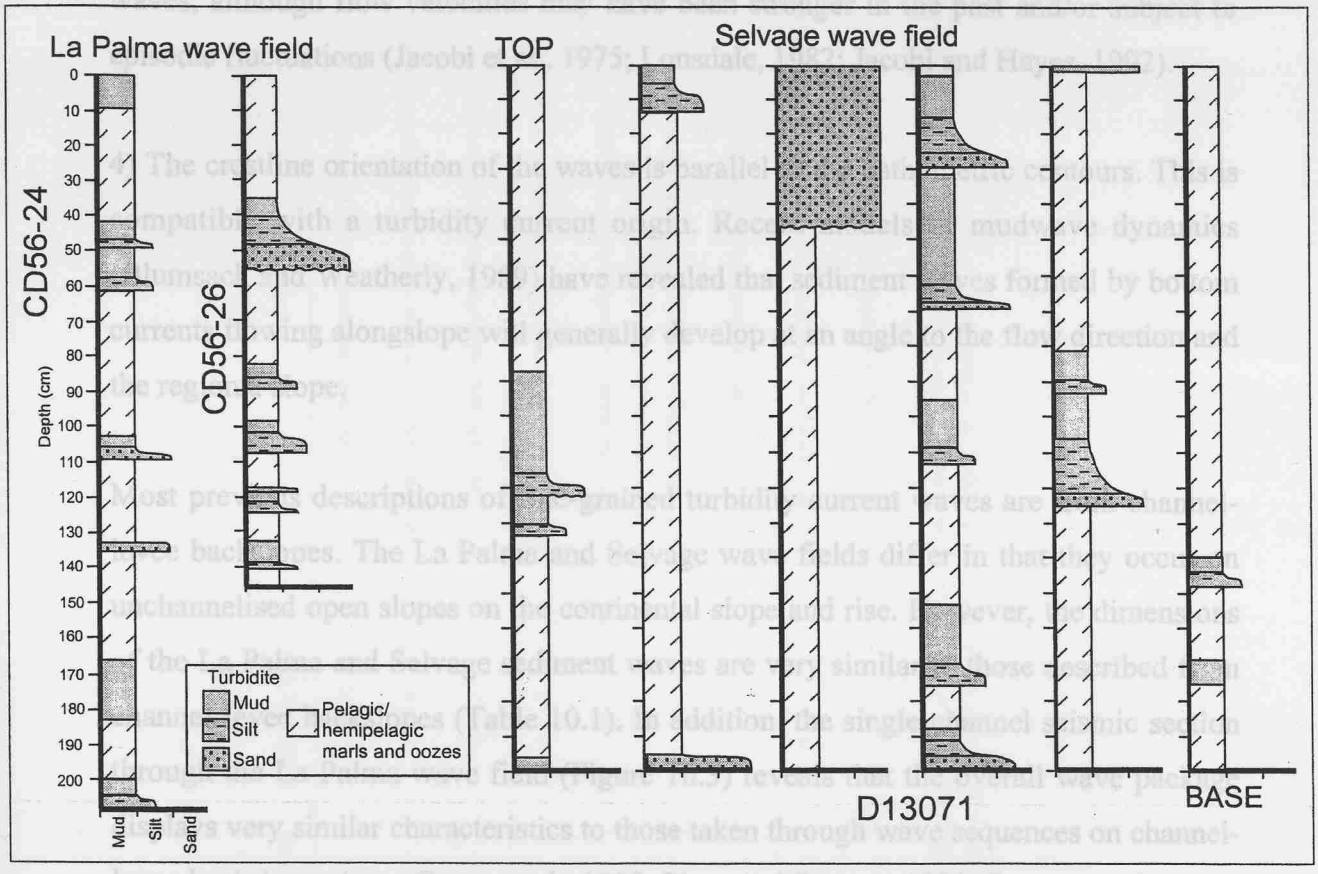

Figure 10.5: Sediment core descriptions from the La Palma and Selvage wave fields. Note the maximum sand-bed thickness of 50 cm. Core locations are shown on Figure 10.1.

2) The regular downslope decrease in wave dimensions is typical of sediment waves formed by unconfined turbidity currents, e.g., Monterey Fan levee backslope (Normark et al., 1980). Bottom current waves typically display more irregular dimensions.

3) The bottom current flow in this area is not strong enough at present to maintain the waves, although flow velocities may have been stronger in the past and/or subject to episodic fluctuations (Jacobi et al., 1975; Lonsdale, 1982; Jacobi and Hayes, 1992).

4) The crestline orientation of the waves is parallel to the bathymetric contours. This is compatible with a turbidity current origin. Recent models of mudwave dynamics (Blumsack and Weatherly, 1989) have revealed that sediment waves formed by bottom currents flowing alongslope will generally develop at an angle to the flow direction and the regional slope.

Most previous descriptions of fine-grained turbidity current waves are from channel-levee backslopes. The La Palma and Selvage wave fields differ in that they occur on unchannelised open slopes on the continental slope and rise. However, the dimensions of the La Palma and Selvage sediment waves are very similar to those described from channel-levee backslopes (Table 10.1). In addition, the single-channel seismic section through the La Palma wave field (Figure 10.3) reveals that the overall wave package displays very similar characteristics to those taken through wave sequences on channel-levee backslopes (e.g., Carter et al., 1990; Piper and Savoye, 1993; Savoye et al., 1993; Nakajima et al., 1998).

These results, therefore, strongly suggest that the sediment waves on the flanks of the Canary Islands were formed by unconfined turbidity currents, and have very similar characteristics to those described from channel-levee backslopes around the world.

Recognition of sediment waves in the subsurface

Turbidity current sediment waves can be recognised in the subsurface at a variety of scales:

On 3.5 kHz-profiles, surficial sediment waves can typically be resolved to subsurface depths of 20-60 m. Migration direction and angle are clearly visible, as well as

Wave field setting	Max WH (m)	Max WL (km)	Slope angle (°)	Comments	Reference
Selvage wave field: lower continental rise	5	1.1	0.13-0.22	WL + WH decrease downslope, crests parallel to slope	this study
La Palma wave field: continental slope/rise	70	2.4	0.4-1.8	WL + WH decrease downslope, crests sinuous and parallel to slope	Wynn *et al.*, 2000b
Bounty Channel: levee backslope	17	6	0.3-0.7	WL + WH decrease downslope, crests parallel to slope	Carter *et al.*, 1990
Toyama Channel: levee backslope	70	3	0.4-1.4	WL + WH decrease downslope, crests sinuous and parallel to slope	Nakajima *et al.*, 1998
Hikurangi Channel: levee backslope	15	3	?	WL + WH decrease downslope, crests subparallel to slope	Lewis *et al.*, 1998
Monterey Fan: levee backslope	37	2.1	0.8	WL + WH decrease downslope, sinuous crests subparallel to slope	Normark *et al.*, 1980
Hueneme Fan: levee backslope	10	0.6	0.8	WL + WH decrease downslope	Piper *et al.*, 1999
Var Fan: levee backslope	50	7	0.5-1.7	WL+ WH increase downslope (slope steepens), crests oblique to slope	Piper and Savoye, 1993
Barra Fan: distal fan slope	5	1.75	?	Crests possibly oblique to slope	Howe, 1996

Table 10.1: Examples of sediment-wave fields formed beneath unconfined turbidity currents. Note that all of the wave fields occur on slopes of 0.1°-1.7°, wave dimensions generally decrease downslope, and wave crests are aligned parallel/subparallel to the slope. WH = wave height, WL = wavelength.

individual wave dimensions. The seismic character is typically one of low to moderate amplitude, more or less continuous, subparallel wavy reflectors. The higher amplitude reflectors most likely correlate with more sandy sections. They can be distinguished from compressional features such as creep folds (e.g., Hill et al., 1982; Mulder and Cochonat, 1996) by the fact that they migrate upslope, and because they show a regular downslope decrease in wave dimensions. Compressional features show no evidence of migration and the varying dimensions are clearly not related to changes in slope angle.

On single-channel seismic profiles, relatively thick and laterally extensive successions of sediment waves can be resolved within the upper few hundred metres of section. The seismic character is one of regular wavy reflectors of moderate amplitude. Individual reflectors appear discontinuous although the whole seismic facies is more continuous. Apparent migration direction can be resolved in some cases, but wave dimensions are not readily determined.

On lower resolution seismic profiles it is generally not possible to recognise subsurface sediment waves on the basis of their morphology. It is therefore likely that sediment wave sequences in turbidite environments, such as occur on channel-levee backslopes and on unconfined slope aprons, are frequently overlooked during hydrocarbon exploration. This has important implications for the reservoir production of thin sands in interpreted levee sequences, as a stacked sequence of migrating waves on a channel levee is likely to impart a marked vertical and lateral heterogeneity to any potential reservoir.

Subsurface applications

As this study has shown, the La Palma and Selvage wave fields have similar characteristics to wave fields described from channel-levee backslopes. Therefore, a series of measurements taken from these wave fields may help to increase our understanding of subsurface levee sequences where sediment waves are present. Nevertheless, how do we determine the presence or absence of sediment waves if they are not resolvable on standard seismics? One possible method involves the use of dipmeter readings. Theoretically, a dipmeter log taken through a wave sequence on a levee backslope should show fluctuating values, because a core taken through such a sequence will penetrate a series of wave crests, upslope faces, wave troughs, and

downslope faces (Figure 10.6). Analyses of measured dip readings from the La Palma wave field, based on high-resolution seismic profiles, have shown that in the upper wave field the overall slope is 1.2°. The upslope faces of the waves dip upslope at an average of 1.5°, while the downslope faces dip downslope at an average of 3.2°. There is, therefore, an average difference of almost 5° in the angle between the upslope and downslope faces. In the lower wave field this value decreases to 1.6°. These results suggest that a dipmeter log taken through a series of stacked migrating waves will display dip readings that show regular fluctuations in the region of 1°-5°. In addition, subsurface sequences that preserve the original palaeoslope (typically 1°-2° on channel levees), may show regular reversals in the dip azimuth. Unfortunately existing cores from known sediment wave fields are not long enough to test this hypothesis.

There are, however, many examples from the deep subsurface where regular fluctuations of dipmeter angle have been noted, but no generally accepted interpretation of these patterns exists. One striking example is from the Upper Jurassic fine-grained turbidite successions seen in several wells in the Brae Field area of the North Sea. According to Stow et al. (1982), these were deposited in an open slope setting distal to the gravels and sands of a coarse-grained slope apron system. They interpret the fluctuating dip motif in these wells in terms of prograding mud lobes, but we suggest here that an alternative model is one of a relatively thick sequence of turbidity current waves deposited by unconfined flows on an open slope.

If sediment waves are recognised within a subsurface sequence, it becomes necessary to understand their reservoir characterisation properties. Although the sand/mud ratios in fine-grained sediment wave fields is generally low, the sands may have high poroperm values and be economically viable (A.H. Bouma, personal commun., 1998). In a stacked sequence of migrating sediment waves these sandy units will be unevenly distributed. There will theoretically be a marked vertical and lateral heterogeneity in sand-bed thickness and grain size that hinders fluid flow through the reservoir (Figure 10.6). Generally, the upslope faces of the waves comprise thicker beds than the downslope faces, and in some cases beds may actually pinch out on the downslope face. Therefore, the thin sandy units within a sediment wave sequence will vary in thickness laterally, and may pinch out downslope. In addition, the grain size may also vary

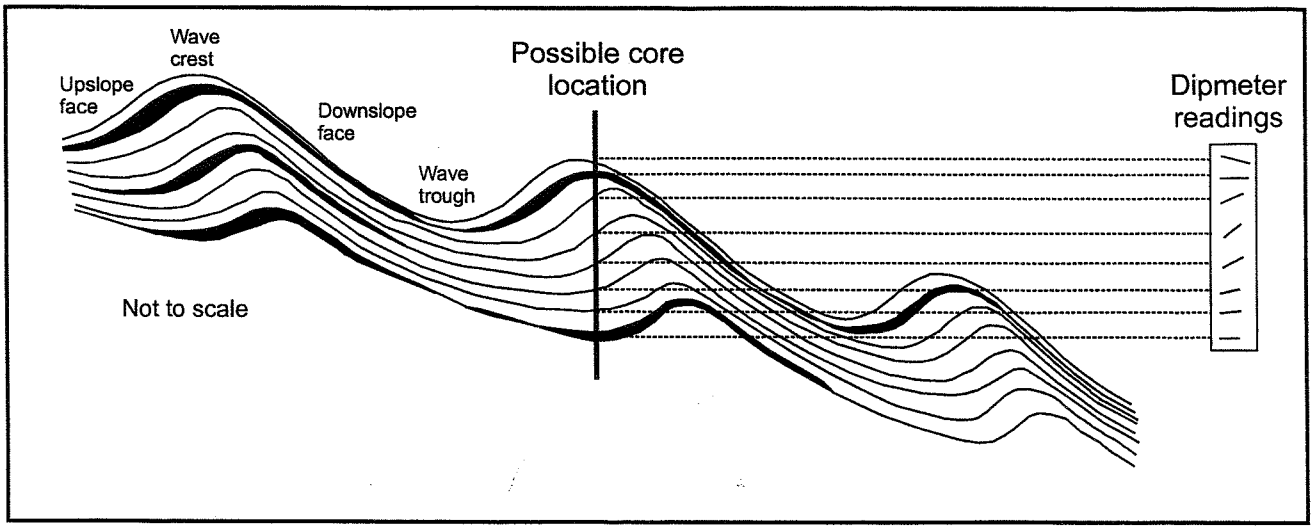

Figure 10.6: Schematic diagram illustrating a hypothetical sequence of migrating sediment waves in the subsurface. A potential series of dipmeter readings is given for a vertical core taken through the waves. Note the fluctuations in dip readings downcore, and also the possible lateral discontinuity and variation of any sandy units within the sequence.

laterally. An individual bed that is laterally continuous across a wave crest may consist of silt-sized sediment on the upslope face, and grades into sand-sized sediment on the downslope face. This heterogeneity will be most marked in the proximal areas of the wave field, where the largest variations in bed thickness and grain size occur.

Conclusions

This study describes two extensive sediment wave fields formed beneath unconfined turbidity currents derived from the flanks of the volcanic Canary Islands. The morphology and distribution of the waves is similar to that described from a number of wave fields on channel-levee backslopes. This allows us to infer that the turbidity current processes acting upon the continental slope and rise north of the Canary Islands are very similar to those occurring in channel-levee backslope environments.

In the subsurface, turbidity current sediment waves can be recognised at a variety of scales. On 3.5kHz- and single-channel seismic profiles, they can be recognised and distinguished from gravitational creep features on the basis of their morphology and upslope migration. On lower resolution seismic profiles individual sediment waves are not generally resolvable in cored sequences, however, they may be detected using detailed dipmeter analysis. Where they do occur, subsurface sequences of migrating sediment waves are likely to impart a marked vertical and lateral heterogeneity to any potential hydrocarbon reservoir. This will lead to complexities at the reservoir production stage.

Acknowledgements

The authors gratefully acknowledge the contribution of the masters and crew of the RRS Charles Darwin and RRS Discovery. Andy Pulham is thanked for helpful comments on various elements of this study. The manuscript benefitted greatly from the reviews of Arnold Bouma, John Bratton and John Southard. RBW acknowledges the PhD research grant supplied jointly by the University of Southampton and the Southampton Oceanography Centre Challenger Division.

10.3: Summary

This final chapter has revealed that sediment waves formed beneath unconfined turbidity currents are probably frequently overlooked during hydrocarbon exploration in turbidite systems. However, they may be recognised on dipmeter records and, when present, form highly heterogeneous sequences.

Overall, the final three chapters of this thesis have shown that sediment waves are abundant in turbidite-dominated environments, and are found on open slopes of the continental rise as well as on levee backslopes and within channels.

CHAPTER 11

DISCUSSION

11.1: Slope apron vs submarine fan vs turbidity current pathway

In Chapter 5, the passive Northwest African margin was classified as a fine-grained clastic slope apron, according to the model of Stow (1985). This is in agreement with Reading and Richards (1994), who described the Northwest African margin as a 'mud-rich slope apron'. Stow's (1985) model describes slope aprons as ranging from mainly constructional, with a smooth convex-concave profile and slope progradation, to mainly erosional, with an irregular surface and abundant mass movements. Facies distribution is highly irregular, with fine-grained sediments dominating and coarse-grained sediments confined to channels, base-of-slope lobes and the shelf break. Slope aprons are also characterised by low sediment supply, often with sediment starvation on the shelf, and an absence of major channels (Stow et al., 1984; Nelson et al., 1991; Reading and Richards, 1994). Overall, large sections of the Northwest African margin fit this slope apron model: fine-grained pelagic and hemipelagic sedimentation is dominant across much of the margin, bottom currents smooth and mould the seafloor sediments, and large-scale mass movements and turbidity currents are infrequent but important events on the margin. However, the margin deviates slightly from the Stow (1985) model where it is affected by topographic complexities such as the volcanic Canary Islands. These topographic features act as diversions for bottom currents, and as nuclei for downslope flows (Figure 5.6, p.80).

The results presented in Chapter 5 suggest that most of the arid Western Saharan margin, and the Moroccan margin north to the Agadir Canyon, should be termed the Northwest African slope apron (Figure 5.1, Foldout 2). To the south, the Mauritania and Senegalese margins appear to be cut by numerous canyons and channels (Jacobi and Hayes, 1982; 1992) and therefore cannot be classified as a slope apron. To the north, the limit of the slope apron is marked by the Agadir Canyon, as further north canyons and channels cut across the slope with increasing frequency in response to the higher terrigenous input on the less arid margin of northern Morocco.

The Agadir Canyon feeds into the Moroccan Turbidite System (MTS), and this system was investigated in detail in Chapter 6. The MTS has previously been termed a turbidity current pathway (e.g. Masson, 1994) but the term turbidite system is now preferred as certain elements, e.g. the intraslope Agadir Basin, are sites of sediment transport and deposition. A more important issue is whether the MTS can be classified as a complex form of elongate fan? Submarine fans are described by Stow (1985) as constructional features at the base-of-slope, that develop as isolated bodies seaward of a major sediment source (e.g. river) or main supply route (e.g. canyon). More specifically, elongate fans are longitudinally extended perpendicular to the margin, have a broad head region, two or more main feeder channels, a complex distributary channel system, and large terminal lobes constructed at the ends of channels in the lower fan region (Reading and Richards, 1994). Elongate fans develop in response to a high to medium sediment input, and contain a high proportion of mud to sand (Stow et al., 1984; Stow, 1985). The Moroccan Turbidite System therefore appears to be a morphologically complex form of elongate fan. It is longitudinally extended perpendicular to the margin (Figure 6.1, p.93), has a broad head region at the top of the Agadir Canyon, a single main feeder canyon, a complex distributary channel system, and large terminal lobes constructed at the ends of channels on the Madeira Abyssal Plain (MAP) (Figure 5.5, p.78). It is dominated by thick muddy turbidites, with sand deposition largely restricted to the Agadir Basin and terminal lobes on the MAP. However, the MTS does show some differences to the standard elongate fan model. The sediment input on the margin is relatively low, being dominated by low frequency, large-volume turbidity currents. In addition, the complex morphology of the MTS is responsible for additional features not accounted for by standard fan models, such as the intraslope Agadir Basin. This basin lies in the 'mid-fan' area, and has a turbidite-fill derived from multiple source areas that can be correlated with the Seine and Madeira Abyssal Plain sequences.

At 1500 km long, the MTS is potentially one of the world's largest submarine fans, being similar in scale to the giant mud-rich Bengal and Indus Fans (Emmel and Curray, 1985; Kolla and Coumes, 1985). Its great size is unusual, as it lies offshore of a semi-arid region with restricted sediment supply. Only about one turbidite every 10,000 years reaches the Agadir Basin, and only one every 30,000 years reaches the MAP. This is in contrast to the Bengal and Indus Fans, which are offshore of major river deltas and are fed by frequent turbidity currents (e.g. Stow et al., 1984; Reading and Richards, 1994).

It is possible that the complex morphology of the slope and rise offshore of Morocco has contributed to the great length of the MTS by funnelling sediments across the flat Agadir Basin. However, even if the Agadir Basin is removed from the total length, the MTS is still some 1200 km long. It is more likely that the huge volume of some of the flows (up to 260 km^3) is the reason for the great length of the MTS. Such large flows require a huge runout distance before they lose enough energy to deposit all of their sediment load. In addition, the results presented in Chapter 6 show that these large-volume flows contain a significant sandy component and can therefore erode a significant amount of material on their passage downslope. This material 'feeds' the turbidity current, allowing it to travel a greater distance than a sand-poor, non-erosive flow. The large volume of the flows is a result of the stable nature of this mature passive margin. Sediments are able to build up on the outer shelf for a long period of time without disturbance from frequent seismic activity. When an earthquake does occur it leads to massive failure of a large volume of sediment (Stow et al., 1984).

11.2: Sediment flux on the Northwest African margin

One of the key questions that has arisen during this study is: what is the driving mechanism for large-volume turbidity currents on a low input margin? As discussed above, the infrequency of trigger events leads to a build up of sediment on the shelf, but where does this sediment come from? The basin-fill sequences of the Moroccan Turbidite System contain a number of thick turbidites derived from the Morocco Shelf. However, the Moroccan margin is semi-arid, and there are few major rivers supplying sediment to the shelf. It therefore seems likely that the sediment within these turbidites is derived from a number of sources, and not just a single fluvial source. The two largest Morocco Shelf turbidites (*AB6/Md* and *AB13/Mf*) were shown in Chapter 6 to have been deposited during a period of rising sea level. The large volume of these turbidites may be explained by multiple sources, and three possible sediment sources have been recognised:

- A large proportion of the muddy sediment on the shelf is derived from the hinterland of the High Atlas Mountains (Summerhayes et al., 1976). At the present day, during an interglacial period, the High Atlas Mountains are high enough to be topped with snow and ice. During a glacial period it is probable that these mountains

would have had a more extensive snow and ice cover, although evidence for this in the literature is lacking. Following glacial periods, these mountains probably supplied large amounts of fine-grained sediment to the shelf as meltwater discharge. Summerhayes et al., (1976) noted that muddy sediments were common on the inner shelf offshore of the Sous River, which drains the High Atlas hinterland and lies immediately landward of the Agadir Canyon.

- A large proportion of the glauconite, pyrite, clastic lithic fragments and biogenic material in the sand and silt fractions of the turbidites is derived from outcropping strata on the Morocco Shelf. During sea level lowstands and the ensuing transgressions, these strata will be more exposed to erosional processes, leading to a build-up of loose sediment on the shelf (Summerhayes et al., 1976).

- TOBI sidescan sonar observations of the Agadir Canyon mouth (Chapter 7) have revealed large-scale erosional scours (Figure 7.2, p.132). These scours were cut by large-volume, high-energy turbidity currents, and the large amount of sediment removed has obviously contributed to the overall turbidite volume. Unfortunately, the complexity of the Agadir channel-lobe transition zone means that it is impossible to estimate the volume of sediment removed by scouring.

The total volumes of turbidites *AB6/Md* and *AB13/Mf* are 125 km^3 and 260 km^3 respectively. However, it is impossible to calculate how much of this material has been derived from each of the three sources listed above. The Moroccan margin is therefore an important example of an area where sediment flux from individual sources is difficult to calculate, due to a complex pattern of sediment derivation. Overall, the driving mechanism for turbidity currents derived from the Morocco Shelf appears to be relatively high sediment accumulation rates following glacial lowstands. The final trigger mechanism is possibly an earthquake, which would explain why individual turbidites appear to have come from two different areas, as an earthquake could trigger multiple failures at the same time (Normark and Piper, 1991).

In contrast, the driving mechanism for large-volume turbidity currents derived from the volcanic Canary Islands appears to be large-scale failure of the island flanks. Turbidites

AB2/Mb and *AB15/Mg* are both related to debris avalanches, although the initial trigger for these events is uncertain.

11.3: Long-distance turbidite correlation

Another key finding of this study is that extensive coring is necessary for long-distance turbidite correlation within basins with multiple source areas. In Chapter 6 the complex turbidite basin-fill of the intraslope Agadir Basin was found to have been sourced from the Morocco Shelf, the volcanic Canary Islands, the Western Sahara slope, and the Casablanca Seamount. The depositional architecture of individual turbidites is revealed by a sequence of widely spaced cores, with core sites located in the eastern, central and western basin, and also on the southern basin flanks (Figure 6.2, p.96). This has important implications for exploration of other deep-water turbidite systems with complex seafloor topography. For example, a single core taken from a complex basin-fill, such as that in the Agadir Basin, could easily lead to a very different interpretation of sand body architecture to that presented in Chapter 6 (Figure 6.10, p.117).

Another advantage of having extensive core control is that it allows individual turbidites to be correlated with confidence between interconnected depositional basins. Therefore, the Agadir Basin turbidites can be correlated with the heavily cored sequences on the Madeira and Seine Abyssal Plains (Figure 6.5, p.104). This is important, as it has revealed that individual turbidites on the Northwest African margin have travelled up to 1500 km, and have total volumes of up to 260 km^3, making the Moroccan Turbidite System one of the largest in the world. In addition, good core control between the Agadir Basin and the Madeira Abyssal Plain has revealed that turbidity currents flowing through the Madeira Distributary Channel System have undergone flow separation. The sandy basal layer is confined within the channels system and interacts with the channel floor sediments, whereas the fine-grained suspended load is unconfined as it crosses over the lower rise and does not interact with the seafloor. These results all indicate that good core control is required to fully understand turbidity current processes and deposits in depositional basins bounded by complex seafloor topography.

11.4: Bottom current vs turbidity current sediment waves

It is interesting to note that in the 1960's and 1970's approximately two-thirds of published studies relating to deep-water sediment waves were focussed on bottom current sediment waves. However, in the 1980's and 1990's there was a major upsurge in the number of published studies relating to turbidity current sediment waves. This change has come about for two reasons: firstly, there has been an upsurge in studies of turbidite systems, in response to the increase in deep-water hydrocarbon exploration of these systems. In addition, there has also been an increasing realisation that sediment waves are a common feature of most turbidite systems, and that not all sediment waves on the slope and rise are necessarily formed by bottom currents. This is partly a result of better quality data being collected, which enables more detailed analysis of the wave-forming processes.

The results presented in Chapters 8-10 of this thesis highlight the need for a high-quality integrated dataset in studies of sediment waves where both turbidity currents and bottom currents are thought to occur. Core data are essential to determine whether turbidites or contourites can be recognised, and multibeam bathymetry or sidescan sonar can give an indication of wave crestline orientation with respect to current flow. Generally, sediment waves have their crestlines aligned roughly perpendicular to the flow. This is true for nearly all turbidity current sediment waves (e.g. Figure 8.2, p.169) and also for bottom current sediment waves on flat seafloors (e.g. Argentine Basin, Flood and Shor, 1988). However, the results of modelling work by Blumsack and Weatherly (1989) and Blumsack (1993), derived from the lee-wave model of Flood (1988), show that due to the Coriolis effect, bottom current sediment waves *developed on slopes* grow at an oblique angle to the current flow. Therefore sediment waves in the northern hemisphere will develop at an angle clockwise to the prevailing bottom current direction, and will migrate upcurrent and to the right of the flow. The opposite will occur in the southern hemisphere. This relationship has been found to be correct in the few studies where it has been tested (e.g. Blumsack and Weatherly, 1989; Cunningham and Barker, 1996). Analysis of crestline orientation can therefore be a useful indicator when assessing whether a sediment-wave field is in the correct alignment for a bottom current or turbidity current origin.

It is generally accepted that bottom current sediment waves are able to form beneath lee waves in the flow, as proposed by Flood (1988). In Chapter 9 it was also demonstrated that the antidune model of Normark et al. (1980) is most applicable to the formation of fine-grained sediment waves beneath turbidity currents. However, it seems unlikely that the antidune model, which relies on sediment preferentially falling out of suspension on the upcurrent face of the wave, is applicable to coarse-grained sediment waves. In Chapter 7 it was shown that coarse-grained sediment waves are a common feature of the channel-lobe transition zone, and are probably formed by tractional processes (e.g. Lowe, 1982; Normark and Piper, 1991). In Chapter 8, TOBI images of coarse-grained sediment waves in the El Julan wave field appear to show evidence for downcurrent migration, similar to most modern sand dunes. Therefore it appears that the process of sediment wave formation and migration is largely dependent on grain size, with fine-grained sediment waves forming as antidunes by suspension fall-out, and coarse-grained sediment waves forming as dunes by bedload traction.

11.5: Applications to hydrocarbon exploration

Several of the studies presented in this thesis have revealed new information and interpretations that are directly applicable to hydrocarbon exploration of deep-water systems. In Chapters 4 and 5, the maps illustrating sediment distribution across large sections of the margin demonstrate how climate, and more specifically the degree of glacial influence, is a key control on sand body distribution:

High-latitude glaciated margins are dominated by stacked, mud-rich, glacigenic debris flows and submarine landslides (e.g. Bugge et al., 1988; Vorren et al., 1998). Sands are not sorted by depositional processes into distinct sand bodies, but are instead dispersed throughout mass movement deposits as muddy or silty sands. On some sections of the continental slope and rise contourite sheet sands are developed, but these are usually relatively thin. Further offshore, the large ocean basin drifts are composed almost entirely of muddy pelagic sediments (Faugeres at al., 1993). Mid-latitude glacially influenced margins are dominated by submarine canyons that supply large quantities of sand to small radial fans situated at the base of slope (e.g. the Celtic Fan, Droz et al., 1999). The continental slope and rise are narrow in this region, allowing rapid transport of sediment to the abyssal plains. The canyons cutting the slope and rise are most active

during lowstands of sea level, and particularly during ice retreat, as more coarse material was transported to the canyon heads at these times. During highstands, the canyons often become partially infilled with fine-grained pelagic/hemipelagic sediments. Low-latitude, non-glaciated margins with low fluvial input are dominated by infrequent, large-scale mass movements. These consist of fine-grained sediments, which accumulate on the upper slope beneath upwelling cells. Sands are transported long distances along linear turbidity current pathways, and are deposited in terminal lobes on abyssal plains far from the shelf-break.

Understanding how sand body distribution is affected by large-scale spatial variations in climate enables us to rapidly classify large sections of the margin according to the climatic regime at any given time. This will vary over time, for example, the glaciated Northwest UK margin is dominated by bottom current processes at the present day, but was largely shaped by glacial processes during the last Ice Age. However, it is also important to understand that tectonic effects also influence this pattern. The Northwest UK margin has been dominated by glacial-interglacial fluctuations during the Pleistocene-Recent, but prior to this the margin was dominated by tectonic forces such as rifting and subsidence (e.g. Roberts, 1975), leading to development of discrete sand bodies that form potential hydrocarbon reservoirs.

In Chapters 5 to 7 the controls on sand body distribution and dimensions within the intraslope Agadir Basin were analysed in detail. Generally, turbidity current volume appears to be the dominant factor in controlling sand body development. Large-volume flows (>100 km^3) excavate giant erosional scours in the Agadir channel-lobe transition zone (Figure 7.2, p.132), and deposit extensive sheet sands on the basin floor (Figure 6.10, p.117). However, most of the large flows have enough energy to continue transporting the bulk of their sediment load westwards to the eastern margin of the Madeira Abyssal Plain. The Agadir Basin therefore acts as a zone of sediment erosion, deposition and bypass for large-volume flows, but is mostly just a zone of deposition for smaller volume flows. The sediment bypassing by large flows is probably a result of the western basin becoming infilled, leading to an almost flat basin floor along its length. Large-volume turbidity currents reaching the western basin margin can now pass into the Madeira Distributary Channel System without encountering any positive topography, whereas in the past they would probably have been ponded on the basin

floor after being deflected by the western basin wall. At the present-day, the Agadir Basin therefore appears to be a dominantly bypassing system for large-volume flows, and may be a useful modern analogue for hydrocarbon exploration of other turbidite systems with complex seafloor topography and intraslope basin development. This includes intraslope basins in areas affected by salt and shale diapirism, such as the Gulf of Mexico and the Nigerian margin (Armentrout et al, 1991; Weimer and Link, 1991). However, it should be noted that the Agadir Basin is an order of magnitude larger than most of the intraslope basins present in the Gulf of Mexico and on the Nigerian margin. Despite this, the observed pattern of sediment erosion, deposition and bypass should still apply in other filled intraslope basins fed by turbidity currents of variable size.

In Chapters 7-10 it was demonstrated that sediment waves are a common feature of many turbidite systems, and are found on channel floors, levee backslopes, and areas of the continental slope and rise crossed by unconfined turbidity currents. In Chapter 10, the possibility of recognising sequences of buried migrating waves using dipmeter readings was discussed. If sediment waves can be recognised using dipmeter readings, or on seismic data, then an understanding of sediment wave orientation in turbidite systems may aid hydrocarbon recovery. Previous research has shown that, on a small scale, cross-bedding orientation can significantly effect directional permeability and residual oil saturation (e.g. Weber, 1982). On a larger scale it seems likely that the orientation of stacked sequences of sediment waves will also affect fluid flow through a potential reservoir sand body. Sediment wave orientation could possibly be detected by comparison of dipmeter data with observed outcrop analogues (e.g. Winn and Dott, 1979), as has been applied to fluvial and shoreface sand bodies based on dip readings of cross-bed foresets (Williams and Soek, 1993). However, if the palaeoslope is known, sediment wave orientation can also be deduced by analysis of modern analogues, as turbidity current sediment waves are generally aligned roughly perpendicular to turbidity current flow direction, and are therefore parallel to the slope. However, further investigations into how sand body orientation fits in with the overall sediment wave package are required. This may be achieved by intensive coring of modern sediment waves, or by recognition and study of outcrop analogues.

CHAPTER 12

CONCLUSIONS

- The Northwest African margin is a passive, arid, non-glaciated margin, and is largely dominated by low frequency, large-scale mass wasting processes. The broad slope and rise are characterised by gentle gradients, although numerous volcanic islands and seamounts give rise to localised areas of rugged relief. The Iberian-Biscay margin to the north is influenced by glacial processes and tectonic activity, leading to high rates of fluvial input. As a result, this margin is steep and narrow, and is frequently swept by turbidity currents that cut numerous canyons. The Northwest European margin, north of 56°N, is dominated by glacial/interglacial cyclicity, with mass wasting processes operating during glacial periods and bottom current processes dominating during interglacials.

- A large section of the Northwest African margin can be classified as a fine-grained clastic slope apron. The slope and rise are affected by a complex interplay of pelagic/hemipelagic sedimentation, alongslope bottom currents and downslope gravity flows. However, volcanic islands and seamounts complicate the picture by acting as nucleii for gravity flows, and as obstacles for bottom currents.

- The Moroccan Turbidite System marks the northern boundary of the Northwest African slope apron. It has a total length of 1500 km, making it one of the longest turbidite systems in the world. Detailed core analysis has revealed that individual turbidites within this system can be correlated between three interconnected deep-water basins.

- The intraslope Agadir Basin contains a complex turbidite-fill, with individual turbidites being sourced from the Morocco Shelf, the volcanic Canary Islands, the Western Sahara slope, and the Casablanca Seamount. Morocco Shelf turbidites dominate the basin-fill, and display a highly variable architecture due to fluctuations in flow volume. The largest turbidity currents have sufficient energy to largely

bypass the basin, leaving behind a thin sheet sand but little mud. Smaller flows tend to be completely ponded on the basin floor.

- A major channel-lobe transition zone is developed at the mouth of the Agadir Canyon, in response to large-volume flows undergoing a hydraulic jump at this point. This zone is dominated by intense scouring, leading to development of large scours and tractional bedforms. Comparison with other channel-lobe transition zones has revealed that their development is controlled by the break of slope angle, canyon/channel size and gradient, and turbidity current volume.

- Turbidity current sediment waves are widespread on the Northwest African margin. They occur on channel floors, in channel-lobe transition zones, and on the submarine slopes of volcanic islands. The largest are up to 70 m high, and have a wave length of up to 2.5 km. Fine-grained turbidity current sediment waves form as antidunes, beneath low-velocity, low-concentration unconfined flows. Coarse-grained waves probably form by bedload traction beneath high energy flows.

CHAPTER 13

FUTURE WORK

- An interesting project that is being worked on by Wynn and Weaver in 2000/2001 is a comparison of the Northeast and Northwest Atlantic continental margins. The results of all the seafloor mapping completed on the Northeast Atlantic margin are presented in Paper 1 (Chapter 4), and in particular on the new sedimentation map (Figure 4.1, Foldout 1). A similar map will be produced for the Northwest Atlantic margin, based on new GLORIA data and previously published studies. It will be interesting to see if the tripartite margin division of the Northeast Atlantic also occurs on the 'opposite side'. If not, what are the controlling factors on any differences? Is the climatic or tectonic regime different in certain regions?

- One aspect of continental margin sedimentation not adequately covered in this study is that of slope/rise sedimentation. On the Northwest African margin there is a large amount of information on turbidite volume and architecture in the deep-water basins, but relatively little knowledge of the thickness and volume of these deposits within interchannel areas on the slope and rise. An increased effort to core some of these marginal areas would give a better idea of the total volumes of turbidites on the margin, and possibly reveal more information on their source area/transport direction. In addition, experimental work on the scale and spreading rates of unconfined turbidity currents on the slope/rise would be useful.

- Further investigation of the channel-lobe transition zone is required in ancient turbidite systems. There is now a fairly good modern database, but these zones are rarely recognised in outcrop. How are they distinguished from channels? What do they look like in the subsurface? What are the implications for hydrocarbon exploration in proximal turbidite environments?

- Although, the mode of formation of turbidity current sediment waves has been analysed in this thesis, there is still scope for laboratory experiments to better understand whether or not sediment waves really can form under antidune

conditions. In addition, more good-quality examples of deep-water sediment waves are required from environments where both turbidity currents and bottom currents are active. In this way it may be possible to unravel the key characteristics of waves formed by each process. This will also apply to mass movement features, which are also frequently misinterpreted as sediment waves. In 2001 there will be a special issue of Marine Geology devoted to the recognition and interpretation of deep-water sediment waves (Guest Editors: Wynn and Stow) which may help to answer some of these questions.

REFERENCES

Allen, J.R.L. (1970) *Physical processes of sedimentation*, Unwin, London, 248pp.

Allen, J.R.L. (1984) *Sedimentary structures, their character and physical basis*, Elsevier, Amsterdam, 663pp.

Armentrout, J.M., Malecek, S.J., Braithwaite, P. and Beeman, C.R. (1991) Seismic facies of slope basin turbidite reservoirs, East Breaks 160-161 Field: Pliocene-Pleistocene, Northwestern Gulf of Mexico. In: *Seismic Facies and Sedimentary Processes of Submarine Fans and Turbidite Systems* (Eds. P. Weimer and M.H. Link), pp.223-239. Springer-Verlag, New York.

Armishaw, J.E., Holmes, R.W and Stow, D.A.V. (1998) Morphology and sedimentation on the Hebrides Slope and Barra Fan, NW UK continental margin. In: *Geological Processes on Continental Margins: Sedimentation, Mass-Wasting and Stability* (Eds. M.S. Stoker, D. Evans, and A. Cramp), Geol. Soc. London Spec. Publ., **129**, 81-104.

Baltzer, A., Holmes, R. and Evans, D. (1998) Debris flow on the Sula Sgeir Fan, NW of Scotland. In: *Geological Processes on Continental Margins: Sedimentation, Mass-Wasting and* Stability (Eds. by M.S. Stoker, D. Evans, and A. Cramp), Geol. Soc. London Spec. Publ., **129**, 105-115.

Belderson, R.H., Kenyon, N.H. and Wilson, J.B. (1973) Iceberg plough marks in the Northeast Atlantic. *Palaeogeog., Palaeoclimatol., Palaeoecol.*, **13**, 215-224.

Bellaiche, G., Droz, L., Aloisi, J.-C., Bouye, C., Got, H., Monaco, A., Maldonado, A., Serra-Raventos, J. and Mirabile, L. (1981) The Ebro and the Rhone deep-sea fans: first comparative study. *Mar. Geol.*, **43**, 75-85.

Best, A.I. and Gunn, D.E. (1999) Calibration of marine sediment core loggers for quantitative acoustic impedance studies. *Mar. Geol.*, **160**, 137-146.

Bhat, H., McMillan, N.J., Aubert, J., Porthault, B. and Surin, M. (1975) North American and African drift – the record in Mesozoic coastal plain rocks, Nova Scotia and Morocco. In: *Canadian Continental Margins and offshore Petroleum Potential* (Eds. C.J. Yorath et al.), Mem. Can. Soc. Petrol. Geol., **4**, 375-389.

Blumsack, S.L. (1993) A model for the growth of mudwaves in the presence of time-varying currents. *Deep-Sea Res. II*, **40**, 963-974.

Blumsack, S.L. and Weatherley, G.L. (1989) Observations of the nearby flow and a model for the growth of mudwaves. *Deep-Sea Res.*, **36/9**, 1327-1339.

Bondevik, S., Svendsen, J.L. and Mangerud, J. (1997) Tsunami sedimentary facies deposited by the Storegga tsunami in shallow marine basins and coastal lakes, western Norway. *Sedimentology*, **44**, 1115-1131.

Bouma, A.H. (1962) *Sedimentology of some flysch deposits*, Elsevier, Amsterdam, 168pp.

Bouma, A.H. (2000) Coarse-grained and fine-grained turbidite systems as end member models: applicability and dangers. *Mar. Petrol. Geol.*, **17**, 137-144.

Bourillet, J-F. and Loubrieu, B. (1995) Atlantique nord-est, bathy-morphologie de la marge des entrees de la Manche. Echelle 1:250 000. (Brest: IFREMER).

Bowen, A.J., Normark, W.R. and Piper, D.J.W. (1984) Modelling of turbidity currents on Navy submarine fan, California Continental Borderland. *Sedimentology*, **31**, 169-185.

British Oceanographic Data Centre (1995) *GEBCO Digital Atlas*, Southampton Oceanography Centre, UK.

Bugge, T., Befring, S., Belderson, R.H., Eidvin, T., Jansen, E., Kenyon, N.H., Holtedahl, H. and Sejrup, H.P. (1987) A giant three-stage submarine slide off Norway. *Geo-Mar. Lett.*, **7**, 191-198.

Bugge, T., Belderson, R.H. and Kenyon, N.H. (1988) The Storegga Slide. *Phil. Trans. Roy. Soc. London, A*, **325**, 357-388.

Carter, L., Carter, R.M., Nelson, C.S., Fulthorpe, C.S. and Neil, H.L. (1990) Evolution of Pliocene to Recent abyssal sediment waves on Bounty Channel levees, New Zealand. *Mar. Geol.*, **95**, 97-109.

Clark, J.D., Kenyon, N.H. and Pickering, K.T. (1992) Quantitative analysis of the geometry of submarine channels: Implications for the classification of submarine fans. *Geology*, **20**, 633-636.

Coumes, F., Delteil, J., Gairaud, H., Ravenne, C. and Cremer, M. (1982) Cap Ferret Deep Sea Fan (Bay of Biscay). *AAPG Bull.*, **42**, 583-591.

Cunningham, A.P. and Barker, P.F. (1996) Evidence for westward-flowing Weddell Sea Deep Water in the Falkland Trough, western South Atlantic. *Deep-Sea Res.*, **45**, 643-654.

Damuth, J.E. (1977) Late Quaternary sedimentation in the western equatorial Atlantic. *Geol. Soc. Am. Bull.*, **88**, 695-710.

Damuth, J.E. (1979) Migrating sediment waves created by turbidity currents in the northern South China Basin. *Geology*, **7**, 520-523.

Damuth, J.E. (1980) Use of high-frequency (3.5-12 kHz) echograms in the study of near-bottom sedimentation processes in the deep sea: a review. *Marine Geology,* **38**, 51-75

Damuth, J.E., Flood, R.D., Kowsmann, R.O., Belderson, R.H. and Gorini, M.A. (1988) Anatomy and growth pattern of Amazon deep-sea fan as revealed by long-range side-scan sonar (GLORIA) and high-resolution seismic studies. *AAPG Bull.*, **72**, 885-911.

Davies, T.L.I., van Niel, B., Kidd, R.B. and Weaver, P.P.E. (1997) Erosional characteristics and turbidity current links between the Seine and Madeira Abyssal Plain

turbidites calculated from reworked coccolith assemblages. *Geo-Marine Letters*, **17**, 147-153.

de Lange, G.J., Jarvis, I., and Kuijpers, A. (1987) Geochemical characteristics and provenance of late Quaternary sediments from the Madeira Abyssal Plain, North Atlantic. In: *Geology and Geochemistry of Abyssal Plains* (Eds. P.P.E. Weaver and J. Thomson), Spec. Pub. Geol. Soc. London, **31**, 147-165.

Dowdeswell, J.A. and Kenyon, N.H. (1997) Long-range side-scan sonar (GLORIA) imagery of the eastern continental margin of the glaciated polar North Atlantic. In: *Glaciated Continental Margins: An Atlas of Acoustic* Images (Eds. T.A. Davies, T. Bell, A.K. Cooper, H. Josenhans, L. Ployak, A. Solheim, M.S. Stoker, and J.A. Stravers), pp. 260-263. Chapman & Hall, London.

Dowdeswell, J.A. and Siegert, M.J. (1999) Ice-sheet numerical modeling and marine geophysical measurements of glacier-derived sedimentation on the Eurasian Arctic continental margins. *Geol. Soc. Am. Bull.*, **111**, 1080-1097.

Dowdeswell, J.A., Kenyon, N.H., Elverhoi, A., Laberg, J.S., Hollender, F.-J., Mienert, J. and Siegert, M.J. (1996) Large-scale sedimentation on the glacier-influenced Polar North Atlantic margins: Long-range side-scan sonar evidence. *Geophys. Res. Lett.*, **23**, 3535-3538.

Dowdeswell, J.A., Kenyon, N.H., Laberg, J.S. and Elverhoi, A. (1997) Submarine debris flows on glacier-influenced margins: GLORIA imagery of the Bear Island fan. In: *Glaciated Continental Margins: An Atlas of Acoustic Images* (Eds. T.A. Davies, T. Bell, A.K. Cooper, H. Josenhans, L. Ployak, A. Solheim, M.S. Stoker, and J.A. Stravers), pp.118-119. Chapman & Hall, London.

Droz, L., and Bellaiche, G. (1985) Rhone deep sea fan: morphostructure and growth pattern. *AAPG Bulletin*, **69**, 460-479.

Droz, L., Rigaut, F., Cochonat, P. and Tofani, R. (1996) Morphology and recent evolution of the Zaire turbidite system (Gulf of Guinea). *Geol. Soc. Am. Bull.*, **108**, 253-269.

Droz, L., Auffret, G.A., Savoye, B. and Bourillet, J-F. (1999) The Celtic Deep-sea fan: Stratigraphy and sedimentary evolution. *C.R Acad. Sci. Paris. Earth Planet. Sci.*, **328**, 173-180.

Dybedal, J. and Boe, R. (1994) Ultra-High resolution sub-bottom profiling for detection of thin layers and objects. *Oceans'94*, Osates, Brest, France.

Ellison, T.H. and Turner, J.S. (1959) Turbulent entrainment in stratified flows. *Journal of Fluid Mechanics*, **6**, 423-428.

Embley, R.W. (1976) New evidence for occurrence of debris flow deposits in the deep sea. *Geology,* **4**, 371-374.

Embley, R.W. (1982) Anatomy of some Atlantic margin sediment slides and some comments on ages and mechanisms. In: *Marine Slides and Other Mass Movements* (Eds. S. Saxov and J.K. Nieuwenhuis), pp.189-214. Plenum Press, New York.

Embley, R.W. and Jacobi, R.D. (1977) Distribution and morphology of large submarine sediment slides and slumps on Atlantic continental margins. *Marine Geotechnology,* **2**, 205-228

Embley, R.W. and Langseth, M.G. (1977) Sedimentation processes on the continental rise of northeastern South America. *Mar. Geol.*, **25**, 279-297.

Emery, K.O. and Uchupi, E. (1984) *The Geology of the Atlantic Ocean.* New York, Springer-Verlag, 1050pp.

Emmel, F.J. and Curray, J.R. (1985) Bengal Fan, Indian Ocean. In: *Submarine Fans and Related Turbidite Systems* (Eds. A.H. Bouma, W.R. Normark and N.E. Barnes), pp.107-112. Springer-Verlag, New York.

Ercilla, G., Alonso, B., Perez-Belzuz, F., Estrada, F., Baraza, G., Farran, M., Canals, M. and Masson, D. (1998) Origin, sedimentary processes and depositional evolution of the Agadir turbidite system (Central Eastern Atlantic). *J. Geol. Soc., London*, **155**, 929-939.

Evans, D., King, E.L., Kenyon, N.H., Brett, C. and Wallis, D. (1996) Evidence for long-term instability in the Storegga Slide region off Western Norway. *Mar. Geol.*, **130**, 281-292.

Ewing, M., Aitken, T. and Eittreim, S. (1968) Giant ripples in the Madagascar Basin. *Trans. Am. Geophys. Union*, **49**, 218-232.

Faugeres, J.C., Gonthier, E., Grousset, F. and Poutiers, J. (1981) The Feni Drift: The importance and meaning of slump deposits on the eastern slope of the Rockall Bank. *Mar. Geol.*, **40**, 49-57.

Faugeres, J.C., Cremer, M., Monteiro, H. and Gaspar, L. (1985) Essai de reconstitution des prosessus d'edification de la ride sedimentaire de Faro (Marge sud-Portugaise) *Bull. Inst. Geol. Bassin Aquit.*, **37**, 229-258.

Faugeres, J-C., Mezerais, M-L, and Stow, D.A.V. (1993) Contourite drift types and their distribution in the North and South Atlantic Ocean basins. *Sedim. Geology*, **82**, 189-203.

Flood, R.D. (1988) A lee wave model for deep-sea mudwave activity. *Deep-Sea Res.*, **35**, 973-983.

Flood, R.D. and Shor, A.N. (1988) Mud waves in the Argentine Basin and their relationship to regional bottom circulation patterns. *Deep Sea Res.*, **35**, 943-971.

Flood, R.D., Hollister, C.D. and Lonsdale, P. (1979) Disruption of the Feni sediment drift by debris flows from Rockall Bank. *Mar. Geol.*, **32**, 311-334.

Fox, P.J., Heezen, B.C. and Harian, A.M. (1968) Abyssal antidunes. *Nature*, **220**, 470-472.

Garcia, M., and Parker, G. (1989) Experiments on hydraulic jumps in turbidity currents near a canyon-fan transition. *Science*, **245**, 393-396.

Gee, M.J.R., Masson, D.G., Watts, A.B. and Allen, P.A. (1999) The Saharan debris flow: an insight into the mechanics of long runout submarine debris flows. *Sedimentology*, **46**, 317-335.

Hampton M.A., Locat, J. and Lee, H.J. (1996) Submarine landslides. *Rev. Geophys.*, **34**, 33-59.

Hand, B.M. (1974) Supercritical flow in density currents. *J. Sedim. Pet.*, **44/3**, 637-648.

Hand, B.M., Middleton, G.V. and Skipper, K. (1972) Antidune cross-stratification in a turbidite sequence, Cloridorme Formation, Gaspe, Quebec. *Sedimentology*, **18**, 135-138.

Heezen, B.C., Tharp, M. and Ewing, M. (1959) The floors of the oceans. *Geol. Soc. Am. Spec. Paper*, **65**, 122-137.

Hesse, R., Chough, S.K. and Rakofsky, A. (1987) The Northwest Atlantic Mid-Ocean Channel of the Labrador Sea. V. Sedimentology of a giant deep sea channel. *Can. J. Earth Sci.*, **24**, 1595-1624.

Hesse, R., Klaucke, I., Ryan, W.B.F., Edwards, M.B. and Piper, D.J.W. (1996) Imaging Laurentide Ice Sheet drainage into the deep sea: impact on sediments and bottom water. *Geol. Soc. Am. Today*, **6**, 3-9.

Hill, P.R., Moran, K.M. and Blasco, S.M. (1982) Creep deformation of slope sediments in the Canadian Beaufort Sea. *Geo-Mar. Lett.*, **2**, 163-170.

Hilton, V.C. (1995) Sandstone architecture and facies from the Annot Basin of the Tertiary SW Alpine Foreland Basin, SE France. In: *Atlas of Deep Water Environments: Architectural style in turbidite systems* (Eds. K.T. Pickering, R.N. Hiscott, N.H. Kenyon, F. Ricci Lucchi, and R.D.A. Smith), pp.227-235, Chapman and Hall, London.

Hinz, K. et al. (1982) Preliminary results from DSDP Leg 79 seaward of the Mazagan Plateau off Central Morocco. In: *Geology of the Northwest African Continental Margin* (Eds. U.von Rad, K. Hinz, M. Sarnthein and E. Seibold), pp.23-33, Springer-Verlag, Berlin.

Holmes, R., Long, D. and Dodd, L.R. (1998) Large-scale debrites and submarine landslides on the Barra Fan, west of Britain. In: *Geological Processes on Continental Margins: Sedimentation, Mass-Wasting and* Stability (Eds. by M.S. Stoker, D. Evans, and A. Cramp), Geol. Soc. London Spec. Publ., **129**, 67-79.

Howe, J.A. (1996) Turbidite and contourite sediment waves in the northern Rockall Trough, North Atlantic Ocean. *Sedimentology*, **43**, 219-234.

Howe, J.A., Livermore, R.A. and Maldonado, A. (1998) Mudwave activity and current-controlled sedimentation in Powell Basin, northern Weddell Sea, Antarctica. *Mar. Geol.*, **149**, 229-241.

Jacobi, R.D. (1976) Sediment slides on the northwestern continental margin of Africa *Mar. Geol.* **22**, 157-173.

Jacobi, R.D. and Hayes, D.E. (1982) Bathymetry, microphysography and reflectivity characteristics of the West African Margin between Sierra Leone and Mauritania. In: *Geology of the Northwest African Continental Margin* (Eds. U.von Rad, K. Hinz, M. Sarnthein and E. Seibold), pp.182-210, Springer-Verlag, Berlin.

Jacobi, R.D. and Hayes, D.E. (1984) Echo character, microphysiography and geologic hazards. In: *Northwest African Continental Margin and Adjacent Ocean Floor off Morocco, Ocean Margin Drilling Program, Regional Atlas Series* (Eds D.E. Hayes, P.D. Rabinowitz, and K. Hinz), pp.12-14, Marine Science International Atlas, Woods Hole, MA.

Jacobi, R.D. and Hayes, D.E. (1992) Northwest African continental rise: Effects of near-bottom processes inferred from high-resolution seismic data. In: *Geologic*

Evolution of Atlantic Continental Rises (Eds. C.W. Poag and P.C. de Graciansky), pp.293-325. Van Nostrand Reinhold, New York.

Jacobi, R.D., Rabinowitz, P.D. and Embley, R.W. (1975) Sediment waves on the Moroccan continental rise. *Mar. Geol.*, **19**, 61-67.

Johnson, G.L. and Schneider, E.D. (1969) Depositional ridges in the North Atlantic. *Earth Planet Sci. Lett.*, **6**, 416-422.

Kenyon, N.H. (1986) Evidence from bedforms for a strong poleward current along the upper continental slope of north-west Europe. *Mar. Geol.*, **72**, 187-198.

Kenyon, N.H. (1987) Mass wasting features on the continental slope of north-west Europe. *Mar. Geol.*, **74**, 57-77.

Kenyon, N.H. and Belderson, R.H. (1973) Bed forms of the Mediterranean undercurrent observed with side-scan sonar *Sed. Geol.* **9**, 77-99.

Kenyon, N.H., and Millington, J. (1995) Contrasting deep-sea depositional systems in the Bering Sea. In: *Atlas of Deep Water Environments: Architectural style in turbidite systems* (Eds. K.T. Pickering, R.N. Hiscott, N.H. Kenyon, F. Ricci Lucchi, and R.D.A. Smith), pp.196-202, Chapman and Hall, London.

Kenyon, N.H., Belderson, R.H. and Stride, A.H. (1978) Channels, canyons and slump folds on the continental slope between south-west Ireland and Spain. *Oceanol. Acta*, **1**, 369-380.

Kenyon, N.H., Millington, J., Droz, L. and Ivanov, M.K. (1995) Scour holes in a channel-lobe transition zone on the Rhone Cone. In: *Atlas of Deep Water Environments: Architectural style in turbidite systems* (Ed. by K.T. Pickering, R.N. Hiscott, N.H. Kenyon, F. Ricci Lucchi and R.D.A. Smith), pp. 212-215. Chapman and Hall, London.

Kenyon, N.H., Ivanov, M.K. and Akhmetzhanov, A.M. (1998) Cold water carbonate mounds and sediment transport on the north-east Atlantic margin: Preliminary results of

geological and geophysical investigations during the TTR-7 cruise of R/V Professor Logachev in co-operation with the CORSAIRES and ENAM 2 programmes, July-August 1997. *IOC Technical Series*, **52**, 178pp.

Kidd, R.B. and Hill, P.R. (1987) Sedimentation on mid-ocean sediment drifts. In: *North Atlantic Paleoceanography* (Ed. by C.P. Summerhayes and N.J. Shackleton), Geol. Soc. London, Spec. Publ. **21**, 87-102.

Kidd, R.B., Simm, R.W. and Searle, R.C. (1985) Sonar acoustic facies and sediment distribution on an area of the deep ocean floor *Mar. Petrol. Geol.* **2**, 210-221

Kidd, R.B., Lucchi, R.G., Gee, M., and Woodside, J.M. (1998) Sedimentary processes in the Stromboli Canyon and Marsili Basin, SE Tyrrhenian Sea: results from side-scan sonar surveys. *Geo-Mar. Lett.*, **18**, 146-154.

King, E.L., Serjup, H.P., Haflidason, H., Elverhoi, A. and Aarseth, I. (1996) Quaternary seismic stratigraphy of the North Sea Fan: glacially-fed gravity flow aprons, hemipelagic sediments, and large submarine slides. *Mar. Geol.*, **130**, 293-315.

Kneller, B.C. and Branney, M.J. (1995) Sustained high-density turbidity currents and the deposition of thick massive sands. *Sedimentology*, **42**, 607-616.

Kolla, V. and Coumes, F. (1985) Indus Fan, Indian Ocean In: *Submarine Fans and Related Turbidite Systems* (Eds. A.H. Bouma, W.R. Normark and N.E. Barnes), pp.129-136. Springer-Verlag, New York.

Kolla, V., Eittreim, S., Sullivan, L., Kostecki, J.A. and Burckle, L.H. (1980) Current-controlled, abyssal microtopography and sedimentation in Mozambique Basin, Southwest Indian Ocean. *Mar. Geol.*, **34**, 171-206.

Komar, P.D. (1971) Hydraulic jumps in turbidity currents. *Geol. Soc. Am. Bull.*, **82**, 1477-1488.

Komar, P.D. (1975) Supercritical flow in turbidity currents: a discussion. *J. Sedim. Pet.*, **45**, 747-749.

Kuijpers, A., Andersen, M.S., Kenyon, N.H., Kunzendorf, H. and van Weering, T.C.E. (1998) Quaternary sedimentation and Norwegian Sea overflow pathways around Bill Bailey Bank, northeastern Atlantic. *Mar. Geol.*, **152**, 101-127.

Laberg, J.S. and Vorren, T.O. (1993) Late Pleistocene submarine slide on the Bear Island trough mouth fan. *Geo-Mar. Lett.*, **13**, 227-234.

Laberg, J.S., Vorren, T.O. and Knutsen, S.-M. (1999) The Lofoten contourite drift off Norway. *Mar. Geol.*, **159**, 1-6.

Lallemand, S. and Sibuet, J-C. (1986) Tectonic implications of canyon directions over the northeast Atlantic continental margin. *Tectonics*, **5**, 1125-1143.

Lancelot, Y. and Winterer, E.L. (1980) Evolution of the Moroccan oceanic basin and adjacent continental margin – a synthesis. *Init. Rep. DSDP*, pp.801-821. Washington DC (US Gov. Printing Office) 50.

Laughton, A.S. (1960) An interplain deep sea channel system. *Deep Sea Res.*, **7**, 75-88.

Lebreiro, S.M. (1995) Sedimentation history off Iberia: Tore seamount, Tagus and Horseshoe abyssal plains. *Unpublished PhD. Thesis.* University of Cambridge.

Lebreiro, S.M., McCave, I.N. and Weaver, P.P.E. (1997) Late Quaternary emplacement of turbidites on the Horseshoe Abyssal Plain. *J. Sed. Res.*, **67**, 856-870.

Lewis, K.B. (1994) The 1500-km long Hikurangi Channel: trench-axis channel that escapes its trench, crosses a plateau, and feeds a fan drift. *Geo-Mar. Lett.*, **14**, 19-28.

Lewis, K.B., Collot, J-V. and Lallemand, S.E. (1998) The dammed Hikurangi Trough: a channel-fed trench blocked by subducting seamounts and their wake avalanches (New Zealand-France GeodyNZ Project). *Basin Res.*, **10**, 441-468.

Lonsdale, P. (1978) Bedforms and benthic boundary layer in the North Atlantic: A cruise report of INDOMED Leg 11. *Scripps Institute of Oceanography, SIO Reference,* **15**, 78-30

Lonsdale, P. (1982) Sediment drifts of the Northeast Atlantic and their relationship to the observed abyssal currents. *Bull. Inst. Geol. Bassin d'Aquitaine, Bordeaux,* **31**, 141-150

Lonsdale, P.F. and Hollister, C.D. (1979) A near-bottom traverse of Rockall Trough: Hydrographic and geologic inferences. *Oceanol. Acta,* **2**, 91-105.

Lowe, D.R. (1982) Sediment gravity flows: II. Depositional models with special reference to the deposits of high-density turbidity currents. *J. Sedim. Petrol.*, **52**, 279-297.

Malinverno, A., Ryan, W.B.F., Auffret, G.A. and Pautot, G. (1988) Sonar images of the path of recent failure events on the continental margin off Nice, France. *Spec. Paper Geol. Soc. Am.*, **229**, 59-75.

Masson, D.G. (1994) Late Quaternary turbidity current pathways to the Madeira Abyssal Plain and some constraints on turbidity current mechanisms. *Basin Research,* **6**, 17-33.

Masson, D.G. (1996) Catastrophic collapse of the volcanic island of Hierro 15 ka ago and the history of landslides in the Canary Islands. *Geology,* **24**, 231-234.

Masson, D.G., Kidd, R.B., Gardner, J.V., Huggett, Q.J. and Weaver, P.P.E. (1992) Saharan continental rise: Facies distribution and sediment slides. In: *Geologic Evolution of Atlantic Continental Rises* (Eds. C.W. Poag and P.C. de Graciansky), pp.327-343. Van Nostrand Reinhold, New York.

Masson, D.G., Huggett, Q.J. and Brunsden, D. (1993) The surface texture of the Saharan Debris Flow and some speculations on submarine debris flow processes. *Sedimentology,* **40**, 583-598.

Masson, D.G., Kenyon, N.H., Gardner, J.V., and Field, M.E. (1995) Monterey Fan: channel and overbank morphology. In: *Atlas of Deep Water Environments: Architectural style in turbidite systems* (Ed. by K.T. Pickering, R.N. Hiscott, N.H. Kenyon, F. Ricci Lucchi and R.D.A. Smith), pp. 74-79. Chapman and Hall, London.

Masson, D.G., Bett, B.J. and Birch, K.G. (1997) Atlantic margin environmental survey. *Sea Technol.*, **38**, 10, 52-59.

Masson, D.G., van Niel, B. and Weaver, P.P.E. (1997) Flow processes and sediment deformation in the Canary Debris Flow on the NW African Continental Rise. *Sedim. Geol.*, **110**, 163-179

Masson, D.G., Canals, M., Alonso, B., Urgeles, R. and Huhnerbach, V. (1998) The Canary Debris Flow: source area morphology and failure mechanisms. *Sedimentology*, **45**, 411-432.

McCave, I.N. and Carter, L. (1997) Recent sedimentation beneath the Deep Western Boundary Current off northern New Zealand. *Deep-Sea Res.*, **44/7**, 1203-1237.

McCave, I.N. and Tucholke, B.E. (1986) Deep current-controlled sedimentation in the western North Atlantic. In: *Geology of North America. Volume M. The Western North Atlantic Region* (Eds. P.R. Vogt and B.E. Tucholke), pp.1117-1126. Geol. Soc. Am., Boulder, Colorado.

Middleton, G.V. (1966) Experiments on density and turbidity currents. II. Uniform flow of density currents. *Can. J. Earth Sci.*, **3**, 627-637.

Mienert, J., Posewand, J. and Baumann, M. (1998) Gas hydrates along the northeastern Atlantic margin: possible hydrate bound margin instabilities and possible release of methane. In: *Gas Hydrates: Relevance to World Margin Stability and Climate Change* (Eds. J.P. Henriet and J. Mienert), Geol. Soc. London Spec. Publ., **137**, 275-291.

Miles, P.R. (1995) Potential distribution of methane hydrate beneath the European continental margins. *Geophys. Res. Lett.*, **22**, 3179-3182.

Milkert, D. and Weaver, P.P.E. (1996) Pleistocene and Pliocene turbidites from the Iberia Abyssal Plain drilled during ODP Leg 149. *Proc. ODP Init. Reports*, **149**, pp.281-294. College Station, TX (Ocean Drilling Program).

Millington, J., and Clark, J.D. (1995) Submarine canyon and associated base-of-slope sheet system: the Eocene Charo-Arro system, south-central Pyrenees, Spain. In: *Atlas of Deep Water Environments: Architectural style in turbidite systems* (Ed. by K.T. Pickering, R.N. Hiscott, N.H. Kenyon, F. Ricci Lucchi and R.D.A. Smith), pp. 150-156. Chapman and Hall, London.

Mohrig, D., Elverhoi, A. and Parker, G. (1999) Experiments on the relative mobility of muddy subaqueous and subaerial debris flows, and their capacity to remobilize antecedent deposits. *Mar. Geol.*, **154**, 117-129.

Moore, J.G., Clague, D.A., Holcomb, R.T., Lipman, P.W., Normark, W.R. and Torresan, M.T. (1989) Prodigious submarine landslides on the Hawaiian ridge. *J. Geophys. Res.*, **94**, 17445-17484

Morris, S.A., Kenyon, N.H., Limonov, A.H. and Alexander, J. (1998) Downstream changes of large-scale bedforms in turbidites around the Valencia channel mouth, north-west Mediterranean: implications for palaeoflow reconstruction. *Sedimentology*, **45**, 365-377.

Mougenot, D. (1985) Progradation on the Portuguese continental margin: interpretation of seismic facies. *Mar. Geol.*, **69**, 113-130.

Mulder, T. and Cochonat, P. (1996) Classification of offshore mass movements. *J. Sedim. Res.*, **66**, 1, 43-57.

Mulder, T. and Syvitski, P.M. (1995) Turbidity currents generated at river mouths during exceptional discharges to the World Ocean. *J. Geol.*, **103**, 285-299.

Murton, B.J., Rouse, I.P., Millard, N.W. and Flewellen, C. (1992) Deep-towed instrument explores ocean floor. *Eos (Transactions, American Geophysical Union),* **73**, 225-228.

Mutti, E. (1979) Turbidites et cones sous-marins profond. In: *Sedimentation detritique (fluviatile, littorale et marine)* (Ed. P. Homewood), pp.353-419. Institut de Geologie, Univ. de Fribourg, Suisse.

Mutti, E. (1985) Turbidite systems and their relations to depositional sequences. In: *Provenance of Arenites* (Ed. G.G. Zuffa), pp.65-93. Reidel.

Mutti, E., and Normark, W.R. (1987) Comparing examples of modern and ancient turbidite systems: problems and concepts. In: *Marine Clastic Sedimentology: Concepts and Case Studies* (Eds. J.K. Leggett and G.G. Zuffa), pp.1-38. Graham and Trotman, London.

Mutti, E., and Normark, W.R. (1991) An integrated approach to the study of turbidite systems. In: *Seismic Facies and Sedimentary Processes of Submarine Fans and Turbidite Systems* (Eds. P. Weimer and M.H. Link), pp.75-106. Springer-Verlag, New York.

Mutti, E., Seguret, M., and Sgavetti, M. (1989) Sedimentation and deformation in the Tertiary sequences of the southern Pyrenees. *AAPG Mediterranean Basins Conf. Guidebook Field Trip No.7, Spec. Publ. Inst. Geol., Univ. of Parma,* Nice, 157p.

Nakajima, T., Satoh, M. and Okamura, Y. (1998) Channel-levee complexes, terminal deep-sea fan and sediment wave fields associated with the Toyama Deep-Sea Channel system in the Japan Sea. *Mar. Geol.*, **147**, 25-41.

Nelson, C.H., Maldonado, A., Barber Jr., J.H. and Alsonso, B. (1991) Modern sand-rich and mud-rich siliclastic aprons: alternative base-of-slope turbidite systems to submarine fans. In: *Seismic Facies and Sedimentary Processes of Submarine Fans and Turbidite Systems* (Eds. P. Weimer and M.H. Link), pp.171-190. Springer-Verlag, New York.

Nelson, C.H., Baraza, J., Maldonado, A., Rodero, J., Escutia, C. and Barber, J.H Jr. (1999) Influence of the Atlantic inflow and Mediterranean outflow currents on Late Quaternary sediment facies of the Gulf of Cadiz continental margin. *Mar. Geol.*, **155**, 99-129.

Normark, W.R. (1970) Growth patterns of deep-sea fans. *Unpublished Ph.D. Dissertation*, University of California, San Diego, 165p.

Normark, W.R., and Piper, D.J.W. (1983) Navy Fan, California Borderland: Growth pattern and depositional processes. *Geo-Marine Letters*, **3**, 101-108.

Normark, W.R. and Piper, D.J.W. (1991) Initiation processes and flow evolution of turbidity currents: implications for the depositional record. In: *From Shoreline to Abyss* (Ed. R.H. Osborne). *Spec. Publ. SEPM*, **46**, 207-230.

Normark, W.R., Piper, D.J.W., and Hess, G.R. (1979) Distributary channels, sand lobes, and mesotopography of Navy Submarine Fan, California Borderland, with applications to ancient fan sediments. *Sedimentology*, **26**, 749-774.

Normark, W.R., Hess, G.R., Stow, D.A.V. and Bowen, A.J. (1980) Sediment waves on the Monterey Fan levee: A preliminary physical interpretation. *Mar. Geol.*, **37**, 1-18.

O'Connell, S., Ryan, W.B.F., and Normark, W.R. (1991) Evolution of a fan channel on the outer Mississippi Fan: evidence from side-looking sonar. In: *Seismic Facies and Sedimentary Processes of Submarine Fans and Turbidite Systems* (Eds. P. Weimer and M.H. Link), pp.365-382. Springer-Verlag, New York.

Palanques, A., Kenyon, N.H., Alonso, B., and Limonov, A. (1995) Erosional and depositional patterns in the Valencia Channel Mouth: an example of a modern channel-lobe transition zone. *Marine Geophysical Researches*, **17**, 503-517.

Pearce, T.J. and Jarvis, I. (1992) Composition and provenance of turbidite sands: Late Quaternary, Madeira Abyssal Plain. *Mar. Geol.*, **109**, 21-51.

Pilkey, O.H. (1987) Sedimentology of basin plains. In: *Geology and Geochemistry of Abyssal Plains* (Eds. P.P.E. Weaver and J. Thomson), Geol. Soc. London Spec. Publ., **31**, 1-12.

Piper, D.J.W. and Kontopoulos, N. (1990) Large gravel waves of turbidite origin: Ancient analogues of features seen by sidescan sonar (abst.). *Geological Association of Canada - Mineralogical Association of Canada Joint Annual Meeting*, Vancouver, B.C., A107.

Piper, D.J.W. and Savoye, B. (1993) Processes of late Quaternary turbidity current flow and deposition on the Var deep-sea fan, north-west Mediterranean Sea. *Sedimentology*, **40**, 557-582.

Piper, D.J.W., Shor, A.N., and Hughes Clarke, J.E. (1988) The 1929 Grand Banks earthquake, slump and turbidity current. *Geological Society of America Special Paper,* **229**, 77-92.

Piper, D.J.W., Hiscott, R.N. and Normark, W.R. (1999) Outcrop-scale acoustic facies analysis and latest Quaternary development of Hueneme and Dume submarine fans, offshore California. *Sedimentology*, **46**, 47-78.

Reading, H.G. and Richards, M. (1994) Turbidite systems in deep-water basin margins classified by grain size and feeder systems. *AAPG Bull.*, **78**, 792-822.

Reynaud, J-C, Tessier, B., Proust, J-N., Proust, D., Bourillet, J-F., de Batist, M., Lericolais., Berne, S. and Marsset, T. (1999) Architecture and sequence stratigraphy of a late Neogene incised valley at the shelf margin, Southern Celtic Sea. *J. Sedim. Res.*, **69**, 351-364.

Roberts, D.G. (1972) Slumping on the eastern margin of the Rockall Bank, North Atlantic Ocean. *Mar. Geol.*, **13**, 225-237.

Roberts, D.G. (1975) Marine geology of the Rockall Plateau and Trough. *Phil. Trans. Roy. Soc. London. A.*, **278**, 447-509.

Roberts, D.G. and Kidd, R. (1979) Abyssal sediment wave fields on Feni Ridge, Rockall Trough: Long range sonar studies. *Mar. Geol.*, **33**, 175-191.

Roberts, D.G., Schnitker, D. et al. (1984) Site 554, *Initial Reports DSDP 81*. US Govt. Printing Office, Washington DC.

Rona, P.A. (1969) Linear "lower continental rise hills" off Cape Hatteras. *J. Sedim. Pet.*, **39**, 1132-1141.

Rothwell, R.G. (1989*) Minerals and mineraloids in marine sediments: an optical identification guide*, Elsevier, London, 279pp.

Rothwell, R.G., Pearce, T.J. and Weaver, P.P.E. (1992) Late Quaternary Evolution of the Madeira Abyssal Plain, Canary Basin, NE Atlantic. *Basin Research*, **4**, 103-131.

Ruddiman, W.F. et al. (1988) *Proc. ODP, Init. Reports, Leg 108*: College Station, Texas, Ocean Drilling Program.

Sarnthein, M., Thiede, J., Pflaumann, U. et al. (1982) Atmospheric and ocean circulation patterns off Northwest Africa during the past 25 million years. In: *Geology of the Northwest African Continental Margin* (Eds. U. von Rad, K. Hinz, M. Sarnthein and E. Seibold), pp.545-604. Springer-Verlag, Berlin.

Saunders, P.M. (1988) Bottom currents near a small hill on the Madeira Abyssal Plain. *J. Phys. Oceanog.*, **18**, 868-879.

Savoye, B., Piper, D.J.W. and Droz, L. (1993) Plio-Pleistocene evolution of the Var Deep-sea fan off the French Riviera. *Marine and Petroleum Geology*, **10**, 550 - 571.

Schemainda, R., Nehring, D. and Schulz, S. (1975) Ozeanologische Untersuchungen zum Produktionspotential der nordwestafrikanischen Wasserauftriebsregion 1970-1973. *Geod. Geophys. Veroff.*, **4**, 88.

Schlager, W. (1980) Mesozoic calciturbidites in DSDP hole 416A – recognition of a drowned carbonate platform. In: *Init. Rep.* DSDP (Eds. Y. Lancelot and E.L. Winterer), pp.733-750. Washington DC (US Gov. Printing Office) 50.

Schmincke, H.-U. (1982) Volcanic and chemical evolution of the Canary Islands. In: *Geology of the Northwest African Continental Margin* (Eds. U.von Rad, K.Hinz, M.Sarnthein and E.Seibold), pp.273-306. Springer-Verlag, New York.

Schmincke, H.-U., Weaver, P.P.E., Firth, J.V. et al. (1995*) Proc. ODP, Init. Reports, Leg 157*: College Station, Texas (Ocean Drilling Program).

Searle, R.C. (1987) Regional setting and geophysical characterisation of the Great Meteor East area in the Madeira Abyssal Plain. In: *Geology and Geochemistry of Abyssal Plains* (Eds P.P.E.Weaver and J.Thomson, J.) *Spec. Publ. Geol. Soc. London*, **31**, 49-70.

Seibold, E. (1982) The northwest African continental margin – an introduction. In: *Geology of the Northwest African Continental Margin* (Eds. U.von Rad, K.Hinz, M.Sarnthein and E.Seibold), pp.3-20. Springer-Verlag, New York.

Shanmugam, G. and Moiola, R.J. (1981) Eustatic control of turbidites and winnowed turbidites. *Geology*, **10**, 231-235.

Shanmugam, G., and Moiola, R.J. (1988) Submarine fans: characteristics, models, classification, and reservoir potential. *Earth Science Reviews*, **24**, 383-428.

Shipboard Scientific Party (1995) Site 930. In: *Proc. ODP, Init. Repts., 155* (Eds. R.D. Flood, D.J.W. Piper, A. Klaus, et al.), pp.87-122. College Station, TX (Ocean Drilling Program).

Shor, A.N., Piper, D.J.W., Hughes Clarke, J. and Mayer, L.A. (1990) Giant flute-like scour and other erosional features formed by the 1929 Grand Banks turbidity current. *Sedimentology*, **37**, 631-645.

Simm, R.W and Kidd, R.B. (1984) Submarine debris flow deposits detected by long-range side-scan sonar 1,000-kilometers from source. *Geo-Mar. Lett.*, **3**,13-16.

Stacey, M.W. and Bowen, A.J. (1988) The vertical structure of density and turbidity currents: Theory and observation. *J. Geophys. Res.*, **93**, 3528-3542.

Stoker, M.S. (1995) The influence of glacigenic sedimentation on slope-apron development on the continental margin off northwest Britain. In: *The Tectonics, Sedimentation and Palaeoceanography of the North Atlantic* Region (Eds. R.A. Scrutton, M.S. Stoker, G.B. Shimmield and A.W. Tudhope), Geol. Soc. London Spec. Publ., **90**, 309pp.

Stoker, M.S., Leslie, A.B., Scott, W.D., Briden, J.C., Hine, N.M., Harland, R., Wilkinson, I.P., Evans, D. and Ardus, D.A. (1994) A record of Late Cenozoic stratigraphy, sedimentation and climate change from the Hebrides Slope, NE Atlantic Ocean. *J. Geol. Soc. London*, **151**, 235-249.

Stow, D.A.V. (1985) Deep-sea clastics: where are we and where are we going? In: *Sedimentology: Recent Developments and Applied Aspects* (Eds P.J.Brenchley and B.P.J.Williams), *Spec. Publ. Geol. Soc. London*, **18**, 67-93.

Stow, D.A.V. and Bowen, A.J. (1980) A physical model for the transport and sorting of fine-grained sediments by turbidity currents. *Sedimentology*, **27**, 31-46.

Stow, D.A.V. and Holbrook, J.A. (1984) North Atlantic contourites: an overview. In: Fine-Grained Sediments: Deep-Water Processes and Facies (Eds. D.A.V. Stow and D.J.W. Piper), *Geol. Soc. London Spec. Publ.*, **15**, 245-256.

Stow, D.A.V. and Lovell, J.P.B. (1979) Contourites: their recognition in modern and ancient sediments. *Earth Sci. Rev.*, **14**, 251-291.

Stow, D.A.V. and Shanmugam, G. (1980) Sequence of structures in fine-grained turbidites: comparison of recent deep sea and ancient flysch sediments. *Sedim. Geol.*, **25**, 23-42.

Stow, D.A.V. and Tabrez, A.R. (1998) Hemipelagites: processes, facies and model. In: *Geological Processes on Continental Margins: Sedimentation, Mass-Wasting and Stability* (Ed. by M.S. Stoker, D. Evans and A. Cramp). *Geol. Soc. London Spec. Publ.*, **129**, 317-337.

Stow, D.A.V., C.D. Bishop, and S.J. Mills (1982) Sedimentology of the Brae oilfield, North Sea: Fan models and controls. *Journal of Petroleum Geology*, **5**, 129-148.

Stow, D.A.V., Howell, D.G. and Nelson, C.H. (1984) Sedimentary, tectonic and sea-level controls on submarine fans and slope-apron turbidite systems. *Geo-Marine Letters*, **3**, 57-64.

Stow, D.A.V., Faugeres, J.C. and Gonthier, E.G. (1986) Facies distribution and textural variation in Faro Drift contourites: Velocity fluctuation and drift growth, *Marine Geology,* **72**, 71-100.

Stow, D.A.V., Reading, H.G. and Collinson, J.C. (1996) Deep seas. In: *Sedimentary Environments and Facies* (Ed. by H.G. Reading). pp. 395-453, Blackwell, Oxford.

Summerhayes, C.P. et al. (1976) Northwest African shelf sediments: influence of climate and sedimentary processes. *J. Geol.*, **84**, 277-300.

Thiede, J., Suess, E. and Muller, P.J. (1982) Late Quaternary fluxes of major sediment components to the sea floor at the northwest African continental slope. In: *Geology of the Northwest African Continental Margin* (Eds. U.von Rad, K.Hinz, M.Sarnthein and E.Seibold), pp.605-631. Springer-Verlag, New York.

Thierstein, H.R., Geitzenauer, K.R., Molfino, B. and Shackleton, N.J. (1977) Global synchroneity of Late Quaternary coccolith datum levels: validation by oxygen isotopes. *Geol.*, **5**, 400-404.

Thomson, J. and Weaver, P.P.E. (1994) An AMS radiocarbon method to determine the emplacement time of recent deep-sea turbidites. *Sedim. Geol.*, **89**, 1-7.

Urgeles, R., Masson, D.G., Canals, M., Watts, A.B., and Le Bas, T. (1999) Recurrent large-scale landsliding on the west flank of La Palma, Canary Islands. *Journal of Geophysical Research*, **104**, 25331-25348.

Vail, P.R., Mitchum Jr, R.M. and Thompson III, S. (1977) Global cycles of relative changes of sea level. In: *Seismic stratigraphy and global changes of sea* level (Eds. P.R. Vail et al.), AAPG Memoir, **26**, 83-98.

van Weering, T.C.E., Nielsen, T., Kenyon, N.H., Akentieva, K. and Kuipers, A.H. (1998a) Large submarine slides on the NE Faeroe continental margin. In: *Geological Processes on Continental Margins: Sedimentation, Mass-Wasting and* Stability (Eds. M.S. Stoker, D. Evans, and A. Cramp), Geol. Soc. London Spec. Publ., **129**, 5-17.

van Weering, T.C.E., Nielsen, T., Kenyon, N.H., Akentieva, K. and Kuijpers, A.H. (1998b) Sediments and sedimentation at the NE Faeroe continental margin; contourites and large-scale sliding. *Mar. Geol.*, **152**, 159-176.

Varnes, D.J. (1978) Slope movement types and processes. In: *Landslides - Analysis and Control* (Eds. R.L.Schuster and R.J.Krizek), *Spec. Rep. Transp. Res. Board, Natl. Res. Counc., Washington D.C*, **176**, 12-33.

Vicente Bravo, J.C., and Robles, S. (1995) Large-scale mesotopographic bedforms from the Albion Black Flysch, northern Spain: characterization, setting and comparison with recent analogues. In: *Atlas of Deep Water Environments: Architectural style in turbidite systems* (Ed. by K.T. Pickering, R.N. Hiscott, N.H. Kenyon, F. Ricci Lucchi and R.D.A. Smith), pp. 216-226. Chapman and Hall, London.

von Rad, U. and Wissmann, G. (1982) Cretaceous-Cenozoic history of the West Saharan continental margin (NW Africa): Development, destruction and gravitational sedimentation. In: *Geology of the Northwest African Continental* Margin (Eds. U. von Rad, K. Hinz, M. Sarnthein and E. Seibold), pp.106-131. Springer-Verlag, Berlin.

Vorren, T.O., Laberg, J.S., Blaume, F., Dowdeswell, J.A., Kenyon, N.H., Mienert, J., Rumohr, J. and Werner, F. (1998) The Norwegian-Greenland Sea continental margins:

morphology and late Quaternary sedimentary processes and environment. *Quat. Sci. Rev.*, **17**, 273-302.

Watts, A.B. and Masson, D.G. (1995) A giant landslide on the north flank of Tenerife, Canary Islands. *J. Geophys. Res.*, **100 (B12),** 24487-24498.

Weaver, P.P.E. (1983) An integrated stratigraphy of the upper Quaternary of the King's Trough Flank area, N.E. Atlantic. *Oceanolog. Acta*, **6**, 451-456.

Weaver, P.P.E. (1993) High resolution stratigraphy of marine Quaternary sequences. In: *High Resolution Stratigraphy* (Eds. E.A. Hailwood and R.B. Kidd), Spec. Publ. Geol. Soc. London, **70**, 137- 153.

Weaver, P.P.E. (1994) Determination of turbidity current erosional characteristics from reworked coccolith assemblages, Canary Basin, north-east atlantic. *Sedimentology*, **41**, 1025-1038.

Weaver, P.P.E. and Kuijpers, A. (1983) Climatic control of turbdite deposition on the Madeira Abyssal Plain. *Nature*, **306**, 360-363.

Weaver, P.P.E. and Rothwell, R.G. (1987) Sedimentation on the Madeira Abyssal Plain over the last 300,000 years In: *Geology and Geochemistry of Abyssal Plains* (Eds. P.P.E.Weaver and J.Thomson), Spec. Pub. Geol. Soc. London, **31**, 71-86.

Weaver, P.P.E., Rothwell, R.G., Ebbing, J., Gunn, D. and Hunter, P.M. (1992) Correlation, frequency of emplacement and source directions of megaturbidites on the Madeira Abyssal Plain. *Mar. Geol.*, **109**, 1-20.

Weaver, P.P.E., Masson, D.G., Gunn, D.E., Kidd, R.B., Rothwell, R.G. and Maddison, D.A. (1995) Sediment mass wasting in the Canary Basin. In: *Atlas of Deep Water Environments: Architectural Style in Turbidite* Systems (Eds. K.T. Pickering, R.N. Hiscott, N.H. Kenyon, F. Ricci Lucchi and R.D.A. Smith), pp.287-29. London, Chapman & Hall.

Weaver, P.P.E., Jarvis, I., Lebreiro, S.M., Alibes, B., Baraza, J., Howe, R. and Rothwell, R.G. (1998) The Neogene turbidite sequence on the Madeira Abyssal Plain: basin filling and diagenesis in the deep ocean In: *Proc. ODP Sci. Results, 157* (Eds. P.P.E.Weaver, H.-U. Schmincke, J.V.Firth and W.Duffield). College Station, Texas.

Webb, D.L. (1993) Seabed and sub-seabed mapping using a parametric system. *Hydrogr. Journal*, **68**, 5-13.

Weber, K.J. (1982) Influence of common sedimentary structures on fluid flow in reservoir models. *J. Petrol. Technol.*, **34**, 665-672.

Weimer, P. and Link, M.H. (1991) Global petroleum occurrences in submarine fans and turbidite systems. In: *Seismic Facies and Sedimentary Processes of Submarine Fans and Turbidite Systems* (Eds. P. Weimer and M.H. Link), pp.9-67. Springer-Verlag, New York.

Whitmarsh, R.B., Sawyer, S., Klaus, A. and Masson, D.G. (1996) Iberia Abyssal Plain: covering Leg 149 of the cruises of the Drilling Vessel "Joides Resolution", Balboa Harbor, Panama, to Lisbon, Portugal, Sites 897-901. *Proc. ODP, Sci. Res., 149*, College Station, Texas (Ocean Drilling Program) 785pp.

Williams, H. and Soek, H.F. (1993) Predicting reservoir sandbody orientation from dipmeter data: the use of sedimentary dip profiles from outcrop studies. In: *The Geological Modelling of Hydrocarbon Reservoirs and Outcrop Analogues* (Eds. S.S. Flint and I.D. Bryant) *Spec. Pub. Int. Assoc. Sediment.*, **15**, 143-156.

Winn, R.D.Jr. and Dott, R.H.Jr. (1979) Deep-water fan-channel conglomerates of Late Cretaceous age, southern Chile. *Sedimentology*, **26**, 203-228.

Wynn, R.B., Masson, D.G., Stow, D.A.V. and Weaver, P.P.E. (2000, a) The Northwest African slope apron: a modern analogue for deep-water systems with complex seafloor topography. *Marine and Petroleum Geology*, **17/2**, 253-265.

Wynn, R.B., Masson, D.G., Stow, D.A.V., and Weaver, P.P.E. (2000, b) Turbidity current sediment waves on the submarine slopes of the western Canary Islands. *Mar. Geol.*, **163**, 185-19

APPENDICES

Appendix 1: Turbidite sand mineralogy in cores recovered from the Agadir Basin and Seine Abyssal Plain

Data presented in this appendix include the turbidite sand mineralogy for Cores D27, D70, D71, D72 and D73 recovered from the Agadir Basin, and D74 recovered from the Seine Abyssal Plain. These data have been used in the construction of the turbidite sand composition graphs presented in Paper 3 (page 105).

Core D12627: Turbidite sand composition

Turbidite AB4

	v.fine sand (63 - 90 um)	fine sand (125 - 180 um)	medium sand (250 - 355 um)	coarse sand (> 500 um)	all grain sizes
Number of grains counted	310	302	0	0	612
Quartz - no.	293	133	0	0	426
Quartz - %	***95***	***44***	***0***	***0***	***70***
Glauconite - no.	10	118	0	0	128
Glauconite - %	***3***	***39***	***0***	***0***	***21***
Clastic lithics - no.	4	30	0	0	34
Clastic lithics - %	***1***	***10***	***0***	***0***	***6***
Other/unidentified - no.	3	21	0	0	24
Other/unidentified - %	***1***	***7***	***0***	***0***	***3***

Turbidite AB6

	v.fine sand (63 - 90 um)	fine sand (125 - 180um)	medium sand (250 - 355 um)	coarse sand (> 500 um)	all grain sizes
Number of grains counted	307	376	340	314	1337
Quartz - no.	282	200	25	25	538
Quartz -%	***92***	***53***	***7***	***8***	***40***
Clastic lithics - no.	7	55	161	214	437
Clastic lithics - %	***2***	***14***	***47***	***68***	***33***
Pyrite - no.	10	63	46	55	175
Pyrite - %	***4***	***17***	***15***	***17***	***13***
Glauconite - no.	7	51	96	13	167
Glauconite %	***2***	***14***	***28***	***4***	***12***
Other/unidientified - no.	0	7	11	6	24
Other/unidentified - %	***0***	***2***	***3***	***3***	***2***

Turbidite AB11

	v.fine sand (63 - 90 um)	fine sand (125 - 180um)	medium sand (250 - 355 um)	coarse sand (> 500 um)	all grain sizes
Number of grains counted	338	347	0	0	685
Quartz - no.	323	266	0	0	589
Quartz - %	***96***	***77***	***0***	***0***	***86***
Glauconite - no.	9	40	0	0	49
Glauconite %	***3***	***12***	***0***	***0***	***7***
Clastic lithics - no.	5	19	0	0	24
Clastic lithics - %	***1***	***5***	***0***	***0***	***4***
Mica - no.	2	18	0	0	20
Mica - %	***0***	***5***	***0***	***0***	***3***
Other/unidentified - no.	2	4	0	0	6
Other/unidentified - %	***0***	***1***	***0***	***0***	***< 1***

Turbidite AB13

	v.fine sand (63 - 90 um)	fine sand (125 - 180um)	medium sand (250 - 355 um)	coarse sand (> 500 um)	all grain sizes
Number of grains counted	337	347	0	0	684
Quartz - no.	309	248	0	0	557
Quartz - %	***92***	***71***	***0***	***0***	***81***
Glauconite - no.	14	61	0	0	75
Glauconite - %	***4***	***18***	***0***	***0***	***11***
Clastic lithics - no.	12	35	0	0	46
Clastic lithics - %	***4***	***10***	***0***	***0***	***7***
Other/unidentified - no.	2	3	0	0	5
Other/unidentified - %	***0***	***1***	***0***	***0***	***3***

Core D13070: Turbidite sand composition

Turbidite AB6

	v.fine sand (63 - 90 um)	fine sand (125 - 180 um)	medium sand (250 - 355 um)	coarse sand (> 500 um)	all grain sizes
Number of grains counted	302	337	333	311	1283
Quartz - no.	274	259	42	31	606
Quartz - %	***91***	***77***	***12***	***9***	***47***
Clastic lithics - no.	5	19	89	207	320
Clastic lithics - %	***2***	***5***	***26***	***66***	***25***
Glauconite - no.	12	33	109	23	177
Glauconite - %	***4***	***10***	***33***	***7***	***14***
Pyrite - no.	9	9	68	28	125
Pyrite - %	***3***	***6***	***21***	***9***	***10***
Other/unidentified - no.	2	6	25	22	55
Other/unidentified - %	***1***	***2***	***8***	***8***	***4***

Turbidite AB8

	v.fine sand (63 - 90 um)	fine sand (125 - 180um)	medium sand (250 - 355 um)	coarse sand (> 500 um)	all grain sizes
Number of grains counted	300	307	0	0	607
Quartz - no.	57	206	0	0	263
Quartz - %	***19***	***67***	***0***	***0***	***43***
Pyrite - no.	69	83	0	0	152
Pyrite - %	***23***	***27***	***0***	***0***	***25***
Volcanic glass - no.	144	0	0	0	144
Volcanic glass - %	***48***	***0***	***0***	***0***	***24***
Other/unidientified - no.	32	18	0	0	50
Other/unidentified - %	***13***	***6***	***0***	***0***	***8***

Turbidite AB9

	v.fine sand (63 - 90 um)	fine sand (125 - 180um)	medium sand (250 - 355 um)	coarse sand (> 500 um)	all grain sizes
Number of grains counted	327	323	308	0	958
Volcanic lithics - no.	305	310	279	0	894
Volcanic lithics - %	***93***	***96***	***91***	***0***	***93***
Quartz - no.	9	11	15	0	35
Quartz - %	***3***	***3***	***5***	***0***	***4***
Volcanic glass - no.	11	2	3	0	25
Volcanic glass - %	***4***	***1***	***1***	***0***	***3***
Other/unidentified - no.	2	0	11	0	13
Other/unidentified - %	***<1***	***0***	***3***	***0***	***<1***

Turbidite AB13

	v.fine sand (63 - 90 um)	fine sand (125 - 180um)	medium sand (250 - 355 um)	coarse sand (> 500 um)	all grain sizes
Number of grains counted	303	359	0	0	662
Quartz - no.	263	257	0	0	520
Quartz - %	***87***	***72***	***0***	***0***	***79***
Volcanic lithics - no.	20	53	0	0	73
Volcanic lithics - %	***7***	***15***	***0***	***0***	***11***
Glauconite - no.	6	25	0	0	31
Glauconite - %	***2***	***7***	***0***	***0***	***5***
Clastic lithics - no.	7	17	0	0	24
Clastic lithics - %	***2***	***5***	***0***	***0***	***4***
Other/unidentified - no.	7	5	0	0	11
Other/unidentified - %	***2***	***1***	***0***	***0***	***1***

Turbidite AB15

	v.fine sand (63 - 90 um)	fine sand (125 - 180um)	medium sand (250 - 355 um)	coarse sand (> 500 um)	all grain sizes
Number of grains counted	330	300	247	0	877
Volcanic glass - no.	327	291	240	0	858
Volcanic glass - %	***99***	***97***	***97***	***0***	***98***
Volcanic lithics - no.	3	9	7	0	19
Volcanic lithics - %	***1***	***3***	***3***	***0***	***2***

Core D13071: Turbidite sand composition

Turbidite AB15

	v.fine sand (63 - 90 um)	fine sand (125 - 180 um)	medium sand (250 - 355 um)	coarse sand (> 500 um)	all grain sizes
Number of grains counted	322	308	321	38	989
Volcanic glass - no.	280	247	268	36	831
Volcanic glass - %	***87***	***80***	***83***	***95***	***84***
Voilcanic lithics - no.	33	48	36	0	117
Volcanic lithics - %	***10***	***16***	***11***	***0***	***12***
Quartz - no.	3	3	12	0	18
Quartz - %	***1***	***1***	***4***	***0***	***2***
Other/unidentified - no.	6	10	5	2	23
Other/unidentified - %	***2***	***3***	***2***	***5***	***2***

Turbidite ? (753 cm)

	v.fine sand (63 - 90 um)	fine sand (125 - 180um)	medium sand (250 - 355 um)	coarse sand (> 500 um)	all grain sizes
Number of grains counted	367	307	322	0	996
Volcanic glass - no.	256	188	3	0	447
Volcanic glass - %	***70***	***61***	***1***	***0***	***45***
Foram casts - no.	13	112	317	0	442
Foram casts - %	***4***	***37***	***99***	***0***	***44***
Volcanic lithics - no.	61	1	1	0	63
Volcanic lithics - %	***17***	***0***	***0***	***0***	***6***
Quartz - no.	17	0	1	0	18
Quartz - %	***4***	***0***	***0***	***0***	***2***
Other/unidientified - no.	20	6	0	0	26
Other/unidentified - %	***5***	***2***	***0***	***0***	***3***

Turbidite ? (794 cm)

	v.fine sand (63 - 90 um)	fine sand (125 - 180um)	medium sand (250 - 355 um)	coarse sand (> 500 um)	all grain sizes
Number of grains counted	312	411	0	0	723
Foram casts - no.	11	341	0	0	352
Foram casts - %	***3***	***83***	***0***	***0***	***49***
Volcanic lithics - no.	193	47	0	0	240
Volcanic lithics - %	***62***	***11***	***0***	***0***	***33***
Volcanic glass - no.	80	12	0	0	92
Volcanic glass - %	***26***	***3***	***0***	***0***	***13***
Quartz - no.	28	8	0	0	36
Quartz - %	***9***	***2***	***0***	***0***	***5***
Other/unidentified - no.	0	3	0	0	3
Other/unidentified - %	***0***	***1***	***0***	***0***	***1***

Turbidite ? (925 cm)

	v.fine sand (63 - 90 um)	fine sand (125 - 180um)	medium sand (250 - 355 um)	coarse sand (> 500 um)	all grain sizes
Number of grains counted	300	329	0	0	629
Volcanic glass - no.	297	204	0	0	501
Volcanic glass - %	***99***	***62***	***0***	***0***	***80***
Volcanic lithics - no.	2	109	0	0	111
Volcanic lithics - %	***1***	***33***	***0***	***0***	***18***
Quartz - no.	1	14	0	0	15
Quartz - %	***0***	***4***	***0***	***0***	***2***
Other/unidentified - no.	0	2	0	0	2
Other/unidentified - %	***0***	***1***	***0***	***0***	***0***

Turbidite ? - (1050 cm) (FORAM SAND)

Core D13072: Turbidite sand composition

Turbidite AB4

	v.fine sand (63 - 90 um)	fine sand (125 - 180 um)	medium sand (250 - 355 um)	coarse sand (> 500 um)	all grain sizes
Number of grains counted	300	300	300	178	1078
Quartz - no.	227	8	0	0	225
Quartz - %	***72***	***3***	***0***	***0***	***21***
Iron oxide flakes - no.	42	244	300	178	763
Iron oxide flakes - %	***14***	***81***	***100***	***100***	***71***
Mica - no.	41	46	0	0	87
Mica - %	***14***	***15***	***0***	***0***	***8***
Unidentified/other - no.	0	2	0	0	2
Unidentified/other - %	***0***	***<1***	***0***	***0***	***<1***

Turbidite AB6

	v.fine sand (63 - 90 um)	fine sand (125 - 180um)	medium sand (250 - 355 um)	coarse sand (> 500 um)	all grain sizes
Number of grains counted	300	309	386	278	1283
Quartz - no.	274	129	29	44	476
Quartz -%	***91***	***42***	***9***	***16***	***37***
Pyrite - no.	7	107	165	77	356
Pyrite - %	***2***	***35***	***43***	***26***	***28***
Clastic lithics - no.	11	56	100	121	288
Clastic lithics - %	***4***	***18***	***26***	***40***	***22***
Glauconite - no.	10	12	76	35	133
Glauconite %	***3***	***5***	***20***	***12***	***10***
Other/unidientified - no.	0	1	7	12	20
Other/unidentified - %	***0***	***< 1***	***2***	***6***	***3***

Turbidite AB11

	v.fine sand (63 - 90 um)	fine sand (125 - 180um)	medium sand (250 - 355 um)	coarse sand (> 500 um)	all grain sizes
Number of grains counted	324	323	0	0	647
Quartz - no.	313	299	0	0	612
Quartz - %	***97***	***93***	***0***	***0***	***95***
Glauconite - no.	4	12	0	0	16
Glauconite %	***1***	***4***	***0***	***0***	***3***
Clastic lithics - no.	5	9	0	0	14
Clastic lithics - %	***1***	***2***	***0***	***0***	***2***
Other/unidentified - no.	2	3	0	0	5
Other/unidentified - %	***1***	***1***	***0***	***0***	***< 1***

Turbidite AB13

	v.fine sand (63 - 90 um)	fine sand (125 - 180um)	medium sand (250 - 355 um)	coarse sand (> 500 um)	all grain sizes
Number of grains counted	307	302	0	0	609
Quartz - no.	278	259	0	0	537
Quartz - %	***91***	***86***	***0***	***0***	***88***
Glauconite - no.	11	25	0	0	33
Glauconite - %	***3***	***8***	***0***	***0***	***5***
Clastic lithics - no.	6	13	0	0	19
Clastic lithics - %	***2***	***4***	***0***	***0***	***3***
Other/unidentified - no.	11	5	0	0	18
Other/unidentified - %	***4***	***2***	***0***	***0***	***3***

Turbidite AB14

	v.fine sand (63 - 90 um)	fine sand (125 - 180um)	medium sand (250 - 355 um)	coarse sand (> 500 um)	all grain sizes
Number of grains counted	316	0	0	0	316
Quartz - no.	299	0	0	0	299
Quartz - %	***96***	***0***	***0***	***0***	***96***
Mica - no.	8	0	0	0	8
Mica - %	***2***	***0***	***0***	***0***	***2***
Glauconite - no.	5	0	0	0	5
Glauconite - %	***1***	***0***	***0***	***0***	***1***
Clastic lithics - no.	4	0	0	0	4
Clastic lithics - %	***1***	***0***	***0***	***0***	***1***

Core D13073: Turbidite sand composition

Turbidite AB4

	v.fine sand (63 - 90 um)	fine sand (125 - 180 um)	medium sand (250 - 355 um)	coarse sand (> 500 um)	all grain sizes
Number of grains counted	310	327	84	0	721
Quartz - no.	287	145	8	0	440
Quartz - %	***92***	***44***	***10***	***0***	***61***
Iron oxide flakes - no.	7	44	33	0	84
Iron oxide flakes - %	***2***	***13***	***39***	***0***	***12***
Glauconite - no.	5	62	19	0	86
Glauconite - %	***2***	***19***	***23***	***0***	***12***
Clastic lithics - no.	6	51	18	0	75
Clastic lithics - %	***2***	***16***	***21***	***0***	***10***
Unidentified/other - no.	5	25	6	0	36
Unidentified/other - %	***2***	***8***	***7***	***0***	***5***

Turbidite ? (37 cm) - FORAM SAND

Turbidite AB6

	v.fine sand (63 - 90 um)	fine sand (125 - 180um)	medium sand (250 - 355 um)	coarse sand (> 500 um)	all grain sizes
Number of grains counted	317	327	300	0	944
Quartz - no.	291	156	39	0	486
Quartz - %	***92***	***48***	***13***	***0***	***51***
Clastic lithics - no.	13	72	158	0	243
Clastic lithics - %	***4***	***22***	***53***	***0***	***26***
Pyrite - no.	5	49	59	0	113
Pyrite - %	***2***	***15***	***20***	***0***	***12***
Glauconite - no.	7	47	37	0	97
Glauconite - %	***2***	***14***	***12***	***0***	***10***
Other/unidentified - no.	1	3	7	0	11
Other/unidentified - %	***0***	***1***	***2***	***0***	***1***

Turbidite AB7

	v.fine sand (63 - 90 um)	fine sand (125 - 180um)	medium sand (250 - 355 um)	coarse sand (> 500 um)	all grain sizes
Number of grains counted	311	339	0	0	650
Quartz - no.	278	141	0	0	419
Quartz - %	***89***	***42***	***0***	***0***	***64***
Glauconite - no.	12	122	0	0	134
Glauconite - %	***4***	***36***	***0***	***0***	***21***
Clastic lithics - no.	17	40	0	0	57
Clastic lithics - %	***6***	***12***	***0***	***0***	***9***
Mica - no.	4	34	0	0	38
Mica - %	***1***	***10***	***0***	***0***	***6***

Turbidite ? (123 cm) - FORAM SAND

Turbidite ? (152 cm) - FORAM SAND

Turbidite ? (178 cm) - FORAM SAND

Turbidite AB11

Medium sand (250 - 355um) - Pyrite framboids + v.rare volcanic glass
Fine sand (125 - 180um) - Pyrite framboids + rare glauconite, qtz, clastic lithics, mica, spicules
V.fine sand (63 - 90um) - Qtz dominant, also glauconite, clastic lithics, pyrite framboids, mica

Turbidite AB13

Fine sand (125 - 180um) - Dominated by spicules and forams
V.fine sand (63 - 90um) - Qtz dominant, also glauconite, spicules, forams, mica, clastic lithics

Turbidite AB17

Fine sand (125 - 180um) - Biotite dominant, also glauconite, quartz, clastic lithics, pyrite
V.fine sand (63 - 90um) - Qtz dominant, also glauconite, clastic lithics, mica

Turbidite ? (493 cm)

Fine sand (125 - 180um) - Biotite dominant, also qtz, glauconite, clastic lithics
V.fine sand (63 - 90um) - Qtz dominant, also glauconite, clastic lithics, mica

Turbidite ? (565 cm)

Fine sand (125 - 180um) - Glauconite (oxidized) dominant, also biotite, qtz, clastic lithics, fish teeth, pyrite, spicules
V.fine sand (63 - 90um) - Qtz dominant, also glauconite, clastic lithics, mica

Turbidite ? (584 cm)

Medium sand (250 - 355um) - Forams dominant, v.rare biotite + glauconite
Fine sand (125 - 180um) - Qtz, glauconite, mica, clastic lithics
V.fine sand (63 - 90um) - Qtz dominant, also glauconite, clastic lithics, mica

Turbidite ? (598 cm)

Fine sand (125 - 180um) - Biotite dominant, also qtz, glauconite, clastic lithics
V.fine sand (63 - 90um) - Qtz dominant, also glauconite, clastic lithics, mica

Turbidite ? (653 cm)

Fine sand (125 - 180um) - Biotite dominant, also qtz, glauconite, clastic lithics
V.fine sand (63 - 90um) - Qtz dominant, also glauconite, clastic lithics, mica

Turbidite ? (676 cm)

Fine sand (125 - 180um) - Mica + pyrite aggregates dominant, also qtz, glauconite, clastic lithics
V.fine sand (63 - 90um) - Qtz dominant, also glauconite, clastic lithics, mica

Turbidite ? (695 cm)

Fine sand (125 - 180um) - Qtz, glauconite, clastic lithics, mica
V.fine sand (63 - 90um) - Qtz dominant, also glauconite, clastic lithics, mica

Turbidite 970 cm)

Fine sand (125 - 180um) - Qtz, glauconite, clastic lithics, mica
V.fine sand (63 - 90um) - Qtz dominant, also glauconite, clastic lithics, mica

Core D13074: Turbidite sand composition					
Turbidite AB6					
	v.fine sand (63 - 90 um)	**fine sand** (125 - 180 um)	**medium sand** (250 - 355 um)	**coarse sand** (> 500 um)	**all grain sizes**
Number of grains counted	308	332	301	96	1037
Quartz - no.	291	265	42	7	605
Quartz - %	***94***	***80***	***14***	***8***	***58***
Clastic lithics - no.	14	24	134	75	247
Clastic lithics - %	***5***	***7***	***45***	***78***	***24***
Glauconite - no.	3	26	79	5	113
Glauconite - %	***1***	***8***	***26***	***5***	***11***
Pyrite - no.	0	8	32	4	44
Pyrite - %	***0***	***2***	***11***	***4***	***4***
Other/unidentified - no.	0	9	14	5	28
Other/unidentified - %	***0***	***3***	***5***	***5***	***3***
Turbidite AB13 - (FORAM-DOMINATED)					
	v.fine sand (63 - 90 um)	**fine sand** (125 - 180um)	**medium sand** (250 - 355 um)	**coarse sand** (> 500 um)	**all grain sizes**
Number of grains counted	301	316	*FORAMS*	0	617
Quartz - no.	275	212	0	0	487
Quartz - %	***91***	***67***	***0***	***0***	***79***
Glauconite - no.	9	50	0	0	59
Glauconite - %	***3***	***16***	***0***	***0***	***10***
Clastic lithics - no.	12	32	0	0	44
Clastic lithics - %	***4***	***10***	***0***	***0***	***7***
Other/unidientified - no.	5	22	0	0	27
Other/unidentified - %	***2***	***7***	***0***	***0***	***4***
Turbidite ? (668 cm)					
	v.fine sand (63 - 90 um)	**fine sand** (125 - 180um)	**medium sand** (250 - 355 um)	**coarse sand** (> 500 um)	**all grain sizes**
Number of grains counted	312	180	0	0	492
Quartz - no.	283	38	0	0	321
Quartz - %	***91***	***21***	***0***	***0***	***65***
Mica - no.	10	95	0	0	105
Mica - %	***3***	***53***	***0***	***0***	***22***
Clastic lithics - no.	16	15	0	0	31
Clastic lithics - %	***5***	***8***	***0***	***0***	***6***
Spicules - no.	0	15	0	0	15
Spicules - %	***0***	***8***	***0***	***0***	***3***
Glauconite - no.	2	8	0	0	10
Glauconite - %	***1***	***5***	***0***	***0***	***2***
Other/unidentified - no.	1	9	0	0	10
Other/unidentified - %	***0***	***5***	***0***	***0***	***2***
Turbidite ? (779 cm) - (FORAM SAND)					

Figure 4.1: Sedimentary features on the Northeast Atlantic margin

THREE PRIMARY MARGIN TYPES

Glaciated margin
North of 56ºN

Dominated by sedimentary processes which occured during glacial times when ice extended across the continental shelf. Some redistribution of sediment by bottom currents and landsliding during the Holocene

Glacially influenced margin
From 26ºN to 56ºN

Margin physiography heavily *influenced by sedimentary processes which occured during glacial times* (e.g. cutting of canyons, filling of abyssal plains), when sediment supply was much greater. Some redistribution of sediments through canyons and by alongslope processes during the Holocene.

Non-Glaciated Margin
South of 26ºN

Low sediment supply from rivers even during glacial times, although high sedimentation in upwelling areas along the upper slope. Some large-scale but infrequent landslides.

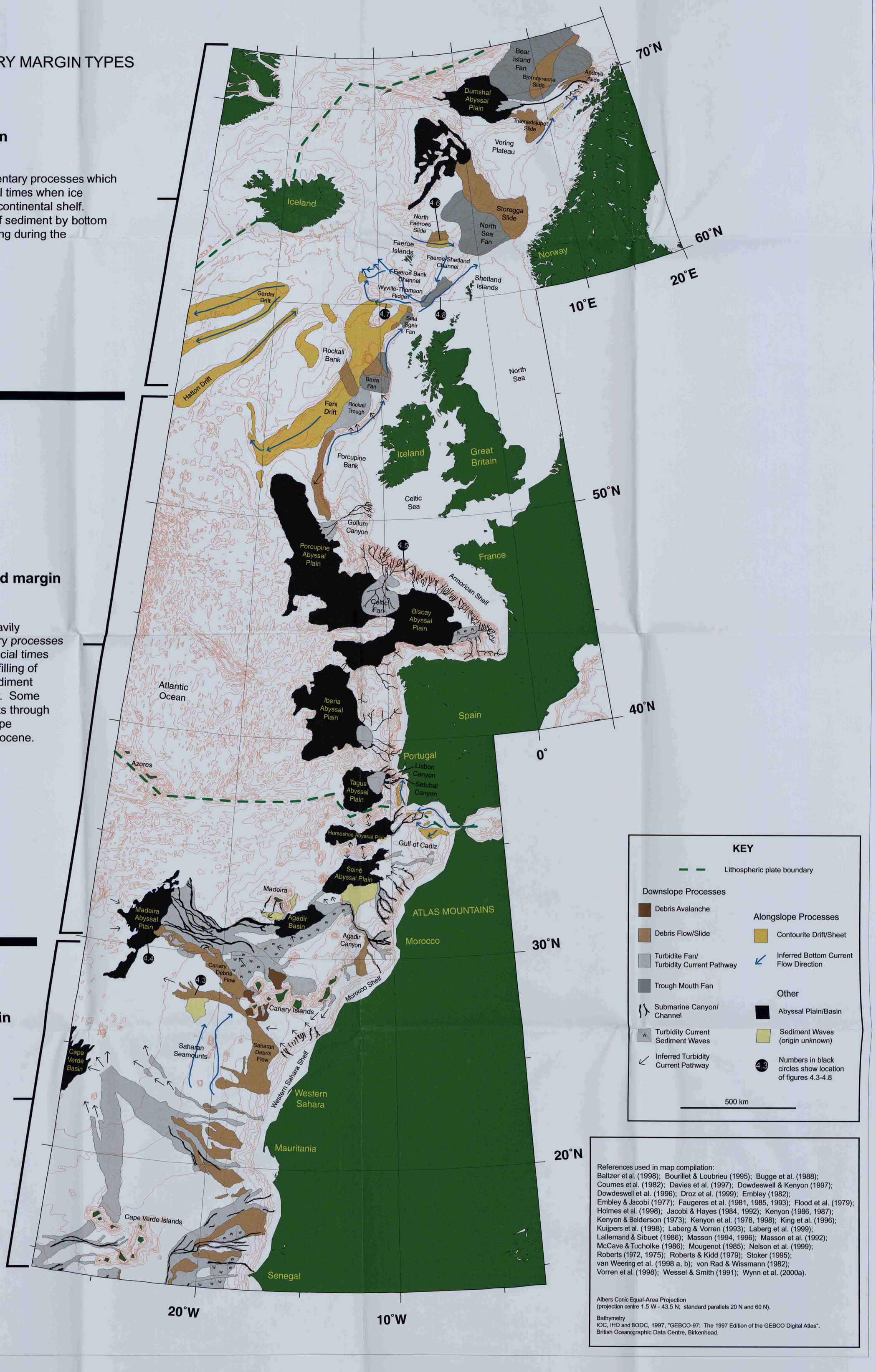

KEY

- Lithospheric plate boundary

Downslope Processes
- Debris Avalanche
- Debris Flow/Slide
- Turbidite Fan/ Turbidity Current Pathway
- Trough Mouth Fan
- Submarine Canyon/ Channel
- Turbidity Current Sediment Waves
- Inferred Turbidity Current Pathway

Alongslope Processes
- Contourite Drift/Sheet
- Inferred Bottom Current Flow Direction

Other
- Abyssal Plain/Basin
- *Sediment Waves (origin unknown)*
- Numbers in black circles show location of figures 4.3-4.8

500 km

References used in map compilation:
Baltzer et al. (1998); Bourillet & Loubrieu (1995); Bugge et al. (1988); Coumes et al. (1982); Davies et al. (1997); Dowdeswell & Kenyon (1997); Dowdeswell et al. (1996); Droz et al. (1999); Embley (1982); Embley & Jacobi (1977); Faugeres et al. (1981, 1985, 1993); Flood et al. (1979); Holmes et al. (1998); Jacobi & Hayes (1984, 1992); Kenyon (1986, 1987); Kenyon & Belderson (1973); Kenyon et al. (1978, 1998); King et al. (1996); Kuijpers et al. (1998); Laberg & Vorren (1993); Laberg et al. (1999); Lallemand & Sibuet (1986); Masson (1994, 1996); Masson et al. (1992); McCave & Tucholke (1986); Mougenot (1985); Nelson et al. (1999); Roberts (1972, 1975); Roberts & Kidd (1979); Stoker (1995); van Weering et al. (1998 a, b); von Rad & Wissmann (1982); Vorren et al. (1998); Wessel & Smith (1991); Wynn et al. (2000a).

Albers Conic Equal-Area Projection
(projection centre 1.5 W - 43.5 N; standard parallels 20 N and 60 N).

Bathymetry
IOC, IHO and BODC, 1997, "GEBCO-97: The 1997 Edition of the GEBCO Digital Atlas". British Oceanographic Data Centre, Birkenhead.

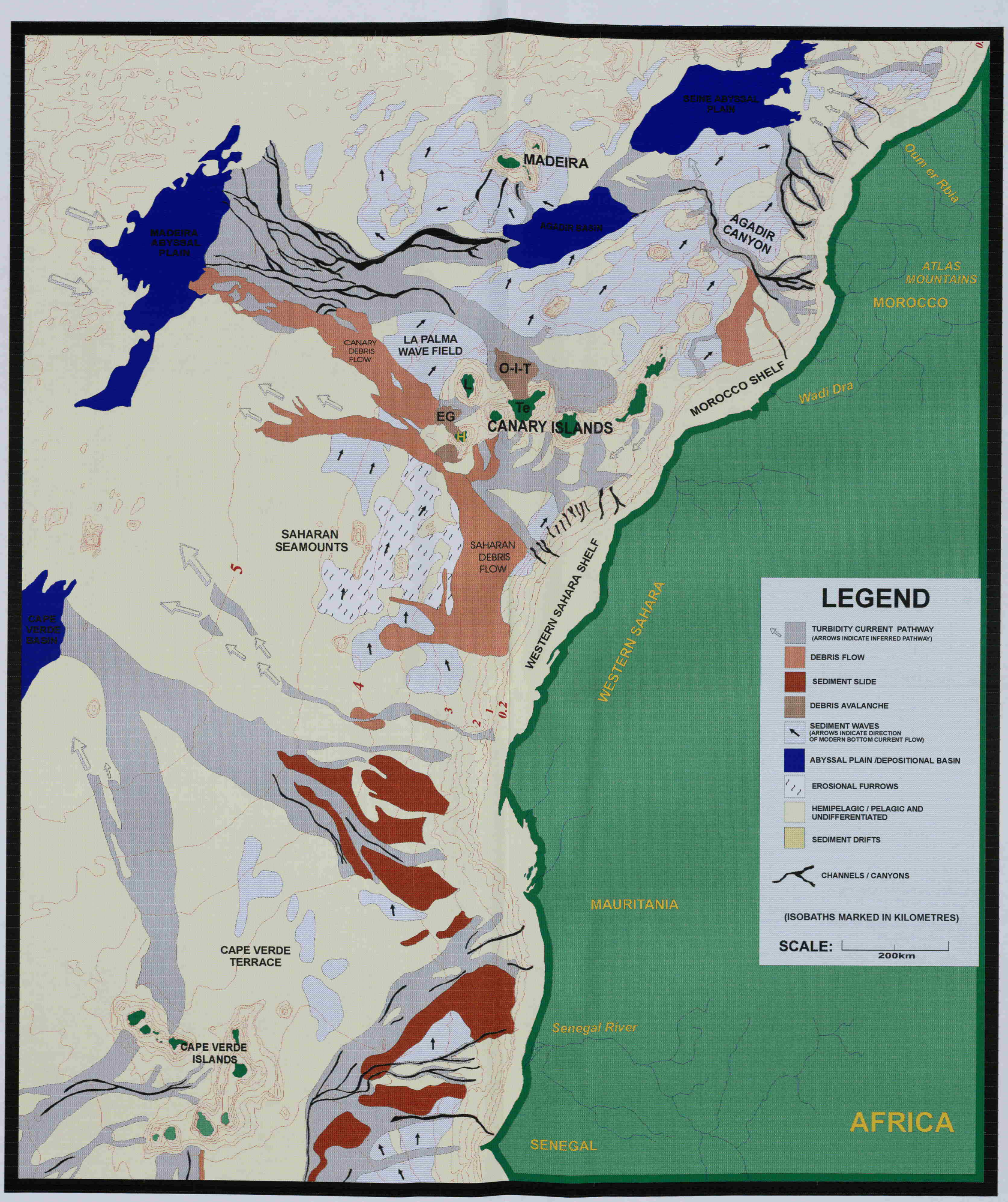

Figure 5.1: Sediment process map of the Northwest African margin. This map is largely based on 3.5kHz profiles and sidescan sonar images, and shows the complex interplay between pelagic/hemipelagic sedimentation, alongslope bottom currents and downslope gravity flows. Bathymetric contours in kilometres. Abbreviations: Te = Tenerife, L = La Palma, H = El Hierro, O-I-T = Oratava-Icod-Tino Debris Avalanche, EG = El Golfo Debris Avalanche.